Summer 8-23-2019

Development of a Hybrid Thermoplastic Composite and Concrete Deck System

Benjamin T. Smith
University of Maine, benjamin.t.smith@maine.edu

DEVELOPMENT OF A HYBRID THERMOPLASTIC COMPOSITE AND CONCRETE DECK SYSTEM

By

Benjamin Tyrell Smith

B.S. University of Maine, 2017

A THESIS

Submitted in Partial Fulfillment of the

Requirements for the Degree of

Master of Science

(in Civil Engineering)

The Graduate School

The University of Maine

August 2019

Advisory Committee:

William Davids, Professor of Civil Engineering, Co-Advisor

Roberto Lopez-Anido, Professor of Civil Engineering, Co-Advisor

Warda Ashraf, Professor of Civil Engineering

DEVELOPMENT OF A HYBRID THERMOPLASTIC COMPOSITE AND CONCRETE DECK SYSTEM

By Benjamin Tyrell Smith

Thesis Advisors: Dr. William Davids, Dr. Roberto Lopez-Anido

An Abstract of the Thesis Presented
in Partial Fulfillment of the Requirements for the
Degree of Master of Science
(in Civil Engineering)
August 2019

Reinforced concrete is a widely used structural system in conventional construction. It is used to create beams, columns, slabs, walls, bridge decks, dams, and many other structures. Concrete is a relatively inexpensive material that is much stronger in compression than in tension. This leads to the need to combine concrete with other materials to make an efficient hybrid structure. In conventional construction, steel reinforcing bars (rebar) are often used to carry the tension in the structure, as they are widely available and their design is well understood. There are some situations where rebar is not effective such as highly corrosive environments.

A continuous fiber-reinforced thermoplastic (CFRTP) panel could be used as non-corrosive tension reinforcement in concrete structures to replace steel rebar. In this research, three sets of composite CFRTP-concrete specimens were designed, manufactured, and tested to evaluate their use as a replacement for steel rebar in reinforced concrete construction. To function as the tension reinforcement for the structure, a shear connection mechanism was needed to create composite action between the CFRTP panel and the concrete. For this research, E-glass fiber-reinforced thermoplastic polyethylene terephthalate glycol (PETg) was selected for its good mechanical and hygro-thermal properties and relatively low cost compared to other thermoplastic composites. Each

set of composite CFRTP-concrete beams was designed to meet the requirements for a bridge deck with stay-in-place formwork given in the AASHTO LRFD Bridge Design Specifications.

The first set of specimens consisted of a flat CFRTP panel with friction welded thermoplastic shear studs as the shear transfer mechanism. When loaded in four-point bending, the specimens failed at the CFRTP-concrete interface at a load that corresponded to about 50% of the ultimate strength of the shear connection from stud testing.

For the second and third iterations of testing, modifications were made to the CFRTP panels to increase their flexural stiffness, allowing them to function as stay-in-place formwork for the structure. This would reduce installation costs and times as formwork and shoring would not need to be erected or removed.

The second set of specimens consisted of a corrugated CFRTP panel with steel dowels run through the webs as a shear transfer mechanism. The corrugations were created by stamp forming a flat panel in a mold. The corrugated hybrid beams were tested in four-point bending and reached 117% of the required design loading prior to failure.

The final set of specimens consisted of a stiffened CFRTP panel where holes were cut into the stiffeners, allowing concrete to flow into the holes creating a concrete dowel that would bear directly onto the CFRTP to transfer shear. The stiffened panels were created by bonding angle-shaped CFRTP panels to a flat CFRTP panel. The stiffened hybrid beams were tested in four-point bending and reach around 128% of the required design loading prior to failure.

ACKNOWLEDGEMENTS

First, I would like to thank my advisors, Dr. Bill Davids and Dr. Roberto Lopez-Anido, as well as the Advanced Structures and Composites Center and the U.S. Army Engineer Research and Development Center for bringing me in to work on this project.

Next, I would not be here without the eternal support of my Mom. You taught me a love of learning that has gotten me this far in life and does not seem to be slowing down anytime soon.

I am grateful for everything my Dad taught me growing up including logical thinking skills and a mentality to work smarter, not harder. I know if you were still here, you would have told me seven things I could have done better with this thesis.

I cannot show enough appreciation for my girlfriend, Laura, for putting up with me staying at the office late and always listening when I wanted to talk about my research.

I would also like to thank all the people at the ASCC who helped me along the way. Camerin, thank you for showing me how to be a graduate student and researcher. I will never forget all the good times we had in and out of the office especially playing Catan and other games. Everybody else in the office, Phil, Dante, Vacation Dante, Justin, Anthony, and Chris, for being great friends and making every day interesting. Everybody else on the ERDC team, Josh, Cody, and the undergrads, for helping with all the testing. The grad students in the other offices, Adam, Anthony, Jay, Pianpian, Hannah, Will, Charlie, Sunil, Reagan, Yi, and all the others for entertaining me when I really did not feel like working. And finally, the rest of the staff, especially Nick for creating and fixing most of my thermoforming problems and the instrumentation team for helping run my tests.

The work contained in this thesis was sponsored by the U.S. Army Engineer Research and Development Center (ERDC) under the project “Engineered Energy Efficient and Low Logistics Burden Materials and Processes" executed under Contract Number CEED-17-0018. Permission to publish was granted by the ERDC Geotechnical and Structures Laboratory.

TABLE OF CONTENTS

LIST OF TABLES

LIST OF FIGURES

CHAPTER 1

INTRODUCTION

1.1 Project Background

Reinforced concrete is a widely used structural system in conventional construction. It is used to create beams, columns, slabs, walls, bridge decks, dams, and many other structures. Concrete is a relatively inexpensive material that is much stronger in compression than in tension. This leads to the need to combine concrete with other materials to make an efficient hybrid structure. In conventional construction, steel reinforcing bars (rebar) are often used to carry the tension in the structure, as they are widely available and well understood, but rebar can degrade quickly in corrosive environments. The goal of this research is to evaluate continuous fiber-reinforced thermoplastic (CFRTP) panels, including stay-in-place formwork, for use as tension reinforcement in reinforced concrete structures.

The Advanced Structures and Composites Center (ASCC) has previously researched an alternative to rebar, a thermoset fiber-reinforced polymer (FRP) plate fastened to the tension side of a concrete beam as a retrofit for old bridges [1], [2]. This concept is shown in Figure 1. To further this line of research, this project aims to develop an effective design to incorporate this type of technology into new construction using thermoplastic FRPs

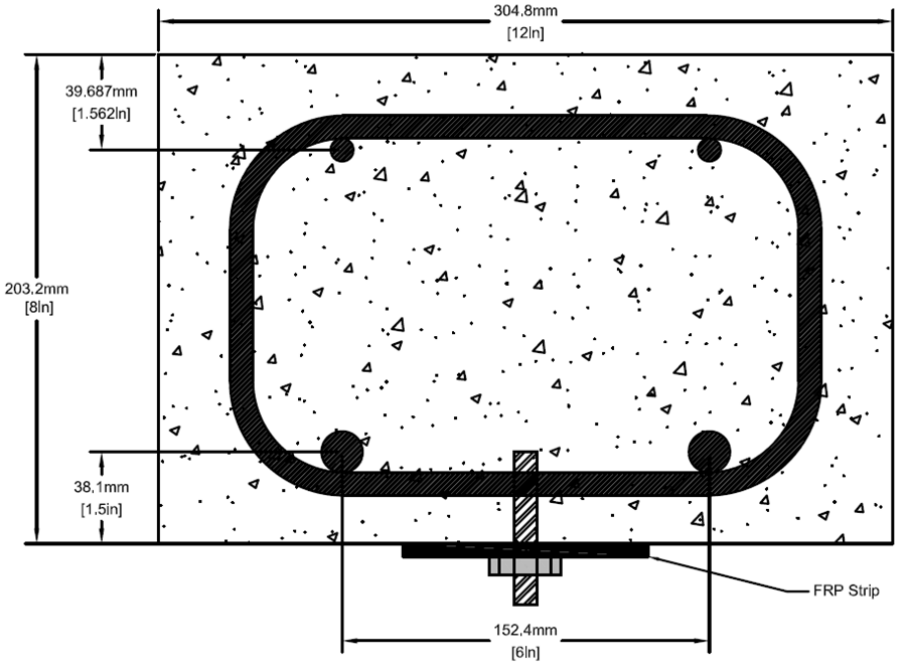

Figure 1: Concept image of FRP retrofit [1]

To improve on the previous design for new construction, the plates could be modified to also serve as stay-in-place formwork. Removable wood or steel formwork is typically used to support concrete structures before they cure and can carry their own weight, see Figure 2. The formwork is removed after the concrete has cured. The construction, placement, and removal of forms are labor-intensive tasks, which makes removable formwork increasingly expensive with the growing cost of labor.

Figure 2: Removable wooden formwork [3]

To reduce the labor cost associated with concrete formwork, stay-in-place formwork can be used. Stay-in-place formwork made of steel has been used in construction but it has several shortcomings that limit its usefulness. One shortcoming is that water can become trapped between the concrete and the formwork, which can cause the formwork to rust. As with steel rebar, steel stay-in-place formwork has a significant weight that must be factored into design. Some owners are also hesitant to use stay-in-place formwork since it prevents visual inspection of the concrete. Steel stay-in-place formwork often has a corrugated shape, shown in Figure 3, with each corrugation running the length of the span of the concrete structure. The corrugations increase the bending stiffness of the formwork so that it can support the weight of the wet concrete before it cures without experiencing large deformations.

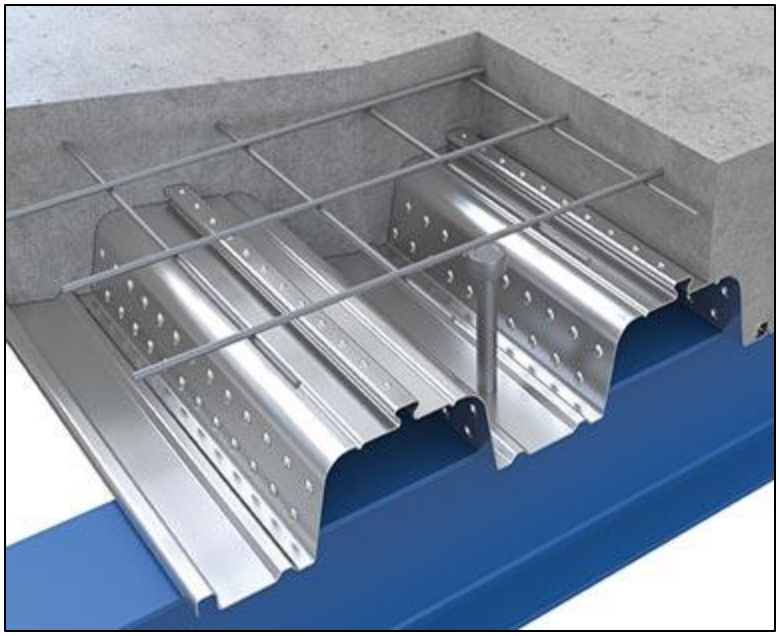

Figure 3: Corrugated steel stay-in-place formwork and shear stud [4]

To have the CFRTP panels also serve as the tension reinforcement for the reinforced concrete structure, a shear connection is needed to connect the CFRTP panel and the concrete mechanically. In conventional construction, this is typically done with welded shear studs. Several types of common shear connectors are discussed by Muhit [5] including shear studs, perfobond ribs, and channel connectors.

This process of transferring shear to another material with a shear connector has been used often in steel girder bridge construction. In this process, the concrete deck was made composite with the girders to increase flexural capacity. As the steel girder and concrete deck deform under load, the shear connectors prevent the relative slip at the steel-concrete interface, which engages the concrete in compression and steel in tension. This greatly increases the flexural stiffness and strength of the system compared to the independent parts.

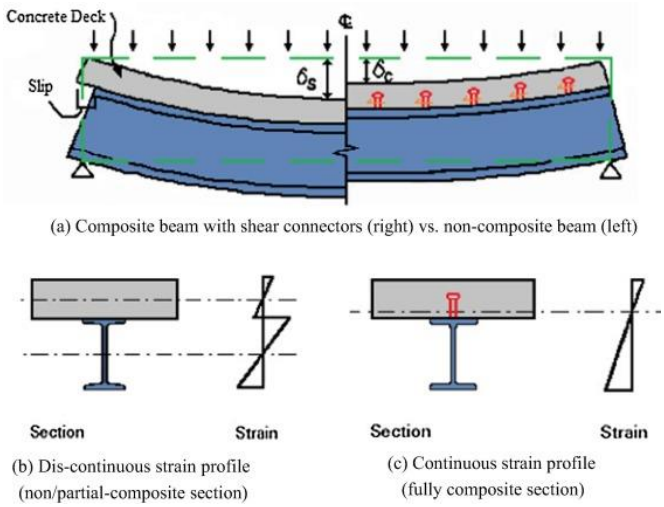

Figure 4: Effect of shear studs on the strain profile of a beam [6]

A study was performed by Seigars [7] at the beginning of this project to determine which thermoplastic materials would be appropriate for this research. From this study, two materials were chosen: Elium and polyethylene terephthalate glycol (PETg).

Elium is an acrylic two-part liquid thermoplastic resin system produced by Arkema. Elium composites are made through a vacuum infusion process similar to what is use to make more conventional thermoset composite. In this process, the liquid parts of the resin are forced through a set of fiber by a vacuum as the polymerization reaction occurs, creating a solid fiber-reinforced thermoplastic part.

PETg is an engineering grade thermoplastic resin, which was available as E-glass reinforced, pre-impregnated (prepreg) unidirectional (UD) tapes from PolyOne. PETg composites are manufactured through a process called stamp forming, where layers of prepreg UD tapes are fused into a solid laminate through heated consolidation.

Seigars [7] used these two materials to design and test two thermoplastic shear connection systems similar to conventional steel shear studs. The first system was an infused, Elium shear stud, shown

in Figure 5. Though these were very strong, the process for manufacturing them was very time-consuming and expensive, and this technology is not pursued here.

Figure 5: E-glass/Elium infused shear stud [7]

The second connection system was a friction welded PETg stud, shown in Figure 6. The studs were formed by spinning a rod of PETg rapidly and pressing it into an E-glass/PETg panel. This would create enough friction to melt the thermoplastic at the base of the rod and the top of the panel. When the spinning stopped, the thermoplastic parts would cool and form together to create a solid part. The method for manufacturing these parts was rapid and could be automated on a large scale. Therefore, this shear connection system was evaluated further in this research in the flat panel tests outlined in Chapter 3.

Figure 6: PETg friction welded shear stud [7]

1.2 Thesis Objective

The objective of this research was to develop a system to provide shear transfer between CFRTP reinforcement and concrete. Three approaches were evaluated using different configurations of reinforcement. The first configuration used a flat CFRTP panel, the second, a corrugated CFRTP panel, and the third, a stiffened CFRTP panel. The second and third configurations added stiffness to the panel which would allow the panel to also serve as stay-in-place formwork for the concrete.

1.3 Scope of Research

The goal of evaluating CFRTP panels, including stay-in-place forms, for use as tension reinforcement in reinforced concrete structures was tackled with a combination of design and experimental evaluation. To support design, computational tools were developed to predict panel capacity. The three CFRTP panel configurations explored in this thesis are briefly described below.

Initially, the PETg friction welded shear studs developed by Seigars [7] were tested in a reinforced concrete beam application. For this test, the thermoplastic shear studs are used to mechanically

bond a flat CFRTP panel to concrete so that the CFRTP panel can act as tension reinforcement for the concrete. This concept is shown in Figure 7. The composite beams were then tested in four-point bending to evaluate the effectiveness of the shear studs and the CFRTP reinforcement.

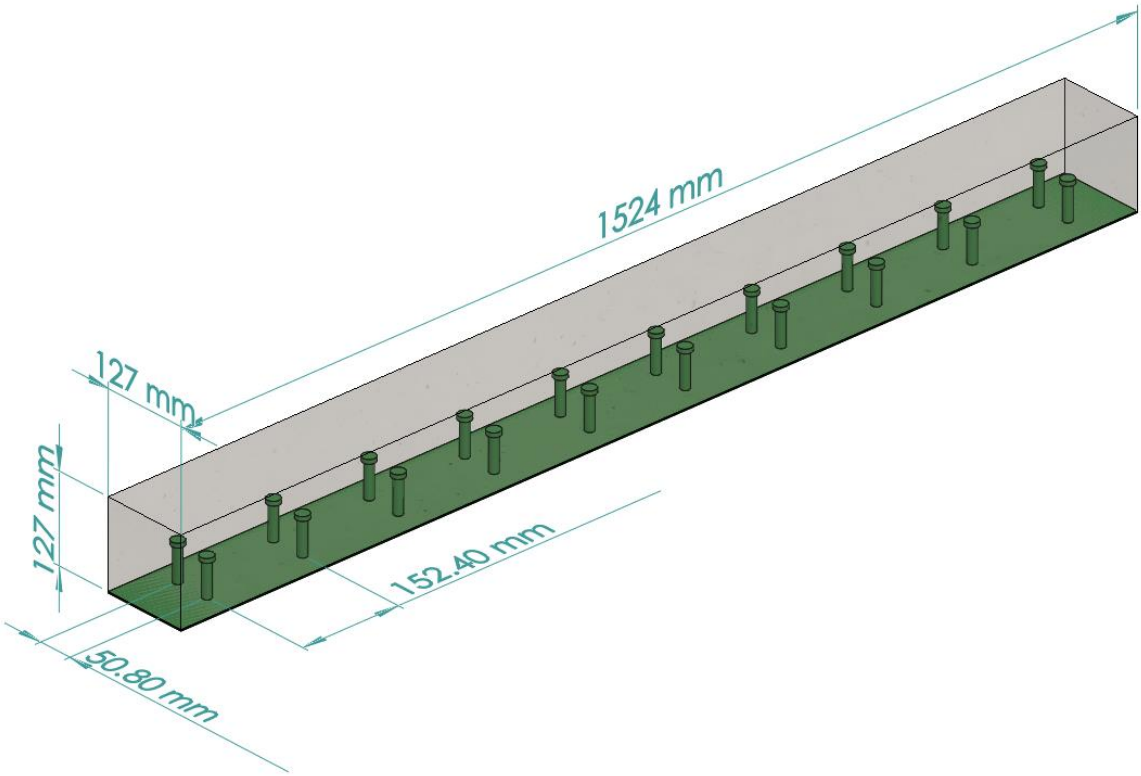

Figure 7: CFRTP reinforced concrete concept with shear studs

Two additional CFRTP configurations were investigated for increasing the flexural stiffness of the CFRTP panels so they can act as stay-in-place formwork. For each method, a new connection system was needed to transfer shear between the CFRTP panel and the concrete.

The first configuration was a corrugated panel similar to the steel formwork shown in Figure 3. To transfer shear between the corrugated CFRTP panel and the concrete, a steel bar was run transversely between the webs of the corrugated panel. The steel bar transferred shear from the concrete to the CFRTP through direct bearing.

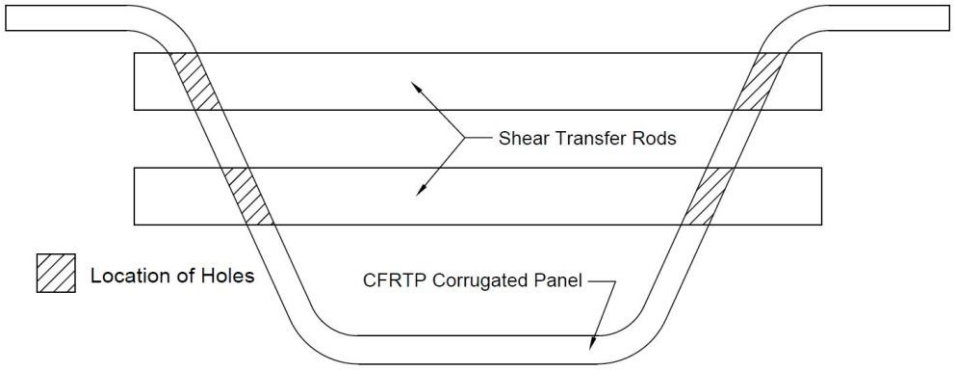

Figure 8: Corrugated panel configuration cross-section

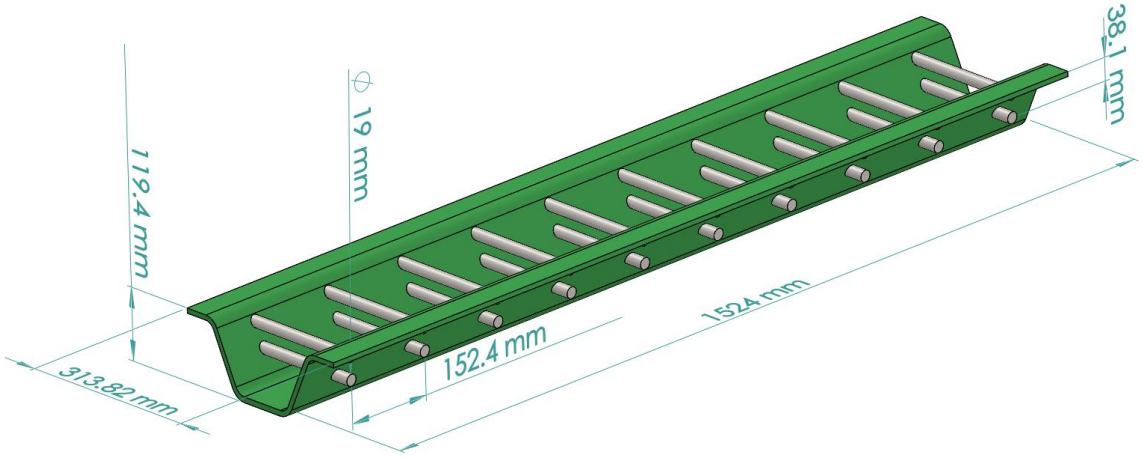

Figure 9: Corrugated panel configuration tentative dimensions

The second configuration was a stiffened panel where vertical stiffeners were bonded to the top of the panel. The vertical stiffeners provided panel stiffness and strength needed to support wet concrete. To transfer shear between the two materials after the concrete cured, holes were cut into the stiffeners to create a connection similar to a perfobond rib shear connector [5]. In this connection, concrete is allowed to flow through the holes in the stiffeners during the concrete pour. This interlocks the concrete and the CFRTP panel together.

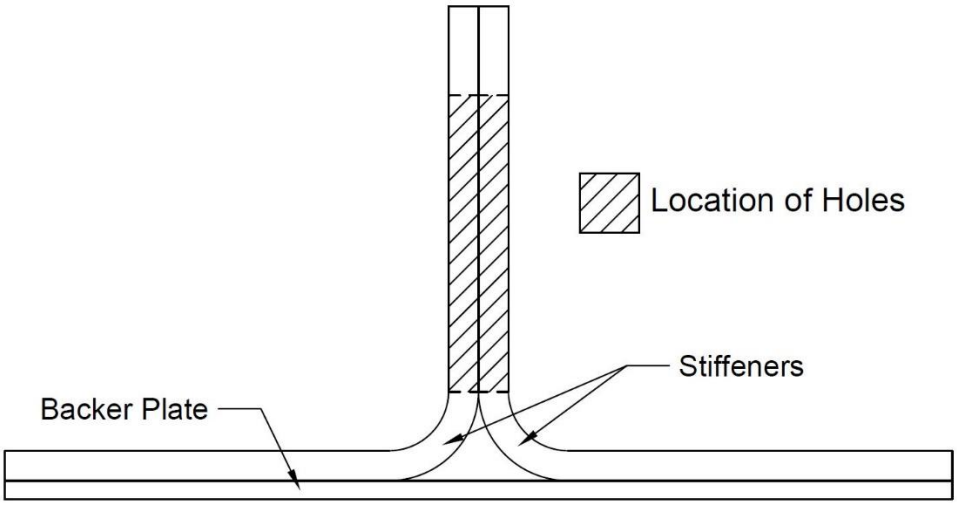

Figure 10: Stiffened panel configuration cross-section

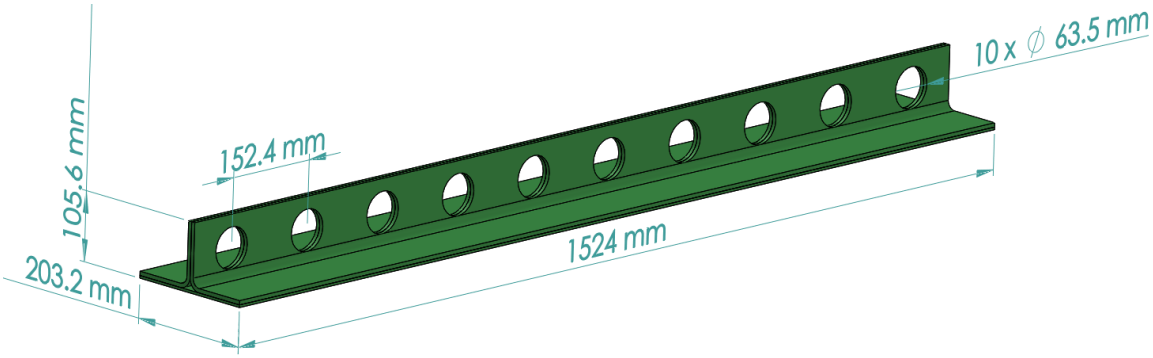

Figure 11: Stiffened panel configuration tentative dimensions

Beams were manufactured and tested for each of the proposed configurations to evaluate their viability as stay-in-place formwork and tension reinforcement.

1.4 Thesis Outline

This thesis contains the five chapters described below in addition to Chapter 1. Supplemental information is included in Appendices and referenced when appropriate.

- Chapter 2: Material Characterization and Analysis discusses the materials that were chosen for this research and the analytical methods that were used to model those materials.

- Chapter 3: Flat Panel Tension Reinforcement Design and Testing covers the design, manufacturing, and testing of the composite flat CFRTP-concrete beams.
- Chapter 4: Corrugated Panel Design and Testing covers the design, manufacturing, and testing of the composite corrugated CFRTP-concrete beams.
- Chapter 5: Stiffened Panel Design and Testing covers the design, manufacturing, and testing of the composite stiffened CFRTP-concrete beams.
- Chapter 6: Conclusions and Recommendations summarizes the essential findings and gives recommendations for the next steps of this research.

CHAPTER 2

MATERIAL CHARACTERIZATION AND ANALYSIS

2.1 Introduction

To design hybrid CFRTP-concrete structural members, the behavior of the individual materials needs to be characterized. This chapter discusses how the strength and stiffness of the materials were evaluated and the basis for CFRTP-concrete member strength and failure predictions.

2.2 Material Characterization

For this research, E-glass reinforced glycolized polyethylene terephthalate (PETg) was chosen for the CFRTP because it has sufficient mechanical properties, given in Table 1, but is still relatively inexpensive. PETg is also an amorphous polymer, which can be formed more easily than crystalline thermoplastics [7]. The E-glass reinforced PETg for this research was manufactured by PolyOne. The material came as unidirectional pre-impregnated tapes that were slit to widths of approximately 50 mm, shown in Figure 12.

Figure 12: E-glass reinforced PETg pre-impregnated tape

Unidirectional stiffness and strength properties developed by Seigars [7] for PETg were utilized here with classical lamination theory to predict the properties of the more complex laminates required for the CFRTP specimens. However, several additional sets of material tests were required to inform design of the test specimens. As a bearing connection was used with the corrugated and stiffened panels, a bearing test was run to determine the approximate bearing strength of the composite. Tests of single laminas to quantify the shrinkage that was observed were also performed. Cylinder tests were also performed on the concrete to assess the compressive strength of the concrete prior to CFRTP member testing.

2.2.1 PETg Unidirectional Properties from Seigars [7]

The strengths and moduli for a unidirectional PETg composite were determined from the material testing done by Seigars [7]. The results of these tests are shown in Table 1.

Table 1: Properties of a E-glass PETg Lamina from Material Testing [7]

Property	Variable	Value	Unit
Fiber Volume Fraction	V_f	36.4%	-
Longitudinal Tensile Strength	F_{1t}	623.0	MPa
Transverse Tensile Strength	F_{2t}	14.5	MPa
Longitudinal Compressive Strength	F_{1c}	309.9	MPa
Transverse Compressive Strength	F_{2c}	65.0	MPa
Longitudinal Elastic Modulus	E_1	28.2	GPa
Transverse Elastic Modulus	E_2	4.4	GPa
In-Plane Shear Strength	F_6	28.5	MPa
In-Plane Shear Modulus	G_{12}	1.5	GPa
In-Plane Poisson's Ratio	ν_{12}	0.353	-

2.2.2 PETg Bearing Capacity

Shear transfer between the CFRTP and the concrete for the corrugated and stiffened panels is accomplished with a bearing connection. To help predict failure at the bearing interface, a bearing test was performed. The web of the corrugated panel and the vertical leg of the stiffened panel both had layups that were approximately half 0° and half 45°, and the layup chosen for the bearing test followed this pattern. It was assumed that the bearing strength would increase proportionally with the thickness of the laminate. For this set of tests, a $[0, 0, \pm 45, \mp 45, 0, 0]$ layup was used.

2.2.2.1 Test Setup

The bearing specimens were tested in tension in a 100-kN Instron test frame using a custom fixture that supported a ¾-inch diameter steel bearing rod. The specimen was placed between two aluminum plates and the bearing rod was run though all three. The specimen was then pulled in tension to create a bearing force between the rod and the CFRTP specimen. A model of the setup is shown in Figure 13. The dimensions of the test specimen and the fixture were chosen to force a bearing failure in the specimen.

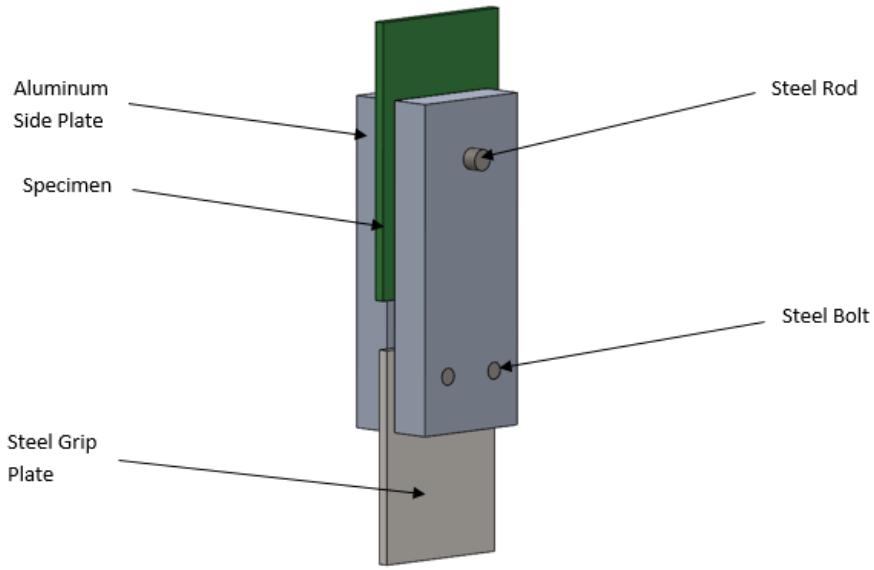

Figure 13: Bearing test fixture

2.2.2.2 Discussion of Results

Eight identical bearing specimens were tested in tension loading. Each specimen failed in the expected mode of bearing. The load-deformation plot for each specimen is shown in Figure 14 and a summary of the peak bearing stress carried by each plate, calculated as the peak bearing load divided by the thickness of the laminate and the diameter of the hole, is given in Table 2. The corrugated and stiffened panels were designed with an approximate bearing capacity of $124.8\ MPa$. This capacity was calculated from the bearing strength of a thermoset composite previously tested at the ASCC by multiplying it by the ratio of the compressive strength of the two

laminates. The ratio of the laminates' compressive strengths was used because the laminates had different layups and matrix materials. The compressive strength of the laminates was found through testing using ASTM 6641 [8].

$$\sigma_{bTP} = \frac{F_{xcTP}}{F_{xcTS}} \sigma_{bTS} \tag{1}$$

$$\sigma_{bTP} = predicted\ bearing\ strength\ of\ the\ thermoplastic\ laminate$$

$$\sigma_{bTS} = bearing\ strength\ of\ the\ thermoset\ laminate$$

$$F_{xcTP} = compressive\ strength\ of\ the\ thermoplastic\ laminate$$

$$F_{xcTS} = compressive\ strength\ of\ the\ thermoset\ laminate$$

The experimental average strength of 179.7 MPa is 44% higher than the estimated design strength, which indicates that the CFRTP panels connection design is conservative.

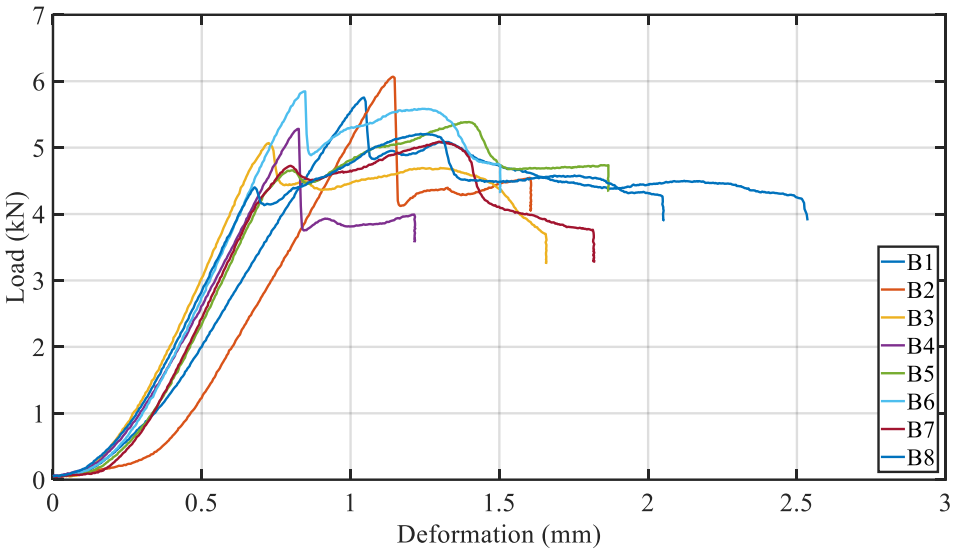

Figure 14: Bearing test load-deformation plot

Table 2: Summary of bearing test results

Specimen	Peak Bearing Stress (MPa)	Deformation at Peak Stress (mm)
1	189.1	1.05
2	199.6	1.14
3	167.0	0.73
4	173.8	0.83
5	177.2	1.40
6	192.7	0.85
7	167.2	1.30
8	171.2	1.23
Average:	179.7	1.06
CoV:	6.9%	21.5%

Figure 15: Failed bearing specimen

2.2.3 Concrete

The concrete chosen for all CFRTP specimens has been previously used for projects at the ASCC. High early strength concrete was used with a design strength of 41.4 MPa. The mix was expected

to reach the design strength within three days. The mix was designed to be self-consolidating and with maximum of 9.55 mm diameter aggregates to ensure flow around the shear connectors. The concrete was prepared and delivered by Sargent Materials of Hermon, Maine.

This technology could potentially be used with conventional concrete mixes as the clear cover and spacing requirements set by the American Association of State Highway and Transportation Officials (AASHTO) [9] for steel shear studs were followed in the design of the specimens. These requirements are discussed further in Section 3.2.2.

2.2.3.1 Cylinder Testing

Two concrete pours were performed, one for the flat panel tests and the other for the corrugated panel tests. Along with the specimen being poured for these tests, 101.6 mm diameter cylinders were poured and tested following ASTM C39 [10]. The results of the cylinder testing can be seen in Figure 16.

The first pour, done for the flat panel beams, behaved as expected. The testing showed that the concrete compressive strength reached the design strength after the third day.

The second pour, done for the corrugated panel beams, did not perform as well. This pour gained strength much more slowly than the previous mixes. After consulting with the manufacturer, Sargent Materials, the cause was determined to be conducting the pour on an abnormally cold day and using a small batch. The concrete lost a significant amount of heat in transport from the manufacturer to the ASCC. The mix was determined acceptable for testing after it reached a 28-day strength of 28.5 MPa.

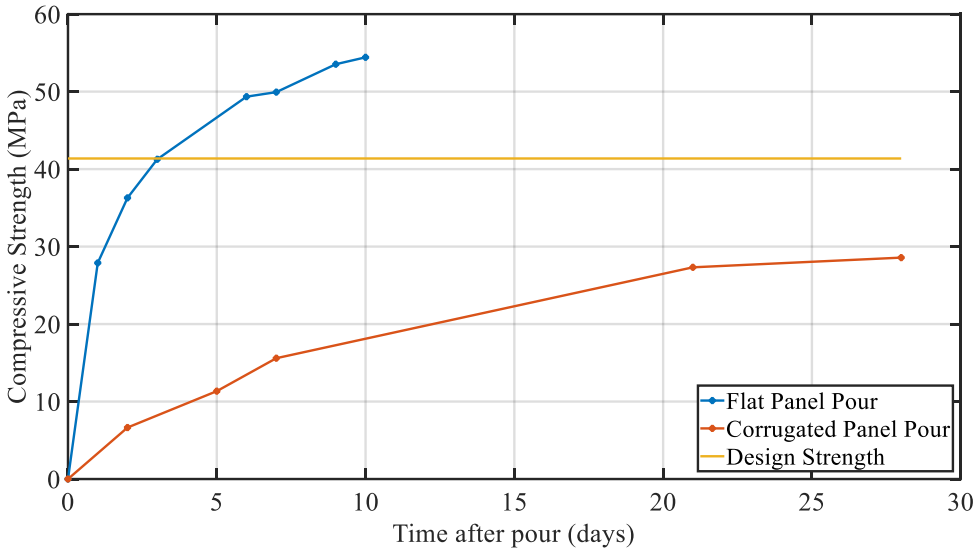

Figure 16: Results of concrete cylinder testing

2.2.3.2 Mold Release Test

As the flat panel tests were designed to test the capacity of the shear studs, any extra composite action developed by a chemical bond between the concrete and the CFTRP panels could skew the results. To counteract this chemical bond, a mold release agent was applied to CFRTP panels before pouring concrete. To verify that the mold release agent would prevent this bond, four 127-mm cubes of concrete were cast with a CFRTP panel on one face. Two of the specimens had the mold release agent while the other two did not. After the concrete cured, the all of the CFRTP panels could be removed by hand, though the specimens with the mold release agent were significantly easier to remove. One of the test specimens is shown in Figure 17. From the results of this test, the mold release agent was applied to all future tests where concrete would contact CFRTP panels.

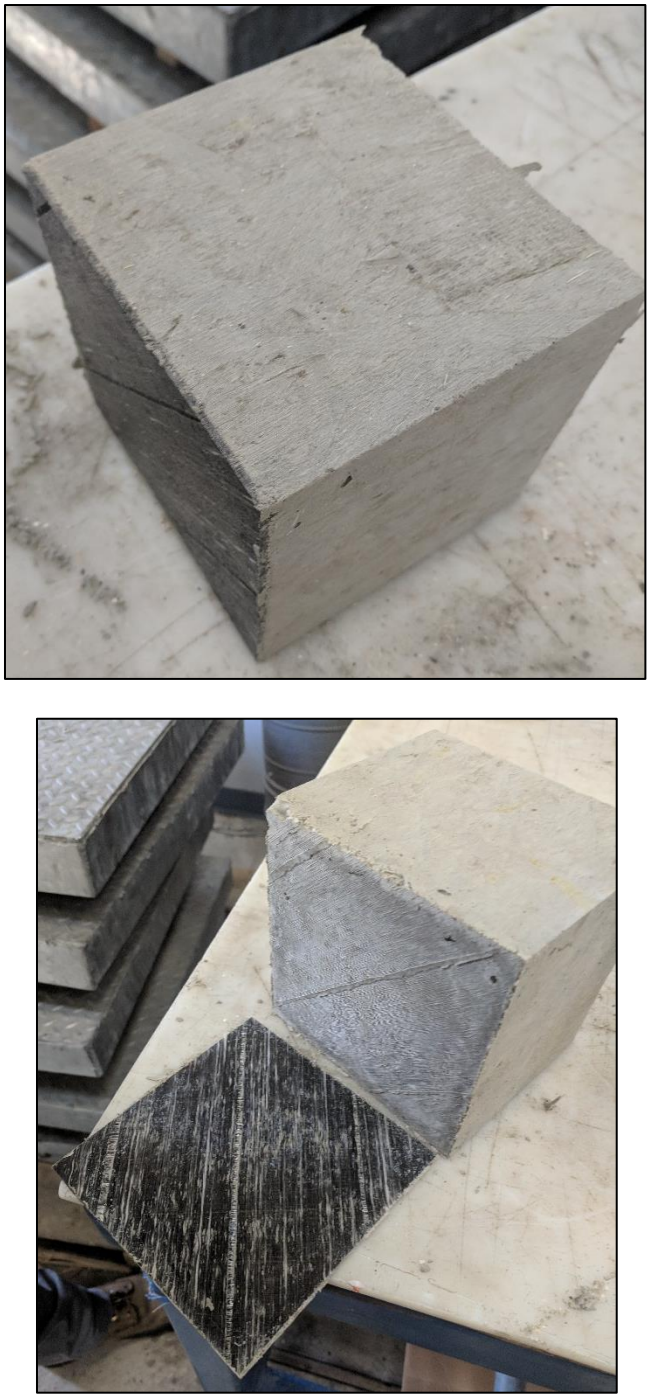

Figure 17: Test of mold release before (left) and after (right) breaking the bond

2.3 Analytical Material Characterization

In this research, two relatively complex materials are being used: CFRTP and concrete. Constitutive relationships and failure criteria for each material required for design of the hybrid CFRTP-concrete structural elements as detailed in Chapters 4-6 are detailed here.

2.3.1 Classical Lamination Theory

CLT is a method of approximating the representative moduli and strengths of a composite laminate. The following sections summarize the theory used to analyze the composite laminates. The equations were taken from Barbero [11].

In this section, the coordinate systems are referred to as follows. Local coordinates are the lamina coordinate system, which is unique to each lamina in a laminate. The local coordinates are shown as the 1 and 2 directions in Figure 18 with the 1 direction defined as the longitudinal (fiber) direction of the lamina, the 2 direction is orthogonal to 1 and in the plane of the lamina, and the 3 direction is normal to the surface of the lamina. Global coordinates are used by the entire structure, represented by x, y, and z in Figure 18. For this section, the x direction was defined as direction along the span of the proposed beam. The y and z directions are perpendicular to the x-axis in the horizontal and vertical directions respectively.

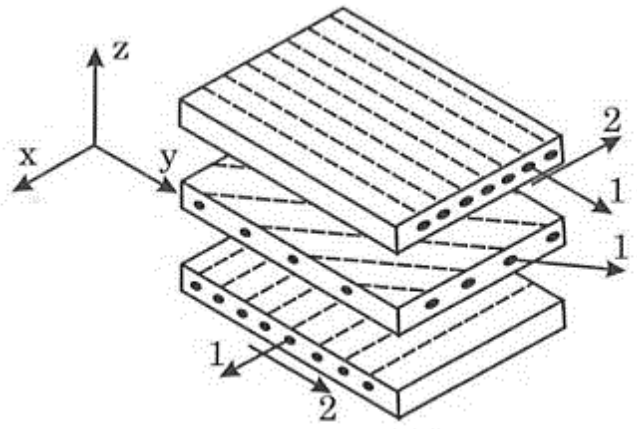

Figure 18: Coordinate systems for lamina and laminates [11]

2.3.1.1 Lamina Stiffness and Compliance Matrices

For each lamina, matrices were constructed to model the performance of the lamina. Reduced stiffness and compliance matrices, [Q] and [S] respectively, were constructed using the lamina moduli. These matrices model the constitutive relationship between the stresses and strains in lamina coordinates, as shown in Equations 2 and 3. [Q] converts the local strains into local stresses. [S] is the inverse of [Q] and thus converts local stresses into local strains.

$$\begin{Bmatrix}\sigma_1\\ \sigma_2\\ \sigma_6\end{Bmatrix} = [Q]\begin{Bmatrix}\varepsilon_1\\ \varepsilon_2\\ \gamma_6\end{Bmatrix} \tag{2}$$

$$\begin{Bmatrix}\varepsilon_1\\ \varepsilon_2\\ \gamma_6\end{Bmatrix} = [S]\begin{Bmatrix}\sigma_1\\ \sigma_2\\ \sigma_6\end{Bmatrix} \tag{3}$$

Transformation matrices, [T], were then constructed using the orientation of the fibers for each lamina. The transformation matrices relate the stresses or strains in local coordinates to the stresses or strains in global coordinates, as shown in Equation 4.

$$\begin{Bmatrix}\sigma_1\\ \sigma_2\\ \sigma_6\end{Bmatrix} = [T]\begin{Bmatrix}\sigma_x\\ \sigma_x\\ \sigma_{xy}\end{Bmatrix} \tag{4}$$

The [Q] and [S] matrices were then transformed into global coordinates, resulting in the transformed reduced stiffness and transformed compliance matrices, $[\overline{Q}]$ and $[\overline{S}]$ respectively. This transformation is shown in Equation 5. The transformed reduced stiffness matrix converts global strains to global stresses, as shown in Equation 6.

$$\left[\overline{Q}\right] = [T]^{-1}[Q][T]^{-T} \tag{5}$$

$$\begin{Bmatrix}\sigma_x\\ \sigma_y\\ \sigma_{xy}\end{Bmatrix} = \left[\overline{Q}\right]\begin{Bmatrix}\varepsilon_x\\ \varepsilon_y\\ \gamma_{xy}\end{Bmatrix} \tag{6}$$

2.3.1.2 Laminate Stiffness and Compliance Matrices

To begin modeling an entire laminate, several more stiffness and compliance matrices were constructed. The in-plane stiffness matrix, [A], was created to relate in-plane strains to in-plane forces. The bending stiffness matrix, [D], was created to relate curvatures to bending moments. The bending-extension coupling matrix, [B], was created to account for relationships between in-plane strains and moments and between curvatures and in-plane forces that would not be present in homogeneous materials. [A], [B], and [D] each depend on [Q] and the thickness of each lamina as well as the distance of each lamina from the center of the composite. Each of these matrices was inverted to obtain the respective stiffness matrices, [α], [β], and [δ] respectively.

$$\begin{Bmatrix}N_x\\ N_y\\ N_{xy}\\ M_x\\ M_y\\ M_{xy}\end{Bmatrix} = \begin{bmatrix}A_{11} & A_{12} & A_{16} & B_{11} & B_{12} & B_{16}\\ A_{12} & A_{22} & A_{26} & B_{12} & B_{22} & B_{26}\\ A_{16} & A_{26} & A_{66} & B_{16} & B_{26} & B_{66}\\ B_{11} & B_{12} & B_{16} & D_{11} & D_{12} & D_{16}\\ B_{12} & B_{22} & B_{26} & D_{12} & D_{22} & D_{26}\\ B_{16} & B_{26} & B_{66} & D_{16} & D_{26} & D_{66}\end{bmatrix}\begin{Bmatrix}\varepsilon_x^0\\ \varepsilon_y^0\\ \gamma_{xy}^0\\ \kappa_x\\ \kappa_y\\ \kappa_{xy}\end{Bmatrix} \tag{7}$$

$$A_{ij} = \sum_{k=1}^{N} \left(\bar{Q}_{ij}\right)_k t_k \,; i,j = 1,2,6 \tag{8}$$

$$B_{ij} = \sum_{k=1}^{N} \left(\bar{Q}_{ij}\right)_k t_k \, \bar{z}_k; i,j = 1,2,6 \tag{9}$$

$$D_{ij} = \sum_{k=1}^{N} \left(\bar{Q}_{ij}\right)_k (t_k \bar{z}_k^2 + \frac{t_k^3}{12}) \,; i,j = 1,2,6 \tag{10}$$

$N = number\ of\ lamina\ in\ the\ laminate$

$t_k = thickness\ of\ the\ k^{th}\ lamina$

$\bar{z}_k = distance\ from\ the\ bottom\ of\ the\ laminate$

$to\ the\ center\ of\ the\ k^{th}\ lamina$

2.3.1.3 Representative Laminate Moduli

Representative moduli were computed from laminate compliance matrices. The longitudinal elastic modulus, E_x, transverse elastic modulus, E_y, in-plane shear modulus, G_{xy}, and Poisson's ratio, ν_{xy}, are found this way. These moduli found were applicable for in-plane loads.

$$E_x = \frac{1}{t * \alpha_{11}} \tag{11}$$

$$E_y = \frac{1}{t * \alpha_{22}} \tag{12}$$

$$G_{xy} = \frac{1}{t * \alpha_{66}} \tag{13}$$

$$\nu_{xy} = -\frac{\alpha_{12}}{\alpha_{11}} \tag{14}$$

When the laminates were expected to be in flexure, different equations were needed for the elastic moduli.

$$E_x^b = \frac{12}{t^3 * \delta_{11}} \quad (15)$$

$$E_y^b = \frac{12}{t^3 * \delta_{22}} \quad (16)$$

$$G_{xy}^b = \frac{12}{t^3 * \delta_{66}} \quad (17)$$

$$\nu_{xy}^b = -\frac{\delta_{12}}{\delta_{11}} \quad (18)$$

2.3.2 Composites Failure Criteria

To predict the failure of the CFRTP panels in the hybrid CFRTP-concrete beams, a set of failure criteria needed to be adopted. Three sets of composites failure criteria for unidirectional composites were potentially applicable to this research. The three were the Hashin failure theory [12], Tsai-Wu failure theory [13], and maximum strain failure theory [11].

Each theory requires knowledge of the strength of a unidirectional laminate under different types of loading. A summary of the strengths needed for the failure criteria is given in Table 3. The values of these variables were found through material testing which is given in 2.2.1.

Table 3: Summary of variables used by failure theories

Type of Force	**Variable Used**			
	Strength	Modulus	Applied Stress	Applied Strain
Longitudinal Tension	F_{1t}	E_1	$\sigma_1(>0)$	$\varepsilon_1(>0)$
Longitudinal Compression	F_{1c}	E_1	$\sigma_1(<0)$	$\varepsilon_1(<0)$
Transverse Tension	F_{2t}	E_2	$\sigma_2(>0)$ $\sigma_3(>0)$*	$\varepsilon_2(>0)$
Transverse Compression	F_{2c}	E_2	$\sigma_2(<0)$ $\sigma_3(<0)$*	$\varepsilon_2(<0)$
In-Plane Shear	F_6	G_{12}	σ_{12}	γ_6
Out-of-Plane Shear	F_4	-	σ_{13}* σ_{23}*	-

*** Considered negligible for all calculations**

2.3.2.1 Hashin Failure Theory

The Hashin failure criteria for unidirectional fiber composites allows for a three-dimensional stress state. This failure theory is based on the two primary failure modes of unidirectional fiber composites: a fiber mode and a matrix mode. The fiber failure mode can be caused by fiber rupture while in tension or fiber buckling while in compression. The matrix failure mode can be caused by a planar crack forming in the matrix material parallel to the fiber direction. The Hashin failure criteria are given as four independent quadratic stress polynomials [12].

- Fiber tension ($\sigma_1 > 0$)

$$F_1(\sigma) = \left(\frac{\sigma_1}{F_{1t}}\right)^2 + \frac{1}{(F_6)^2}(\sigma_{12}^2 + \sigma_{13}^2) = 1 \tag{19}$$

- Fiber compression ($\sigma_{11} < 0$)

$$F_2(\sigma) = \frac{-\sigma_1}{F_{1c}} = 1 \tag{20}$$

- Matrix tension ($\sigma_2 + \sigma_3 > 0$)

$$F_3(\sigma) = \frac{1}{(F_{2t})^2}(\sigma_2 + \sigma_3)^2 + \frac{1}{(F_4)^2}(\sigma_{23}^2 - \sigma_2\sigma_3) + \frac{1}{(F_6)^2}(\sigma_{12}^2 + \sigma_{13}^2) = 1 \tag{21}$$

- Matrix compression ($\sigma_2 + \sigma_3 < 0$)

$$\begin{aligned} F_4(\sigma) = \frac{1}{F_{2c}}\left[\left(\frac{F_{2c}}{2F_4}\right)^2 - 1\right](\sigma_2 + \sigma_3) + \frac{1}{4(F_4)^2}(\sigma_2 + \sigma_3)^2 \\ + \frac{1}{(F_4)^2}(\sigma_{23}^2 - \sigma_2\sigma_3) + \frac{1}{(F_6)^2}(\sigma_{12}^2 + \sigma_{13}^2) = 1 \end{aligned} \tag{22}$$

For this research, only plane stresses were considered. This means that $\sigma_3 = \sigma_{13} = \sigma_{23} = 0$, which simplifies the failure criteria to the following.

- Fiber tension ($\sigma_1 > 0$)

$$F_1(\sigma) = \left(\frac{\sigma_1}{F_{1t}}\right)^2 + \left(\frac{\sigma_{12}}{F_6}\right)^2 = 1 \tag{23}$$

- Fiber compression ($\sigma_{11} < 0$)

$$F_2(\sigma) = \frac{-\sigma_1}{F_{1c}} = 1 \tag{24}$$

- Matrix tension ($\sigma_2 + \sigma_3 > 0$)

$$F_3(\sigma) = \left(\frac{\sigma_2}{F_{2t}}\right)^2 + \left(\frac{\sigma_{12}}{F_6}\right)^2 = 1 \tag{25}$$

- Matrix compression ($\sigma_2 + \sigma_3 < 0$)

$$F_4(\sigma) = \frac{\sigma_2}{F_{2c}}\left[\left(\frac{F_{2c}}{2F_4}\right)^2 - 1\right] + \left(\frac{\sigma_2}{2F_4}\right)^2 + \left(\frac{\sigma_{12}}{F_6}\right)^2 = 1 \quad (26)$$

2.3.2.2 Tsai-Wu Failure Theory

The Tsai-Wu failure criteria uses strength tensors to provide a single quadratic failure criterion equation. This method is analogous to a von Mises criterion except that it is applicable to a unidirectional composite lamina. As this failure theory provides just one criterion, the mode of failure of the lamina cannot be determined from this analysis. The reduced version of the criterion was used which assumes a two-dimensional state of stress (i.e. $\sigma_3 = \sigma_{13} = \sigma_{23} = 0$) [13].

$$f_1 = \frac{1}{F_{1t}} - \frac{1}{F_{1c}}$$

$$f_{11} = \frac{1}{F_{1t}F_{1c}}$$

$$f_2 = \frac{1}{F_{2t}} - \frac{1}{F_{2c}}$$

$$f_{22} = \frac{1}{F_{2t}F_{2c}}$$

$$f_{66} = \frac{1}{F_6^2}$$

$$a = f_{11}\sigma_1^2 + f_{22}\sigma_2^2 + f_{66}\sigma_{12}^2 - \sqrt{f_{11}f_{22}}\sigma_1\sigma_2$$

$$b = f_1\sigma_1 + f_2\sigma_2$$

$$F = \frac{-b + \sqrt{b^2 + 4a}}{2a} = 1 \quad (27)$$

2.3.2.3 Maximum Strain Failure Theory

Maximum strain failure theory is the most common failure theory used in industry today. The maximum longitudinal, transverse, and shear strains are compared to the corresponding ultimate strain of a unidirectional lamina. Each ultimate strain was found by dividing the corresponding ultimate stress by the corresponding elastic or shear modulus [11].

- Longitudinal tension

$$F_1 = \frac{\left(\frac{F_{1t}}{E_1}\right)}{\varepsilon_1} = 1 \tag{28}$$

- Transverse tension

$$F_2 = \frac{\left(\frac{F_{2t}}{E_2}\right)}{\varepsilon_2} = 1 \tag{29}$$

- Longitudinal compression

$$F_3 = \frac{\left(\frac{F_{1c}}{E_1}\right)}{\varepsilon_1} = 1 \tag{30}$$

- Transverse compression

$$F_4 = \frac{\left(\frac{F_{2c}}{E_2}\right)}{\varepsilon_2} = 1 \tag{31}$$

- In-Plane Shear

$$F_5 = \frac{\left(\frac{F_6}{G_{12}}\right)}{\gamma_6} = 1 \tag{32}$$

2.3.3 Concrete Constitutive Model

To model the crushing failure of concrete at ultimate loading, the ACI Code [14] allows the use of the Whitney stress block to model the constitutive relationship of concrete. The Whitney stress

block is a simple, rectangular approximation of the true constitutive relationship of concrete that is easy to use, making it ideal for normal reinforced concrete design. However, for the hybrid CFRTP-concrete beams in this project, the more complex and accurate Hognestad model [15], was used to model the constitutive relationship of concrete. The Hognestad model provides equations that approximate the entire stress-strain relationship of concrete. The ascending portion of the curve is modeled by a second-degree polynomial, given in Equation 33, until the compressive stress reaches the concrete's compressive strength, commonly referred to as f_c'. The strain at which the stress in the concrete reaches f_c', called ε_m, can be approximated using Equation 34. After the peak of the curve, the model descends linearly with Equation 35 until failure. The slope of this descent was interpolated from given Z values of 100 with a f'_c of 25 MPa and 250 with a f'_c of 50 MPa. For this research, the design strength of 41.4 MPa would result in a Z value of 200. Failure was assumed to occur at 3000 $\mu\varepsilon$.

$$\sigma = \sigma_m \left[2\frac{\varepsilon}{\varepsilon_m} - \left(\frac{\varepsilon}{\varepsilon_m}\right)^2 \right] \tag{33}$$

$\sigma = stress$

$\sigma_m = concrete\ compressive\ strength, f_c'$

$\varepsilon = strain$

$\varepsilon_m = 0.00165 + 0.0000163\sigma_m$ where σ_m is in MPa (34)

$$\sigma = \sigma_m[1 - Z(\varepsilon - \varepsilon_m)] \tag{35}$$

Concrete is primarily used in compression as it cracks under a relatively small tensile load. For this model, the concrete was assumed behave linear-elastically until reaching the modulus of rupture, after which it is assumed to carry no load. The modulus of rupture was calculated using Equation 36 as defined in ACI-318 [14]. The slope of the linear-elastic behavior prior to rupture was calculated using an approximate modulus of elasticity, found through Equation 37 [15].

$$f_r = -0.62\sqrt{f_c'} \text{ where } f_c' \text{ is in MPa} \quad (36)$$

$$E_c = 4{,}730\sqrt{f_c'} \text{ where } f_c' \text{ is in MPa} \quad (37)$$

The entire concrete constitutive model for the design concrete strength used for this research of 41.4 MPa is shown in Figure 19.

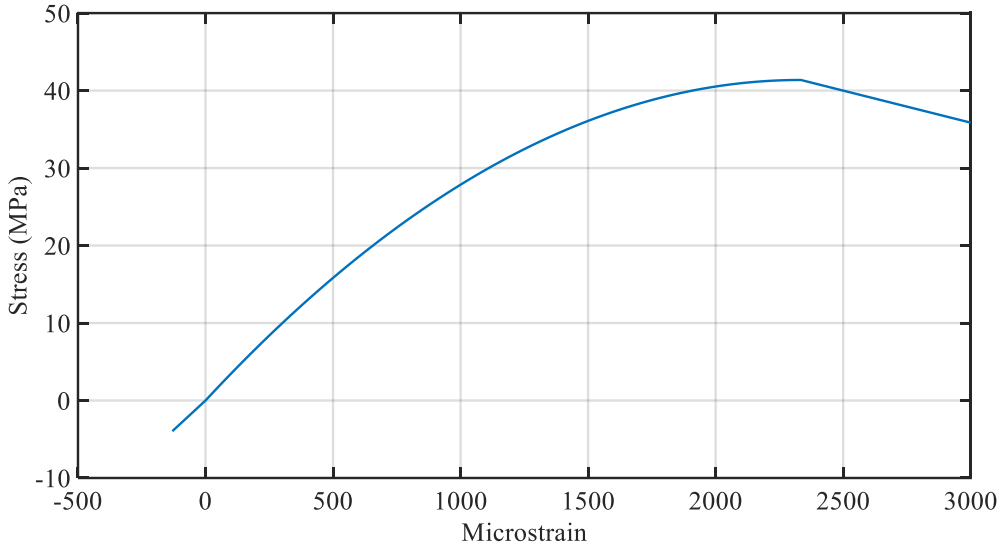

Figure 19: Stress-strain curve for 41.4 MPa concrete using Hognestad constitutive model

2.4 Discussion

Understanding how the concrete and the E-glass reinforced PETg each behaved formed the foundation for designing the composite beams described in the following three chapters. The Hognestad method was used to model the behavior of the concrete where a crushing failure in the concrete is assumed to occur at a strain of 0.003. The E-glass reinforced PETg was assumed to behave linear-elastically until failure. The maximum strain theory was used to design the panels in Chapters 4 and 5 though each was evaluated. The maximum strain theory was chosen because the Tsai-Wu failure theory does not discern the applicable failure mode and the Hashin theory is more suited for scenarios with complex loading.

CHAPTER 3

FLAT PANEL TENSION REINFORCEMENT DESIGN AND TESTING

3.1 Introduction

The first full-scale testing done for this research was on a concrete beam reinforced by a flat CFRTP panel in four-point bending as shown in Figure 20. Shear transfer between the CFRTP panel and the concrete was achieved using PETg shear studs developed by Seigars [7].

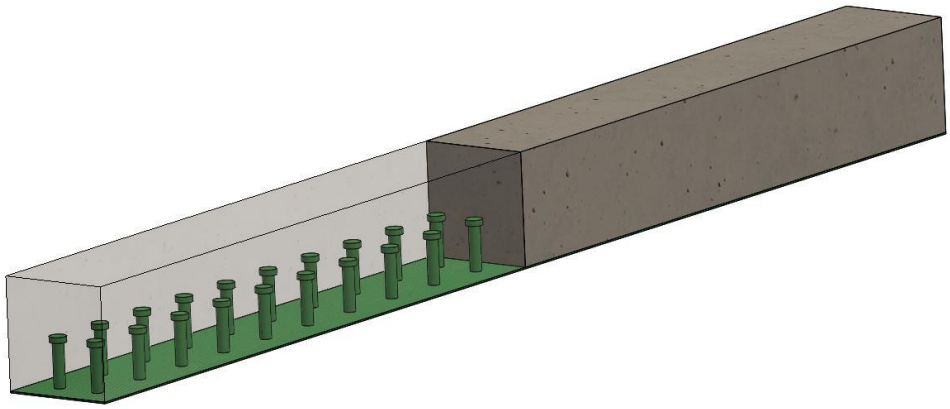

Figure 20: Flat panel beam model with shear studs and concrete

3.2 Design

The length of the flat panel hybrid beam was limited by the size of CFRTP panel that could be produced at the ASCC. The largest panel that could be manufactured was 1580 mm long, which allowed a 1524 mm (60 inch) specimen to be used.

A span to depth ratio of 12 was chosen to reduce the likelihood of shear failure of the beam. This allowed a stud failure to occur without the need for shear reinforcement in the concrete. This led to a beam depth of 127 mm.

The largest diameter stud that can be used with the friction welder developed by Seigars [7], 13 mm was adopted for these specimens.

3.2.1 Strength Design

A MATLAB code was developed that used CLT, discussed in Section 2.3.1 to approximate the strength and stiffness of the flat CFRTP panel. These properties were then used to perform a transformed section analysis on the hybrid beam. In this analysis, a Whitney Stress Block [14] was used to model the concrete at ultimate loads. Force equilibrium was used to locate the neutral axis. The CFRTP panel was designed iteratively, where the fiber architecture of the panel was updated based on output flexural capacities.

The design indicated that two layers of unidirectional fibers would be strong enough in tension for the designed specimens to fail at the shear interface. To provide dimensional stability, layers with fibers running 45° and 90° from the longitudinal fibers were also included. A balanced, symmetric laminate was also desired to avoid any warping in the panels. This lead to using $[\pm 45°, 90°, 0°, 0°, 90°, \mp 45°]$ as the layup for the flat CFRTP panels.

3.2.2 Shear Connection Design

The guidelines in the AASHTO LRFD Bridge Design Specifications [9] for steel shear studs were assumed to apply to thermoplastic shear studs as well. These guidelines were used to determine the minimum spacing and height of studs that could be used in the beam.

The longitudinal center-to-center spacing of the studs was required to be at least six stud diameters but no more than $610\ mm$. To produce the maximum strength of this size beam, the minimum stud spacing was used. For the chosen diameter stud, the minimum longitudinal spacing was calculated to be $76\ mm$. This spacing is conventionally referred to as the pitch of the shear studs. To investigate the effect of varying the pitch on the strength of the studs, half of the specimens were made with the minimum pitch of $76\ mm$ while the other half had double that spacing, $152\ mm$.

The transverse center-to-center spacing of the studs was required to be at least four stud diameters, giving a minimum transverse of $51\ mm$. The required clear distance from the face of the stud to

the edge of the panel was required to be at least $25\ mm$. From these dimensional restraints, the minimum width of the beam was calculated to be $114\ mm$ assuming two studs across the width. To simplify the design, a $127\ mm$ square concrete cross-section was chosen for the beam specimens.

The shear studs were required to penetrate into the concrete at least $51\ mm$ and have at least $51\ mm$ of concrete cover above them. The ratio of the height of the stud to its diameter must be at least four. To meet these requirements, the studs were required to be between 51 and $76\ mm$.

To check the stress in the shear studs when the concrete begins to crush, the shear flow at the interface between the CFRTP panel and the concrete was calculated with the Equation 38 [16]. It must be emphasized that Equation 38 applies for beams made of linearly elastic materials, and therefore was only be applicable near the ends of the beam where moments are small.

$$q = \frac{V * Q}{I} \tag{38}$$

$q = Shear\ flow$

$V = Internal\ shear\ force\ taken\ as\ half\ of\ the\ total\ applied\ load\ in\ four-point\ bending, where\ the\ total\ applied\ load\ is\ that\ required\ to\ produce\ a\ moment\ failure$

$Q = First\ moment\ of\ the\ area\ above\ the\ point\ of\ interest\ taken\ about\ the\ neutral\ axis$

$I = Moment\ of\ inertia$

The maximum shear flow in the beam was used to calculate a force on each stud using Equation 39. This force was compared to the shear strength of the studs gathered during individual stud testing by Seigars [7] of $25.4\ MPa$ multiplied by the cross-sectional area of the studs.

$$F = \frac{q * pitch}{n} \tag{39}$$

$F = Shear\ force\ on\ a\ single\ stud$

$pitch = Longitudinal\ spacing\ between\ studs$

$n = number\ of\ rows\ of\ studs$

The factor of safety for the shear stud connectors failing in shear under the load that would crush the concrete was less than one for both stud spacings so the shear studs were expected to fail first.

3.2.3 Laminate Properties from Seigars [7]

The effective strengths and moduli for a CFRTP laminate with the flat panel layup of $[\pm 45°, 90°, 0°, 0°, 90°, \mp 45°]$ were determined from the material testing done by Seigars [7]. The results of these tests are shown in Table 4 as well as predictions of some of these quantities from first-ply failure based CLT and second-ply failure CLT.

Table 4: Flat CFRTP panel material testing results [7]

	Experimental Results (CoV)	**CLT Results First-Ply Failure**	**CLT Results Second-Ply Failure**
Fiber Volume Fraction, V_f (%)	41.1 (1.6 %)	-	-
Tensile Strength, F_{xt} (MPa)	223 (11.6 %)	39.5	152
Compressive Strength, F_{xc} (MPa)	106 (10.9 %)	133	143
In-Plane Shear Strength, F_{xy} (MPa)	90.8 (13.9 %)	29.5	36.1
Tensile Elastic Modulus, E_{xt} (GPa)	10.9 (8.67 %)	12.1	13.0
Compressive Elastic Modulus, E_{xc} (GPa)	10.7 (9.71 %)	12.1	13.0
In-Plane Shear Elastic Modulus, G_{xy} (GPa)	5.20 (2.79 %)	4.5	5.5
Poisson's Ratio, ν_{xy} (-)	0.32 (3.54 %)	0.338	0.655
Longitudinal Ultimate Tensile Strain, ε_{xt}^{u} (με)	24,200 (8.34 %)	-	-
Longitudinal Ultimate Compressive Strain, ε_{xc}^{u} (με)	11,300 (14.2 %)	-	-
Longitudinal Ultimate In-Plane Shear Strain, ε_{xy}^{u} (με)	20,800 (13.1 %)	-	-
Average Composite Thickness, t (mm)	2.0	-	-

3.3 Manufacturing

Eight $127\ mm$ by $1524\ mm$ panels were manufactured in the ASCC's thermoforming line with the designed layup of $[\pm 45°, 90°, 0°, 0°, 90°, \mp 45°]$. More information on this process is detailed in Appendix A.

Figure 21: Flat CFRTP panel

Next, studs were friction welded onto the beams through the process developed by Seigars [7]. The optimal parameters that were recommended by Seigars and used for this set of testing are shown in Table 5.

Table 5: Friction welding parameters used for flat CFRTP panel testing

Welding Pressure (kPa)	**Forging Pressure (kPa)**	**Welding Time (sec)**	**Spinning Velocity (m/sec)**
50	300	15	10

Each stud was cut to a length of $57\ mm$ prior to installation. This length was chosen because the studs were expected to shrink during the spin welding process and it was found that a stud of this length would minimize the amount of material needed while maintaining the required concrete

penetration of 51 mm after welding. The mobile friction welding tool developed by Seigars [7] is shown in Figure 22. Four of the beams had studs with a pitch of 76 mm, shown in Figure 23, while the other four had a pitch of 152 mm, shown in Figure 24. Each stud had a self-tapping screw and washer drilled into the top of the stud to prevent pullout of the stud from the concrete, shown in Figure 25. The final height of each stud was verified to be between 51 and 76 mm.

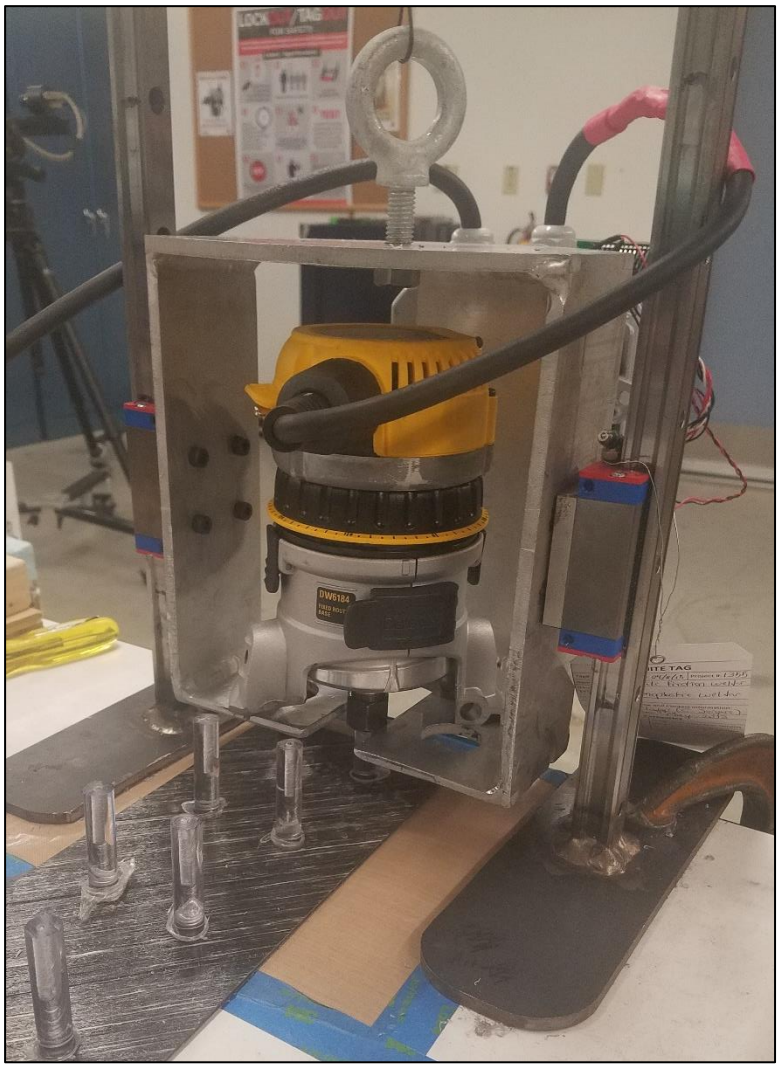

Figure 22: Mobile spin welder developed by Seigars [7]

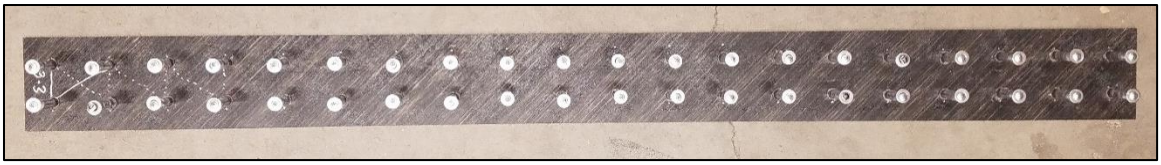

Figure 23: Flat CFRTP panel with shear studs at 76 mm spacing

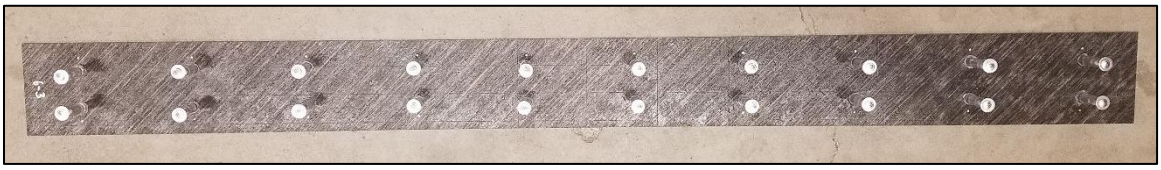

Figure 24: Flat CFRTP panel with shear studs at 152 mm spacing

Figure 25: Spin welded shear studs with pull out resistance

Each of the panels was then put in a set of wooden formwork. The panels and studs were covered in a mold release agent before concrete was poured. The high-early strength concrete mix discussed in Section 2.2.3 was then poured to the top of the molds. Wooden clamps were included to limit any bowing in the sides of the formwork.

Figure 26: Flat CFRTP panels in formwork before (left) and after (right) concrete pour

3.4 Quasi-Static Testing

A four-point bend was chosen for this set of testing because it induces constant moment and no shear in the region between the two load heads and constant shear between each load head and the closest support.

3.4.1 Test Setup

Throughout the analysis, the beam was modelled as a simply supported. To emulate this in the test setup, both supports were allowed to rotate, while only one was allowed to roll.

Between each support and each end of the beam, a 51 by $127\ mm$ piece of neoprene that was $19\ mm$ thick was added to distribute the force applied to the beam by the support. The center of this neoprene was placed directly over the center of each roller and the neoprene was aligned with the end of the beam. The effective span of the beam from center of support to center of support was reduced to $1473\ mm$.

An aluminum spreader beam was attached to an actuator, which applied the load. Two load heads were spaced to divide the effective span of the beam into thirds. For this beam, the two load heads were spaced at $491\ mm$. A $6\ mm$ thick piece of neoprene was put under each load head to distribute the loads and avoid any stress concentrations.

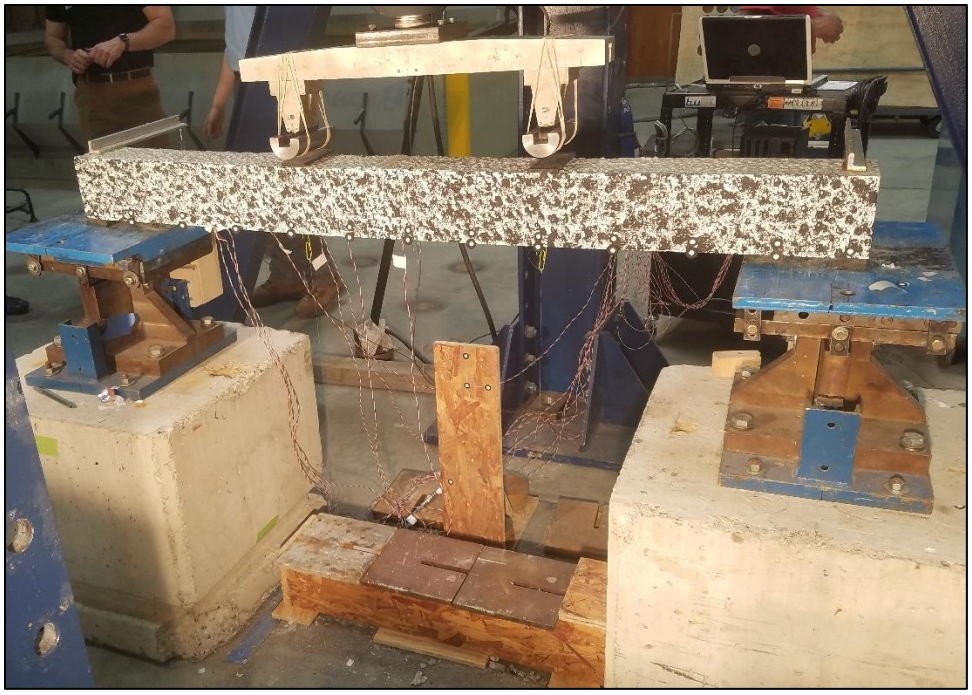

Figure 27: Hybrid flat CFRTP-concrete beam test setup

Eight strain gauges were bonded to the bottom of the flat CFRTP panel. The strain gauges were placed along the bottom of the panel to monitor the strains in the CFRTP to validate the models that were used to design the hybrid beam. The strain gauges were only placed on one half of the beam. It was assumed the strain in the CFRTP panel would be symmetric about the centerline of the span. The spacing of the strain gauges varied with the spacing of the studs. To reduce any influence from stress concentrations from the studs above, the strain gauges were located in the gaps between rows of studs. The location of each strain gauge for the two stud spacings are shown in Figure 28. For both stud spacings, strain gauges 1 through 3 fall between the load heads in the constant moment region of the beam. It was expected that those three gauges would read the same strain as there is the same internal moment at each location. The other five strain gauges were in the constant shear region of the beam and were expected to read linearly decreasing strains the farther from the load head that they were.

Because the shear is transferred between the two materials at discrete points, the locations of the shear studs, the change in strain between strain gauges on either side of the shear studs could be used to calculate the how much force was transferred by each set of studs. For the 152 mm spacing specimens, two strain gauges were placed between each set of studs. Strain gauge 2 (SG2) and SG3 should read a similar strain as there is no stud between them. The same should apply for SG4/SG5 and SG6/SG7. The difference in strain between SG3 and SG4 (as well as SG5/SG6 and SG7/SG8) should correspond to the change in force due to the shear stud. If the studs share the load evenly between each set, the change in strain between those sets should be constant. The same concept also applies to the 76 mm specimens, though there is only one strain gauge between each set of studs.

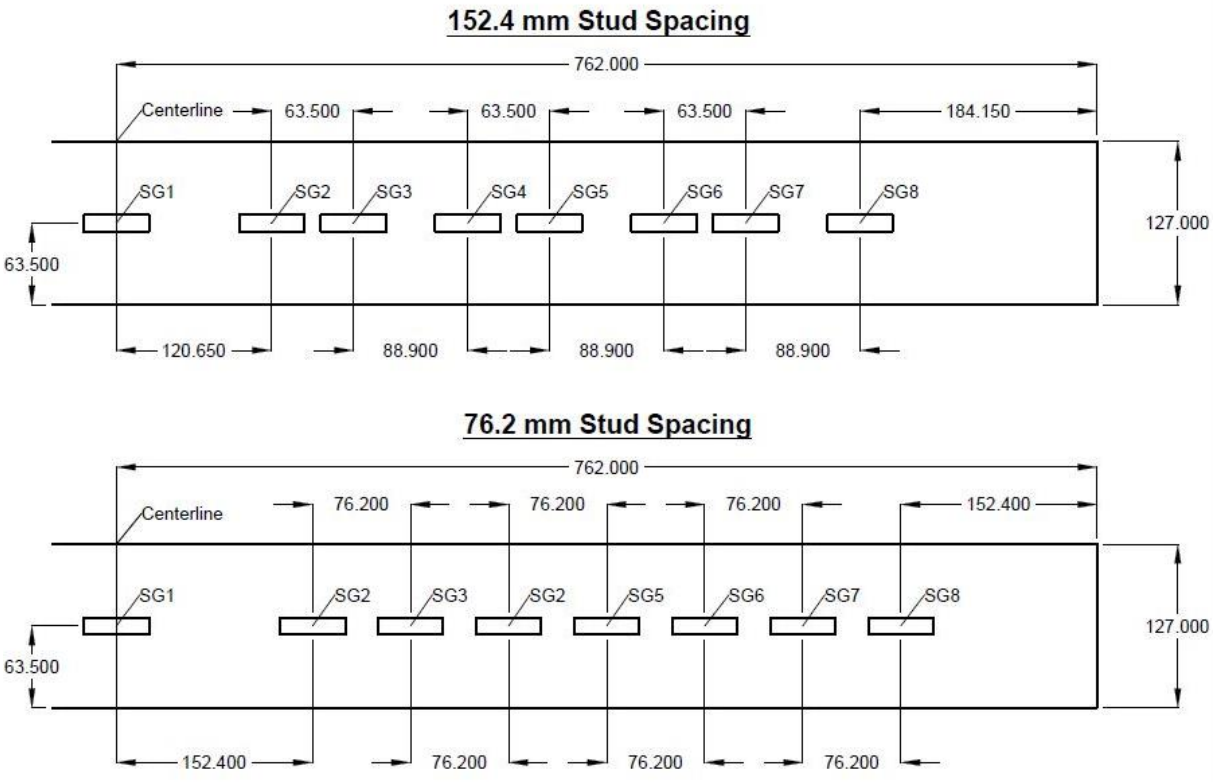

Figure 28: Strain gauge locations (mm)

String potentiometers were attached to the bottom of the CFRTP panel to measure the deflection of beam. One string potentiometer was located at center-span while the other two were located directly under each load head at the third points of the effective span of the beam.

A linear displacement transducer (LDT) was attached to the beam in line with the center of each support. This was used to measure the displacement of the neoprene at the support so that the displacement of the beam from the bending alone can be calculated.

Digital image correlation (DIC) was used to corroborate the other instrumentation. An ARAMIS speckle pattern was applied to one side of each beam to give strain data along the span for the duration of the test. PONTOS dots were applied to the CFRTP panel and the concrete starting at mid-span and extending each direction every $127\ mm$. PONTOS dots were also put on the concrete directly above the support. The side of the CFRTP panel was too small to fit a PONTOS dot on it so a bracket was designed and 3D printed out of polylactic acid (PLA) to mount the dots to the bottom of the CFRTP panel but have them be in line with center of the CFRTP panel. A flat wooden reference panel was also included for each specimen to define the plane for the program to use. The PONTOS dots were used to track, as well as verify displacement data from the string potentiometers and LDTs and calculate relative displacement between the CFRTP panel and concrete. The relative displacement between the CFRTP panel and the concrete can be used to approximate the degree of composite action that is being achieved by the shear studs.

This test was run in displacement control. A load rate of $6\,mm$ per minute was used. The displacement was measured by a displacement transducer inside the testing frame. The load applied by the hydraulic actuator is determined by the displacement transducer to keep the displacement rate constant. The load applied by the hydraulic actuator is measured by a $45\ kN$ load cell attached between the actuator and the spreader beam.

3.4.2 Test Results

Before ultimate failure, tension cracks formed in the constant moment region of each beam. Generally, a crack formed near each load head and around mid-span. The ultimate failure of each beam occurred when the studs in the constant shear region of the beam at one end failed in shear at the CFRTP-concrete interface. This occurred because the highest shear was on the studs in the constant shear region, which would load those studs the most. In theory, each stud in the constant shear region is loaded equally, though this is not necessarily true after the concrete has cracked. Once the studs failed, the concrete beam had no reinforcement to keep the cracks closed and the crack extended to the top of the beam causing collapse of the structure. The peak load applied to each specimen is tabulated in Table 6.

Table 6: Summary of ultimate loads from hybrid flat CFRTP-concrete beams

Ultimate Load (kN)		**Stud Spacing**	
		76 mm	152 mm
Specimen Number	1	12.7	5.98
	2	8.51	5.24
	3	11.8	5.32
	4	11.1	7.74
Average		11.0	6.07
Standard Deviation		1.79	1.16
Coefficient of Variation		16.2%	19.1%

The load vs mid-span deflection data recorded for each specimen are shown in Figure 29 and Figure 30 for the $76\,mm$ stud spacing and the $152\,mm$ stud spacing respectively. The significant drops in load that can be seen at around $5\,kN$ and at several points after that correlate to the formation of cracks in the concrete. The mid-span deflection data comes from the middle string potentiometer with the LDT deflection from the supports taken out. The slope of the initial portion of this curve, before the formation of any cracks is given in Table 7 for each specimen.

For specimens 3-1 and 3-3, the LDTs were mounted to the specimen incorrectly which resulted in a false reading of the compression of the neoprene at the supports. This was fixed for the rest of the specimens. The linear portion from the correct sets of LDT data from specimen 6-2 was used to create a linear load vs displacement model for the neoprene at each support. A line was fit to the LDT data of specimen 6-2 between approximately $2\,kN$ and $4\,kN$. The slope of this line was used as a constitutive model that was then used to model the behavior of the neoprene for every specimen.

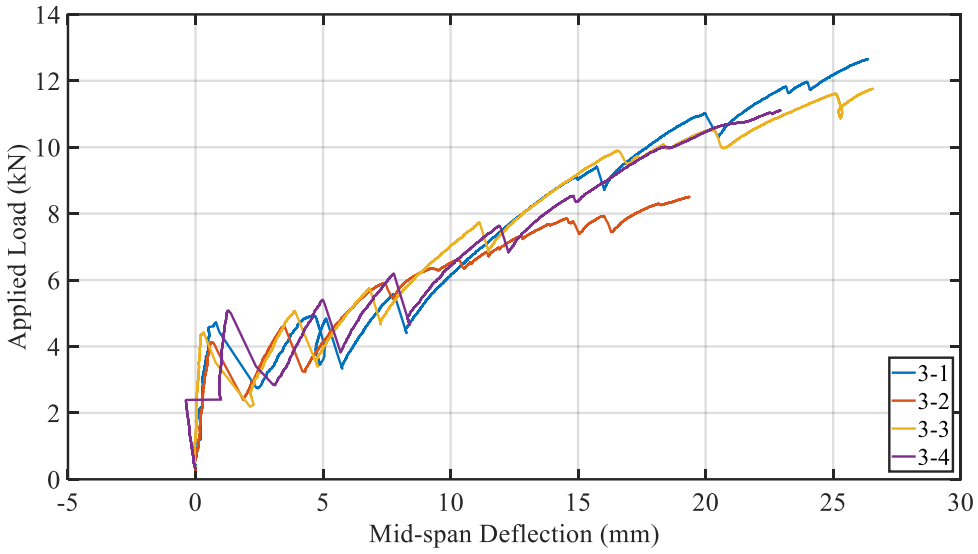

Figure 29: Load vs deflection for 76.2 mm stud spacing

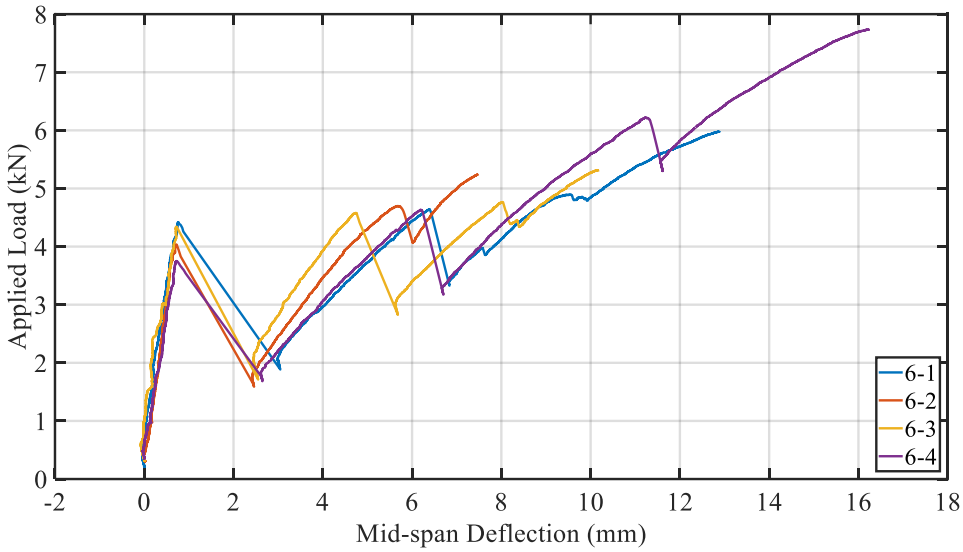

Figure 30 - Load vs deflection for 152.4 mm stud spacing

Table 7: Summary of initial stiffness from hybrid flat CFRTP-concrete beams

Initial Stiffness (kN/mm)		**Stud Spacing**	
		76 mm	152 mm
Specimen Number	1	8.44	5.86
	2	7.74	6.18
	3	20.33	6.10
	4	4.07	5.33
Average		10.14	5.87
Standard Deviation		6.11	0.33
Coefficient of Variation		60%	6%

The load vs mid-span strain data recorded for each specimen is shown in Figure 31 and Figure 32 for the 76.2 *mm* stud spacing and the 152.4 *mm* stud spacing respectively. Several strain gauges broke off specimen 3-3 during testing so that data has not been reported.

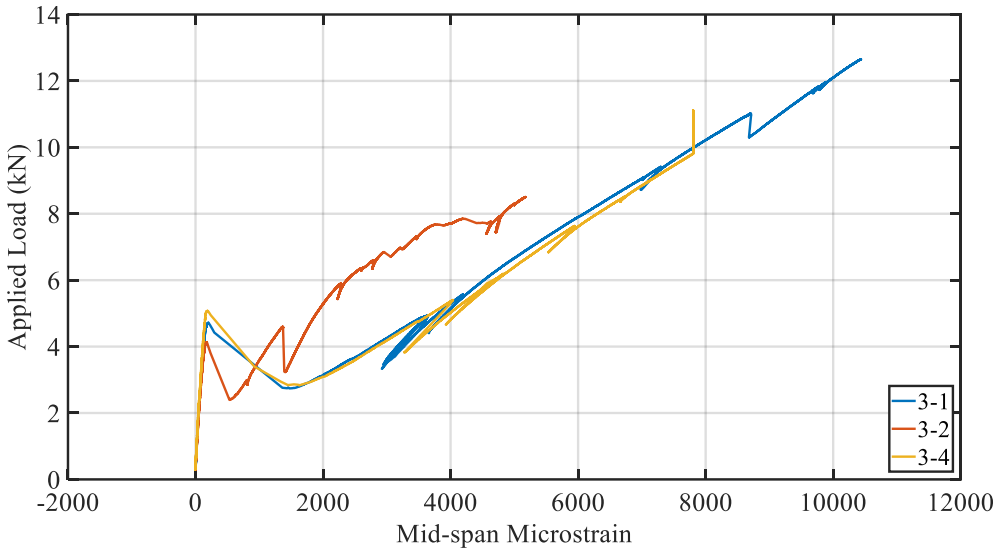

Figure 31 - Load vs strain for 76.2 mm stud spacing

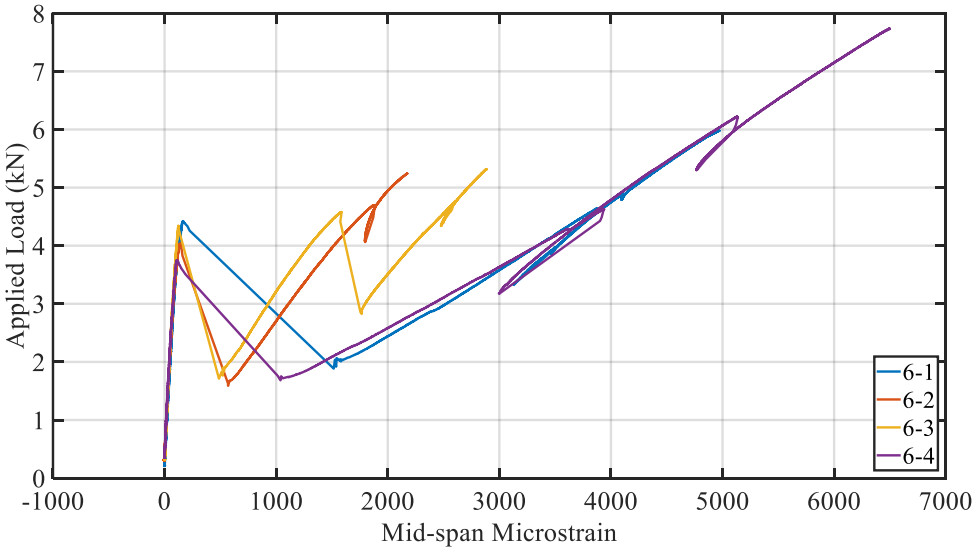

Figure 32 - Load vs strain for 152.4 mm stud spacing

The failure strain data recorded for each specimen is shown in Figure 33 and Figure 34 for the 76.2 mm stud spacing and the 152.4 *mm* stud spacing respectively and tabulated in Table 8. As with

Figure 31, strain gauges 1-3 on specimen 3-3 were not reported because they failed during the test. As was expected, the shape of the plot mostly follows the shape of the moment diagram for the beam. The strain is constant and at a maximum between the two load heads and decreases nearly linearly in the outside third of the span. The only deviation was for specimens 3-2, 6-2, and 6-3, where the strain at midspan dropped uncharacteristically. The cause of this drop in strain is unknown.

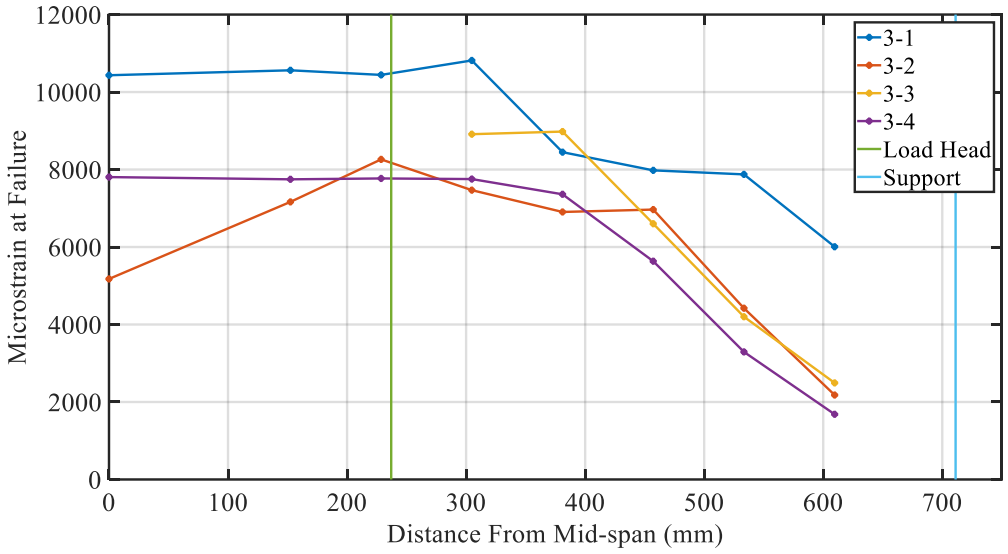

Figure 33 - Failure strain for 76 mm stud spacing

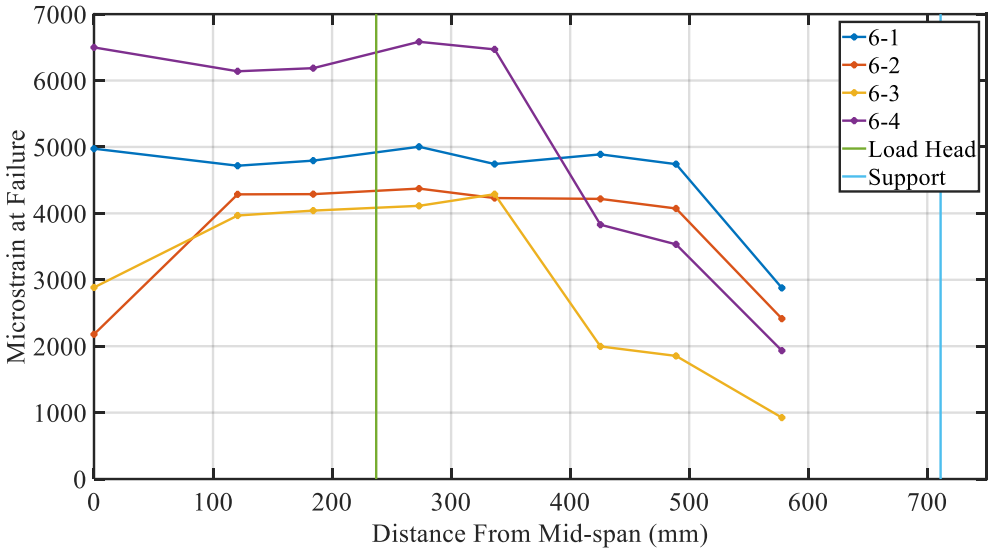

Figure 34 - Failure strains for 152 mm stud spacing

Table 8: Summary of failure microstrain data

Specimen	SG1	SG2	SG3	SG4	SG5	SG6	SG7	SG8
3-1	10434	10561	10443	10815	8448	7979	7875	6007
3-2	5176	7165	8262	7468	6905	6967	4421	2180
3-3	-	-	-	8912	8980	6601	4201	2492
3-4	7805	7748	7770	7754	7361	5633	3293	1682
3-Ave	7805	8491	8825	8737	7924	6795	4948	3090
6-1	4974	4717	4794	5003	4743	4889	4741	2878
6-2	2179	4286	4290	4373	4231	4218	4074	2415
6-3	2885	3968	4042	4113	4289	1997	1854	925
6-4	6499	6139	6186	6584	6469	3830	3533	1933
6-Ave	4134	4778	4828	5018	4933	3734	3551	2038

In the constant shear region, the drop in strain between gauges around a shear was expected to be constant if the studs were evenly sharing the shear load. The drop in strain for each of these instances is given in Table 9 and Table 10 for the $76\ mm$ and $152\ mm$ stud spacing respectively. The high coefficient of variations suggest that the shear was not being shared well between the studs causing some to be loaded more than others. It appears that more load was carried by the studs closer to the end of the beam as the strain differences there are generally higher than the strain differences closer to the load head.

Table 9: 76 *mm* spacing microstrain differences around studs

Specimen	SG4/SG5	SG5/SG6	SG6/SG7	SG7/SG8	CoV
3-1	2367	469	104	1868	78%
3-2	563	62	2546	2241	78%
3-3	68	2379	2400	1709	58%
3-4	393	1728	2340	1611	47%
3-Ave	848	1160	1848	1857	31%

Table 10: 152 *mm* spacing microstrain differences around studs

Specimen	SG5/SG6	SG7/SG8	CoV
6-1	146	1863	85%
6-2	13	1659	98%
6-3	2292	929	42%
6-4	2639	1600	25%
6-Ave	1273	1513	9%

In the 152 mm spacing specimens, where two strain gauges were fit between each set of studs, there was expected to be no difference between these strains. The data shown in Table 11 supports this, as the average difference between the studs was about 10% of the average difference around a stud.

Table 11: 152 mm spacing microstrain differences between studs

Specimen	SG2/SG3	SG4/SG5	SG6/SG7
6-1	77	260	148
6-2	4	142	144
6-3	74	176	143
6-4	47	115	297
6-Ave	51	173	183

Using the strain differences between studs given in Table 9 and Table 10, the approximate shear stress on each set of studs was calculated. To do this, each difference in strain was assumed uniform over the entire panel. The difference in stress in the panel was then calculated by multiplying the difference in strain by the elastic modulus of the CFRTP panel of 12.1 GPa, which was calculated using CLT as described in Section 2.3.1. The difference in stress was the multiplied by the cross-sectional area of the panel to get the change in force carried between both sides of each set of studs. The stress on each set of studs was then found by dividing that change in force by the combined cross-sectional area of the two studs. The resulting stresses are given in Table 12 and Table 13. The average stud stress was 13.8 MPa for the 76 mm specimens and 13.5 MPa for the 152 mm specimens.

Table 12: 76 mm spacing stress between each set of studs (MPa)

Specimen	SG4/SG5	SG5/SG6	SG6/SG7	SG7/SG8	CoV
3-1	22.9	4.5	1.0	18.1	78%
3-2	5.5	0.6	24.6	21.7	78%
3-3	0.7	23.0	23.2	16.5	58%
3-4	3.8	16.7	22.7	15.6	47%

Table 13: 152 mm spacing stress between each set of studs (MPa)

Specimen	SG5/SG6	SG7/SG8	CoV
6-1	1.4	18.0	85%
6-2	0.1	16.1	98%
6-3	22.2	9.0	42%
6-4	25.5	15.5	25%

The displacement data gathered from the string potentiometers is summarized in Table 14. This data includes the linear model created to account for the neoprene displacement at the supports.

Table 14 - Summary of Failure Displacement Data

Displacement at Failure (mm)		**Location**		
Stud Spacing	Specimen	Left Load Head	Mid-span	Right Load Head
76 mm	1	-22.4	-26.4	-24.8
	2	-19.9	-19.4	-17.8
	3	-25.7	-26.6	-23.5
	4	-20.6	-22.9	-18.7
	Average	-22.2	-23.8	-21.2
152 mm	1	-9.80	-12.9	-12.4
	2	-5.02	-7.48	-9.02
	3	-9.99	-10.2	-9.37
	4	-15.2	-16.3	-14.5
	Average	-10.0	-11.7	-11.3

3.4.3 Discussion

The average shear stress in the shear studs at failure was calculated to be 13.8 MPa and 13.5 MPa respectively for the 76 mm and 152 mm pitches from the strain data gathered along the CFRTP panel. These average shear stresses were about 54% of the 25.4 MPa shear strength (coefficient of variation of 1.3%) found by Seigars [7]. All but two of the specimens (6-1 and 6-2) showed at least one set of studs was experiencing a shear stress within 20% of the reported strength, while many

were much lower. For specimens 6-1 and 6-2, the first stud to fail was most likely one that did not have strain gauges around it. There appeared to be very little load sharing between the studs compared to the ductility that steel studs achieve when they begin to yield, as is shown by the coefficient of variations given in Table 12 and Table 13.

Once a stud breaks, the other studs on that end of the beam would have to pick up that load until all of the studs on that side are broken. In the tested specimens, this phenomenon lead to many studs failing in rapid succession causing a sudden ultimate failure of the structure. Because of the poor load sharing observed in the PETg studs and the brittle nature of the structure, the shear studs were abandoned for the remainder of this research in favor of a mechanical bearing connection.

CHAPTER 4

CORRUGATED PANEL DESIGN AND TESTING

4.1 Introduction

The first method that was used to add flexural stiffness to the CFRTP panels was adding corrugations. Corrugations are used commonly in industry increase flexural stiffness in metal stay-in-place formwork, roofs, pipes, and retaining walls.

A new method for shear transfer was also needed as the welded shear studs had been abandoned. The main issue with the welded shear studs was that it relied on the strength of the matrix material instead of the fibers. A mechanical bearing connection was chosen, as this would engage the fibers in the composite. To make the bearing connection, horizontal holes were cut into the webs of the corrugation and steel bars were run through them. This configuration can be seen in Figure 35. This method was chosen because it would engage the fibers in the corrugated panel and it was relatively simple to manufacture.

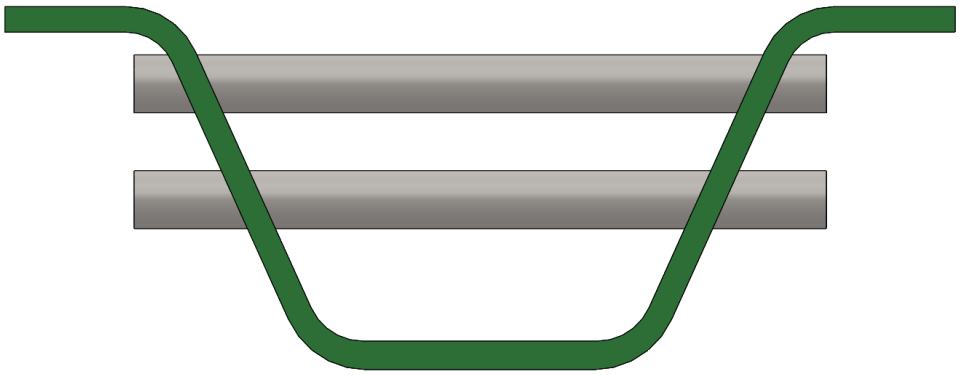

Figure 35: Cross-section of corrugated CFRTP panel

4.2 Design

With the proof-of-concepts parts successfully manufactured, the next step was to begin designing full-scale hybrid corrugated CFRTP-concrete test specimens. These specimens were designed to

meet the factored AASHTO Strength I requirements for a bridge deck with stay-in-place formwork. Two load conditions were considered:

- The weight of the wet concrete before it cures on the corrugated CFRTP panel
- The maximum positive moment from the AASHTO HL-93 truck or tandem on the hybrid beam

The length of the corrugated panel and hybrid beam was chosen to be five feet, the longest panel that can be thermoformed at the ASCC using automated manufacturing.

A MATLAB code was developed that analyzed the corrugated beam with input cross-sectional properties. The analytical tool evaluated two load cases and considered several failure modes.

4.2.1 Final Design

The final design of the hybrid corrugated CFRTP-concrete beam is given in this section. A cross-sectional shape similar to the proof-of-concept parts was chosen because of favorable results from the second set of trial specimens. The material chosen for these specimens was IE 5842b. To achieve composite action between the corrugated CFRTP panel and the concrete, two layers of steel bars were run horizontally through the two webs.

The designed cross-section of the corrugated CFRTP panel is shown in Figure 36. The width of the top and bottom flange were unchanged from the proof-of-concept parts discussed in Appendix B. The vertical distance between the top of the bottom flange and the bottom of the top flange was increased to $102\ mm$ to provide acceptable clearances for two layers of shear transfer rods to be included. The thickness of each laminate was determined by the number of layers required. The layup for the bottom flange was designed to have mostly unidirectional fibers, as it served as the main tension reinforcement for the structure. Some biaxial fibers were also included to transfer the shear from the web into the bottom flange. The web was designed with an even mix of unidirectional and biaxial fibers to provide shear and bearing resistance. The top flange was chosen

to be the same layup as the web for ease of manufacturing as it was not expected to experience much load in the hybrid beam. The layups chosen are the following:

$$Bottom\ Flange = [0_2/\pm 45/0_7/\pm 45/0_7/\pm 45/0_3/\mp 45/0_7/\mp 45/0_7/\mp 45/0_2]$$

$$Web =$$

$$[0_2/\pm 45/0_2/\pm 45/0_2/\pm 45/0_2/\pm 45/0_2/\pm 45/0_2/\mp 45/0_2/\mp 45/0_2/\mp 45/0_2/\mp 45/0_2/\mp 45/0_2]$$

The inner radius of each of the four curves was chosen to be twice the thickness of the webs to avoid springback and fiber wrinkling at the recommendation of James Anderson of the ASCC. The outer radius of each curve was chosen to be thrice the thickness of the webs for the same reason.

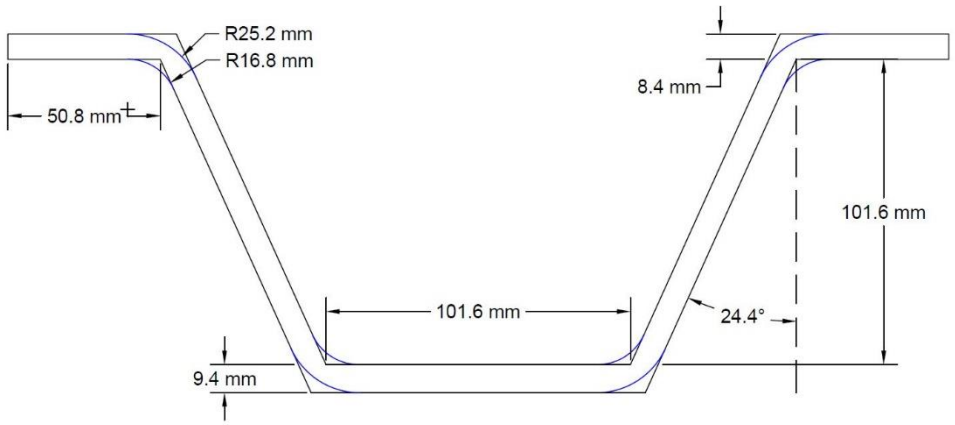

Figure 36: Design dimensions of corrugated cross-section

The diameter of the steel shear transfer bars was chosen to be $19\ mm$. The locations of these bars are shown in Figure 37 and Figure 38. Longitudinally, there are 10 sets of bars along the beam spaced a t $152\ mm$ on center. The first set of bars starts $76\ mm$ from the end of the beam. The center of each of the upper bars is 25 mm below the top of the top flange of the corrugated CFRTP panel. The center of each of the lower bars is 38 mm below the center of the respective upper bar.

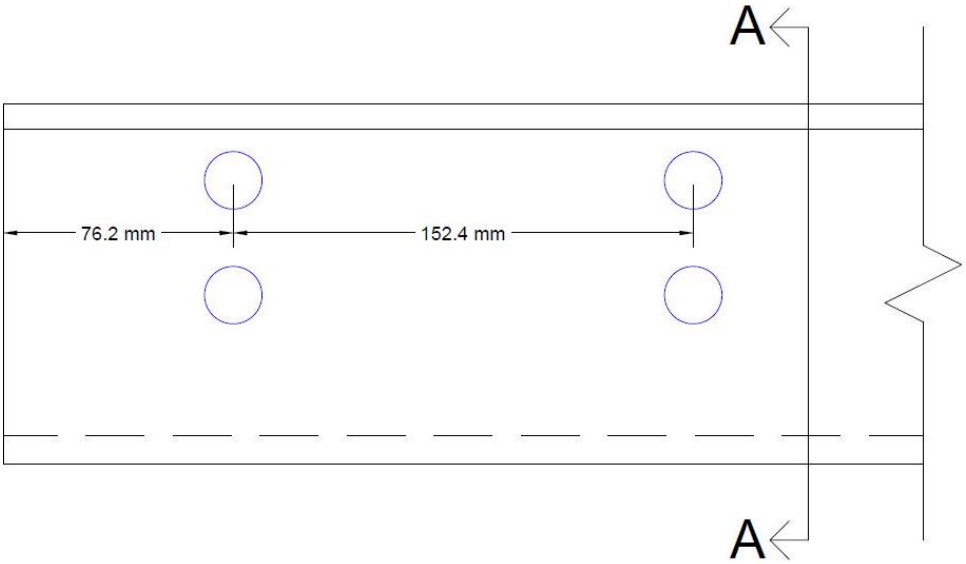

Figure 37: Side view of corrugated beam showing longitudinal spacing of bars

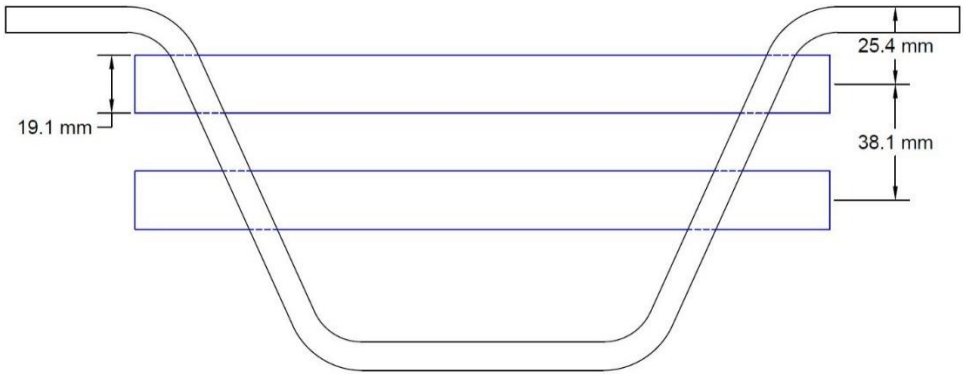

Figure 38: Section A-A of corrugated beam showing vertical spacing of shear transfer bars

The corrugated CFRTP panels were then filled with concrete up to $64\ mm$ above the top flange. The width of concrete was chosen to be the full width of the corrugated CFRTP panel of $314\ mm$. The location of the concrete relative to the corrugated CFRTP panel is shown in Figure 39

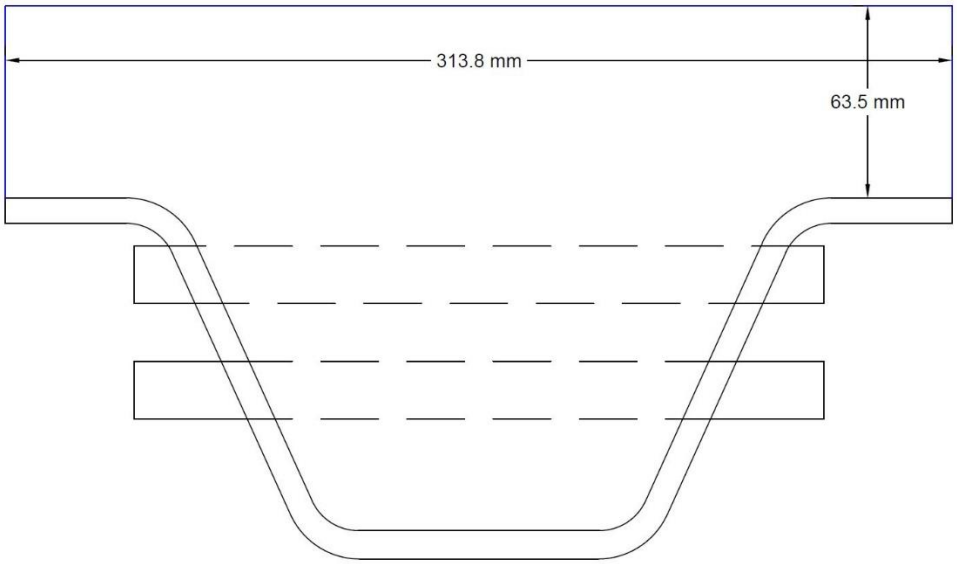

Figure 39: Design dimensions of concrete on the corrugated cross-section

4.2.2 Construction Loading on CFRTP Corrugated Panel

Stay-in-place formwork has to carry the load of the wet concrete without breaking or deforming excessively before the concrete cures and gains compressive strength.

The provisions for stay-in-place formwork given in the AASHTO Bridge Design Specification [9] require that the stay-in-place formwork be designed for at least a construction loading that consists of the following:

- The self-weight of the form
- The weight of the concrete slab
- An additional 50 pounds per square foot (approximately 2.4 kPa)

AASHTO also specifies a maximum deflection equal to the minimum of the span length divided by 180 or 0.5 inches (13 mm). These deflection limits apply to span lengths of ten feet or less.

4.2.2.1 Loading

The maximum moment and shear expected to be experienced by the corrugated panel under this loading were calculated according to AASHTO [9]. In a real-life scenario, the loading would best

be modeled by a constant distributed load, but these tests were loaded in four-point bending. The maximum shear under a constant distributed load was found to be $1.19\ kN$ through Equation 40 [17]. The maximum moment under a constant distributed load was found to be $423\ Nm$ through Equation 41 [17]. Equations 42 and 43 [17] were used to back-calculate an appropriate load for the four-point bend test. To get the same maximum shear as under a distributed load in the four-point bend test, a total load of $2.38\ kN$ was needed. To get the same maximum moment, a total load of $1.78\ kN$ was needed. The larger load of $2.38\ kN$ was chosen as the benchmark for this set of testing.

$$V = \frac{w * L}{2} \tag{40}$$

$$V = Maximum\ shear\ in\ beam$$

$$w = Distributed\ load\ on\ beam$$

$$L = Length\ of\ beam$$

$$M = \frac{w * L^2}{8} \tag{41}$$

$$M = Maximum\ moment\ in\ beam$$

$$V = P \tag{42}$$

$$P = Load\ applied\ at\ each\ third\ point$$

$$M = \frac{P * L}{3} \tag{43}$$

4.2.2.2 Flexural Analysis

To begin determining the nominal moment capacity of the beam, first, the location of the neutral axis was determined as a distance from the bottom of the section by Equation 44. The distance to the neutral axis was determined by weighting the distance from the bottom of the section to the center of each part by its respective area and longitudinal elastic modulus.

$$\bar{z} = \frac{\sum E_{xi} A_i z_i}{\sum E_{xi} A_i} \tag{44}$$

The relationship between the bending moment and the curvature of the beam was then calculated using Equation 45. First, the moment of inertia of each part about its centroid was calculated. Next, the parallel axis theorem was used to find the contribution of each part to the moment of inertia about the centroid of the entire beam. Each part's contribution was then weighted by that part's longitudinal elastic modulus then the stiffness contribution for each part was summed to find the total flexural rigidity of the stiffened panel.

$$EI = \sum E_{xi}(I_{0i} + A_i d_i^2) \tag{45}$$

From the flexural rigidity and the internal moment, the curvature can be calculated using the moment-curvature equation [16], shown in Equation 46.

$$\kappa = \frac{M}{EI} \tag{46}$$

4.2.2.3 Material Strength Analysis

Next, the analysis tool checked that the composite laminate does not fail earlier in any other location. The tool calculated the longitudinal strain, transverse strain, and shear strain in each lamina across the entire height of the corrugated panel to check for failure under their combined effects.

The longitudinal strain from bending for any point on the cross-section can be found using Equation 47 where z is the distance to the point from the neutral axis.

$$\varepsilon_x = \kappa * z \tag{47}$$

Transverse strains from Poisson's effect were also considered and were calculated through Equation 48.

$$\varepsilon_y = -\nu_{xy} * \varepsilon_x \tag{48}$$

Shear stresses were found using Equation 49 [16]. The stresses were converted to strains using the shear modulus of elasticity shown in Equation 50. The shear modulus comes from CLT, which is detailed in Section 2.3.1.3.

$$\tau = \frac{VQ}{Ib} \tag{49}$$

$$\gamma = \frac{\tau}{G_{xy}} \tag{50}$$

Using the three strains, the corresponding stresses were found using by multiplying them with the transformed reduced stiffness matrix, $[\bar{Q}]$. The stresses and strains were then transformed into lamina coordinates using the transformation matrix $[T]$. The ply mechanics methods used for stress and strain transformations are described in more detail in Section 2.3.1. These stresses and strains were compared with three failure theories, discussed in Section 2.3.2, to check for failure.

4.2.2.4 Stability and Serviceability Analysis

The analysis tool also checked some stability and serviceability criteria. For steel stay-in-place formwork, AASHTO limits the acceptable mid-span deflection for spans up to 3 meters (10 feet) to be the lesser of the span length divided by 180 and half an inch [9]. This requirement is meant to prevent excess concrete being added which would increase the weight and the load on the

structure. This problem would also apply to thermoplastic composite stay-in-place formwork so it was checked in the design of the panels. The deflection was calculated using the linear elastic deflection equation for a simply supported beam with an applied distributed load [17].

$$\delta = \frac{5 * w * L^4}{384 * EI} \tag{51}$$

An elastic buckling equation, shown in Equation 52, was checked that is meant for an anisotropic rectangular plate, simply supported on all sides [18].

$$F_{LT}^{cr} = \begin{cases} (2.7 + 1.7\eta_{LT})\left(\frac{t}{b}\right)^2 \sqrt[4]{E_L E_T^3} & 0 < \eta_{LT} \leq 1 \\ \left(3.9 + \frac{0.47}{\eta_{LT}^2}\right)\left(\frac{t}{b}\right)^2 \sqrt{E_T(E_T\nu_{LT} + 2G_{LT})} & \eta_{LT} > 1 \end{cases} \tag{52}$$

$$\eta_{LT} = \frac{2G_{LT} + E_T\nu_{LT}}{\sqrt{E_L E_T}} \tag{53}$$

4.2.2.5 Expected Failure Modes

Several common types of failure modes were analyzed to predict a failure load of the corrugated CFRTP panel.

The first mode considered was CFRTP failure from the combined effects of longitudinal, transverse, and shear strains. Figure 40 shows the minimum strength ratio, defined as the failure strain or stress at that location within the cross-section divided by the respective applied stain or stress at that location, across the entire height of the cross-section. The three failure criteria presented in Section 2.3.2 were used to predict failure. For the Hashin and Maximum strain criteria, the minimum of their respective failure modes for each lamina is taken. For the Tsai-Wu criteria, there is only one failure mode so the minimum of each lamina is taken.

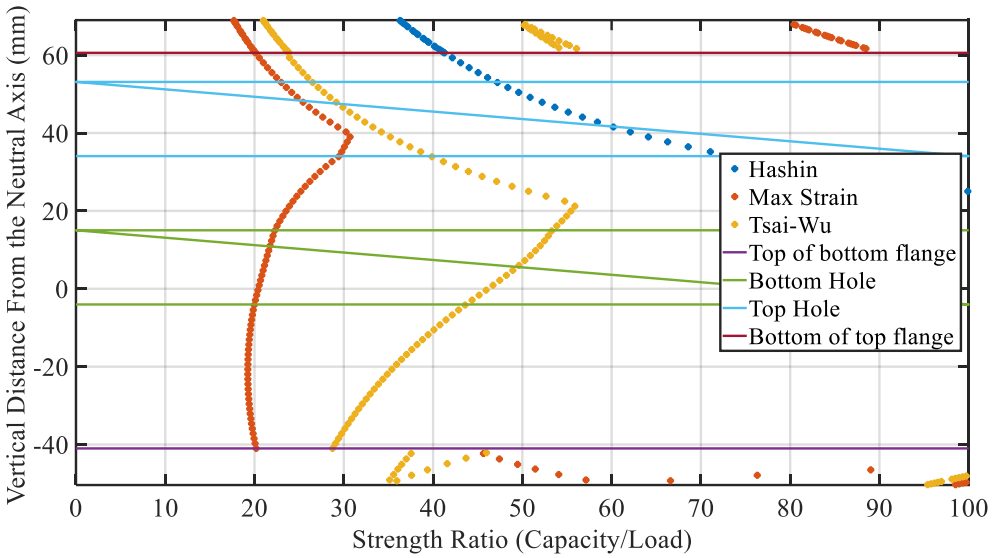

Figure 40: First-ply failure strength ratios over the section under wet concrete loads

Using the maximum strain failure criteria, the minimum strength ratio was 17.7 in the extreme compression fiber. This indicated that first-ply failure would occur at a significantly higher load than the expected construction loading case.

The elastic buckling failure modeled by Equation 52 was also investigated. Under the considered construction loads, the strength ratio was found to be 1.33, which would correspond to a failure load in a four-point bending test of 3.16 kN.

4.2.3 Ultimate Loading on Composite CFRTP-Concrete Corrugated Beam

The analysis tool then considers the corrugated panel once the concrete has cured to form a composite-concrete hybrid beam. Three types of loads were considered on the CFRTP-concrete member for this load case:

- The maximum positive live load moment from Table A4-1 in AASHTO
- An assumed two-inch thick, non-structural asphalt wearing surface
- Pre-stress in the stiffened panel from self-weight of the panel and concrete slab

The loads were factored using the Strength I load combination from Table 3.4.1-1 in AASHTO [9]. The other design considerations were the concrete in shear near the supports and the stiffened panel in bearing at the connection with concrete.

4.2.3.1 Loading

Three types of loading were considered. The specimen was treated as a deck spanning transversely between supporting longitudinal beams. The applied live load on the beam was found using the equivalent strip width analysis required by the AASHTO LRFD Bridge Design Specifications [9]. The strip width, which is the effective width of the slab that can be used to resist the loading, was calculated to be $1443\ mm$. It was assumed that the panel was simply supported so the worst-case load was one wheel located at midspan. The $71\ kN$ wheel load was applied which resulted in an applied moment of $25.3\ kN\ m$. Equation 54 was used to calculate the design moment of $8.8\ kN\ m$ for a single corrugation.

$$M_{LL} = \frac{M}{SW} * m * IM * b \tag{54}$$

$$M = 25.3\ kN\ m = applied\ moment$$

$$SW = 1443\ mm = strip\ width$$

$$m = 1.2 = multiple\ presence\ factor$$

$$IM = 1.33 = impact\ factor$$

$$b = 314\ mm = width\ of\ single\ corrugation$$

A two-inch thick, non-structural, asphalt wearing surface was assumed to rest on top of the concrete slab. A pre-stress in the CFRTP reinforcement from the construction loading case was also considered for this design. The Strength I load combination was used combine these loadings. This load case is meant to replicate normal vehicular use of the bridge without any lateral loads. This load case is shown in Equation 55.

$$M_u = \gamma_{LL} * M_{LL} + \gamma_{DC} * M_{DC} + \gamma_{DW} * M_{DW} \quad (55)$$

$$\gamma_{LL} = 1.75$$

$$\gamma_{DC} = 1.25$$

$$\gamma_{DW} = 1.50$$

For this set of testing, the corrugated CFRTP panel was allowed to deflect under the weight of the wet concrete during the pour so the dead load of the structure is carried by the corrugated CFRTP only, not the hybrid structure. For this calculation, it was assumed that $M_{DC} = 0$, as the strains in the CFRTP from the dead load of the structure were added into the analysis later. For the final designed beam, M_u was calculated to be $11.5\ kN * m$. For a four-point bend test, an applied load of $48.5\ kN$ would create this internal moment. As was done for the construction loading case in Section 4.2.2.1, a higher load was needed to match the shear from a distributed load. This lead to setting the benchmark loading at $64.5\ kN$.

4.2.3.2 Nominal Moment Capacity

To start the analysis, the failure mode was assumed to be crushing in the extreme compression fiber in the concrete. The location of the neutral axis was determined numerically by solving for the root of a function that calculated the difference between the total compressive force and the total tensile force. The Hognestad model, discussed in Section 2.3.3, was used to model the concrete compressive forces while the CFRTP reinforcement were assumed to remain linear-elastic. The strains in the CFRTP from the dead weight of the structure were also included.

$$0 = \sum C(c) - \sum T(c) \quad (56)$$

$$c = depth\ to\ the\ neutral\ axis\ from\ the\ top\ of\ the\ concrete$$

The curvature in the section was then found using Equation 57, which depends on the location of the neutral axis and an assumed ultimate strain of 0.003 in the extreme compression fiber of the concrete.

$$\kappa = \frac{\varepsilon_c}{c} \tag{57}$$

The tensile force in each part of the CFRTP reinforcement and the compressive force in each part of the concrete was calculated using the found curvature and distance from the neutral axis. The nominal moment capacity of the hybrid beam was found summing the product of each part's resultant force and the eccentricity of that force from the neutral axis as shown in Equation 58.

$$M_n = \sum F_i z_i \tag{58}$$

4.2.3.3 Strength Analysis

To verify the assumption that the concrete fails first, the curvature generated from Equation 57 was used to calculate the strains through the corrugated panel. The longitudinal and transverse strains were calculated in the same manner as the linear analysis using Equations 47 and 48. It was found that first-ply failure in the corrugated panel occurred significantly before the concrete would crush. This failure mode is discussed further in Section 4.2.3.6.

As Equation 49 assumes a linear-elastic system to calculate the shear stress, it cannot be used for this analysis. A non-linear method for calculating the shear stress was developed for this analysis. This method assumed that the critical section for shear occurred at load head, which was the location of the taken moment and shear.

Two vertical cuts were made to the beam that were separated by a small finite value; Δx. After several iterations, the results showed convergence with $\Delta x = 0.25mm$ and below so this value was chosen for design. The cuts formed the element shown in Figure 41. The internal moments in

the beam for either side of the element are taken as M_1 and M_2 respectively. The bending stresses acting on the element are shown in Figure 41.

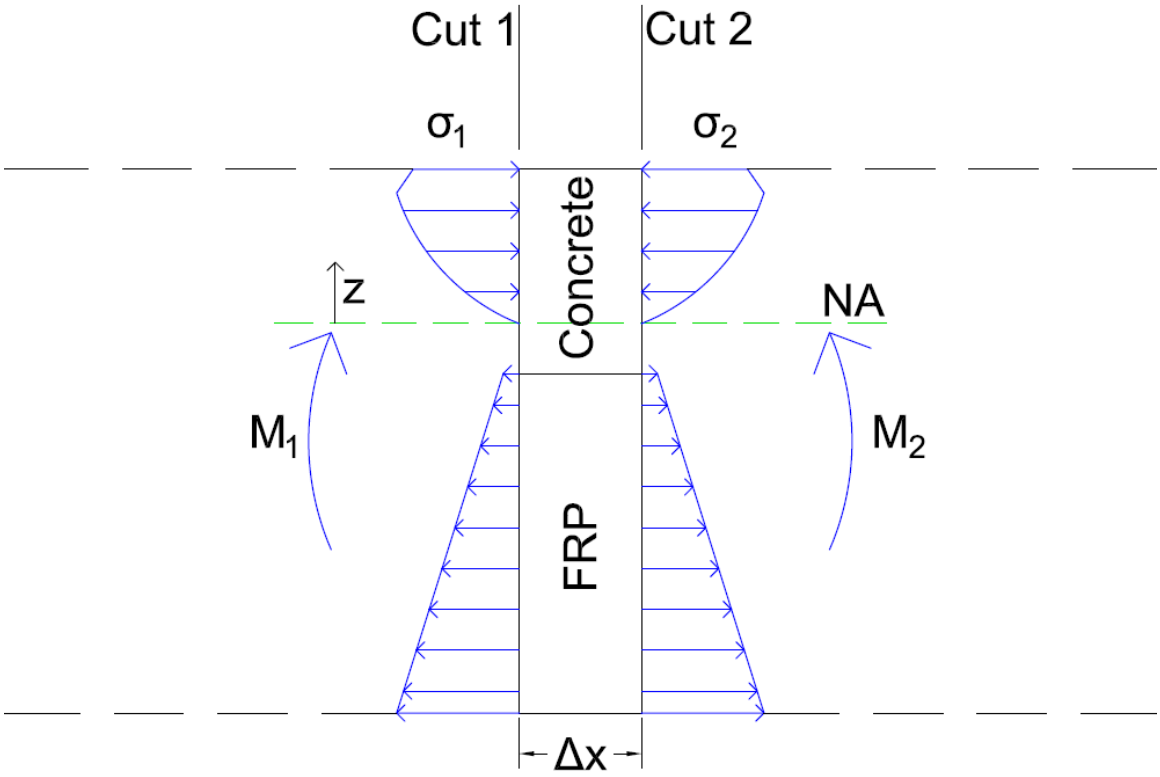

Figure 41: Side view of element of the hybrid beam

The moments, M_1 and M_2, can be found by solving the integral in Equation 59.

$$M = \int_A \sigma(z, \kappa)\, z\, dA \tag{59}$$

M_1 was taken as the maximum moment in the beam and was found using Equation 59. For the stress, the CFRTP was assumed to remain linear-elastic and the Hognestad constitutive model [15] was used to approximate the behavior of the concrete.

The change in moment over the length Δx is approximately equal to the shear force multiplied by the length for small distances. This relationship is shown in Equation 60. As the testing for these

specimens was done in 4-point bending, Equation 61 was used to solve for the shear corresponding to M_1 [17].

$$V = \frac{\Delta M}{\Delta x} = \frac{M_2 - M_1}{\Delta x} \tag{60}$$

$$V = \frac{3M}{L} \tag{61}$$

Equation 60 was used to solve for M_2. The curvature that would cause this moment, κ_2, was then solved for numerically.

Next, a horizontal cut was made to the element shown in Figure 41. The vertical location of this cut would correspond to the location that the shear stress is being determined. This cut formed a sub-element between the cut surface and the outside of the part. The shear stress along the cut, τ, is the stress that needs to be solved for. The two bending stresses on the sub-element, shown in Figure 42, were simplified to forces using Equations 62 and 63. The shear stress was assumed constant across the width of the beam and could then be written as a force using Equation 64.

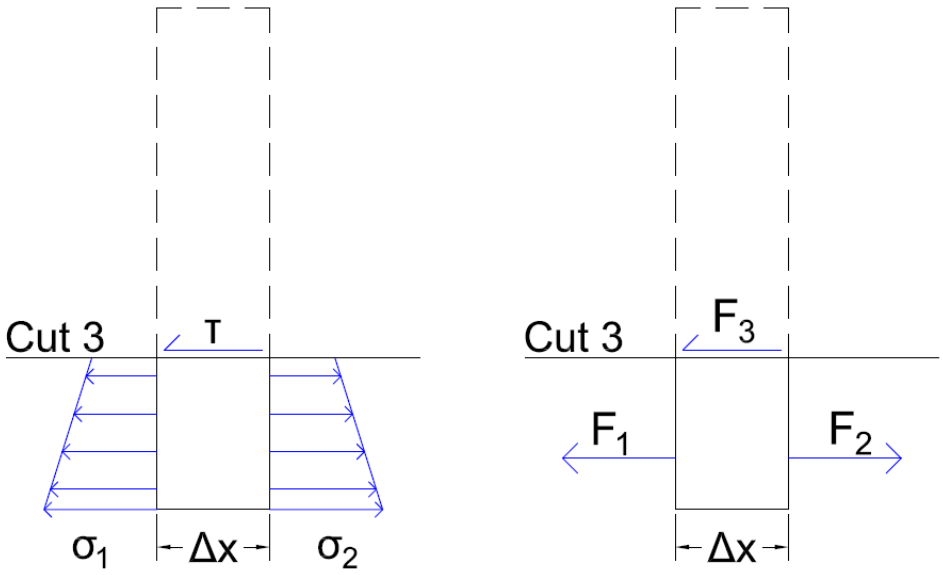

Figure 42: Side view of the sub-element of the hybrid beam

$$F_1 = \int \sigma_1(z, \kappa_1) dA \tag{62}$$

$$F_2 = \int \sigma_2(z, \kappa_2) dA \tag{63}$$

$$F_3 = \tau b \Delta x \tag{64}$$

Using equilibrium, the three forces can be related and the shear stress can be calculated.

$$F_3 = F_2 - F_1 \tag{65}$$

$$\tau = \frac{\int (\sigma_1(z, \kappa_1) - \sigma_2(z, \kappa_2)) dA}{b \Delta x} \tag{66}$$

As the corrugated panel is assumed to remain linear-elastic, the in-plane shear modulus was used to calculate the shear strain in the composite through Equation 50.

The strains in each lamina can be found using the same methods as were outlined in Section 4.2.2.3 for the linear analysis.

4.2.3.4 Bearing Connection

To calculate the shear flow for the connection, a similar non-linear approach as was used in Section 4.2.3.3, except that Equation 66 is modified to the following to calculate shear flow instead of shear stress and the area used for the sub-element was taken as only the area of the corrugated panel tributary to the rod being examined.

$$q = \frac{\int (\sigma_1(z, \kappa_1) - \sigma_2(z, \kappa_2)) dA}{\Delta x} \tag{67}$$

To calculate the bearing force on one of the holes, the shear flow is multiplied by the center-to-center spacing of the holes.

$$F_{bear} = q * p \tag{68}$$

The reduction factor for bearing was taken as 0.7 [9] for bearing on concrete. The factor of safety for bearing was obtained by dividing the reduced nominal capacity of the composite by the calculated bearing force.

$$FS = \frac{\Phi_{bear} * F_{nbear}}{F_{bear}} \tag{69}$$

4.2.3.5 Concrete Shear Capacity

To check if shear reinforcement would be needed in the concrete, the shear capacity of concrete was compared to the maximum shear in the hybrid beam. The shear strength of normal weight concrete was calculated as per the American Concrete Institute (ACI) [14]

$$V_{nc} = 2A_c\sqrt{f_c'} \tag{70}$$

The strength ratio for concrete shear was obtained by dividing the nominal capacity of the concrete by the maximum factored shear force.

$$FS = \frac{V_{nc}}{V_u} \tag{71}$$

This method of analysis assumed that the concrete would carry all of the shear forces in the beam. This assumption is most likely incorrect, as the corrugated panel could resist some of the shear. It should also be noted that no shear reinforcement was used in concrete, though in a real bridge deck a minimum amount of shear reinforcement would be required.

4.2.3.6 Expected Failure Modes

Several common types of failure modes were analyzed to predict a failure load of the hybrid structure.

The first mode considered was concrete crushing at the top of the beam between the load application points. Crushing of concrete was assumed to occur at 0.3% strain. The Hognestad model [15] was used as the constitutive model for the concrete. Crushing was expected to occur at a total load of $187.7\ kN$ in 4-point bending.

Next, first-ply failure of the composite laminates was considered. Three failure theories were considered: Hashin, Tsai-Wu, and Maximum Strain. All of the failure theories predicted the first failure to be in the web region. Maximum strain predicted the lowest failure load of $60.9\ kN$. This was a matrix-dominated failure mode so it was not expected to cause ultimate failure of the structure. The specimen was expected to reach a load of $470.2\ kN$ before any of the unidirectional fibers in the bottom flange would fail in tension according to the maximum strain criterion. The Tsai-Wu criterion predicted a slightly smaller failure load of $455.5\ kN$.

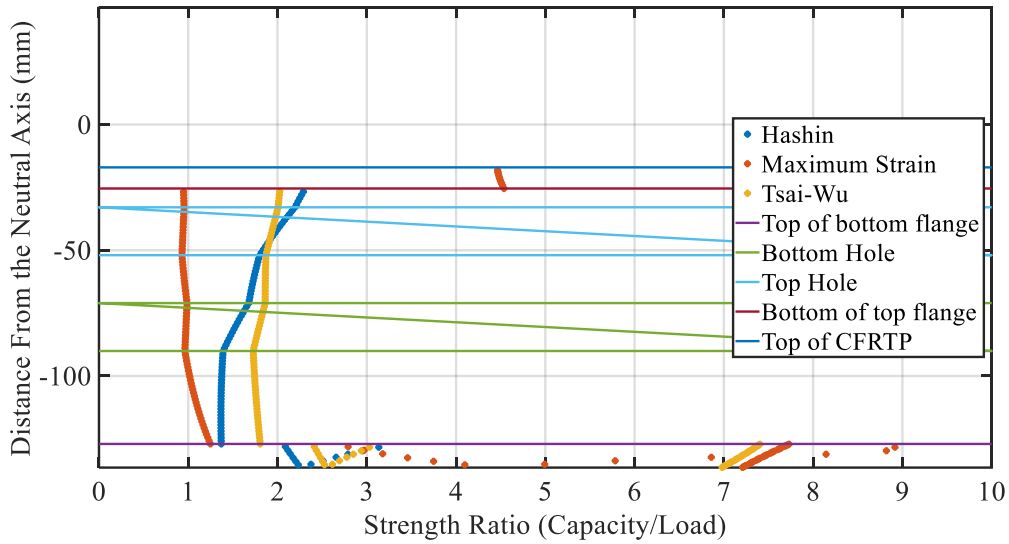

Figure 43: First-ply failure strength ratios over the hybrid section under ultimate loads

After that, failure at the bearing connection was considered. Two types of failures were considered: shear failure of the steel bearing rod and bearing failure of the CFRTP. To approximate the distribution of shear force between the two rods, the ratio of internal tensile force in the CFRTP

below the midpoint of the rods to the total tensile force carried by the CFRTP was used to determine the proportion of the shear stress carried by the lower rod. This method assumed linear elastic behavior of the rod and the CFRTP. This resulted in a significantly higher load on the lower bearing rod. The steel rods were expected to fail in shear at a load of $235.3\ kN$ and the CFRTP was expected to fail in bearing at a load of $105\ kN$.

Ignoring the matrix cracking in the web and bottom flange, the expected failure mode was the CFRTP in bearing at a load of $105\ kN$.

4.3 Manufacturing

Six corrugated CFRTP beams were manufactured at the ASCC. The first two were trial specimens made with a wooden mold to refine the manufacturing parameters. More information on the trial specimens made with the wooden mold can be found in Appendix B. The final four were constructed with a full-size aluminum mold, and then concrete was cast on them to create four hybrid corrugated CFRTP-concrete beams.

4.3.1 Full-Scale Parts

Four full-scale, $1524\ mm$-long corrugated CFRTP panels were constructed for quasi-static testing. A new full-size mold was constructed for this iteration of manufacturing.

4.3.1.1 Full-Scale Mold

An aluminum 6061 mold was created for these specimens after successful trials with an aluminum mold for the manufacturing of stiffened panels, which is discussed in Appendix B. As that mold was deemed mostly successful, another aluminum mold was manufactured at the ASCC for the construction of the full-scale corrugated panels.

The information learned during the finite element analysis (FEA), design, and manufacturing of the previous molds was used in the design and construction of the aluminum corrugated mold.

Some design changes were implemented for this mold to solve some of the minor issues observed in the stiffened panel. They are given in the following list:

- Thicker aluminum gussets were used for additional stiffness in the mold surface plate. This created a more consistent pressure distribution on the part during the forming process
- Thicker aluminum mold surfaces were used to compensate for lost material during the CNC machining process used to get the designed mold surface and maintain the desired stiffness for the forming process
- A thicker aluminum base plate was used to reduce warping from welding thermal stresses
- Mold cross-section design changes were made to reduce overall heat input from the welding process and reduce distortion from remaining welding thermal stresses

Figure 44 and Figure 45 show the aluminum mold constructed for this deliverable.

Figure 44: Aluminum corrugation mold, side view

Figure 45: Aluminum corrugation mold, end view

4.3.1.2 Manufacturing Process

The four full-scale corrugated CFRTP panels were manufactured using the process given in Appendix A. the final design for the composite laminates given in Section 4.2.1 was used for these specimens. The arrangement of the layers were changed from the trials to allow more of the biaxial fibers to be continuous between the two layups and to minimize the number of sequential discontinuous layers. For this iteration of the testing, all of the biaxial fibers in the bottom flange layup were continuous into the web, to maximize the shear strength at the interface. In the trial parts, only one third of the biaxial layers in the bottom flange were continuous into the web.

$$Bottom\ Flange = [0_2/\pm45/0_7/\pm45/0_7/\pm45/0_3/\mp45/0_7/\mp45/0_7/\mp45/0_2]$$

$$Web =$$

$$[0_2/\pm45/0_2/\pm45/0_2/\pm45/0_2/\pm45/0_2/\pm45/0_2/\mp45/0_2/\mp45/0_2/\mp45/0_2/\mp45/0_2/\mp45/0_2]$$

The dimensions of the tailored blank for the parts are shown in Figure 46. The dimensions were identical to the trial part except the length was extended to $1524\ mm$.

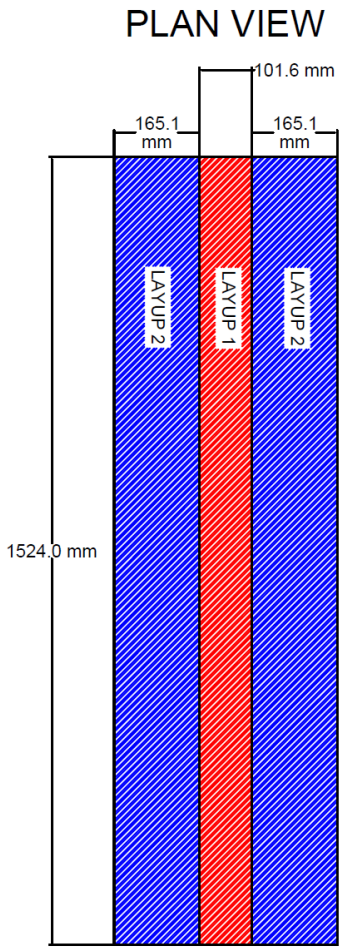

Figure 46: Dimensions of the tailored blank for the corrugated CFRTP panels

The tailored blank was created in four sections on the tape layup machine. The layers that were in each section are shown in Table 15.

Table 15: Full-scale corrugated CFRTP panel layups

Layer	Bottom Flange Layup	Web Layup	Section
1	0	0	
2	0	0	
3	45	45	
4	-45	-45	
5	0	0	1
6	0	0	
7	0	45	
8	0	-45	
9	0	-	
10	0	0	
11	0	0	
12	45	45	
13	-45	-45	
14	0	0	
15	0	0	
16	0	45	
17	0	-45	2
18	0	-	
19	0	0	
20	0	0	
21	45	45	
22	-45	-45	
23	0	0	
24	0	-	
25	0	0	
26	-45	-45	
27	45	45	
28	0	0	
29	0	0	
30	0	-	
31	0	-45	3
32	0	45	
33	0	0	
34	0	0	
35	-45	-45	
36	45	45	
37	0	0	
38	0	0	
39	0	-	
40	0	-45	
41	0	45	
42	0	0	
43	0	0	4
44	-45	-45	
45	45	45	
46	0	0	
47	0	0	

Four flat panels were consolidated using the process described in Appendix A. Figure 47 shows one of the consolidated flat CFRTP panels. Two aluminum plates were included on one side during the consolidation to have constant thickness across the entire part. Including the aluminum plates reduced the observed dry spots from the trial parts.

Figure 47: Consolidated Flat CFRTP Panel

The consolidation platens were then removed from hydraulic press and replaced with the aluminum mold discussed in Section 4.3.1.1. The same forming parameters from the trials, discussed in Appendix B, were used for the full-scale specimens.

4.3.1.3 Discussion of Results

The four full-scale specimens were successfully formed. One of the formed panels is shown in Figure 48. Fewer dry spots and wrinkles were observed than for the trial specimens. The wrinkling and most of the dry spots were restricted to the regions above the supports near the ends of the specimens.

Figure 48: Formed corrugated CFRTP panel

4.3.2 Composite CFRTP-Concrete Corrugated Beam

Before the construction loading test, discussed in Section 4.4.1, the shear transfer bars were installed into the corrugated panels to model the actual construction process as the rods would need to be installed prior to the concrete pour. After the construction loading test, concrete was poured onto the corrugated specimens to imitate a concrete bridge deck being poured.

4.3.2.1 Manufacturing Process

After the forming of the corrugated panels, steel bearing rods were installed into the panels to provide a shear connection between panel and concrete. A CNC router was used to cut 19 mm

diameter horizontal holes into the angles webs of the panel. A plywood mold was made to secure the panels in place during the cutting. The holes being cut into one of the specimens is shown in Figure 49.

Figure 49: Bearing holes being cut into a corrugated panel

Steel rods with a 19 mm diameter were then inserted into the holes. A rubber mallet was used to force some of the rods through the holes. If the rod was not snug, cable ties on the outside of the corrugation were used to secure the rod. One of the specimens with all of the bearing rods installed is shown in Figure 50.

Figure 50: Corrugated panel with bearing rods

Next, six strain gauges were installed on the bottom side of each corrugated panel at mid-span to measure the strain in the panel during testing. The exact locations of these gauges are given in Section 4.4.1.1.

Plywood formwork was constructed to facilitate the concrete pour. Each box had 4-inch long raised supports that would allow the beam to deflect during the pour. Each specimen was placed in the formwork then silicone was used to seal around the edges of the panel to prevent water from getting below the panel and interfering with the attached strain gauges. Concrete was then poured into the formwork and allowed to cure. As was discussed in Section 2.2.3.1, this concrete pour did not reach the design strength of 41.4 MPa after 3 days. The concrete was determined adequate for testing after 28 days when the compressive strength of the concrete reached 28.5 MPa.

Figure 51: Corrugated CFRTP panel installed in the formwork

Figure 52: Wet concrete in plywood formwork

Figure 53: Composite CFRTP-concrete beam specimen, 2 days after pour

4.3.2.2 Discussion of Results

Four hybrid CFRTP-concrete beam specimens were successfully manufactured. The silicone seal worked to keep the moisture from the concrete away from the strain gauges. Each strain gauge continued to function after the pour. In all four beams, the strain gauges had detected the increased strain from the deformation in the corrugated CFRTP panel from the weight of the concrete.

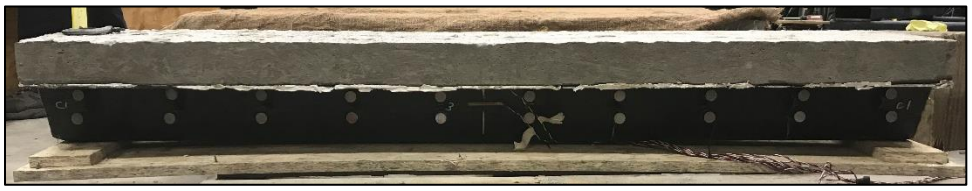

Figure 54: Composite CFRTP-concrete beam specimen one

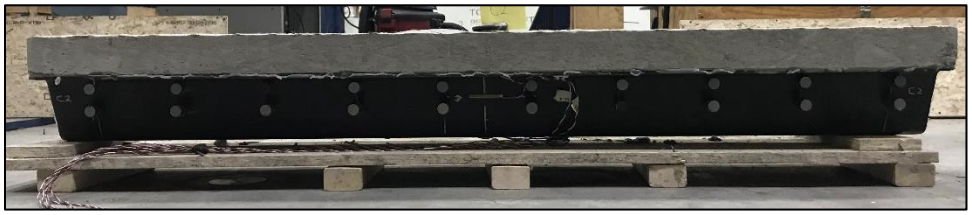

Figure 55: Composite CFRTP-concrete beam specimen two

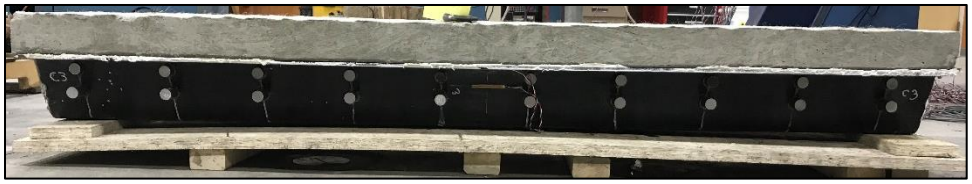

Figure 56: Composite CFRTP-concrete beam specimen three

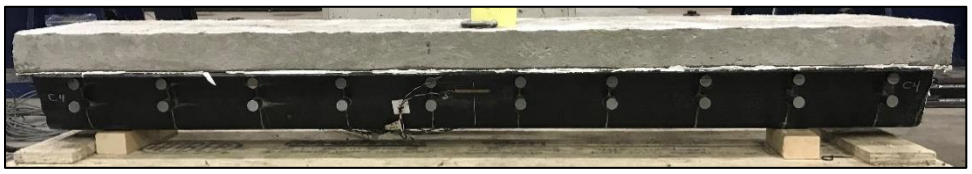

Figure 57: Composite CFRTP-concrete beam specimen four

4.4 Quasi-Static Testing

Two sets of quasi-static testing were done with the corrugated CFRTP panels. For the first test, two of the bare panels were loaded in four-point bending up to the factored AASHTO Strength I required load for stay-in-place formwork for a bridge deck. Then concrete was poured onto all four of the panels. For the second test, each of the composite CFRTP-concrete beams were loaded in four-point bending until failure.

4.4.1 Construction Loading Test

The purpose of the construction loading test was to verify that the corrugated CFRTP panel could carry the weight of the wet concrete during construction without excessive deformation or damage. Two of the specimens were loaded in four-point bending to a load of $2.38\ kN$ then unloaded. The loading of $2.38\ kN$ was chosen as this created a maximum shear in the beam under four-point bending equal to the design distributed load specified by AASHTO for stay in place formwork. The loading is discussed further in Section 4.2.2.1.

4.4.1.1 Test Setup

As can be seen in Figure 58, a steel I-beam was used as spreader beam to load the beam at the third-points of the span. Tilt-tables were used at each support to create a pin connection. Aluminum bars

were added under each load head to distribute the load directly into the top flange and to prevent the top flanges from spreading apart. 13 mm-thick neoprene pads were used at each support and under each load head to distribute the loads and lessen the effects of any stress concentrations.

Figure 58: Construction loading test setup

4.4.1.2 Instrumentation

A string potentiometer was used at midspan to measure the maximum deflection in the beam, and a linear displacement transducer (LDT) was attached at each support to measure any deflection in the neoprene at the support. Six strain gauges were also installed at mid-span to measure curvature: one on each top flange, one on each web, and two on the bottom flange.

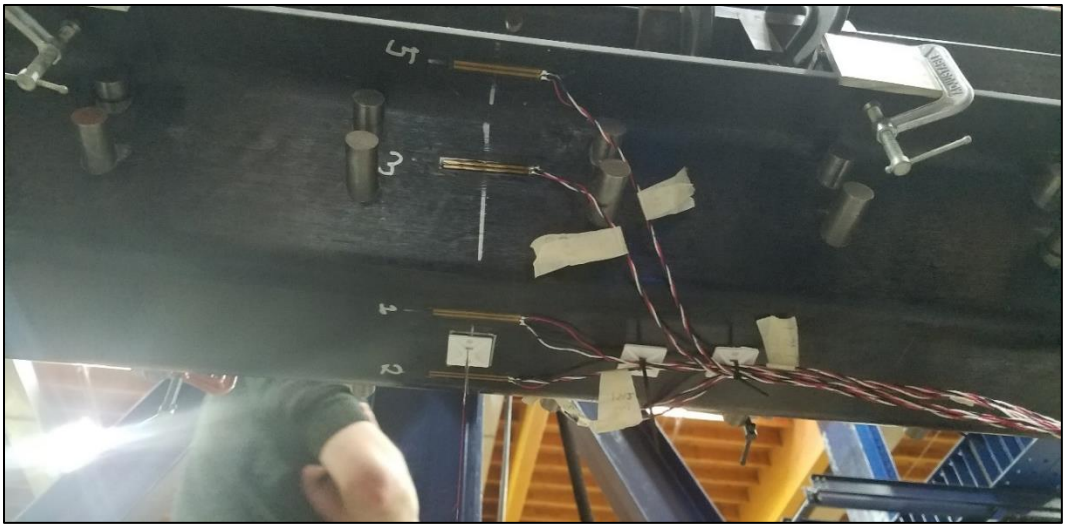

Figure 59: Strain gauges and string potentiometer installed on specimen

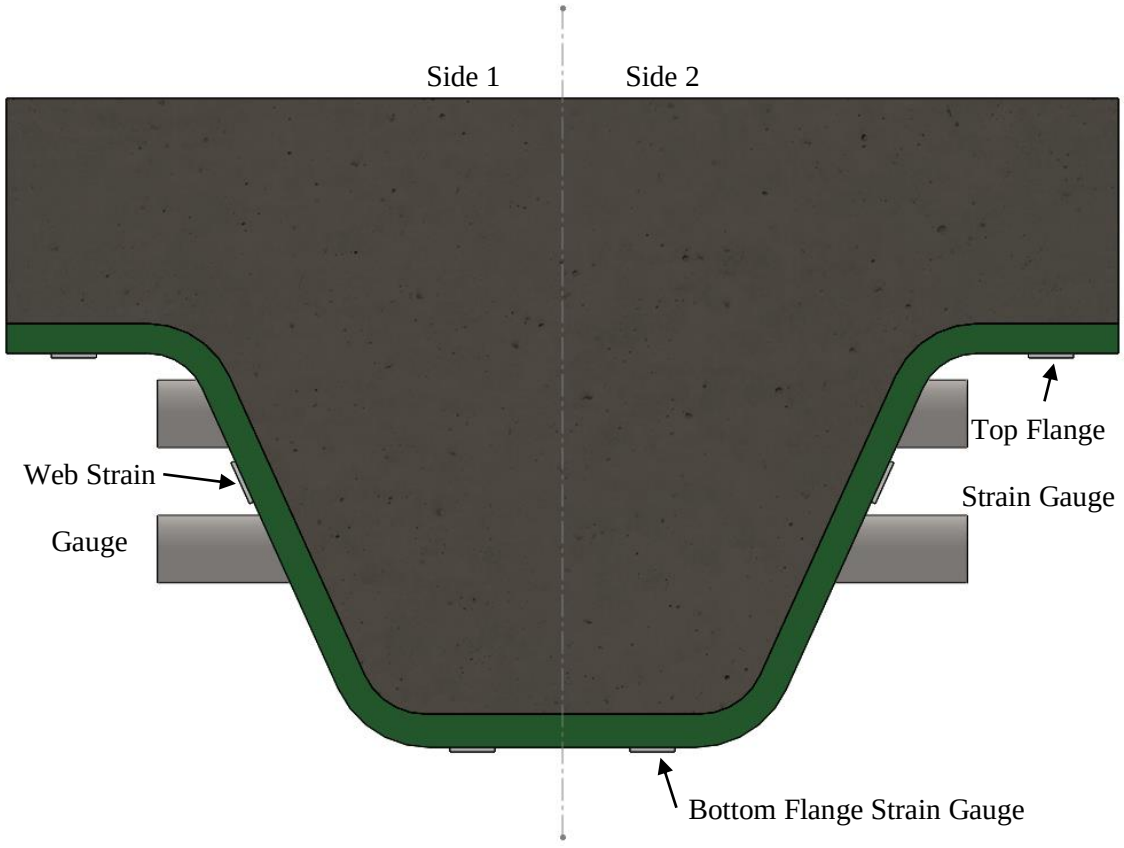

Figure 60: Strain gauge locations on hybrid beam cross-section

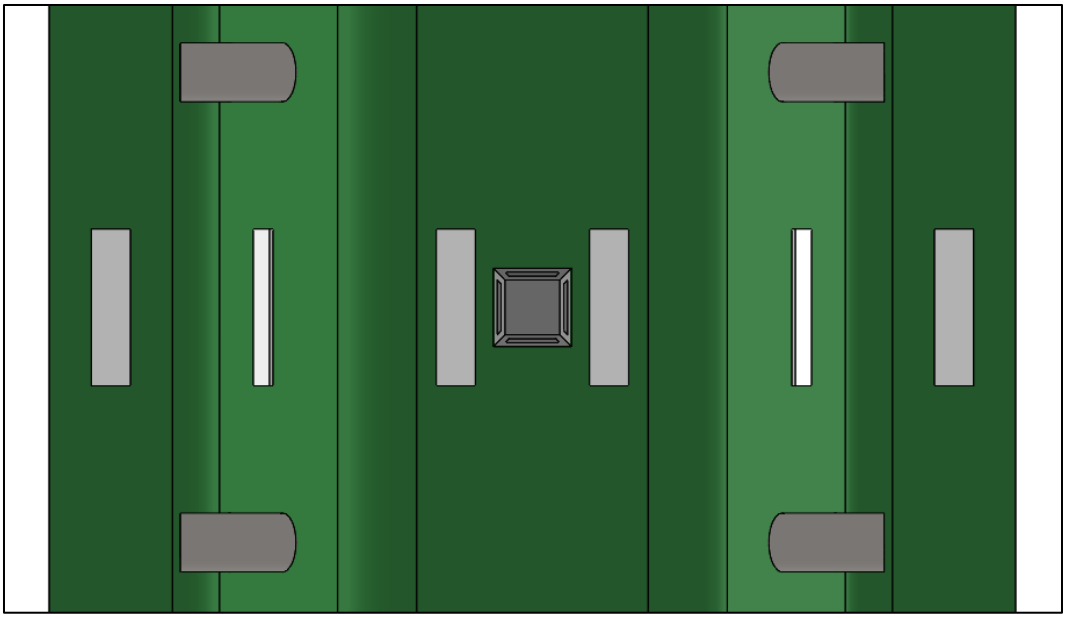

Figure 61: Strain gauge locations at midspan from bottom

4.4.1.3 Test Procedure

The two corrugated panels were quasi-statically loaded in four-point bending. After the instrumentation was installed, the load head was lowered manually until it was in contact with the specimen. The load head was then lowered at a constant rate of $0.76\ mm/minute$. Once the test reached the required loading of $2.38\ kN$, the load head was raised at the same constant rate.

4.4.1.4 Discussion of Results

Both specimens tested under construction loading reached the required AASHTO Strength I design loading without sustaining visible damage. Figure 63 shows the load-midspan deflection plot for one of the specimens that was tested. The midspan beam deflection was computed by subtracting the support compression, measured by the LDT at each support, from the total midspan deflection, measured by a string potentiometer at midspan. The data below $0.44\ kN$ was very noisy so it was discarded. A line was fit to the data between 0.44 and $2\ kN$ and the slope of that line was used to model the behavior below $0.44\ kN$. The fitted line also represents the stiffness of the beam in bending. The stiffness for this specimen was calculated to be approximately $1.17\ \frac{kN}{mm}$. The expected

stiffness based on CFRTP properties of the nominal section estimated using laminate analysis was $1.05\frac{kN}{mm}$. The calculation of this expected stiffness included some assumptions such as using a model, shown in Figure 62, which does not include rounded corners and disregards all CFRTP horizontally between the holes in the web, which could explain the difference seen between the expected and experimental stiffness. The second tested specimen had a higher experimental stiffness of approximately $1.4\frac{kN}{mm}$.

Figure 62: Cross-sectional model of the corrugated CFRTP panel

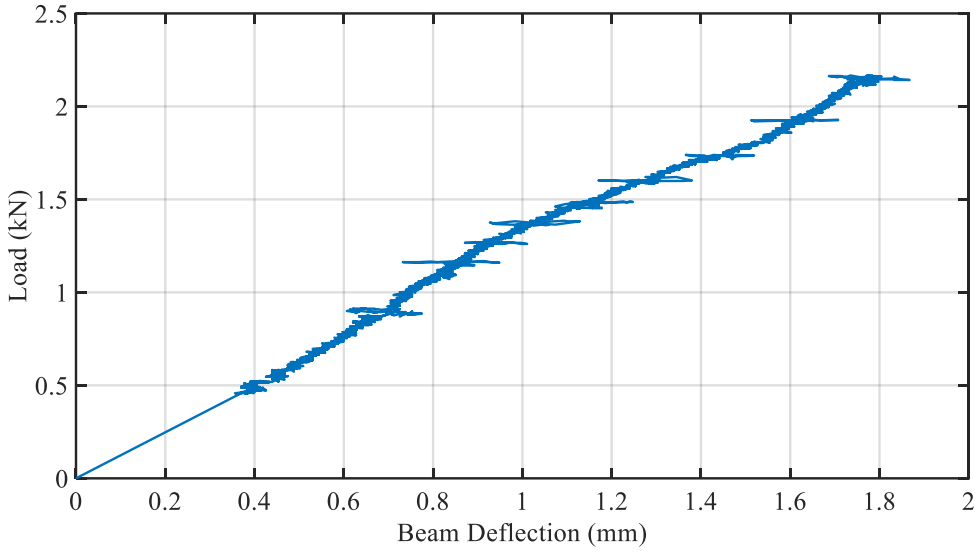

Figure 63: Construction loading test load vs midspan deflection

4.4.2 Ultimate Loading Test

The purpose of the ultimate loading test was to verify that the composite CFRTP-concrete beam could carry the expected loads on a bridge deck as given by AASHTO [9]. All four of the specimens were loaded in four-point bending until failure. The benchmark loading derived from the AASHTO Strength I specifications was 64.5 kN. The loading is discussed further in Section 4.2.3.1.

4.4.2.1 Test Setup

The test setup and instrumentation for the ultimate loading test was similar to the construction loading test. The only difference being that the aluminum brace bars were not needed under each load head. The test setup is shown in Figure 64.

Figure 64: Ultimate loading test setup

4.4.2.2 Test Procedure

The four hybrid beams were quasi-statically loaded in four-point bending. A forklift was used to load each specimen into the frame. After the instrumentation was installed, the load head was

lowered manually until it was in contact with the specimen. The load head was then lowered at a constant rate of 10 $mm/minute$. The test was run until the specimen failed.

4.4.2.3 Discussion of Results

The four composite CFRTP-concrete hybrid beams were tested until failure in four-point bending. Each specimen failed in nearly the same manner. Near a load of 100 kN, shear cracks formed in the deck on one or both ends of the specimen. These cracks can be seen in Figure 65. More cracks then formed and grew until the concrete at one end completely separated from the rest of the specimen. At this point, the specimen was considered failed. A failed specimen can be seen in Figure 66.

Figure 65: Shear cracks forming in the hybrid beam

Figure 66: Failure of hybrid beam specimen

The load-deflection curves for the four specimens are shown in Figure 67. Whenever a shear crack formed, there was a noticeable drop in the load-deflection curve and the stiffness dropped. The failure load, the load at the first shear crack, and the stiffness for each specimen are summarized in Table 16. The stiffness for each specimen was estimated by calculating the slope of each load-deflection curve between 22 and 89 kN. The average peak load and load at first shear crack were both significantly larger than the load required by AASHTO of 64.5 kN. All specimens also endured a higher load than the expected bearing failure load. This could mean that calculations used to predict the bearing load on the lower rod were conservative and that more load was shared to the upper rod. As expected, if matrix cracking occurred at the expected load of the CFRTP first-ply failure, it did not cause ultimate failure of the beam.

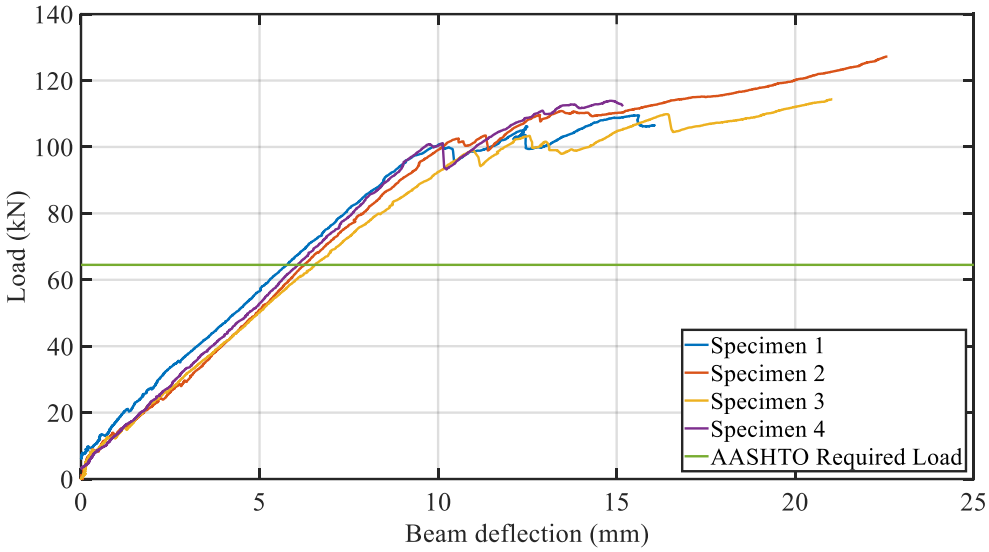

Figure 67: Ultimate loading test load vs midspan deflection plot

Table 16: Summary of ultimate loading test results

		Peak Load (kN)	Load at First Shear Crack (kN)	Stiffness (kN/mm)
Specimen	C1	109	101	9.79
	C2	127	102	9.72
	C3	114	99.2	8.70
	C4	114	101	10.1
Average		116	101	9.56
CoV		6.5%	1.4%	6.2%

4.4.2.3.1 Flexural Strain Analysis

Six strain gauges at midspan were used to measure longitudinal strains in the CFRTP during the test. As discussed in Section 4.4.1.2, two strain gauges were installed on the bottom of the bottom

flange, one on the bottom of each top flange, and one on the outside of each web located evenly between the bearing rods. The strain through the cross-section of each specimen under a load of $89\ kN$ is shown in Figure 68 through Figure 71. A line was fit to the six points to check linearity as shown in Figure 68 through Figure 71. The load of $89\ kN$ was chosen as the shear cracks had not formed yet and the hybrid beam was still behaving linearly. A summary of that data taken at that load is shown in Table 17. From comparing the average difference between sides 1 and 2, it can be seen that the strains in web showed the most variation between sides while the bottom showed the most consistency. The bottom flange being the most consistent could be due to those strain gauges being the closest to each other. The variability of strains in the web could have been caused by stress concentrations around the bearing holes. The bottom flange strain gauges also showed the most consistency between specimens. To approximate curvature, the strain values from the web were not included because of their variability so a line was fit between the top and bottom flange strain values.

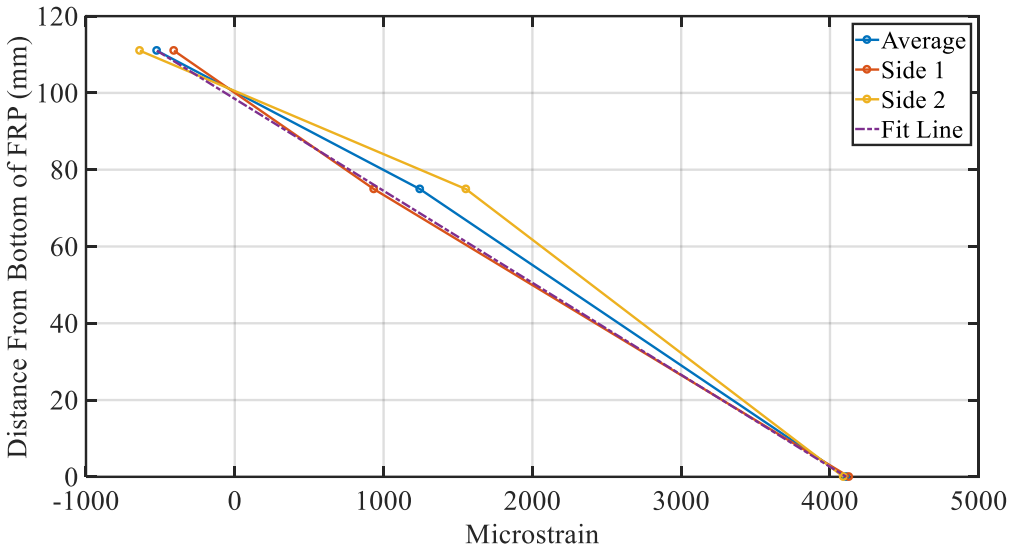

Figure 68: Strain through the cross-section of C1 at midspan under a load of 89 kN

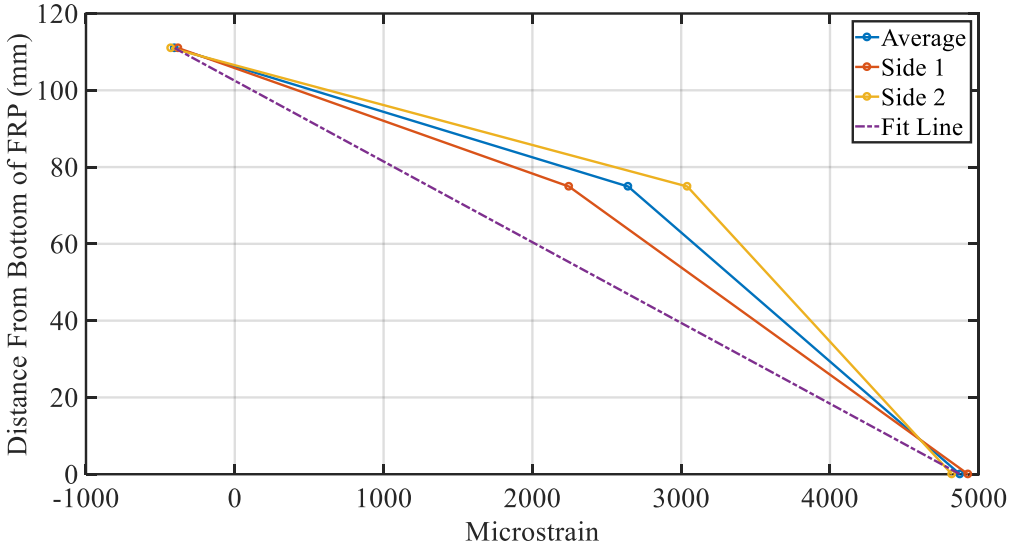

Figure 69: Strain through the cross-section of C2 at midspan under a load of 89 kN

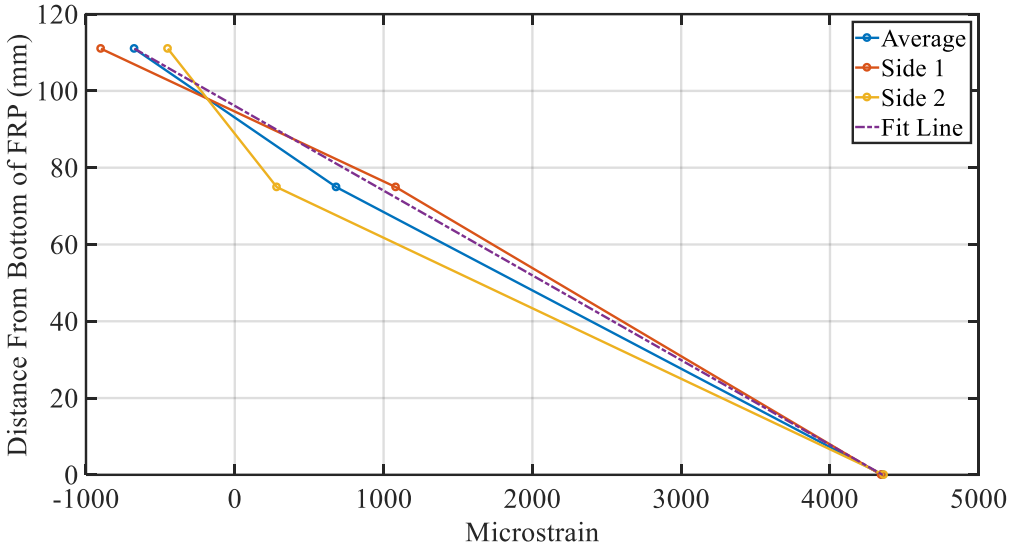

Figure 70: Strain through the cross-section of C3 at midspan under a load of 89 kN

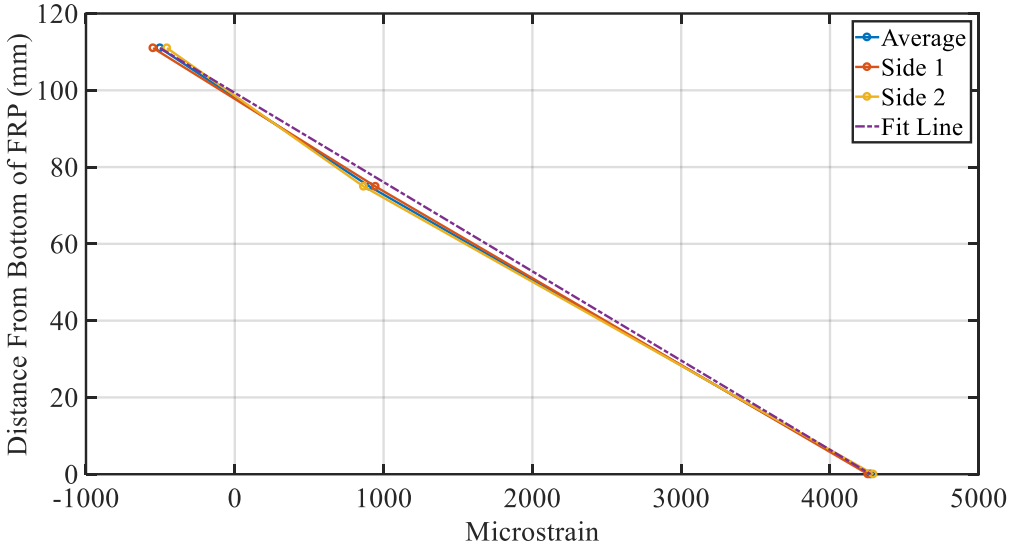

Figure 71: Strain through the cross-section of C4 at midspan under a load of 89 kN

Table 17: Summary of strain results at a load of 89 kN at midspan

		C1	C2	C3	C4	Average	CoV (%)
Top Flange Microstrain	Side 1	-408.6	-380.4	-899.6	-548.7	-559.3	36.9
	Side 2	-638.1	-429.1	-449.9	-455.5	-493.2	17.1
	Average	-523.3	-404.7	-674.7	-502.1	-526.2	18.4
	Difference	229.5	48.7	449.7	93.2	205.3	76.0
Web Microstrain	Side 1	935.4	2246	1083	945.8	1302.6	42.1
	Side 2	1554	3042	282.6	866.4	1436.3	71.8
	Average	1245	2644	682.6	906.1	1369.4	55.7
	Difference	618.6	796	800.4	79.4	573.6	51.4
Bottom Flange Microstrain	Side 1	4128	4928	4345	4256	4414.3	6.9
	Side 2	4091	4819	4362	4291	4390.8	6.1
	Average	4109	4874	4354	4274	4402.8	6.5
	Difference	37	109	17	35	49.5	71.2

Using a cracked section analysis, the neutral axis was predicted to be in the top flange. From the strains shown in Figure 68 through Figure 71, the neutral axis appears to be below the top flange.

This is a difference of approximately 13 mm from the predicted location of the neutral axis. Using a numerical model, the strain in the extreme fiber of the bottom flange was predicted to be 3,900 microstrain at a load of 89 kN. This is approximately 11% lower than the average strain of 4402.8 microstrain observed during testing. Both of these results are consistent with partial composite action in the specimen.

The average strains at loads of 89 kN and 111 kN in Specimen 4 are shown in Figure 72. As the strains after the shear cracks form appear to remain linear through the depth of the section, the plane section assumption remains acceptable near midspan in the CFRTP after the shear cracks form. The other specimens behaved similarly after cracking. Figure 73 shows that the midspan curvature increased linearly with bending moment until the shear cracks formed.

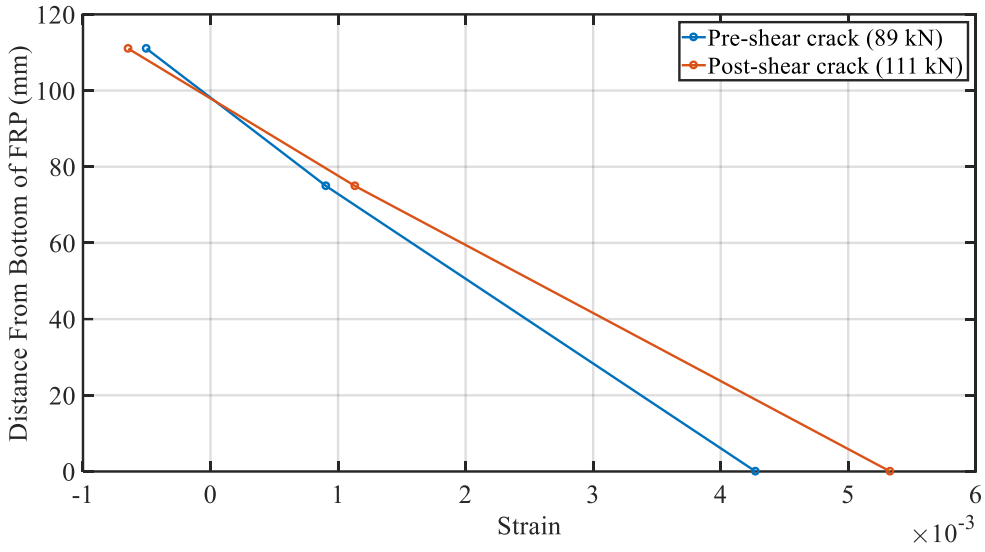

Figure 72: Average strains in Specimen 4 before and after the formation of shear cracks

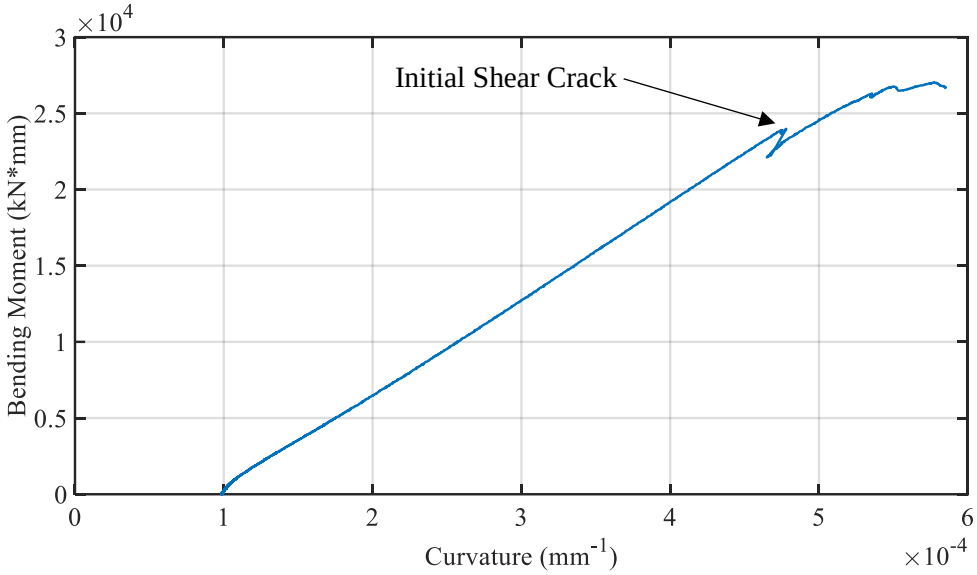

Figure 73: Bending moment vs midspan curvature for Specimen 4

4.4.2.3.2 Flexural Stiffness Analysis

The flexural stiffness of the hybrid beam, defined as the product of the elastic modulus and the section moment of inertia (EI), was calculated from the test results by two methods. For the first method, the flexural stiffness was calculated using the load and deflection data. The second method calculates the flexural stiffness from the relationship between moment and curvature.

For a beam in four-point bending, the relationship between load and midspan deflection without considering shear deformations is given in Equation 72 [17].

$$\Delta = \frac{P * L^3}{28 * EI} \tag{72}$$

$\Delta = midspan\ deflection\ of\ the\ beam$

$P = load\ applied\ by\ one\ load\ head$

$L = length\ of\ the\ beam$

$EI = flexural\ stiffness\ of\ the\ beam$

The flexural stiffness of the beam is also the ratio between bending moment and curvature, given in Equation 46, which is repeated below. The internal moment can be calculated from the load through Equation 43, which is repeated below. The curvature was found from the strain fit line shown in Figure 68 through Figure 71. The flexural stiffness was calculated as the tangent slope of the moment-curvature curve through Equation 73.

$$M = \frac{P * L}{3} \tag{43}$$

$$M = bending\ moment$$

$$\kappa = \frac{M}{EI} \tag{46}$$

$$EI = \frac{M_2 - M_1}{\kappa_2 - \kappa_1} \tag{73}$$

Using these equations, Figure 74 through Figure 77 were generated. From these plots, it can be seen that both methods show a flexural stiffness approaching infinity below a load of $20\ kN$. Above a load of $20\ kN$, the methods show a mostly constant flexural stiffness of $6 * 10^8\ kN * mm^2$. Using a cracked section analysis, the flexural modulus was predicted to be $8.15 * 10^8\ kN * mm^2$. The flexural stiffness observed in the testing was roughly 26% lower than the predicted flexural stiffness. This lower flexural stiffness is consistent with the model's under-prediction of strain in the bottom flange and the difference between predicted and measured neutral axis locations. These differences between the modeled and observed quantities could all be attributed to imperfect composite action.

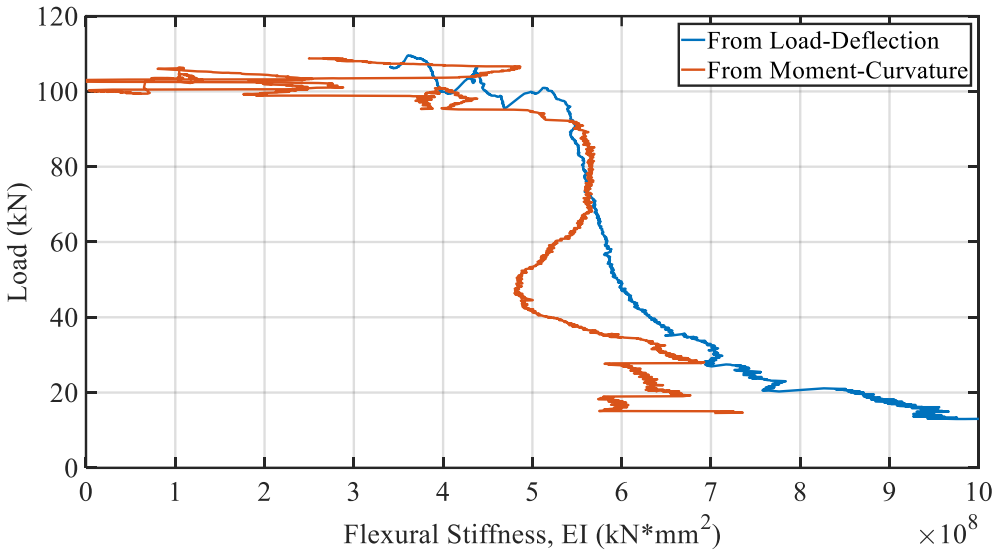

Figure 74: Flexural stiffness vs load of Specimen 1

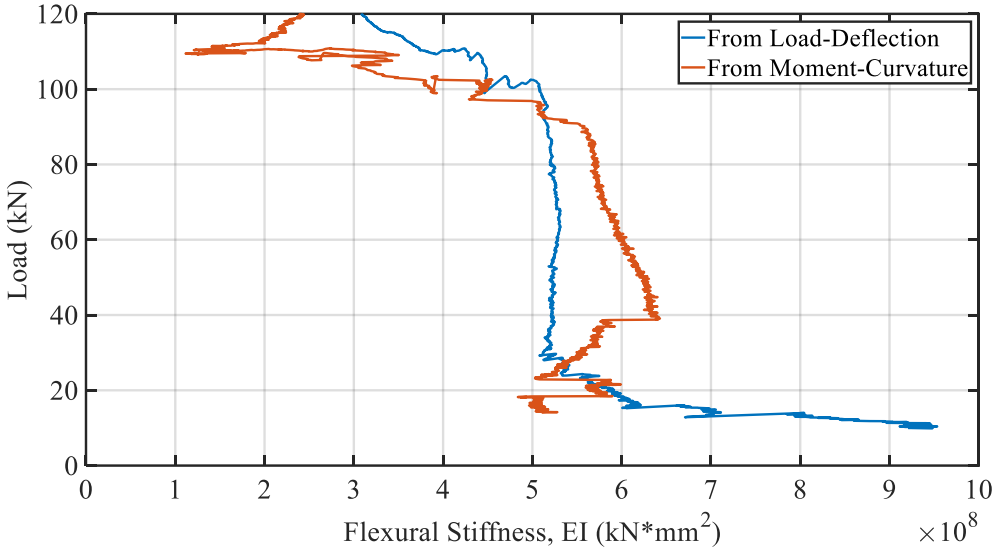

Figure 75: Flexural stiffness vs load of Specimen 2

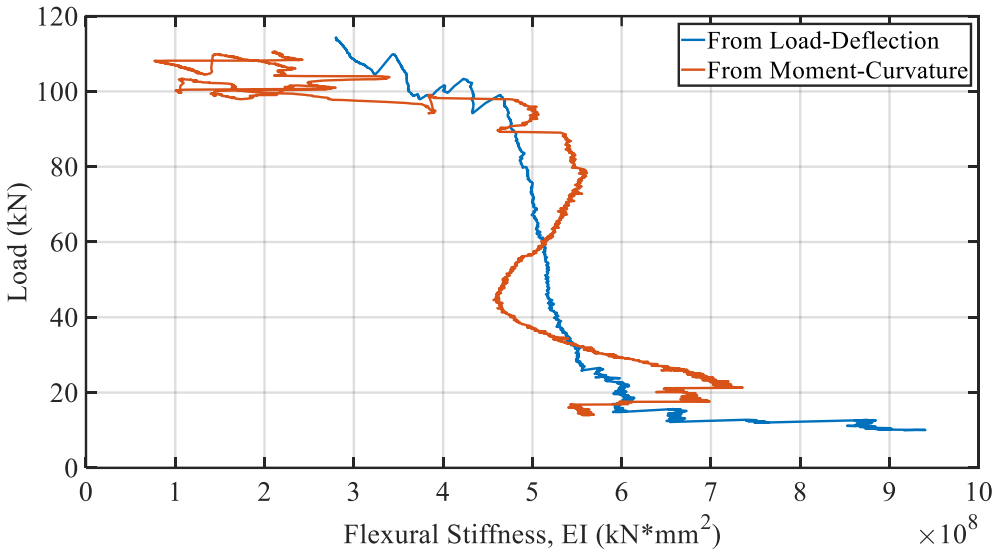

Figure 76: Flexural stiffness vs load of Specimen 3

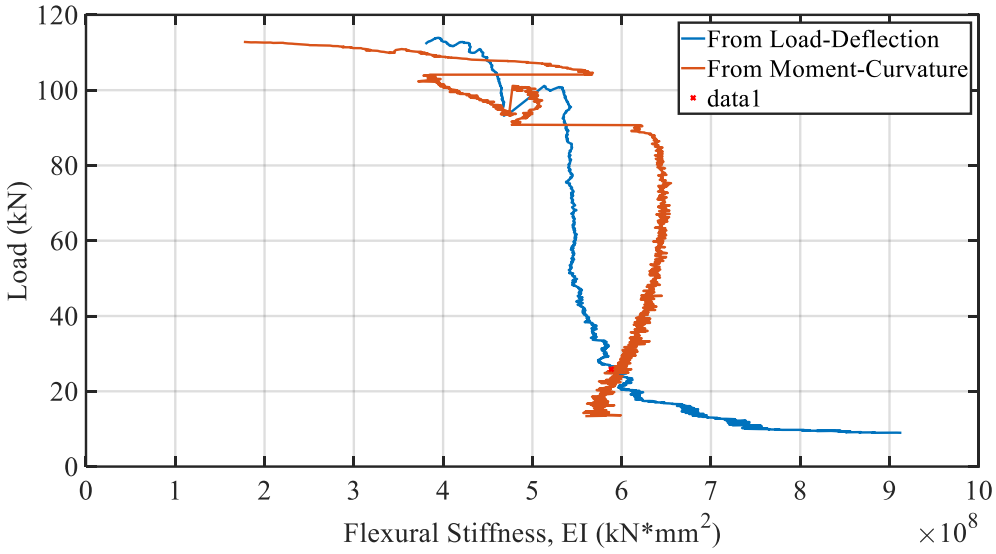

Figure 77: Flexural stiffness vs load of Specimen 4

4.5 Summary

Each of the four specimens was successfully manufactured and tested in four-point bending. The manufacturing of the corrugated CFRTP panels was a time-intensive process as the thermoforming parameters had to be determined through repeated testing. Installing the steel rods into the CFRTP

panel was a labor-intensive process that would not scale well into large-scale manufacturing. A CNC router similar to the one used at the ASCC would not be able to be used to cut the holes in the CFRTP if there were multiple corrugations in one part. A possible solution to this could be to cut the holes into the part before forming, but this could create a low quality part if the resin got too hot during the process. Each hole would also have to be aligned exactly to allow steel rods to run through multiple corrugations.

When each specimen was tested, it met the required load set by AASHTO for stay-in-place formwork and bridge decking before failure. No cracks formed during the stiffness tests. The ultimate failure of the beams resulted from a shear failure in the concrete. Two layers of reinforcing steel are used in conventional bridge decks, which help to contain temperature and shrinkage cracks as well as resist shear in the concrete. With this technology, extra reinforcement would be required along the top face of the concrete in a real scenario, which could potentially increase the capacity of the beam, as this reinforcement would help resist the shear that caused failure in the tests.

Overall, the testing found that this configuration was strong enough to meet the required loads set by AASHTO's Strength I load case, but the time and effort required to manufacture these was significant. To reduce the manufacturing time for the next round of testing, the size of the bearing holes was increased, which would allow concrete to flow through the holes. This eliminated the need for exact hole placement.

CHAPTER 5

STIFFENED PANEL DESIGN AND TESTING

5.1 Introduction

The second method that was used to add flexural stiffness to the CFRTP panels was adding stiffeners. The added stiffeners would allow the panel to carry the weight of the wet concrete during construction. Holes were cut through the stiffeners, similar to a perfobond rib shear connector [5], to facilitate shear transfer between the CFRTP panel and the concrete.

The configuration chosen for this set of testing was a flat panel that would act as the main tension reinforcement for the concrete beam with two angle stiffeners welded to the top of it. The two stiffeners were oriented such that their respective vertical flanges ran back to back along the center of the flat panel. A cross-section of this concept is shown in Figure 78. Holes drilled through both vertical, parallel legs are filled with concrete during the deck pour, and serve to transfer shear from the CFRTP to concrete in direct bearing much like a perfobond rib shear connector.

When used with a steel beam, perfobond rib shear connectors are welded to the steel beams. While welding is still possible with a thermoplastic like PETg, the strength of a PETg weld is considerably less than that of a steel weld, as evidenced by the results of the flat panel tests discussed in Chapter 4. To offset this weakness, the angle section shear connectors used for this testing were continuously welded to the bottom plate to maximize the area of the weld.

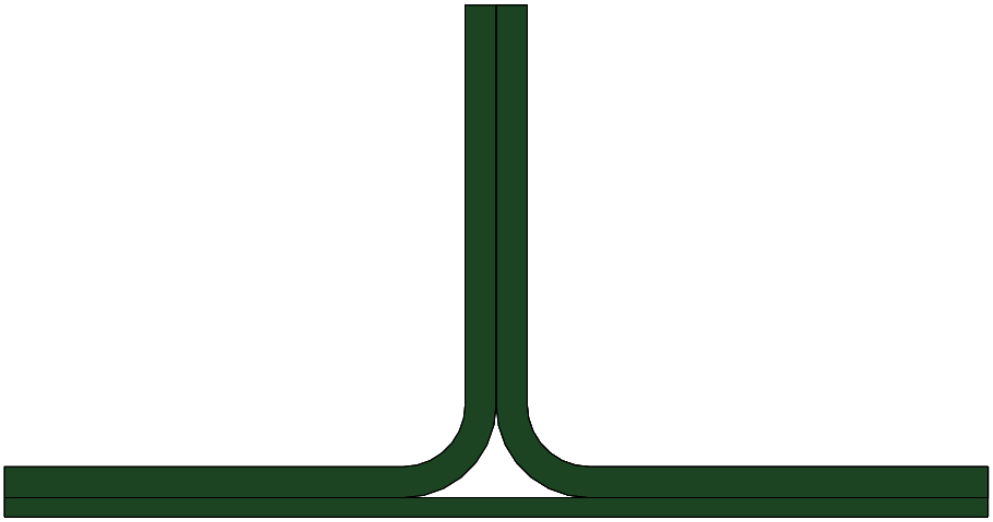

Figure 78: Cross-section of stiffened CFRTP panel

5.2 Design

Full-scale hybrid corrugated CFRTP-concrete test specimens were designed to meet the factored AASHTO Strength I requirements for a bridge deck with stay-in-place formwork. The same two load conditions were considered:

- The weight of the wet concrete before it cures on the stiffened CFRTP panel
- The maximum positive moment from the AASHTO HL-93 truck or tandem on the hybrid beam

The length of the corrugated panel and hybrid beam was chosen to be $1524\ mm$, the longest panel that can be thermoformed at the ASCC using automated manufacturing.

The MATLAB code developed for the corrugated panels was modified to accommodate the stiffened panel geometry and unique differences. For the design, the section was broken into four parts as shown in Figure 79. The four parts are the bottom plate, the horizontal legs of the angles, the vertical legs of the angles below the hole, and the vertical portion of the angles above the hole. The simplified model used for design of the panel did not include the curves in the angles and

ignored the portions of the angles' vertical legs that coincide with the holes drilled for shear transfer.

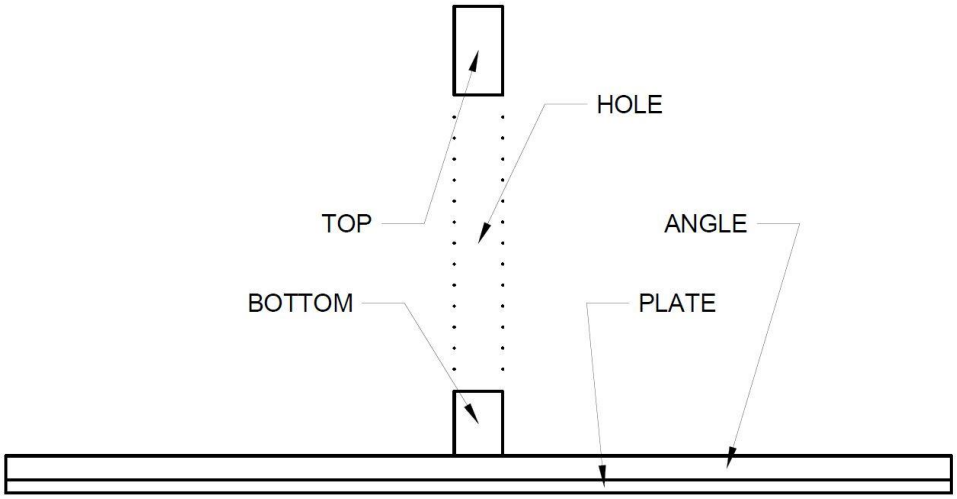

Figure 79: Simplified model of the stiffened panel used for design

5.2.1 Final Design

The final design of the cross-section of the stiffened CFRTP panel is shown in Figure 80. The length of each flange of the angles was chosen to be $102\ mm$ to allow enough room for a $64\ mm$ hole to be cut into the vertical flange and still have enough material above the hole to carry most of the compressive forces during the construction loading test. The length of each flange of the angle was chosen to be equal for ease of manufacturing. The width of the backer plate was chosen to be equal to the width of the two angles back to back. In a real application, the stiffeners could be spaced on a wider backing plate to optimize the design. As with the corrugated panel, the thickness of each laminate was determined by the number of layers required. The layup for the bottom flange was designed to have mostly unidirectional fibers, as it served as the main tension reinforcement for the structure. The angles were designed with an even mix of unidirectional and biaxial fibers to provide shear and bearing resistance.

$$Backer\ Plate = [0_3/\pm 45/0_3/\pm 45/\mp 45/0_3/\mp 45/0_3]$$

$$Angle = [0_2/\pm 45/0_2/\pm 45/0_2/\pm 45/\mp 45/0_2/\mp 45/0_2/\mp 45/0_2/\mp 45/0_2]$$

As with the corrugated panels, the inner and out radii for the angles was chosen to be twice and thrice the thickness of the angle respectively to avoid springback and fiber wrinkling at the recommendation from ASCC staff members' experience in composites fabrication (J. Anderson, personal communication, July, 2018).

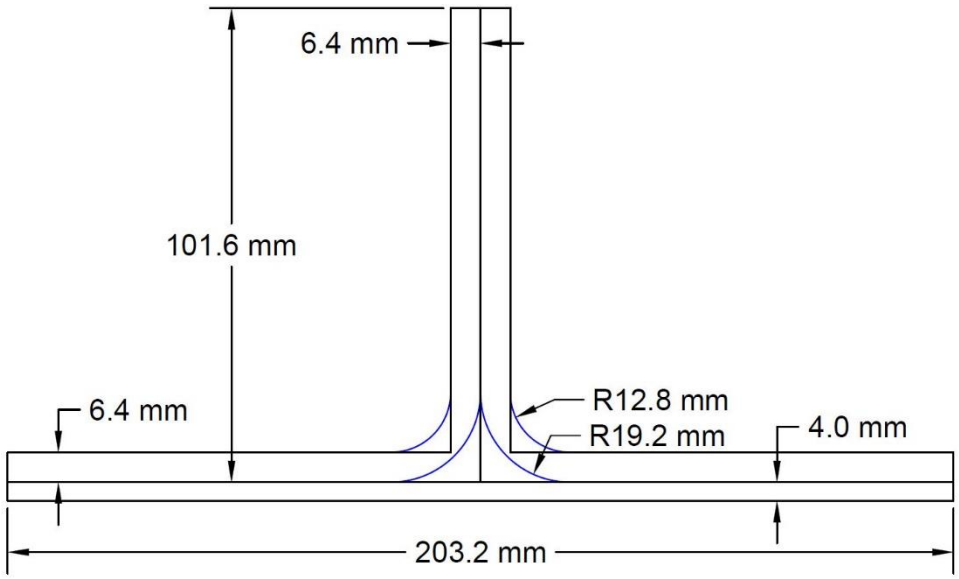

Figure 80: Design dimensions of stiffened CFRTP cross-section

To transfer shear between the stiffened CFRTP panel and the concrete, holes were cut out of the vertical flange of each angle during manufacturing. These holes allowed concrete to flow through the CFRTP panel and form a dowel, which would transfer the bending forces between the two parts through bearing. The diameter of the holes was chosen to be $64\ mm$. This diameter was chosen to allow a #4 (US customary) rebar to run through the center of the hole while leaving about $25\ mm$ of clear space on all sides to allow the concrete aggregate to enter the hole. Rebar would be required in an in-service deck to resist temperature and shrinkage. Each angle had ten holes cut out of it, which were spaced at $152\ mm$ on center. The center of the hole at each end was $76\ mm$ from the end face of the beam. The center of each hole was $51\ mm$ below the top face of the vertical flange

of the angles. This left 19 mm of continuous fibers above the holes to carry the compressive forces in the stiffened panel. The location of the holes is shown in Figure 81.

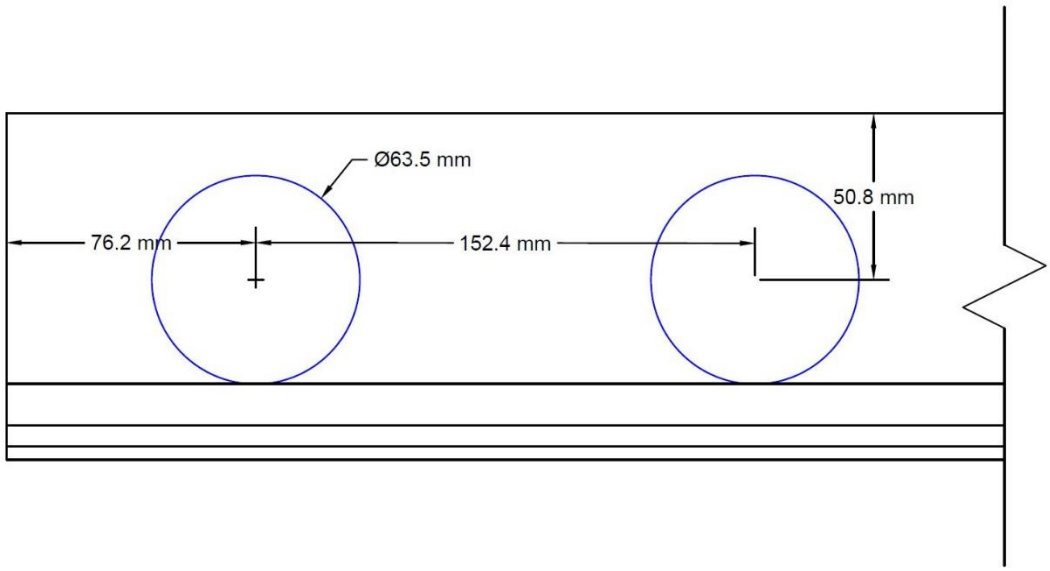

Figure 81: Side view of stiffened panel showing the size and location of the holes

Two #3 (US customary) bars were also run longitudinally just above the transverse rebar to prevent the premature transverse concrete cracking that was observed in the corrugated panel tests detailed in Section 4.4.2.3, 38 mm of clear cover was included at the end of each bar. The longitudinal rebar was not considered in any of the flexural calculations.

The stiffened CFRTP panels were then filled with concrete up to 64 mm above the top of the vertical flange of the angles. The width of concrete was chosen to be the full 203 mm width of the stiffened CFRTP panel. The location of the concrete relative to the stiffened CFRTP panel is shown in Figure 82.

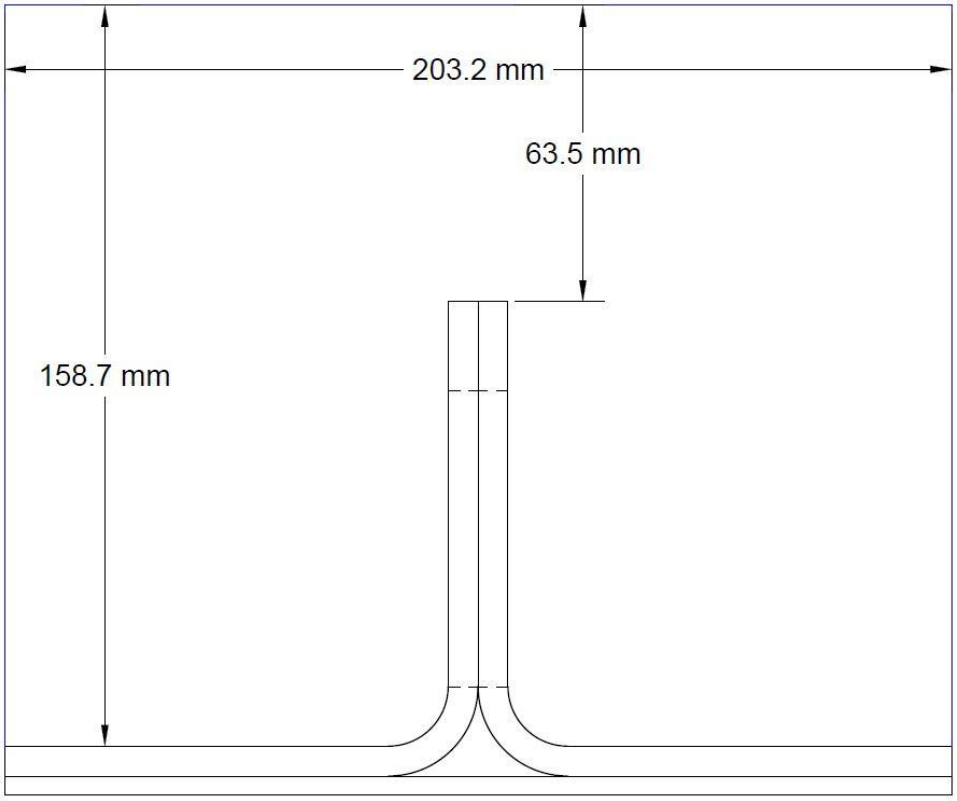

Figure 82: Design dimensions of concrete on the stiffened panel cross-section

5.2.2 Construction Loading on CFRTP Stiffened Panel

The design for the construction loading case for the stiffened panel was performed similarly to the design done with the corrugated panel discussed in Section 4.2.2. The differences are given in this section.

As the panel is narrower, the loads that needed to be applied to meet the AASHTO Strength I requirements were smaller. The required maximum shear and moment in the beam from the distributed load given by the AASHTO Strength I loading requirements were $0.88\ kN$ and $314\ Nm$ respectively. The load that needed to be applied in a four-point bend test to match those shear and moment requirements were $1.77\ kN$ and $1.33\ kN$ respectively. As the higher of those two loads, $1.77\ kN$ was chosen as the benchmark for this set of testing.

The nominal moment capacity calculations and the strength analysis were performed in the same manner as with the corrugated panels.

5.2.2.1 Stability and Serviceability Analysis

As the vertical flange was unrestrained for buckling under the construction loads besides at the load heads, two buckling checks were included in the analysis. First, the angles were checked using an elastic buckling check meant for steel angles [17] shown in Equation 74, which was assumed to apply to a thermoplastic angles even though it is not an isotropic material.

$$F_{cr} = \frac{0.71E_x}{\left(\frac{b}{t}\right)^2} \tag{74}$$

$E_x = longitudinal\ elastic\ modulus$

$b = width\ of\ the\ plate, taken\ as\ the\ length\ of\ the\ stiffener\ leg$

$t = thickness\ of\ the\ plate$

Another elastic buckling equation, shown in Equation 75, was checked that is meant for a rectangular plate, simply supported on three sides [18]. This equation does not assume that the material is isotropic.

$$F_L^{cr} = \left(\frac{t}{b}\right)^2 \frac{\pi}{6}\left(\frac{1}{2}\left(\frac{b}{a}\right)^2 E_L + \frac{6}{\pi^2}G_{LT}\right) \tag{75}$$

$t = thickness\ of\ plate$

$b = unbrace\ length\ \left(\frac{L}{3}\right)$

$a = width\ of\ the\ plate, taken\ as\ the\ length\ of\ the\ stiffener\ leg$

$E_L = longitudinal\ elastic\ modulus$

$G_{LT} = In - plane\ shear\ modulus$

5.2.2.2 Expected Failure Modes

Several common types of failure modes were analyzed to predict a failure load of the corrugated CFRTP panel. The first mode considered was CFRTP failure from the combined effects of longitudinal, transverse, and shear strains. Figure 40 shows the minimum strength ratio, defined as the failure stress or strain at that location within the cross-section divided by the respective internal stress or strain at that location, across the entire height of the cross-section. The three failure criteria discussed in Section 2.3.2 were each used to evaluate the section. For the Hashin and Maximum strain criteria, the minimum of their respective failure modes for each lamina is taken. For the Tsai-Wu criteria, there is only one failure mode so the minimum of each lamina is taken.

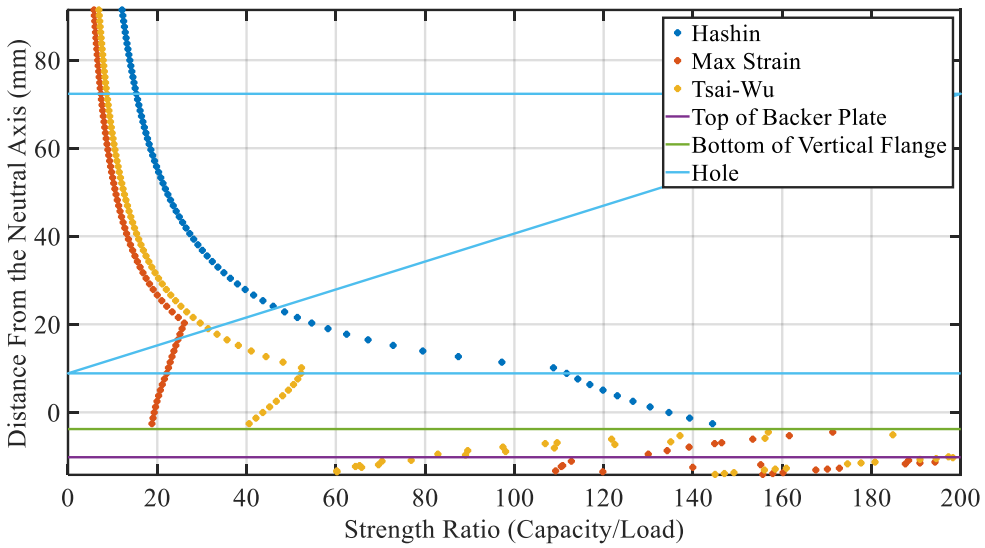

Figure 83: First-ply failure strength ratios over the section under wet concrete loads

Using the maximum strain failure criteria, the minimum strength ratio was 5.8 in the extreme compression fiber. This indicated that first-ply failure would occur at a load of 10.3 kN, more than the AASHTO required load of 1.77 kN.

The elastic buckling failure modeled by Equation 74 was also investigated. Under the considered construction loads, the strength ratio was found to be 5.5, which would correspond to a four-point

bend failure load of $9.8\ kN$. If the two vertical legs of the angles were fastened or formed together, the load in a four-point bend test that would cause this failure would increase to $19.6\ kN$.

For the elastic buckling failure modeled by Equation 75, the strength ratio was found to be 2.7, which would correspond to a four-point bend failure load of $4.7\ kN$. If the two vertical legs of the angles were fastened or formed together, the load in a four-point bend test that would cause this failure would increase to $9.4\ kN$.

5.2.3 Ultimate Loading on Composite CFRTP-Concrete Beam

The design for the ultimate loading case for the stiffened panel was performed similarly to the design done with the corrugated panel discussed in Section 4.2.3. The differences are given in this section.

As with the construction loading case, the loads that needed to be applied to meet the AASHTO Strength I requirements were smaller for the stiffened panel than the corrugated panel because the specimen is not as wide. The required maximum shear and moment in the beam from the distributed load given by the AASHTO Strength I loading requirements were $28.2\ kN$ and $10{,}042\ Nm$ respectively. The load that needed to be applied in a four-point bend test to match those shear and moment requirements were $56.5\ kN$ and $21.2\ kN$ respectively. As the higher of those two loads, $56.5\ kN$ was chosen as the benchmark for this set of testing.

The other analyses were performed in the same manner as with the corrugated panels.

5.2.3.1 Expected Failure Modes

The same failure modes that were examined for the ultimate loading of the composite CFRTP-concrete corrugated panel were also evaluated for the composite CFRTP-concrete stiffened panel. The first mode considered was concrete crushing at the top of the beam between the load application

points in the constant moment region. Crushing was expected to occur at a total load of $237\ kN$ in 4-point bending.

Next, first-ply failure of the composite laminates was considered. All of the failure theories predicted the first failure to be in the vertical flange of the angle. Maximum strain predicted the lowest failure load of $224\ kN$. This was a matrix-dominated failure mode so it was not expected to cause ultimate failure of the structure.

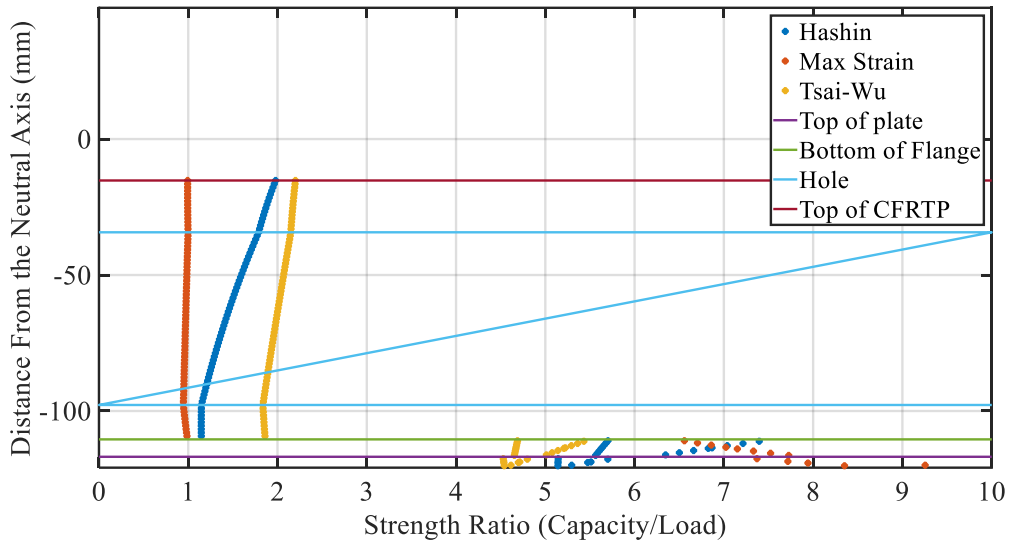

Figure 84: First-ply failure strength ratios over the hybrid section under ultimate loads

After that, failure at the bearing connection was considered. Two types of failures were considered: shear failure of the concrete dowel that was formed and bearing failure of the CFRTP. For failure of the concrete dowel to occur, the concrete and rebar at either end of the dowel would have to fail in shear. To predict the failure, the concrete shear strength was found using Equation 70 where the area considered was twice the area of the hole less the area of the rebar. The shear strength of the rebar was found using Equation 76 [19]. The sum of these two strengths was compared with the shear force calculated with the method described in Section 4.2.3.4 to determine a failure load. The

shear strength of the concrete portion was found to be $6.6\ kN$. The shear strength of the rebar was found to be $35.2\ kN$. The total strength of one dowel was then calculated to be $41.8\ kN$.

$$V_n = 0.6F_yA_s \tag{76}$$

The concrete dowels were expected to fail in shear at a four-point bending load of $1312\ kN$. However, without the #3 (US customary) rebar that was run through each hole, the concrete dowels would have been expected to fail in shear at a load of $212\ kN$. To evaluate a CFRTP bearing failure, the strength was determined as the product of the bearing strength, found through testing as described in Section 2.2.2, and the approximate bearing area, which was taken as the product of hole diameter and the total thickness of the two stiffeners. The bearing strength of each hole was found to be 146 kN. The CFRTP was expected to fail in bearing at a four-point bending load of $4569\ kN$.

The concrete alone was expected to carry a load of XX kN before failing in shear. This was calculated using the concrete shear strength equation used by ACI, given in Equation 70.

The expected failure mode was the concrete crushing at a load of $237\ kN$.

5.3 Manufacturing

Eleven stiffened panels were manufactured at the ASCC. The first four were trial specimens that were used to evaluate different manufacturing methods. The next two panels were tested to failure in four-point bending. The remaining five panels had concrete poured on them to form composite CFRTP-concrete beams and were then also tested to failure in four-point bending.

Each stiffened panel was made by combining three pieces: one backer plate and two angles. For all of the trial and test specimens, the process for manufacturing the tailored blanks and consolidating them was identical.

The usable dimensions of each tailored blank was 203 mm by 1524 mm. Each tailored blank consisted of a constant layup throughout the entire laminate. The design layups chosen for the two different layups are given below. The backer plate tailored blanks were 20 layers thick. The angle tailored blanks were 32 layers thick.

$$Backer\ Plate = [0_3/\pm 45/0_3/\pm 45/\mp 45/0_3/\mp 45/0_3]$$

$$Angle = [0_2/\pm 45/0_2/\pm 45/0_2/\pm 45/0_2/\pm 45/\mp 45/0_2/\mp 45/0_2/\mp 45/0_2/\mp 45/0_2]$$

Each tailored blank was consolidated by heating them while under pressure in a hydraulic press. Six panels could be consolidated simultaneously using two sets of three panels side by side separated by an aluminum panel. One of the consolidated panels is shown in Figure 85. A consistent consolidation and clean finish was achieved for the panels in this set of manufacturing. The panels were then trimmed using a waterjet to the design dimensions of 203 mm by 1524 mm.

Figure 85: Consolidated panel for the angle stiffened panel

5.3.1 Angle Forming

The next step in manufacturing was to form the consolidated angles into the angled shape. To do this, the consolidation platens inside the hydraulic press were replaced with the aluminum mold shown in Figure 86. Each panel was heated in the IR oven, and then moved with the robot arm into the mold.

Figure 86: Angle mold in the hydraulic press

The first several trials were made with the mold inverted from what is shown in Figure 86 so the female mold was on the bottom side of the press. For the first two trials, the bearing holes were cut into panels between consolidation and forming. The holes combined with the female mold being on bottom led to the angles becoming very misaligned inside of the mold as the mold closed. One of the panels formed with this method is shown in Figure 87.

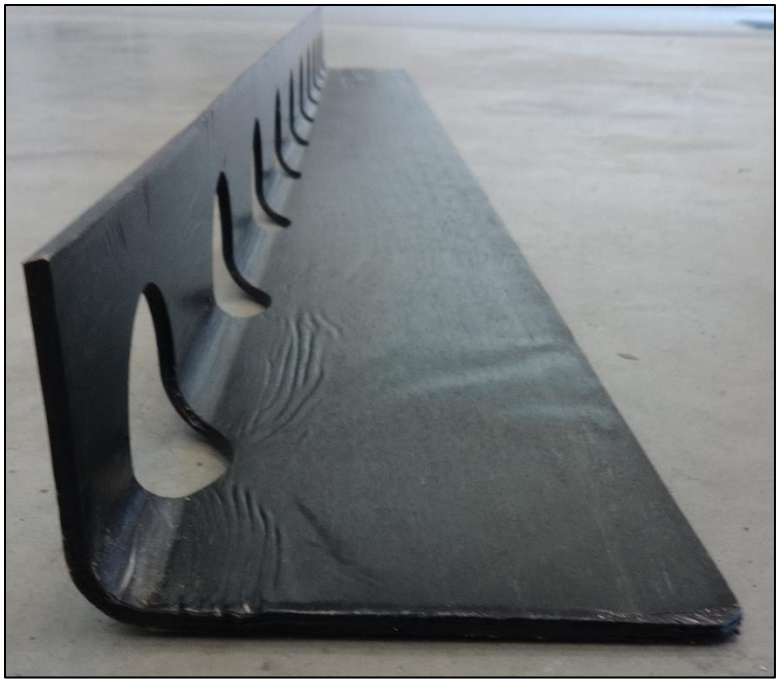

Figure 87: Misaligned angle with holes cut before forming

To attempt to fix the misalignment problems observed in the initial trials, holes were not cut into angles until after forming for the remaining trials and test specimens. The next trial, formed without holes and with the female mold on bottom, also turned out misaligned but to a lesser extent than the previous trials.

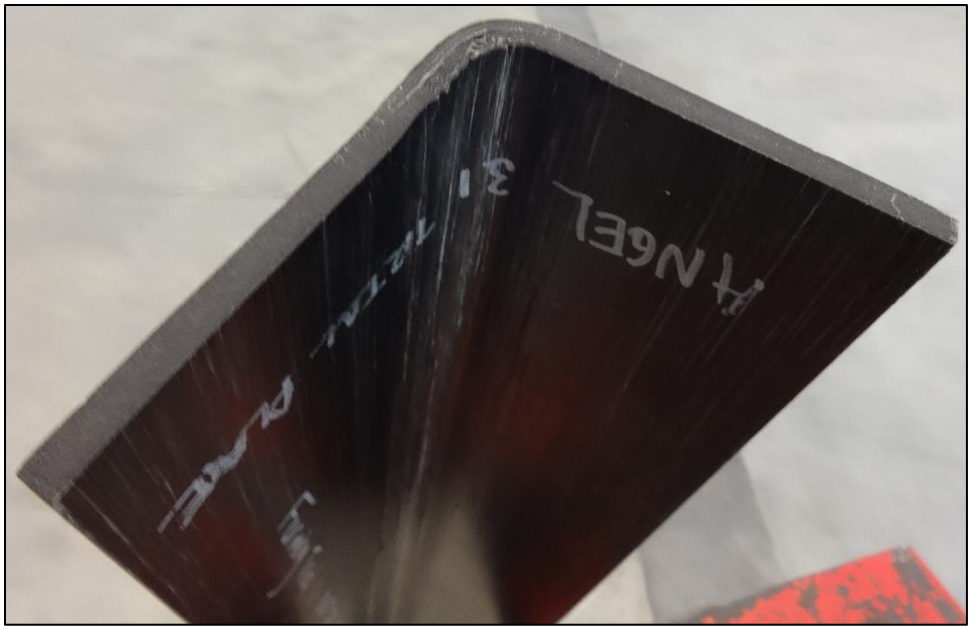

Figure 88: Misaligned angle with holes cut after forming

After that trial, the male and female molds were switched into the alignment that is shown in Figure 86. The next trial was also placed into the mold misaligned, but it was extracted and flattened before it solidified in a misaligned shape. To force alignment in the rest of the specimens, alignment pins were installed into the mold at each end. Holes were cut into the ends of each consolidated panel to line up with the alignment pins. Figure 89 shows one of the successfully formed panels while it is still on the mold with the alignment pin holding it in place. This method provided good, repeatable results so it was used to form the rest of the angles for the test specimens.

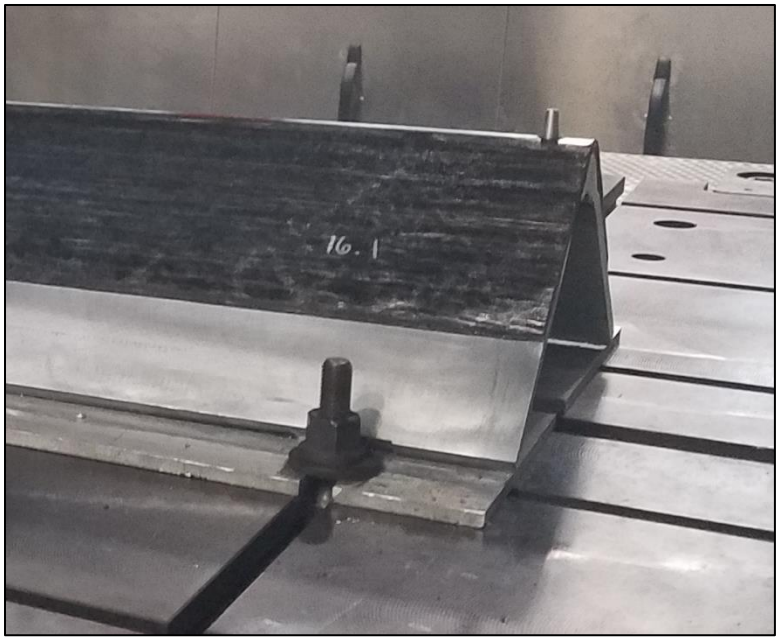

Figure 89: Male angle mold with alignment pins

5.3.2 Stiffened Panel Forming

Next, two stiffeners were attached to each backer plate. To do this, the angle mold was removed from the press, and the top platen and the structure mold were installed. The structure mold is shown in Figure 90. Two stiffeners were then loaded into the mold with the flange with the holes cut out of it pointing down; this is shown in Figure 91. Once the stiffeners were loaded into the mold, the two halves were clamped together to prevent any movement during the manufacturing process.

Figure 90: Structure mold in the hydraulic press

Figure 91: Structure mold with angles inserted

A piece of PET foam core material was pressed into the gap between the two curves in the angles to fill the void than would form there. The PET core was not expected to carry any load so it was discounted in all calculations.

The next step was to fasten the backer plate to the stiffeners. Several methods were tried to achieve this with varying success.

For the first method, the backer panel was put into place by hand then the top platen was lowered until there was $690\ kPa$ on the part. The top platen and the mold were then heated from the press. The press was heated until the interface between the backer plate and stiffeners reached the desired forming temperature. The temperature at the interface was monitored with a series of

thermocouples mounted between the two laminates. The part was then allowed to cool under pressure. As the press had no method of cooling itself, the part was left to cool overnight. The part was removed from the mold the next morning.

The formed part is shown in Figure 92. The backer plate was successfully bonded to the two stiffeners, but the vertical flanges of the stiffeners were heated more than expected. This caused the top of the stiffeners and the holes to deform. Some fiber wash near the edges of the backer plate was also observed. It also appeared that one side of the press was getting significantly warmer than the other as most of the issues were limited to one-half of the specimen, the left half in Figure 92.

Figure 92: First method of forming stiffened panel

Figure 93: Observed issues with the first stiffened panel forming method

Next, a similar method was used except that only the top platen was heated. With this method, the interface would not have reached the desired bonding temperature without overheating the top, which could cause burning, fiber wash, and dry spots in the backer plate. It is expected that the mold and bottom of the press acted as a heat sink, which pulled the heat out of the bottom of the part faster than the heat would penetrate through the backer plate to the bonding interface.

The third method was a combination of the first two trials. Both the top platen were heated until they reached $93°C$ then the bottom heating was cut out so only the top platen kept heating. To confirm the above suspicion that the press was heating unevenly, only one-half of the surface was bonded during this process. The part was removed from the press and rotated 180° then replaced into the mold. The same process was repeated to bond the other half of the surface. This method took two days to make one panel as the heating and cooling cycle had to be performed twice. Some fiber wash was observed at the edges of the backer plate but the holes and the vertical flange of the stiffener remained intact.

The fourth method was different from the others in an attempt to reduce the cycle time. The backer plate heated in the IR oven to a temperature of $188°C$ then held at that temperature for 90 seconds

to allow the heat to penetrate into the center of the laminate. While this was happening, the top platen was lowered until it was near the stiffeners, but not touching them. The top platen was then heated until the face of the stiffeners reached $93°C$. The press and the IR oven then opened and a robot arm moved the heated backer plate from the oven onto the preheated stiffeners. The press then lowered until there was $690\ kPa$ on the part. The part was then allowed to cool for an hour then removed from the mold. This method yielded the best results. No fiber wash or deformations were observed and an even bond appeared to have been achieved. This method was used also to form the remaining four stiffened panels. Each panel was then trimmed to the design width of $203\ mm$ on a wet tile saw.

Figure 94: Stiffened panel made with the fourth forming method

5.3.3 Composite CFRTP-Concrete Beam Manufacturing

Each of the seven complete stiffened panels (one from forming method one, one from method three, and five from method four) then had strain gauges soldered onto them for testing. The locations of these strain gauges are discussed in Section 5.4.1.1. The two panels formed with method one and three were tested as bare panels to assess their performance as stay-in-place formwork; this testing

is discussed in Section 5.4.1. The remaining five specimens were cast into concrete beams to form a composite CFRTP-concrete beam.

To enable concrete casting, wooden formwork was made for each specimen. $102\ mm$-long spacers were included at each end of the formwork to mimic supports. These spacers allowed the CFRTP to deform during the concrete pour; this was done to mimic the real-life scenario where stresses would be locked into the stay-in-place CFRTP formwork before the concrete cured. A graphic of a stiffened panel sitting in the formwork can be seen in Figure 95 including the longitudinal and transverse rebar detailed previously. The transverse bar at each end was held in place by plastic ties that were attached to wooden blocks above the formwork, and the longitudinal bars rested on top of the transverse bars. The remaining transverse bars were tied to the longitudinal bars to keep them in place. One of the panels is shown in Figure 96 inside the formwork.

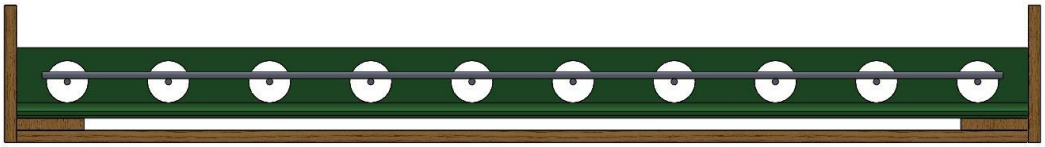

Figure 95: Side view of stiffened panel in the formwork (sides removed)

Figure 96: Stiffened panel in the formwork with rebar and instrumentation installed

Silicone was used to seal around the edges of the panel to prevent water from getting below the panel. The concrete detailed in 2.2.3 was then poured around the specimen to create the composite CFRTP-concrete beams.

Figure 97: Composite stiffened CFRTP-concrete beam specimen, 3 days after pour

5.4 Quasi-Static Testing

As with the corrugated panels, two sets of quasi-static testing were done with the stiffened CFRTP panels. For the first set of tests, two of the panels were initially loaded in four-point bending up to the AASHTO required load for stay-in-place formwork for a bridge deck three times to measure the stiffness. Those panels were then loaded until failure to measure the ultimate capacity. Concrete was poured on the five remaining panels to create composite CFRTP-concrete beams. For the second set of tests, the five beams were initially loaded in four-point bending up to the AASHTO required load for a transversely spanning bridge deck three times to measure stiffness. Those panels were then also loaded until failure to measure the ultimate capacity.

5.4.1 Construction Loading Test

The purpose of the construction loading test was to verify that the stiffened CFRTP panel could carry the weight of the wet concrete during construction without excessive deformation or damage. Two of the specimens were loaded in four-point bending to a load of $1.77\ kN$ then unloaded three

times. The loading of 1.77 kN was chosen as this created a maximum shear in the beam under four-point bending equal to the design distributed load specified by AASHTO for stay in place formwork. The loading is discussed further in Section 4.2.2.1. The panel was then loaded until failure.

Specimen 1 was formed using the first method to bond the backer plate to the angles. Specimen 2 was formed using the third method. Both of these methods were outlined in Section 5.3.2.

5.4.1.1 Test Setup and Instrumentation

The fixtures used for this testing were similar to those used for the testing of the corrugated panels. As can be seen in Figure 98, two back-to-back steel channels were used as a spreader to separate the load points to the third points of the span. Custom load heads were manufactured that slid onto the spreader beam, applied the load directly to the horizontal leg of the angles, and braced the vertical leg against buckling. 13 mm-thick neoprene pads were used at each support and under each load head to distribute the loads and lessen the effects of any stress concentrations.

Figure 98: Construction loading test setup

Three string potentiometers were used to measure the vertical deflection at midspan and directly under each load head. A linear displacement transducer (LDT) was attached at each support to measure any deflection in the neoprene at the support. Six strain gauges were installed at two points along the span of the beam: at midspan and 305 mm from one end of the beam. As is shown in Figure 99, two were installed on either side of the vertical leg and two were installed on the bottom of the panel.

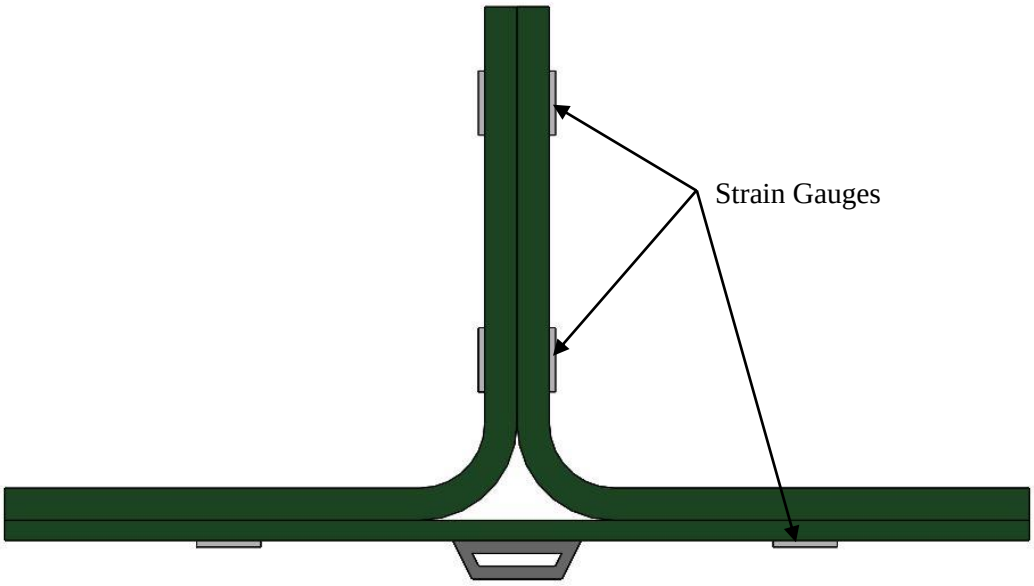

Figure 99: Strain gauge locations on stiffened panel cross-section

5.4.1.2 Test Procedure

The two stiffened panels were quasi-statically loaded in four-point bending. After the instrumentation was installed, the load head was lowered manually until it was in contact with the specimen. The load head was then lowered at a constant rate of $2.54\ mm/minute$ until the load on the specimen reached the AASHTO required load of $1.77\ kN$, at which point the load head was raised at the same rate. This cycle was repeated two more times to evaluate the stiffness of the stiffened panel. The load head was then lowered at the same rate until the stiffened panel failed.

5.4.1.3 Discussion of Results

Both specimens tested under the construction loading reached the required AASHTO design loading without sustaining visible damage. Figure 100 shows the load-midspan deflection plot for the data gathered during the stiffness tests. Each specimen was displaced until it was had $2\ kN$ of load on it, except for the third cycle of Specimen 1, which was only loaded to the required load of $1.77\ kN$. The difference in the magnitude of the loads shown in the data was likely caused by the load being measured with a $490\ kN$ load cell, which was significantly larger than the applied loads.

The midspan beam deflection was computed by subtracting the support compression, measured by the LDT at each support, from the total midspan deflection, measured by a string potentiometer at midspan.

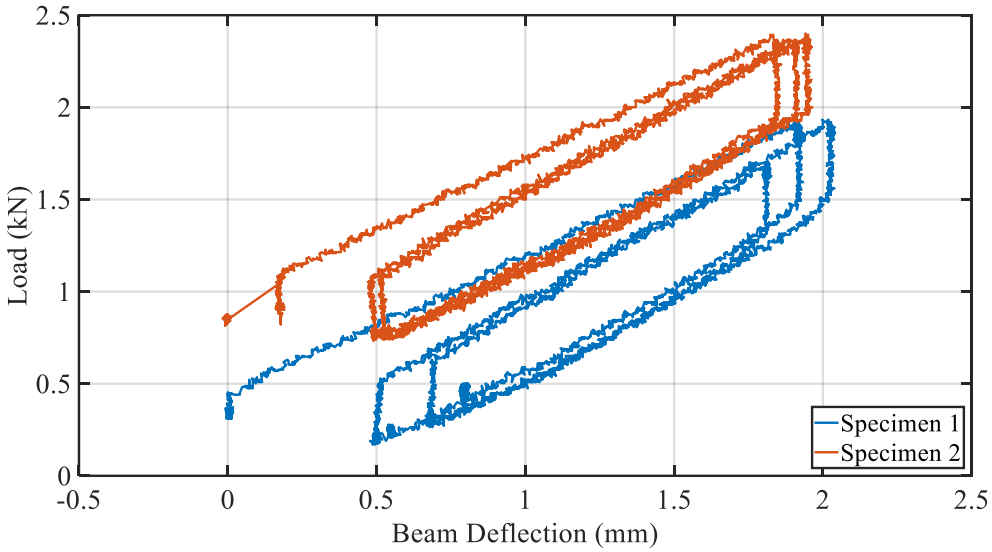

Figure 100: Construction loading stiffness test load vs midspan deflection

The stiffness during the loading in each cycle is summarized in Table 18. This stiffness was found by calculating the slope between two points during the loading in each cycle. For Specimen 1, the slope was taken between loads of 0.89 kN and 1.33 kN. For Specimen 2, slope was taken between loads of 1.33 kN and 2.22 kN. An approximate stiffness of 0.61 kN/mm was calculated using Equation 72. The approximate stiffness was about 30% lower than the average measured stiffness of 0.89 kN/mm. The higher observed stiffness could come from the simplified model, shown in Figure 79, which removed some material to provide a simple, conservative model.

Table 18: Stiffness results from construction loading test (kN/mm)

Specimen	Cycle			Average
	1	2	3	
S1	0.82	0.92	1.01	0.92
S2	0.77	0.89	0.90	0.85

Following the stiffness tests, both specimens were loaded until failure. The load-deflection plot for the failure tests are shown in Figure 101. The two specimens behaved differently during the loading, but failed in the same failure mode of buckling the vertical legs between the load heads. Specimen 1 showed a much higher initial strength, but failed at a much lower deflection than Specimen 2. The expected cause of the higher strength was that during the manufacturing of Specimen 1, the two vertical legs were inadvertently bonded together creating one thick leg instead of two thin legs. The two peaks in the curve around a load of 9 kN correspond to the bond between the two vertical legs breaking. After the legs separate, the load carried by Specimen 1 drops to a load similar to that carried by Specimen 2 at a similar deflection.

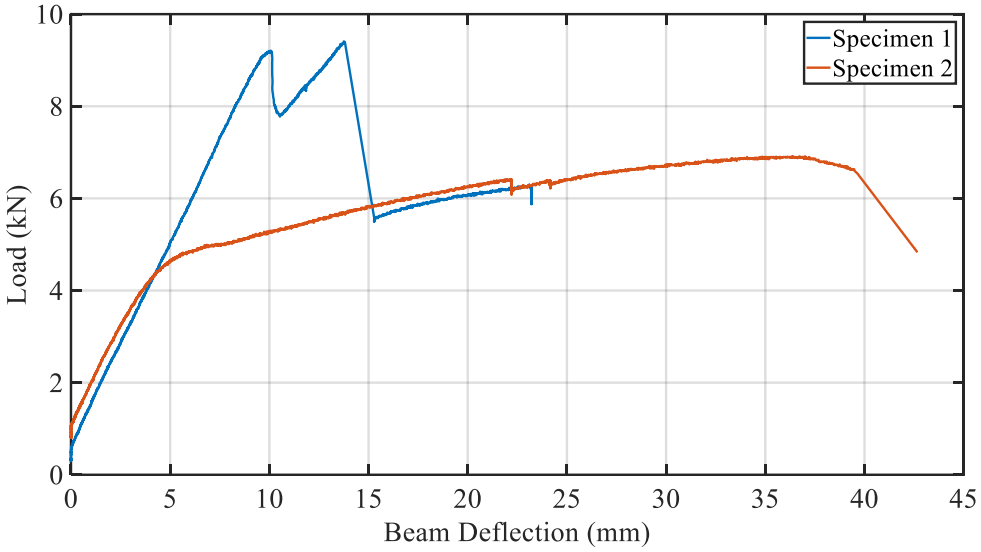

Figure 101: Construction loading failure test load vs midspan deflection

The buckling observed in Specimen 1 after the bond between the two vertical legs broke, shown in Figure 102, was not symmetrical.

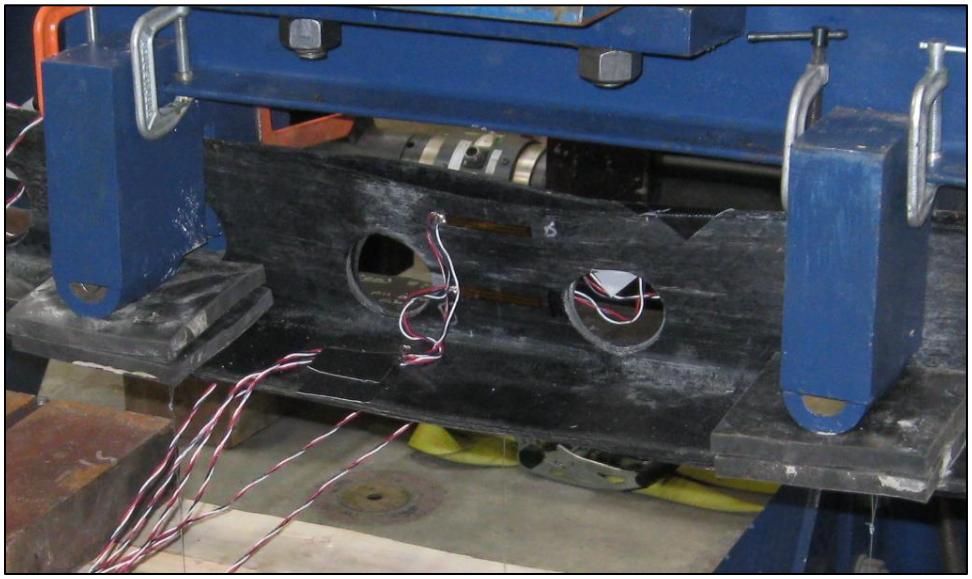

Figure 102: Buckling failure on Specimen 1

The initial buckling observed in Specimen 2, shown in Figure 103, was symmetric starting around a load of 4 kN. The buckling increased until failure, shown in Figure 104, around a load of 7 kN.

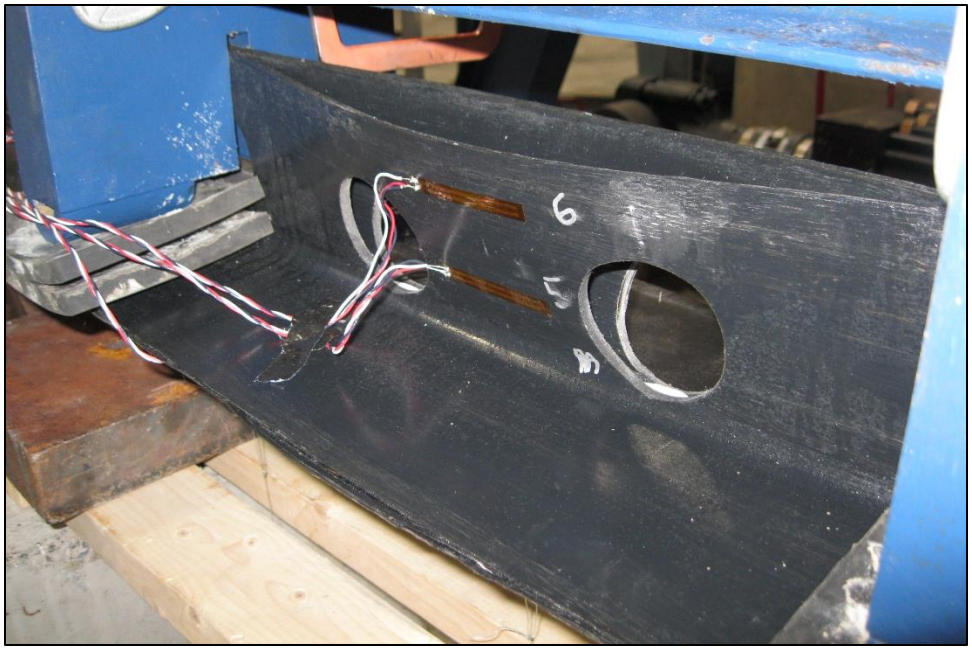

Figure 103: Initial Buckling of Specimen 2

Figure 104: Buckling failure of Specimen 2

5.4.2 Ultimate Loading Test

The purpose of the ultimate loading test was to verify that the composite CFRTP-concrete beam could carry the expected loads on a bridge deck as given by the AASHTO Strength I load case [9]. Five specimens were loaded in four-point bending until failure. The benchmark loading derived from the AASHTO Strength I specifications was $56.5\ kN$. The loading is discussed in Section 4.2.3.1.

All five specimens were manufactured using the fourth method of bonding the backer plate to the angles, outlined in Section 5.3.2.

5.4.2.1 Test Setup

The test setup and instrumentation for the ultimate test were similar to the construction loading test, the major difference being that the concrete support blocks were replaced with a steel I-beam to allow more room to load the specimen into the testing frame. The instrumentation fixtures were modified to fit with the new supports. The test setup is shown in Figure 105.

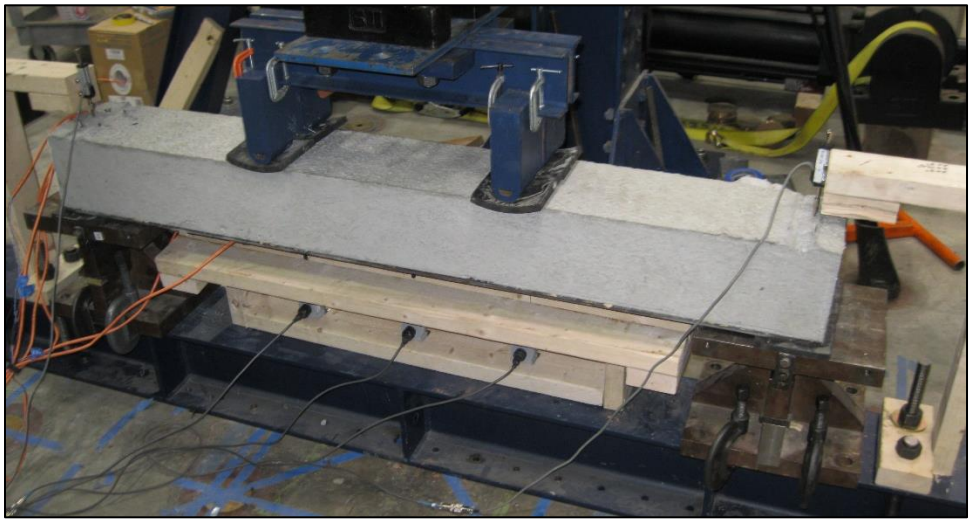

Figure 105: Ultimate Loading Test Setup

5.4.2.2 Test Procedure

A forklift was used to load each specimen into the frame. After the instrumentation was installed, the load head was lowered manually until it was in contact with the specimen. The load head was then lowered at a constant rate of $6.4\ mm/minute$ until the load on the specimen reached the AASHTO Strength I required load of $56.5\ kN$, at which point the load head was raised at the same rate. This cycle was repeated two more times to evaluate the stiffness of the stiffened panel. The load head was then lowered at the same rate until the specimen failed.

5.4.2.3 Discussion of Results

The five composite CFRTP-concrete hybrid beams were tested for stiffness and then to failure in four-point bending. Each specimen failed in nearly the same manner. During the stiffness portion of the test, flexural cracks formed in the constant moment region of the beam. Each of the flexural cracks formed in between two of the holes where the concrete was not continuous between the two sides of the beam. Near a load of $90\ kN$, shear cracks formed in the deck on one or both ends of the specimen. These cracks can be seen in Figure 106. The shear cracks continued to grow until the beam failed. A failed specimen can be seen in Figure 107. For four of the five specimens, this also caused to bond between the backer plate and the angles to break. One of the specimens that broke the bond is shown in Figure 108.

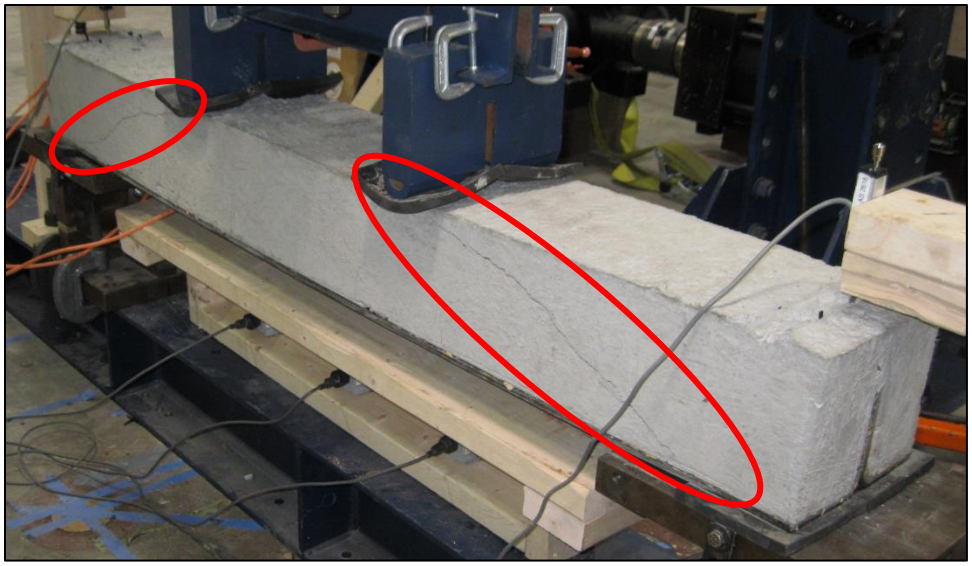

Figure 106: Shear cracks forming in the hybrid beam

Figure 107: Shear failure of hybrid beam specimen

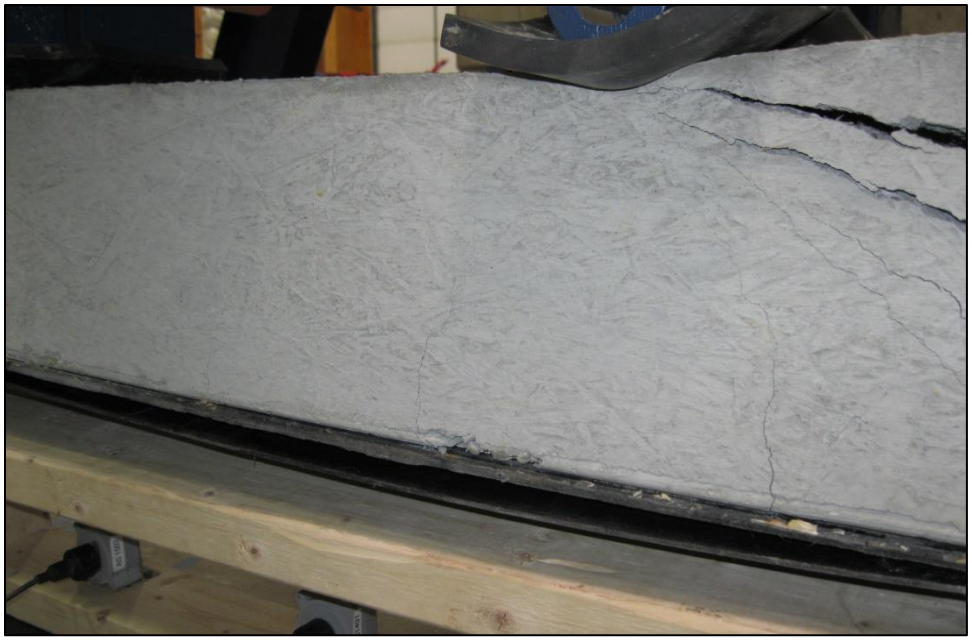

Figure 108: Broken bond between the angles and backer plate

The load-deflection curves for the stiffness tests of the five specimens are shown in Figure 109. Each specimen was brought up to the required AASHTO Strength I load of $56.5\ kN$ three times to evaluate the stiffness of the composite beam. The stiffness values, calculated as the slope of the load-displacement curve between 20 and 50 kN, are given in Table 19. The average stiffness across all tests was 11.7 kN.

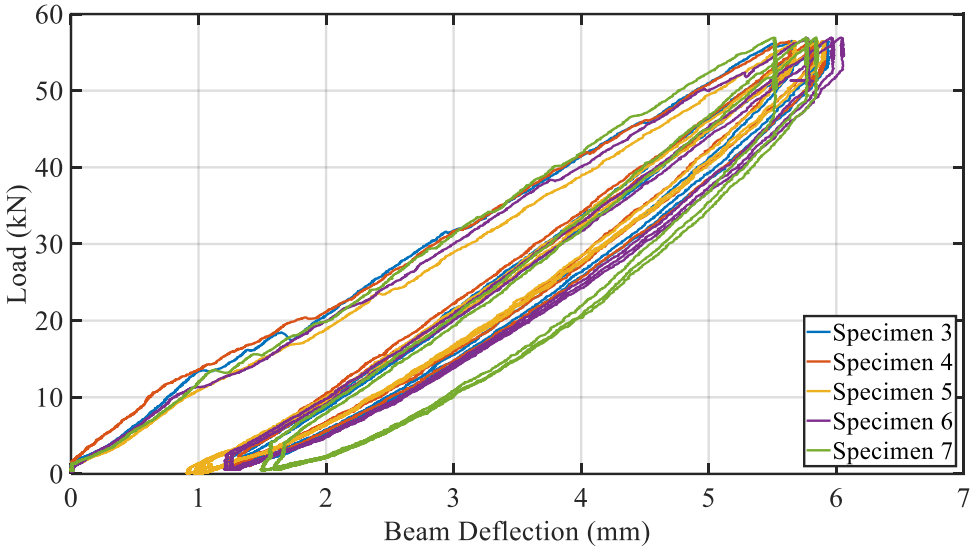

Figure 109: Ultimate loading stiffness test load vs midspan deflection

Table 19: Stiffness results from ultimate test (kN/mm)

Specimen	Cycle			Average
	1	2	3	
S3	10.1	12.5	12.3	11.6
S4	9.57	12.1	12.0	11.2
S5	10.2	12.4	12.2	11.6
S6	10.2	12.2	12.1	11.5
S7	10.9	13.3	13.1	12.4

The load-deflection curves for the ultimate tests of the five specimens are shown in Figure 110. The ultimate failure load for each specimen is given in Table 20. The average peak load for each specimen was significantly larger than the load required by AASHTO for Strength I of $56.5\ kN$.

As expected, if matrix cracking occurred at the expected load of the CFRTP first-ply failure, it did not cause ultimate failure of the beam.

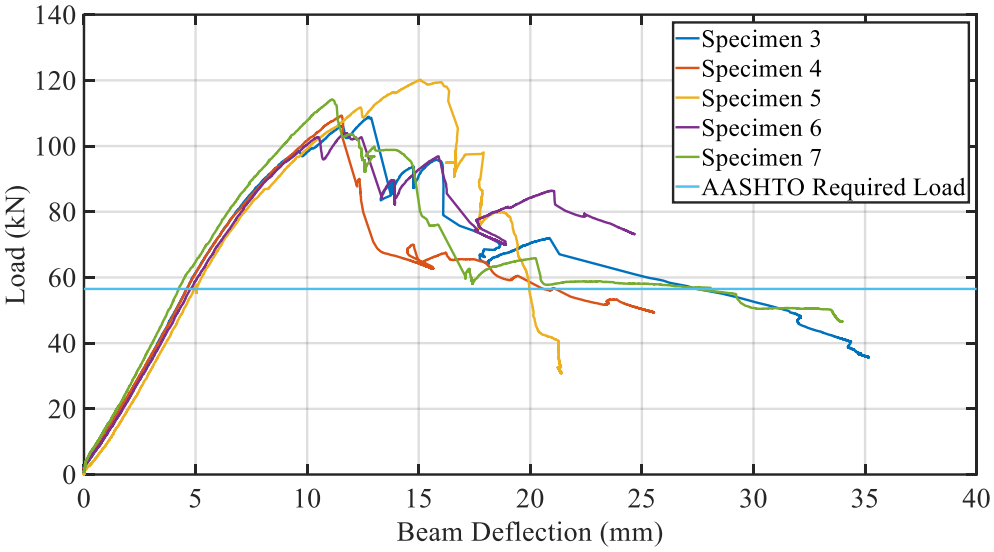

Figure 110: Ultimate loading test load vs midspan deflection plot

Table 20: Summary of ultimate loading test results

		Peak Load (kN)
Specimen	S3	108.9
	S4	109.2
	S5	120.2
	S6	104.0
	S7	114.2
Average		111.3
CoV		4.9%

5.4.2.3.1 Flexural Strain Analysis

Twelve strain gauges at midspan and in the constant moment region were used to measure longitudinal strains in the CFRTP during the test. As discussed in Section 5.4.1.1, two strain gauges were installed on the bottom of the backer plate and two on each on each side of the vertical portion of the angle at each location. The strain through the cross-section of each specimen under AASHTO Strength I loads is shown in Figure 111 through Figure 115. A line was fit to the top and bottom points to check linearity. A summary of that data taken at that load is shown in Table 21. From comparing the average difference between sides 1 and 2, it can be seen that the strains in web showed the most variation between sides while the bottom showed the most consistency, the same as the corrugated specimens behaved. The variability of strains in the web could have been caused by stress concentrations around the bearing holes and the bends in the laminate. The bottom flange strain gauges also showed the most consistency between specimens by having the lowest coefficients of variation. To approximate curvature, the strain values from the web were not included because of their variability so a line was fit between the top and bottom flange strain values.

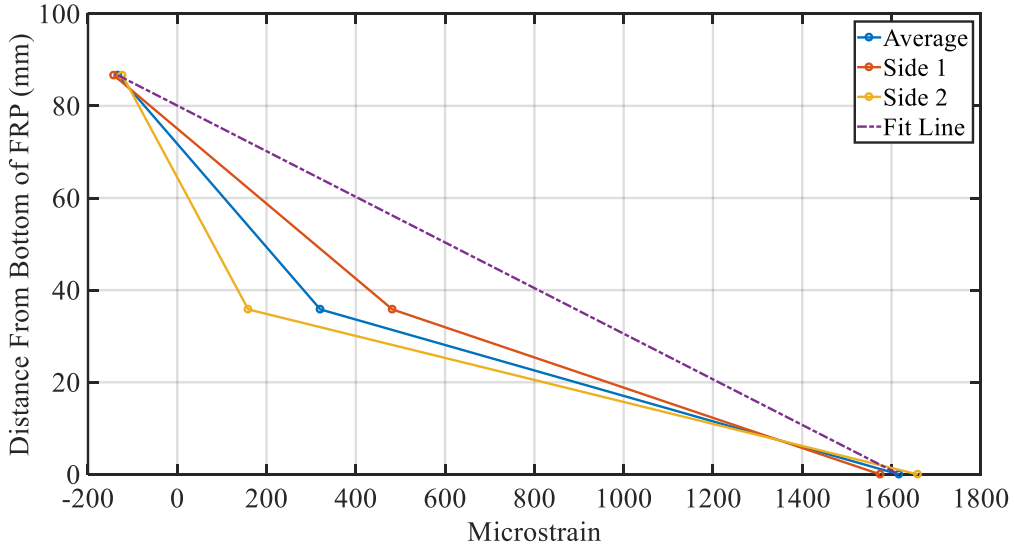

Figure 111: Strain in S3 at midspan under AASHTO Strength I loads

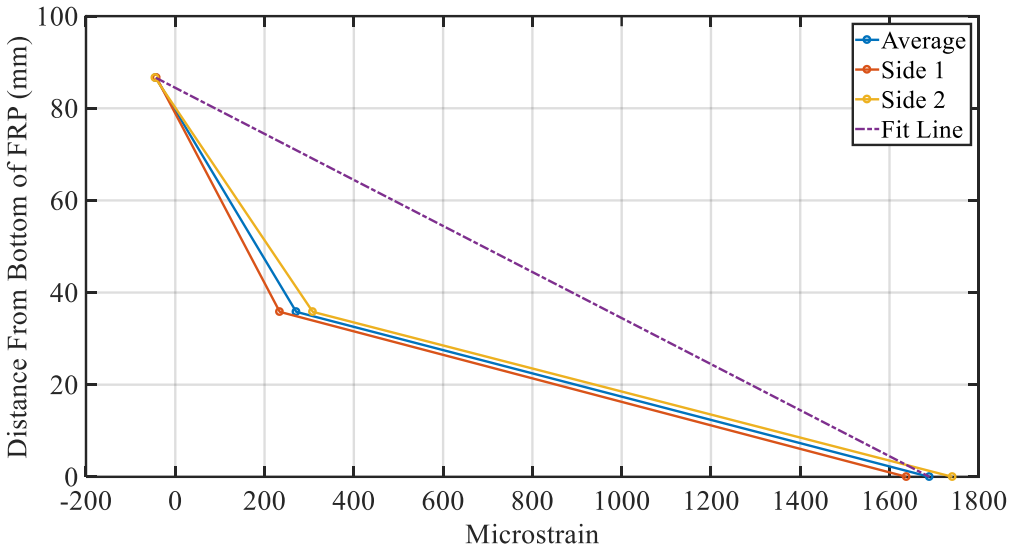

Figure 112: Strain in S4 at midspan under AASHTO Strength I loads

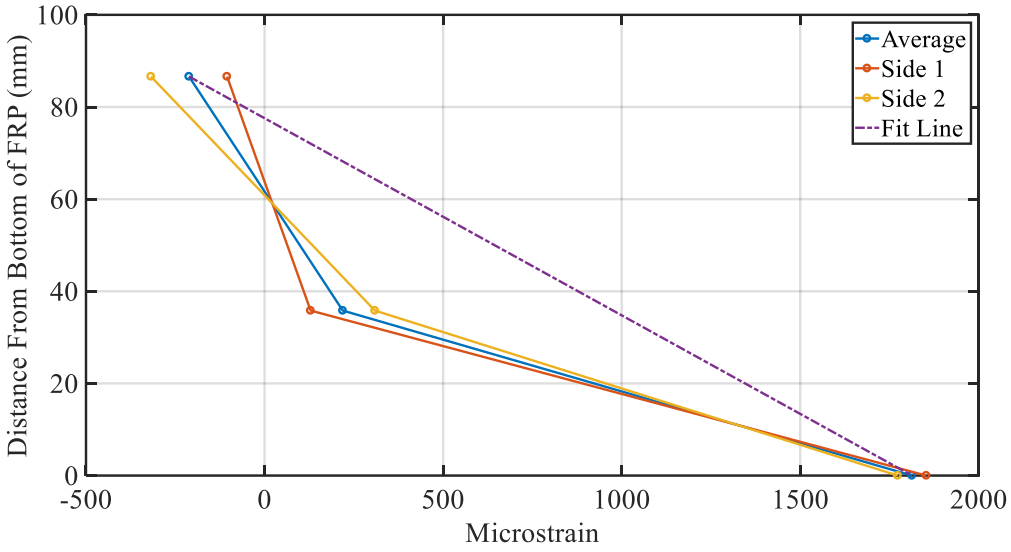

Figure 113: Strain in S5 at midspan under AASHTO Strength I loads

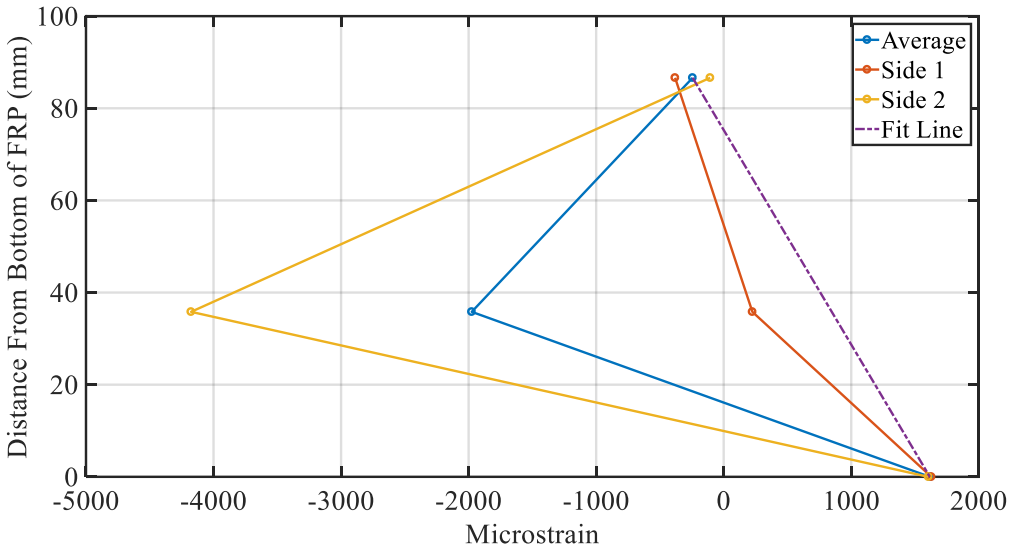

Figure 114: Strain in S6 at midspan under AASHTO Strength I loads

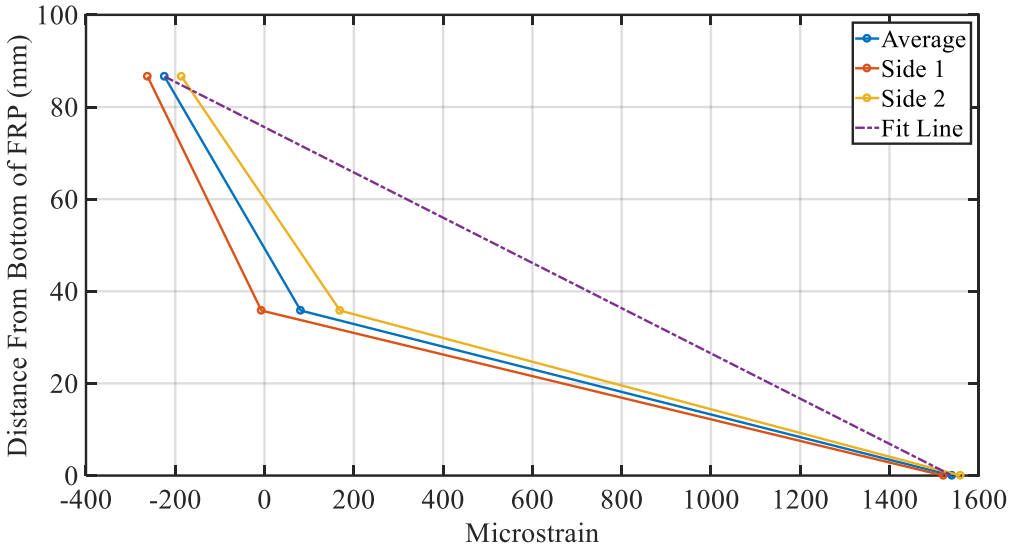

Figure 115: Strain in S7 at midspan under AASHTO Strength I loads

Table 21: Summary of strain results at AASHTO Strength I loads at midspan

		S3	S4	S5	S6	S7	Average	CoV (%)
Top Microstrain	Side 1	-142	-42	-105	-381	-262	-186.4	-65%
	Side 2	-123	-45	-318	-106	-186	-155.6	-60%
	Average	-132.5	-43.5	-211.5	-243.5	-224	-171	-43%
	Difference	19	3	213	275	76	117.2	92%
Middle Microstrain	Side 1	482	234	129	225	-7	212.6	75%
	Side 2	159	308	309	4180	169	1025	154%
	Average	320.5	271	219	2202.5	81	618.8	129%
	Difference	323	74	180	3955	176	941.6	160%
Bottom Microstrain	Side 1	1580	1640	1850	1630	1520	1644	7%
	Side 2	1660	1740	1770	1610	1560	1668	5%
	Average	1620	1690	1810	1620	1540	1656	5%
	Difference	80	100	80	20	40	64	46%

5.5 Summary

Each of the seven specimens was successfully manufactured and tested in four-point bending. When each specimen was tested, it met the required load set by AASHTO for stay-in-place

formwork and bridge decking before failure. No cracks formed during the stiffness tests below the load required by AASHTO. The ultimate failure of the beams resulted from a shear failure in the concrete, which lead to the backer plate debonding from the stiffeners. The rebar added in the bearing holes was not sufficient to prevent shear cracks from opening. Another layer of reinforcement above the vertical part of the stiffener could help to prevent the shear cracking.

CHAPTER 6

CONCLUSIONS AND RECOMMENDATIONS

6.1 Introduction

The goal of this research is to evaluate continuous fiber-reinforced thermoplastic (CFRTP) panels, including stay-in-place forms, for use as tension reinforcement in reinforced concrete structures. This goal was tackled through a combination of design and experimental evaluation. To support design, computational tools were developed to predict panel capacity. Three reinforcing configurations were investigated, each with their own shear connection mechanism.

6.2 Hybrid Beam

Three composite CFRTP-concrete hybrid beam concepts were chosen for exploration in this research. The three concepts were a flat panel (tension reinforcement only), a corrugated panel, and a stiffened panel. Each style of panel was designed and then $1524\ mm$-long specimens were manufactured to evaluate the concept. Each panel was manufactured in the Alfond Advanced Manufacturing Laboratory for Structural Thermoplastics at the ASCC out of an E-glass/PETg thermoplastic composite provided by PolyOne.

6.2.1 Flat Panel

The goals of the flat panel testing were to determine if thermoplastic composite panels could function as the tension reinforcement in a reinforced concrete structure and if the thermoplastic welded shear studs developed by Seigars [7] would be adequate to provide composite action in this application.

Eight specimens were manufactured for testing. Four of the specimens had shear studs spaced at $76\ mm$ on center, which is the minimum distance that AASHTO [9] would allow for steel shear studs of the same size. The rest of the specimens had shear studs spaced at $152\ mm$ on center, twice the other spacing. $127\ mm$ of concrete was then poured over the panel and studs.

The composite beams were then tested in four-point bending until ultimate failure of the beams. Each of the beams failed in the same mode where several flexural cracks would form along the bottom of the concrete in the constant moment region, until one of the studs in the constant shear region would break. After the first stud broke, each other stud on that side of the beam became overloaded causing all of the studs in that region to break in quick succession. This resulted in a brittle failure in the beam where the tension crack spread through the entire height of the beam until the beam collapsed.

The average ultimate load carried by the $76\ mm$ and $152\ mm$ spaced specimens was $11\ kN$ and $6\ kN$ respectively. The stress on each stud was calculated to be 13 MPa and 14 MPa respectively, about 50-55% of the strength reported by Seigars [7].

Because of the low observed strength of the PETg studs and the brittle nature of the structure, the shear studs were abandoned for the remainder of this research in favor of a mechanical bearing connection. There was no visible damage in the CFRTP panel so it appeared that the CFRTP would be strong enough to carry the tensile loads if an adequate shear transfer mechanism was used.

6.2.2 Corrugated Panel

The goal of the corrugated and stiffened panel tests were to develop a CFRTP panel that was strong enough to support the weight of wet concrete and to serve as the tension reinforcement once the concrete had cured. For the corrugated panel, a CFRTP panel was formed into a single corrugation with the groove running in the span direction of the beam. The alternating ridges and grooves increased the bending stiffness of the panel enough for it to function as stay-in-place formwork for the concrete. To develop composite action between the corrugated CFRTP panel and the concrete, steel rods were run transversely between the webs of the corrugation to create a bearing connection between the two materials.

Two tests were performed with the corrugated panels. The first was a construction loading test with the bare corrugated CFRTP panels. In that test, the panels were loaded in four-point bending until the factored AASHTO Strength I load was reached then the specimen was unloaded. Each specimen that was tested this way completed the test successfully while sustaining no visible damage during the process.

The second test was an ultimate loading test of the composite CFRTP-concrete hybrid beam. The panels were tested in four-point bending until failure. Each of the specimens failed in the same failure mode where shear cracks formed in the concrete, which eventually grew until the end of the specimen broke off. The first shear cracks formed at an average load of $101\ kN$ (minimum of $99.2\ kN$), which is 16% higher than the factored AASHTO Strength I load of $87.2\ kN$. The ultimate failure of the specimens occurred at an average load of $116\ kN$, which is 33% higher than the factored AASHTO Strength I load. As each specimen failed in the concrete and there was no visible damage to the CFRTP panels, the reported ultimate loads should be considered a lower bound for the true ultimate load of the CFRTP panels. The specimens could have potentially reached a higher load before failure if shear reinforcing was included in the concrete.

6.2.3 Stiffened Panel

For the stiffened panel, the flexural stiffness and strength of the panel was increased by bonding stiffeners to the top of the CFRTP panel. The stiffeners increased the bending stiffness and strength of the panel enough for it to function as stay-in-place formwork for the concrete. To develop composite action between the stiffened CFRTP panel and the concrete, transverse holes were cut into the vertical sections of the stiffeners. During the concrete pour, concrete flowed into the hole, forming a concrete dowel that would bear directly onto the CFRTP panel.

As with the corrugated panels, two tests were performed with this configuration. The first was a construction loading test with the bare stiffened panels. In that test, the panels were loaded in four-

point bending until they reached the AASHTO Strength I load then were unloaded. This process was repeated two more times to determine the stiffness of the panel, and then they were loaded to failure. Each panel did not accrue any visible damage during the stiffness portion of the test. The failure method of both specimens was buckling of the vertical sections of the stiffeners in the constant moment region between the loading points where they were restrained.

The second test was an ultimate loading test of the composite CFRTP-concrete hybrid beam. The panels were tested in four-point bending until failure. Each of the specimens failed in the same failure mode where shear cracks formed in the concrete. In most of the specimens, the large deformations resulting from the shear cracks forming caused the bond between the backer plate and the stiffeners to break in some places. The beams failed at an average peak load of $111\ kN$ (minimum of $104\ kN$), which is 96% higher than the factored AASHTO Strength I load of $56.5\ kN$. As with the corrugated panel, the specimens could have potentially reached a higher load before the bond broke if reinforcing was included in the concrete.

6.3 Overall Performance Assessment of Three CFRTP Panel Configurations

Five categories were used to assess the performance of the three configurations. The following categories were used:

- Design
- Manufacturing
- Stiffness
- Strength
- Durability

6.3.1 Design

The design of the shear connection of each configuration involved different issues. The design of the CFRTP panels in tension was relatively simple. CFRTP is a linear elastic material, which was designed similarly to steel reinforcement prior to yielding.

For the flat panel configuration, the shear studs were designed similarly to steel shear studs. The issue with this method was that the PETg material did not show the same ductility and load sharing that a shear stud would. This resulted in premature failure of the connection. To better design this connection in the future, a higher factor of safety would be required as a brittle failure was observed.

For the corrugated panel configuration, a similar method to the flat panel was used to determine the shear force that had to be carried by each pair (spaced vertically) of rods. A crude solution was used to distribute this shear force into each rod. This method under predicted the strength of the connection. A more sophisticated model of the distribution would be required to better design this connection in the future.

For the stiffened panel configuration, the design of the shear connection was simple and effective relative to the other configurations. The only issue with the design of this configuration was that this geometry made the vertical part of the stiffeners prone to buckling before the concrete cured. A finite element model would give a better understanding of the buckling capacity around the holes.

6.3.2 Manufacturing

As with the design, the manufacturing of each configuration involved different issues. As the same concrete was used for each configuration, this comparison focused on the differences before the respective concrete pours.

For the flat panel configuration, the CFRTP panel did not require forming post consolidation, which simplified the process of manufacturing the panels. To attach the shear studs, a machine developed by Seigars [7] was used to spin weld each stud individually. A more sophisticated spin welding

machine could be developed using CNC to control the location, pressure, and time of each weld automatically.

For the corrugated panel configuration, the manufacturing of the CFRTP panel required the extra stem to form the panel into a three-dimensional shape. This extra step required several trial runs to determine the proper parameters. Forming the corrugation itself is a quick process with the proper parameters though new parameters would be required with different materials or equipment. The cross-section was constant which means it could also be manufactured on a larger scale through conventional methods such as pultrusion or roll forming. The next step in manufacturing, adding the bearing rods, was simple with a CNC router though it becomes much harder to access the necessary areas if more than one corrugation are formed into one panel. The holes also need to be cut precisely to allow a steel bar to be run through multiple holes.

For the stiffened panel configuration, the manufacturing of the panels and forming the stiffeners was a similar process to the corrugated panels. The difference being the process to attach the stiffeners to the backer plate. This process should be similar to the consolidation of a flat panel. This bond breaking during ultimate testing of the specimens could indicate that a sub-optimal bond was formed at the interface. This could have been caused by mold release that was applied to the plates for consolidation not being completely removed prior to attaching the stiffeners. As the bearing holes do not have to snugly contain bars through them, the alignment of the holes is less critical with this configuration than with the corrugated panels.

6.3.3 Stiffness

The stiffness of each configuration was calculated using the testing data. The stiffness of the beam was calculated as the change in load divided by the change is midspan deflection below a load where the specimen diverged from linear behavior. A comparison of the three average stiffnesses is given in Table 22. As each specimen was a different width, a straight comparison of the stiffness

of each would not be accurate. To compare the stiffness of each configuration, the stiffnesses were normalized to a unit width of beam.

Table 22: Comparison of beam experimental stiffness values

	Flat Panel		Bare Corrugated Panel	Corrugated Panel	Bare Stiffened Panel	Stiffened Panel
	76 mm	152 mm				
Stiffness (kN/mm)	10.14	5.87	1.29	9.56	0.89	11.7
Width (mm)	127	127	313.8	313.8	203.2	203.2
Stiffness per unit width (kN/mm^2)	0.080	0.046	0.004	0.030	0.004	0.058

As would be expected, the flat panel with $152\ mm$ spacing of the studs had approximately half the unit stiffness as the specimen with a $76\ mm$ spacing. Each hybrid beam configuration had similar unit stiffness to the others while the bare panels had significantly less stiffness. The flat panel with $76\ mm$ stud spacing had the highest initial unit stiffness, though those specimens formed flexural cracks at a relatively low load, which reduced the stiffness as can be seen in Figure 29.

6.3.4 Strength

The peak load for each configuration was compiled into Table 23. Similar to the stiffness values, the ultimate strengths of each configuration are not comparable as each beam has a different width. To compare the strengths, a factor of safety was calculated.

The LRFD nominal moment capacity reduction factor for a CFRTP reinforced beam in bending was taken from the AASHTO LRFD Guide Specifications for Design of Concrete-Filled FRP Tubes for Flexural and Axial Members. This reduction factor was taken as 0.65 [20]. The factor of safety for the beams were calculated by dividing the reduced nominal capacity of the beam by the factored ultimate moment.

$$FS = \frac{\Phi_b M_n}{M_u} \tag{77}$$

The flat panel configuration was not designed to meet the AASHTO Strength I loading, only to determine the strength of the studs, so a factor of safety was not calculated for that configuration. The bare corrugated panels were not taken to an ultimate loading, so a factory of safety was not calculated for that configuration either.

Table 23: Comparison of beam experimental strengths

	Flat Panel		Bare Corrugated Panel	Corrugated Panel	Bare Stiffened Panel	Stiffened Panel
	76 mm	152 mm				
Ultimate Strength (kN)	11.0	6.07	-	116	8.16	111.3
Reduced Ultimate Strength (kN)	-	-	-	75.4	5.30	72.3
Factored AASHTO Strength I Load (kN)	-	-	2.38	64.5	1.77	56.5
Factor of Safety	-	-	-	1.17	2.99	1.28

As was expected from the design, the ultimate loading controlled over the construction loading for the stiffened panel configuration by having a smaller factor of safety. Both the corrugated panel and stiffened panel configurations had factors of safety above 1.0 though as previously mentioned, both configurations failed in shear in the concrete. This would be unlikely in a real structure as extra reinforcement included in the slab for temperature and shrinkage resistance is usually sufficient to control shear cracks.

6.3.5 Durability

For the two configurations that could see potential use in future testing, long-term durability should be considered as a comparison. As both are forms of stay-in-place formwork, some durability issues can arise from that. Water can become trapped between the CFRTP formwork and the concrete, which can create issues during freeze-thaw cycles. In addition, many owners are hesitant to use any type of stay-in-place formwork as it restricts inspection of the concrete from below, which can be important in gauging the condition and remaining strength of the structure later in its design life.

The corrugated panel configuration has more potential issues in that the bearing rod is exposed from below. If this rod is made of steel, as it was during this testing, this could open up the potential for rust issues. If the rods begin to rust out, the strength of the slab could become compromised.

6.3.6 Comparison

To summarize the comparisons made in the last five sections, a summary table, shown in Table 24, was created to determine the best solution. Each configuration was given a rating between one and five for its performance in each category where one was poor and five was excellent. A zero is given for a category that is not applicable.

Table 24: Comparison of each configuration over five categories

	Flat Panel	Corrugated Panel	Stiffened Panel
Design	2	3	3
Manufacturing	2	3	4
Stiffness	4	2	3
Strength	1	4	4
Durability	0	2	4
Total	9	14	18

From Table 24, the stiffened panel was found to be the best candidate for future research.

6.4 Recommendations for Future Research

The results of this research open several avenues for future research into this technology. Some potential avenues could be further investigation into the stiffened panel and investigation into other configurations of CFRTP reinforcement.

6.4.1 Stiffened Panel

The results of this research show that the stiffened panel configuration could meet the strength requirements set by AASHTO for stay-in-place formwork and a hybrid bridge slab. To progress this research, the design and manufacturing processes should be optimized to improve this technology.

One possible avenue of future research is to conduct more testing into the individual components of the stiffened panel in order to provide more accurate and efficient designs. One potential test could be to investigate how to create a stronger bond between the backer plate and the stiffeners and to run lap shear tests to determine the actual strength of the bonds. Another potential test could be to perform push out tests in concrete with the bearing shear connection, similar to the push out tests done by Seigars [7] to characterize the shear stud strength. Fatigue of the hybrid beams was not assessed in this research and could be a potential controlling load case so fatigue testing of this technology is recommended. It is also recommended to perform more quasi-static testing on the hybrid beams with reinforcing steel and span length comparable to a conventional bridge deck to better assess the strength and applicability of the CFRTP panels.

Another possible avenue is to optimize the design process. The analysis tool developed for this research could be iterated to find more optimal sizes and layups for the CFRTP panel. Finite element modeling could also help to analyze the buckling of the stiffeners. Other thermoplastic materials such as PA6 could be also be involved in the optimization process in place of PETg to assess their relevance to this technology.

Another avenue is to investigate the use of large-scale manufacturing methods to create the stiffened panels. Pultrusion and role forming are common industrial practices that could suit this technology as it has a constant cross-section. This would also remove the issue of a secondary bond between the stiffeners and the backer plate if the part was created in one step. A secondary step would still be needed to cut the holes out of the stiffeners for the bearing connection.

6.4.2 Other Configurations

Only three configurations of CFRTP reinforcement were investigated in this research so it likely that there are other configurations that are just as or more promising. One potential configuration could be use a CFRTP panel as internal reinforcement for concrete by cutting holes into a flat panel

similar to the stiffeners in the stiffened panel then suspending the panel inside a concrete beam similar to conventional rebar. The holes would create composite action as concrete flowed through the panel and continuous fibers outside of the hole would carry the tension. This could remove the issues with stay-in-place formwork though temporary formwork and shoring would be required during construction.

Another possible configuration could be to incorporate a CFRTP-concrete bearing connection into the corrugated panel. This could possibly be done by welding a plate similar to the internal reinforcement discussed above to the top flanges of the corrugation. This would eliminate the exposed steel and complications with the hole cutting that were observed in this research.

REFERENCES

[1] H. Breton, "Mechanically Fastened Fiber-Reinforced Polymer (FRP) Flexural Retrofit Systems for Reinforced Concrete Flat-Slab Bridges," University of Maine, Orono, Maine, 2013.

[2] H. B. Loring and W. G. Davids, "Mechanically fastened hybrid composite strips for flexural strengthening of concrete beams," *Constr. Build. Mater.*, vol. 76, pp. 118–129, 2015.

[3] UFP Ranson, "UFP Ranson, LLC." [Online]. Available: http://www.ufpi.com/ranson.

[4] Tata Steel, "ComFlor 80." [Online]. Available: https://www.tatasteelconstruction.com/en_GB/Products/structural-buildings-and-bridges/Composite-floor-deck/Comflor®-80.

[5] Imrose Bin Muhit, "Various Types of Shear Connectors in Composite Structures: A Review," Composite Structures Lab, Chung-Ang University, Seoul, Korea, Apr. 2015.

[6] G. Merryfield, A. El-Ragaby, and F. Ghrib, "New shear connector for Open Web Steel Joist with metal deck and concrete slab floor system," *Constr. Build. Mater.*, vol. 125, pp. 1–11, 2016.

[7] C. Seigars, "Feasibility of Hybrid Thermoplastic Composite-Concrete Load Bearing System," University of Maine, Orono, Maine, 2018.

[8] ASTM International, "Standard Test Method for Compressive Properties of Polymer Matrix Composite Materials Using a Combined Loading Compression (CLC) Test Fixture," D6641/D6641M − 14.

[9] AASHTO, "AASHTO LRFD Bridge Design Specifications," American Association of State Highway and Transportation Officials, Washington, D.C., 2012.

[10] ASTM International, "Standard Test Method for Compressive Strength of Cylindrical Concrete Specimens," C39/C39M-17B.

[11] E. J. Barbero, *Introduction to Composite Materials Design*, 2nd ed. New York: CRC Press, 2011.

[12] Z. Hashin, "Failure Criteria for Unidirectional Fiber Composites," *J. Appl. Mech.*, vol. 47, pp. 329–334, Jun. 1980.

[13] I. M. Daniel and O. Ishai, *Engineering Mechanics of Composite Materials*, 2nd ed. New York: Oxford University Press, Inc., 2006.

[14] American Concrete Institute, "Building Code Requirements for Structural Concrete," ACI, Farmington Hills, MI, USA, ACI 318-14, Sep. 2014.

[15] A. E. Naaman, *Prestressed Concrete Analysis and Design: Fundamentals*, 2nd ed. Ann Arbor, Michigan, USA: Techno Press 3000, 2004.

[16] J. M. Gere and B. J. Goodno, *Mechanics of Materials*, 8th ed. United States: Cengage Learning, 2013.

[17] AISC, *Steel Construction Manual*, 14th ed. United States of America: American Institute of Steel Construction, 2011.

[18] American Society of Civil Engineers (ASCE), "Chapter 7. Design of Plates and Built-up Members," in *Standard for Load & Resistance Factor Design (LRFD) of Pultruded Fiber Reinforced Polymer (FRP) Structures*, Reston, VA, 2018.

[19] W. T. Segui, *Steel Design*, 5th ed. United States: Cengage Learning, 2013.

[20] AASHTO, "LRFD Guide Specifications for Design of Concrete-Filled FRP Tubes for Flexural and Axial Members," American Association of State Highway and Transportation Officials, Washington, D.C., 2012.

[21] Sheffield Plastics Inc., "PETG Sheet: Product Data," Bayer Material Science, Sheffield, Massachusetts, 2003.

[22] PolyOne, "Polystrand IE 5842 Technical Data Sheet." 2017.

[23] S. Bhandari, "Feasibility of Using 3D Printed Molds For Thermoforming Thermoplastic Composites," University of Maine, 2016.

[24] Sheffield Plastics Inc., "PETG Sheet: Product Data," Sheffield, Massachusetts, 2003.

[25] Z. Padovec, M. Růžička, and V. Stavrovský, "Springback analysis of thermoplastic composite plates," *Appl. Comput. Mech.*, vol. 6, no. 1, pp. 25–34, 2012.

APPENDIX A

THERMOFORMING PROCESS AND PARAMETERS

A.1 Introduction

The manufacturing done through thermoforming for this research was performed at the Advanced Structures and Composites Center. The majority of the work was completed on the automated thermoforming line in the Alfond Advanced Manufacturing Laboratory for Structural Thermoplastics. The remainder was performed with an oven and a smaller hydraulic press. This section discusses on the process used in the automated thermoforming line and the parameters that were found to work best during testing.

A.2 Equipment

Five main pieces of equipment in the thermoforming line were used for this research.

- Fortus 900mc 3D Production System
- Fiberforge RELAY 2000
- Sopara Infrared Oven
- 650-Tonnes Utah Hydraulic Press
- ABB IRB 6650S Industrial Robot

A.2.1 Fortus 900mc 3D Production System

The Fortus 900mc 3D Production System is a large 3D printer used to create molds for thermoforming. This printer has a build volume of $914\ mm$ x $610\ mm$ x $914\ mm$ and is capable of printing with 13 engineering-grade thermoplastics.

Figure A-1: Fortus 900mc 3D Production System

A.2.2 Fiberforge RELAY 2000

The Fiberforge RELAY 2000 is a tape layup machine that uses rolls of pre-impregnated thermoplastic tape to create tailored blanks. Slices of tape are cut and arranged automatically according to an input file to form each layer of the desired laminate. The tapes are held down using a vacuum system built into the table. Each layer is attached to the previous layer with a series of ultrasonic spot welds.

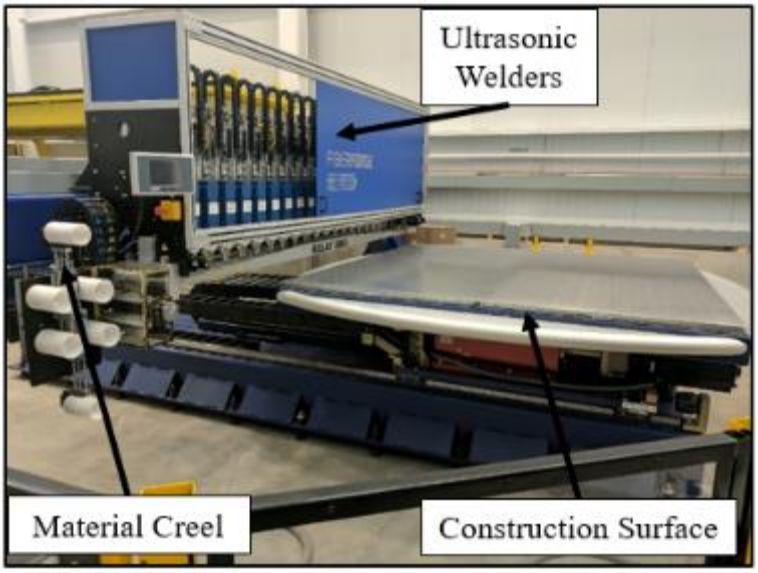

Figure A-2: Fiberforge RELAY 2000

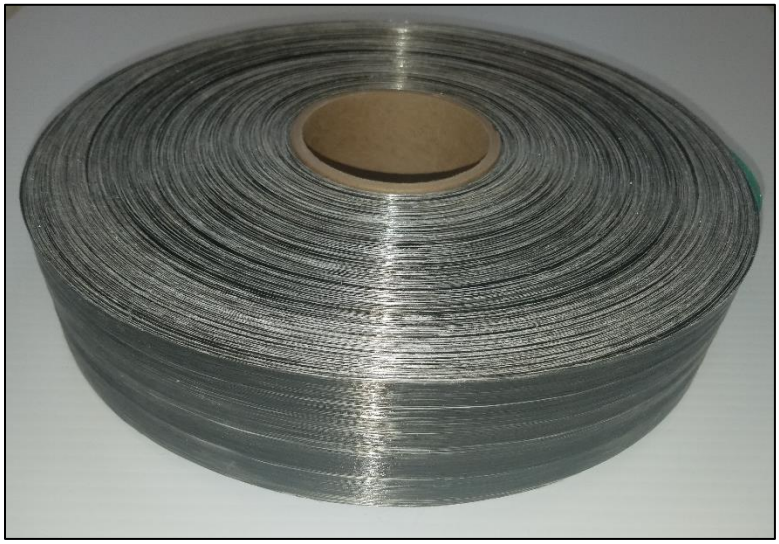

Figure A-3: Roll of PETg pre-impregnated tape used for this research

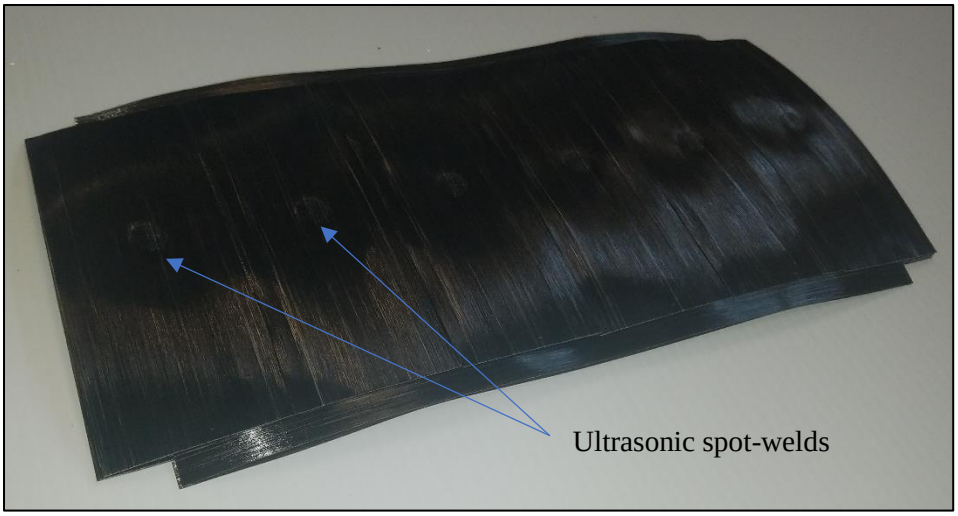

Figure A-4: Tailored blank created on the Fiberforge RELAY 2000

A.2.3 Sopara Infrared Oven

The Sopara Infrared (IR) Oven is an oven that is used to heat composite tailored blanks and laminates before consolidation and forming respectively.

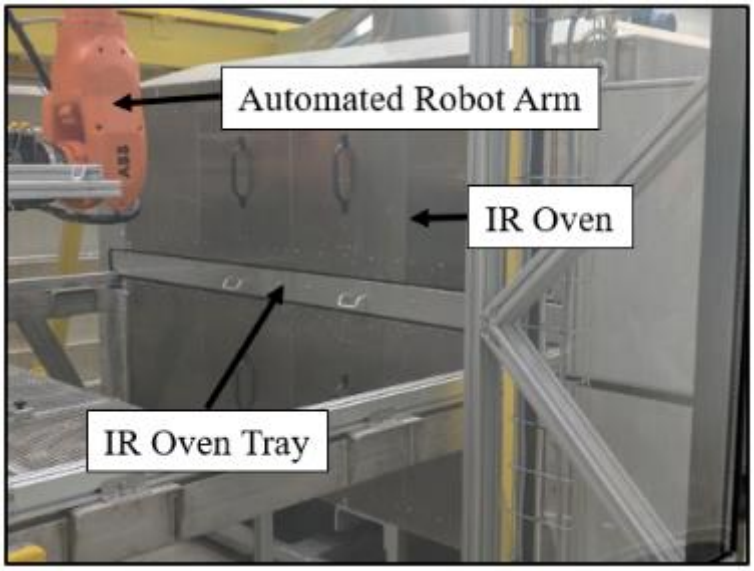

Figure A-5: Sopara Infrared Oven

A.2.4 650-Tonnes Utah Hydraulic Press

The 650-Tonnes Utah Hydraulic Press is used to consolidate and form composite materials. Flat consolidation platens can be used to consolidate tailored blanks or the platens can be removed and replaced with a mold to form composite materials.

Figure A-6: 650-Tonnes Utah Hydraulic Press

A.2.5 ABB IRB 6650S Industrial Robot

The ABB IRB 6650S Industrial Robot is a mechanical arm, which uses a series of suction cups to transport parts along the manufacturing line automatically. It is especially useful to transport heated composites from the IR oven to the hydraulic press quickly without risking burns.

Figure A-7: ABB IRB 6650S Industrial Robot

A.3 Process

This section follows a part going through the thermoforming line from tape to formed part. Before this process starts, decisions need to be made on the desired layup and material to be used.

A.3.1 Tape Layup

First, a control file needs to be created and loaded into the RELAY for the desired layup. A roll of the desired material needs to be loaded into the creel to be fed into the machine. The Fiberforge RELAY 2000 then follows the program and build the laminate up layer by layer. The table rotates and translates for each piece of tape put down so that it is placed in the correct location. A vacuum built into the table holds the bottom layer in place and each successive row above that is attached to the previous layer using ultrasonic spot welds. The final part created is a tailored blank which is a pile of layered strips of thermoplastic tape held together with discrete ultrasonic welds. For the next part, the tailored blank is moved into the thermoforming cell.

Figure A-8: Tailored blank for a stiffened panel stiffener being created

A.3.2 Consolidation

The next step in the process is to consolidate the tailored blank into a solid plate. To do this, the tailored blank is placed inside the press and put under pressure. The platens are then heated to bond the layers of thermoplastic tape together. Once the part has reached the desired temperature, the temperature is held for an amount of time referred to as a dwell time. The part is then allowed to cool while still under pressure. As the hydraulic press at the ASCC did not have active cooling, this was a time consuming process. This process also forces out any air bubbles in the part.

Figure A-9: Tailored blank, before (left) and after (right) consolidation

If the goal was to make a flat CFRTP panel, such as for the flat panel configuration discussed in this thesis, the thermoforming process is now complete. If not, forming the flat panel into a three-dimensional part, such as a corrugated panel or stiffener, is the next step.

A.3.3 Forming (Optional)

To form the CFRTP panel into a three-dimensional shape, the platens in the hydraulic press need to be removed and replaced with a mold. The mold needs to be centered on the press and bolted down to get a consistent pressure across the part. It is often best to trim the part to the correct size before forming, as it can be difficult to cut a three-dimensional part. The flat panel needs to be heated again in the IR oven until it is hot enough to form. It is recommended to let the part dwell at the desired heat to ensure that the inside of the part reaches the correct temperature. Once the flat panel is heated adequately, the robot arm moves it into the mold which then closes to cool the part

in the desired shape under pressure. Alignment pins were found to be helpful during forming, as parts would tend to shift while the mold was closing creating misaligned fibers and skewed parts.

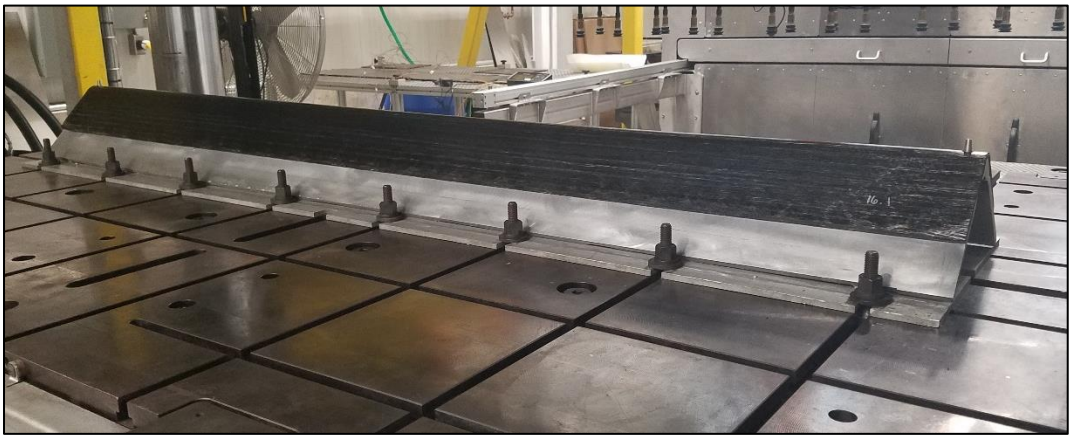

Figure A-10: Formed stiffener in the mold in the hydraulic press

After this step, the corrugated panels were finished, but the stiffened panels still required one more manufacturing step.

A.3.4 Bonding (Optional)

To bond the backer plate to the stiffeners, a new mold was loaded into the bottom of the press and the top platen was returned to the press. Achieving a bond between two consolidated plates is a similar process to consolidating a tailored blank. The two plates need to be sufficiently heated then allowed to cool under pressure. For the stiffened panel, this was done by heating the backer plate in the IR oven and using a heated top platen to heat the face of the stiffeners that would be bonded to the backer plate. As the hydraulic press at the ASCC did not have built in cooling at the time, this was a time intensive process, as the part would take a while to cool since the top platen was also heated to begin the process.

Figure A-11: Stiffeners in the mold for bonding in the hydraulic press

A.4 Recommended Parameters

For each round of manufacturing in this research, the parameters used were varied to determine the optimal method of manufacturing these parts. Several trial specimens were manufactured for most of the specimens to allow the parameters to be trialed to find a successful way to make each part.

The parameters that were found to work for each specimen varied as the layups, sizes, and thicknesses changed. If the material were varied, this would also affect the required parameters. The manufacturing of the stiffened panels resulted in the highest quality parts of the three trials, so the parameters used to manufacture them are given in Table A-1.

Table A-1: Manufacturing parameters used for stiffened panels

	Press Pressure (MPa)	Press Dwell Time (min)	Press Temperature (°C)	IR Oven Dwell Time (sec)	IR Oven Temperature (°C)
Angle Plate Consolidation	1	60	177	-	-
Angle Forming	1	2	66	180	179
Attaching Backer Plate	1	2	93 (top only)	90	188

APPENDIX B

SUPPLEMENTAL TESTING AND MANUFACTURING TRIALS

B.1 PETg Material Shrinkage Test

During initial prototype manufacturing using the PETg tapes, gabs between the outer layers of tape were observed. An example of the shrinkage observed in one of the trial flat panels is shown in Figure B-1.

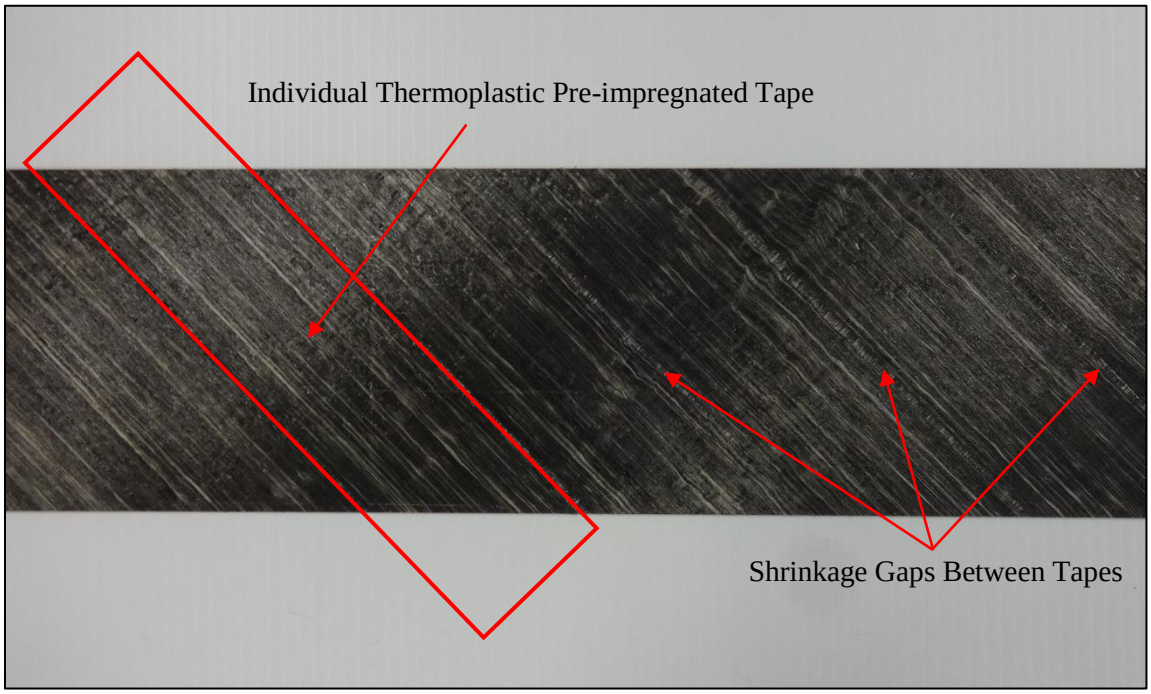

Figure B-1: Shrinkage observed in outer layers of trial flat panel

To determine if the shrinkage occurred during heating or during consolidation, the heating of the next round of manufacturing was investigated more thoroughly. It was found that the shrinkage occurred during heating, as the gaps were clearly visible before the part was formed. The tailored blank after being heated is shown in Figure B-2.

Figure B-2: Gaps observed after heating of tailored blank

To quantify the observed shrinkage, a short test was performed. Specimens were cut out of a single layer of tape that were 50.8 mm by 50.8 mm. Specimen were taken from the rolls of tape shown in Figure 12 and from uncut rolls of PETg that had not been slit or dyed black. It was also observed that some of the dyed tapes that were received were significantly lighter in color so these were considered a different material for this test. The manufacturer confirmed that the change in color was between different batches of the same material. The dark and light dyed tapes came from separate rolls of tape as the color of the tape remained relatively constant throughout a role. Examples of the three materials are shown in Figure B-3.

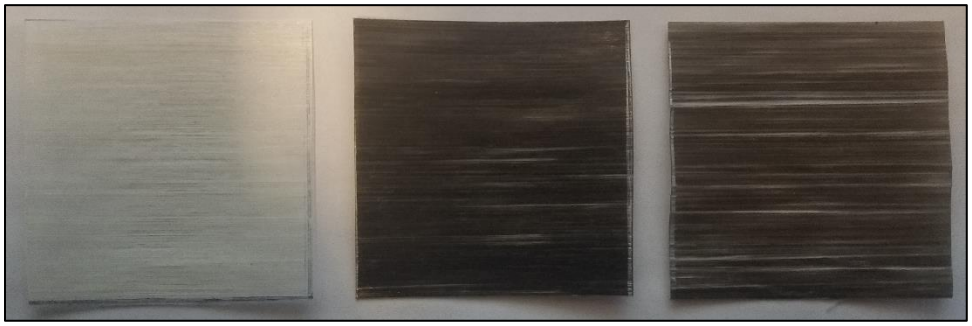

Figure B-3: Shrinkage test specimens

Five temperatures were chosen for this test: $93.3°C$, $121.1°C$, $148.9°C$, $176.7°C$, and $204.4°C$. These temperatures were chosen to bound the recommended forming temperatures of 137.8°C to 160.0°C of PETg [21].

B.1.1 Test Procedure

To prepare for the test, each specimen was measured longitudinally (fiber direction) and transversely. Then eight specimens of each material were arranged on a steel sheet covered with Taconic tape. One more sacrificial specimen was added with a thermocouple taped to it to measure the temperature. This arrangement is shown in Figure B-4.

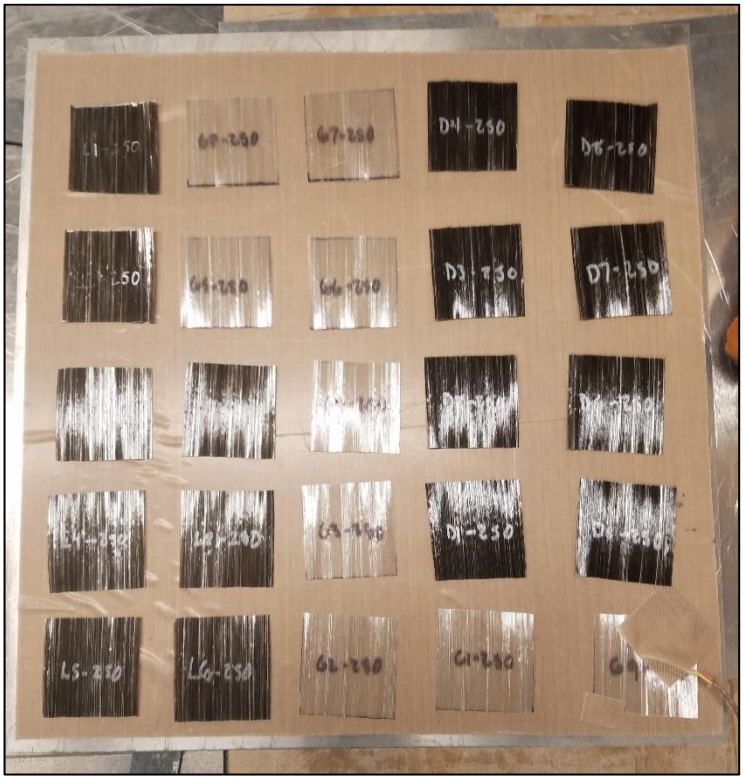

Figure B-4: Arrangement of shrinkage test specimens

The steel sheet was then placed in a convection oven. The oven was then heated until the thermocouple read the desired steady-state temperature. The heating took from 10 to 50 minutes to reach a steady state. The specimen were then removed from the oven and allowed to cool overnight.

Each specimen was then measured again in the longitudinal and transverse directions. This was repeated for each desired temperature.

B.1.2 Discussion of Results

As expected, the transverse dimension of each specimen reduced after being heated, but the longitudinal dimension remained relatively constant. The average reduction in the transverse dimension and the longitudinal dimension are shown in **Error! Reference source not found.** and **Error! Reference source not found.** respectively.

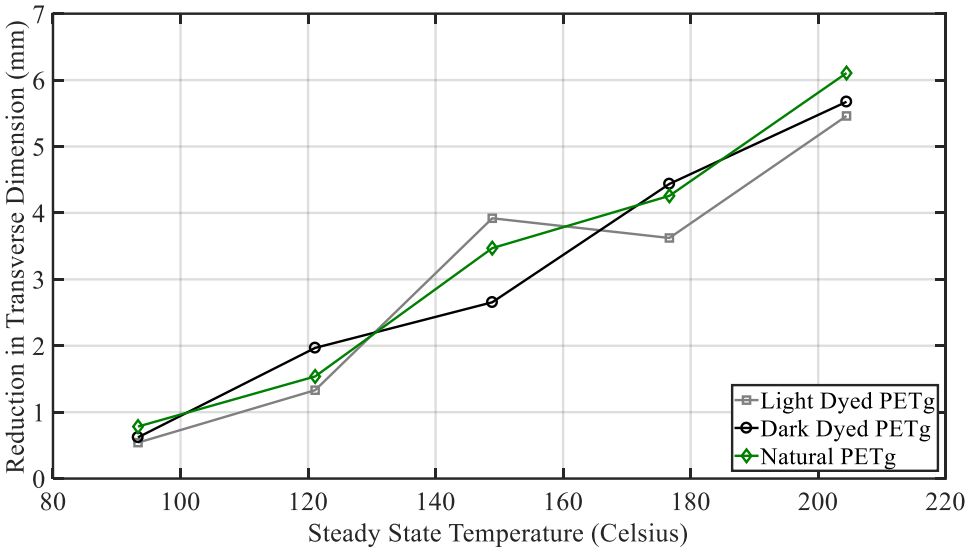

Figure B-5: Average reduction in transverse dimension with temperature

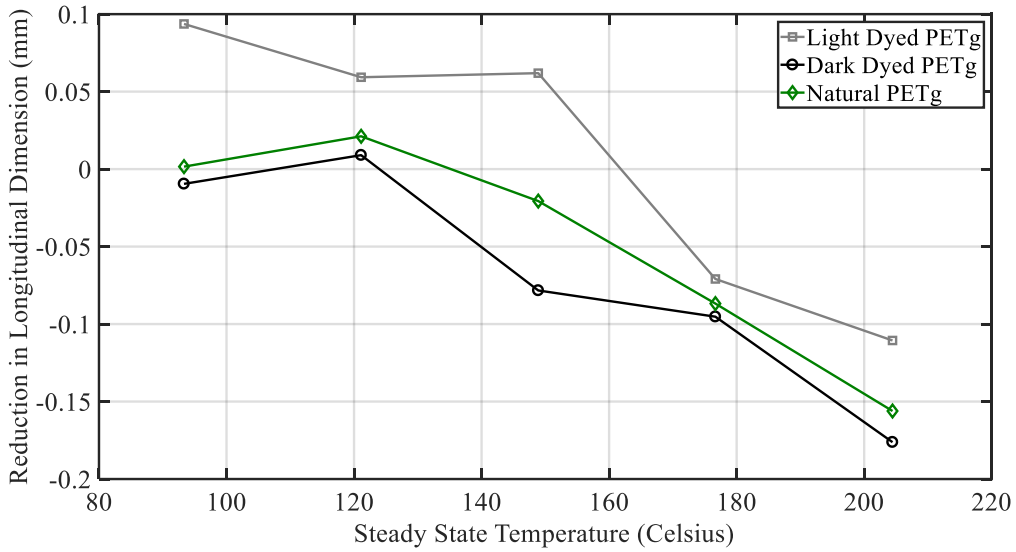

Figure B-6: Average reduction in longitudinal dimension with temperature

B.1.3 Conclusions

After consulting with the tape manufacturer, it was determined that the probable cause of the shrinkage was internal stresses in the material resulting from the manufacturing of the tapes. Heating unrestrained tapes releases these internal stresses. This explained why the shrinkage was only seen in the external layers as the internal layers were restrained through friction with the tapes above and below them.

To prevent this issue moving forward, two solutions were found through trial and error testing. First, when using the convection oven to heat the tailored blank, high-temperature silicon rubber sheets included on either side of the part during heating and forming restrained the external tapes during the heating. The inclusion of the silicone sheets also helped to reduce heat loss during transport from the oven to the mold. The improvement to the final part realized with this method can be seen in Figure B-7.

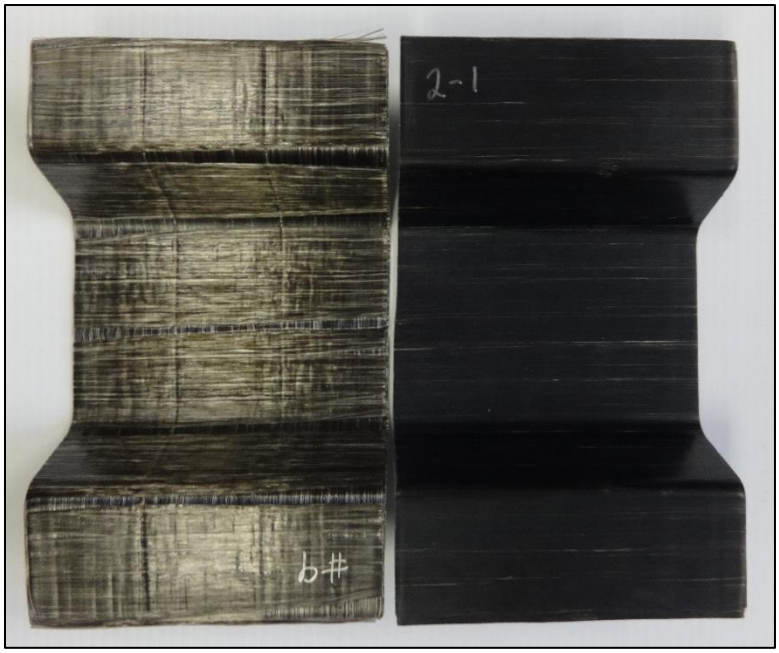

Figure B-7: Consolidated parts without (left) and with (right) silicone during heating

The second solution applied when using the thermoforming line at the ASCC. In this situation, the tailored blanks needed to be heated and cooled while under pressure in the hydraulic press. As the hydraulic press is much larger for this option, the cooling was a more time-intensive process, but larger and higher quality parts could be created.

B.2 Proof-of-Concept Parts

Initially, short, single corrugations were manufactured to demonstrate that corrugations could be manufactured at the ASCC through heated consolidation in a shaped mold. For the process of heated consolidation, a flat CFRTP panel is heated, then placed in a shaped mold and allowed to cool under pressure

B.2.1 Part Design

A simple corrugated cross-section was desired for this set of manufacturing trials. A corrugated part is comprised of three main parts: the top flange, the web, and the bottom flange. Common sizes of metal corrugations used in industry were investigated and used to size the part. The height of

corrugation, the vertical distance between the top flange and the bottom flange was chosen to be 50.8 mm. The width of the top flange and bottom flange were each chosen to be 101.6 mm. An inclination of 20° was chosen for the webs. These dimensions were chosen based on previous corrugations manufactured at the ASCC. As a single corrugation is being used for these trials, the top flange was divided into two parts to create a symmetric section.

B.2.2 Thermoplastic material

For this trial, the E-glass reinforced PETg discussed in Section 2.2 was used. Two variations of PETg provided by PolyOne were used: rolls of IE 5842 and rolled tapes of IE 5842b. PETg is an engineering grade thermoplastic with relatively low processing parameters such as forming temperature.

IE 5842 is PETg in its natural color. The material comes in 635 mm wide rolls. It is semi-transparent material with a green tint. The roll must be hand cut to get the orientation of the fibers and the dimensions that are needed.

The main difference between IE 5842b and IE 5842 is that dye has been added to the resin, which turns the IE 5842b solid black. The IE 5842b comes on a similar roll to the IE 5842, but it has since been slit into approximately $50.4\ mm$ wide tapes. Both PETg tapes have a reported fiber weight fraction of 58% [22]. The advantage of having the dye in the resin is that the black color allows the material to be used with the automated tape layup machine at the ASCC without recalibration and improves the heating rate in the infrared oven.

B.2.3 Fiber Material

Both types of PETg have continuous unidirectional, E-glass fibers in the direction of the roll.

B.2.4 Fiber Architecture

Two fiber layups were chosen for this task. For each layup, at least two were manufactured with each thermoplastic resin. For these fiber layups, 0° is in the direction of the corrugations, shown in Figure B-8. The two are as follows:

$$[\pm 45°, 0°, 0°, 0°, 0°, 0°, 0°, \mp 45°]$$

$$[0°, 90°, 0°, 0°, 0°, 0°, 0°, 0°, 90°, 0°]$$

The two fiber layups were chosen to assess whether having fibers cross the corners directly or at angle affected the quality of the final part.

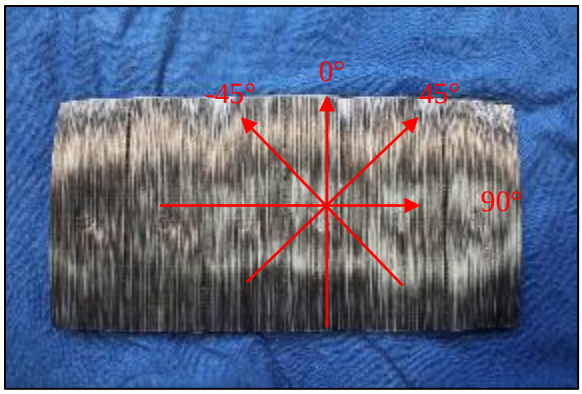

Figure B-8: Fiber orientations

B.2.5 Mold Design

The mold was designed using the program SOLIDWORKS which was developed by Dassault Systèmes. The mold was designed in two parts, male and female, shown in Figure B-9. The mold was designed to have a 5 mm gap between the two parts of the mold when the corrugated GFRTP is being formed. This gap includes the thickness of the part, 2.5 mm, and the thickness of a layer of high-temperature silicone used to distribute the pressure equally into the GFRTP and achieve a uniform consolidation. For the first set of trials, a 3 mm thick sheet of silicone was used which was expected to compress under the pressure to the correct thickness. For the second set of trials, two

1.5 mm thick sheets of silicone were used with one on either side of the part. The mold was designed to fit the part except that the mold was made wider to accommodate for the GFRTP possibly not being centered on the mold.

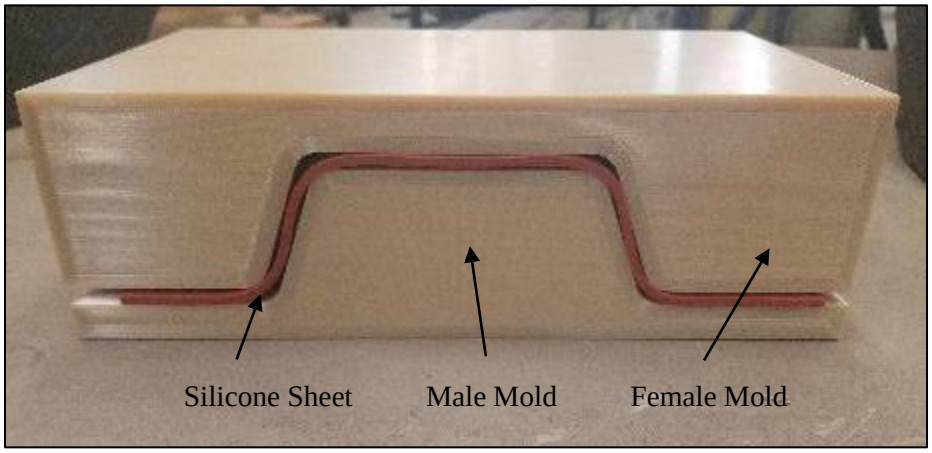

Figure B-9: Parts of proof-of-concept mold

B.2.6 Mold Manufacturing

Each part of the mold was individually 3D printed in the Alfond Advanced Manufacturing Lab for Structural Thermoplastics at the ASCC. The mold was printed on the Fortus 900mc 3D Production System discussed in Appendix A.2.1. Each part of the mold was printed on its side to achieve a smoother surface around the curves and the webs; this is shown in Figure B-10.

The feasibility of using 3D printed molds for thermoforming thermoplastic composites was investigated by Bhandari [23]. Based on the recommendations from Bhandari, ULTEM 9085 material was selected for the molds because it exhibited a glass transition temperature higher than the temperature needed to consolidate the PETg tapes. The glass transition temperature of ULTEM 9085 is $180°C$ and the heat distortion temperature is $153°C$.

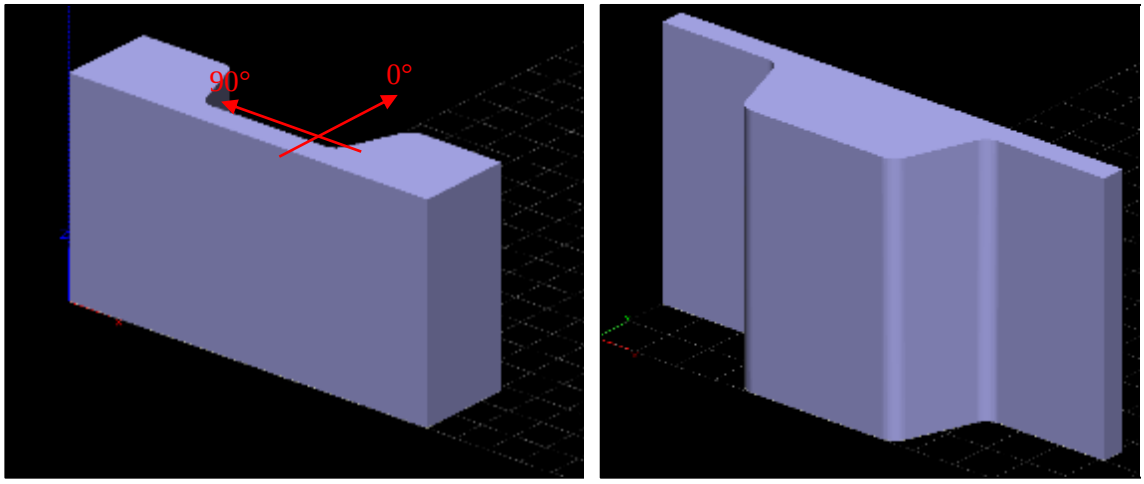

Figure B-10: Female mold (left) and male mold (right) in the orientation used for printing

The molds were printed with eight solid layers around the outside of the part to allow for sanding of the corners if necessary. The infill of each mold had the following repeating pattern: eight layers of alternating 0° and 90° sparse-double dense layers followed by two solid layers. The sparse layers had $0.66\ mm$ thick strands arranged across the part that were spaced at $2.54\ mm$. The direction of the 0° and 90° layers is shown in Figure B-10.

The female mold required $1333\ cm^3$ of filament and took approximately 18 hours and 15 minutes to print. The male mold required $1006\ cm^3$ of filament and took approximately 13 hours and 30 minutes to print. After the printing process was initiated, it required no supervision until completion.

B.2.7 Part Manufacturing

The first step in manufacturing the corrugated GFRTP parts was to assemble the layers of materials with the desired orientation of fibers. The IE 5842 tape was measured and cut by hand so that each layer was a solid piece. The IE 5842b tape was cut and arranged automatically with the

Dieffenbacher-FiberForge RELAY 2000 discussed in Appendix A.2.2. One of the unconsolidated tailored blanks is shown with the hand cut PETg 5842 in Figure B-11.

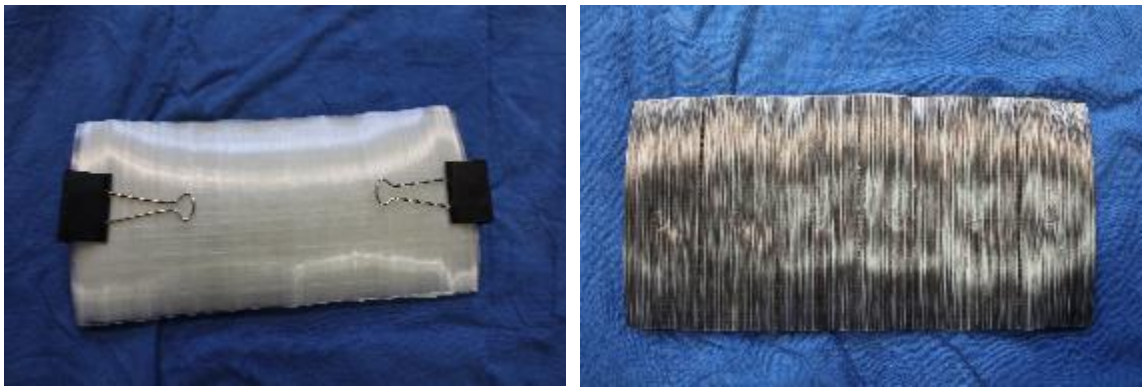

Figure B-11: Cut layers of PETg 5842 (left) and IE 5842 (right)

The unconsolidated PETg tailored blank is then heated in an oven to get the plastic to its forming temperature. The forming temperature for PETg is $160°C$ [24]. The temperature of the oven used to heat the blank was $250°C$. The higher oven temperature was used to counteract any cooling that would occur while the part was being moved between the oven and the mold. Heating the part took between 5 and 20 minutes depending on the starting temperature of the oven and number of times the door was opened to inspect the plastic.

This process worked well for the IE 5842, but the IE 5842b experienced some individual tape shrinkage on the unrestrained top layer. After the investigation discussed in Appendix B.1, two silicone sheets were included in the heating phase. This eliminated the shrinkage observed on the external layers of tape.

After the PETg tape reached the desired temperature, it was hand-placed into a 50-ton hydraulic press containing the 3D printed mold, shown in Figure B-12. The male mold was fixed to the bottom platen of the press using double-sided tape. The female mold was attached to the top platen with the same tape. For the first round of trials, the 3 mm thick silicone sheet was inserted into the mold before the plastic. Before the plastic was consolidated, steel spacers were put into the press

to calibrate the pressure. The hydraulic gage pressure for the press was calibrated to between 5.52 and $6.21\,MPa$, which corresponds to 0.63 and $0.72\,MPa$ on the gross surface area of the corrugated part.

After the part was placed in the mold, the press was closed. The pressure was adjusted to compensate for any lost pressure. The part was then left to cool for two minutes. The part is shown being placed in the press and consolidated in Figure B-13.

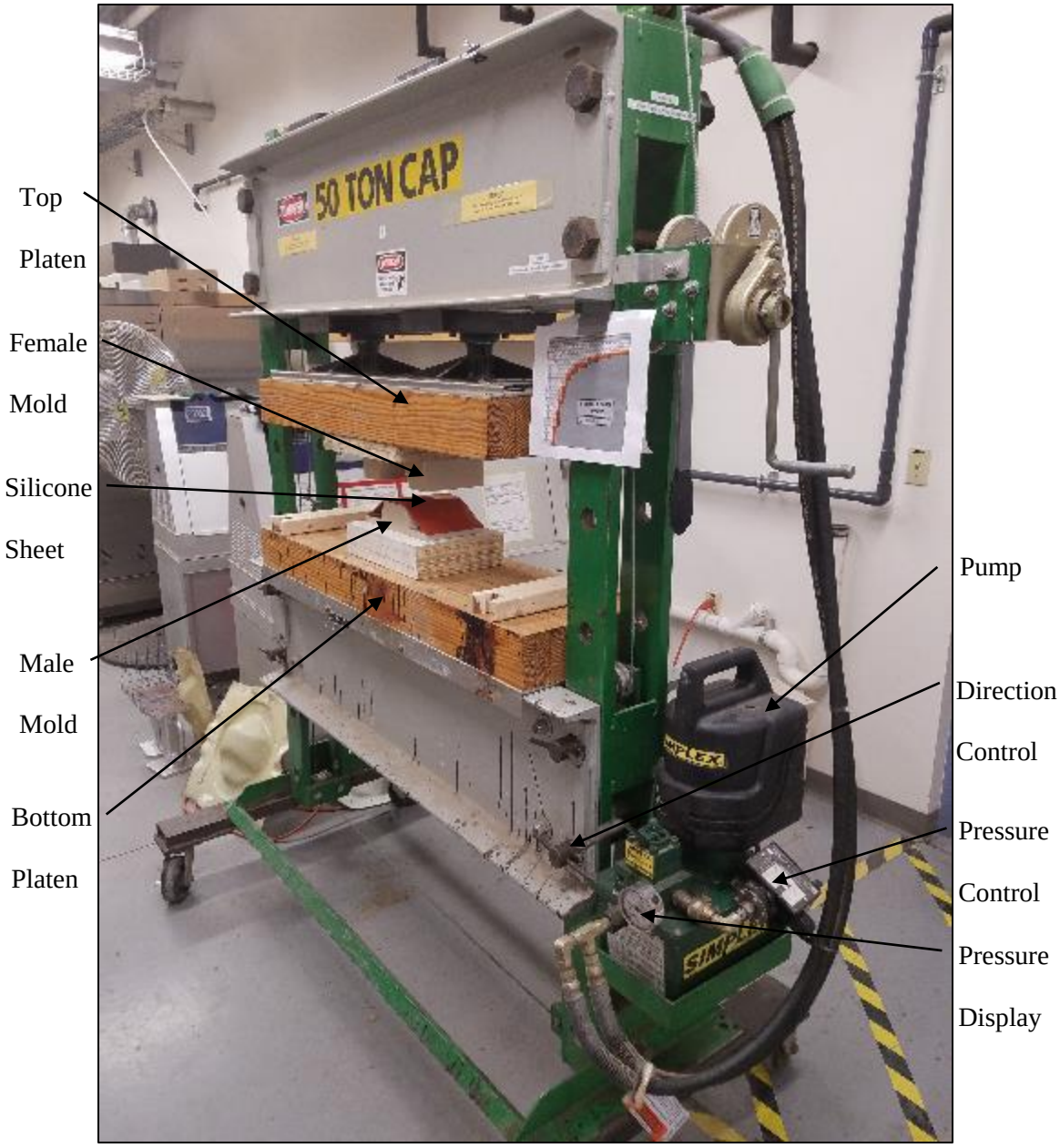

Figure B-12: ASCC's 50-ton hydraulic press

Figure B-13: Heated PETg put into the press (left) and the press closed (right)

B.2.8 First Trial Results

Three parts were made with the 45° layup out of the IE 5842 tape to test the method then two more of each layup for each material were made with varying degrees of success. Overall, the IE 5842 parts came out with a higher quality than the initial IE 5842b parts and the 45° layups were higher quality than the 0°/90° layups. All of the parts showed varying degrees of fibers washing out, which is the splaying out of fibers that are carried out along with flowing thermoplastic material during consolidation of the heated tapes.

B.2.9 IE 5842 Tape

Based on visual inspection, these parts appeared to be the highest quality. When manufacturing these parts, the individual layers of tape were not always aligned. The tapes were still curved from the roll so it was difficult to keep them together. Keeping the layers aligned could possibly be fixed

for future iterations by ultrasonically welding the layers together before they are put in the oven. Some fiber wash was observed near the curves that were closest to the outside of the part. This might have been caused by the composite not being restrained on one side unlike the interior curves. This problem might disappear if multiple corrugations are used or if the part was made to be larger than necessary then trimmed to the correct size. These issues are shown in Figure B-14.

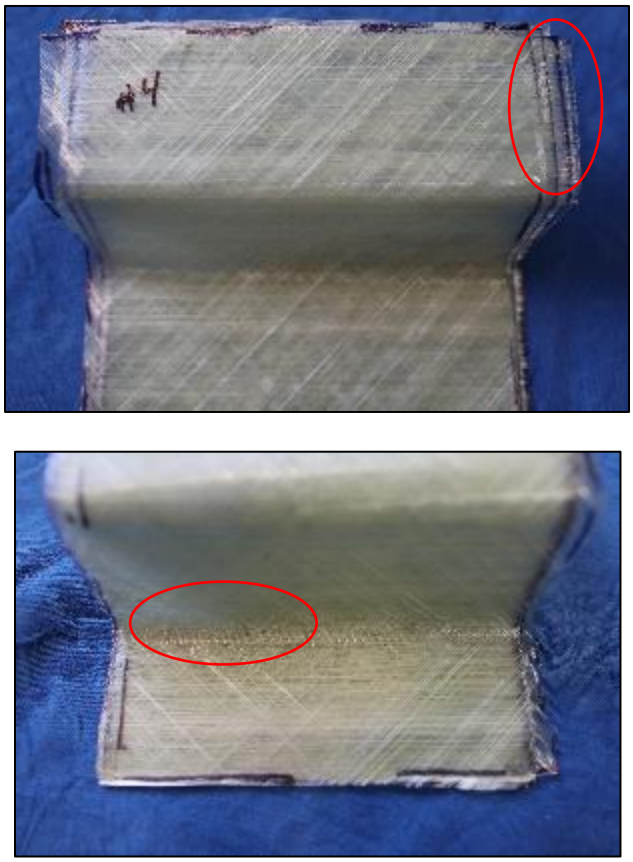

Figure B-14: 45° PETg 5842 showing misaligned layers (top) and fiber wash (bottom)

B.2.10 0°/90° IE 5842 Tape

For these parts, the largest problems were the outside 0° layer washing out and the stability of the shape post forming. As can be seen in Figure B-15, the outside layer of the fibers washed out in a similar location to the 45° IE 5842 tape. After the part had been consolidated, it was difficult to remove from the mold as the corrugation tried to flatten due to residual stresses and locked itself in the female mold. Under closer observation, it appeared that residual stresses increased the corner

radius. This phenomenon has been documented before by Padovec and is referred to as springback [25]. This can be seen in Figure B-15 where a gap formed between the part and the female mold. The springback could be avoided in the future by increasing the temperature of the part when it enters the mold.

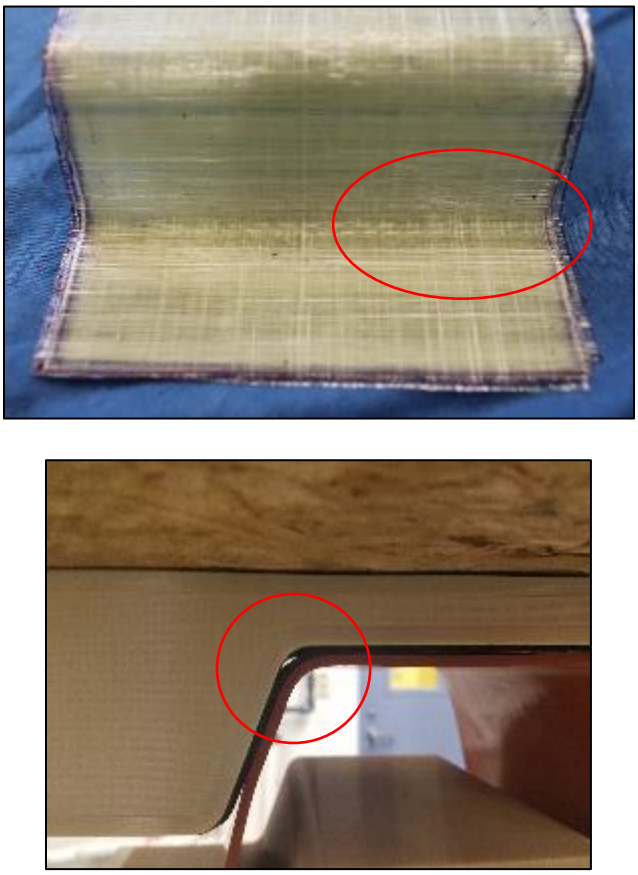

Figure B-15: 0°/90° IE 5842 showing fiber wash (top) and springback (bottom)

B.2.11 45° IE 5842b Tape

The largest problem observed for these parts was the tapes shrinking on the side of the part not restrained in the oven as can be seen in Figure B-16. This has been a common occurrence with composites made with this tape. This problem was investigated and the results are documented in Appendix B.1. These parts also required an extra step in manufacturing to trim them to the correct size, as the tailored blank had to be made larger than the desired part to have all layers cover the

entire area of the part. Fiber wash was difficult to detect in these parts as many of the fibers were already out of alignment from the tapes shrinking.

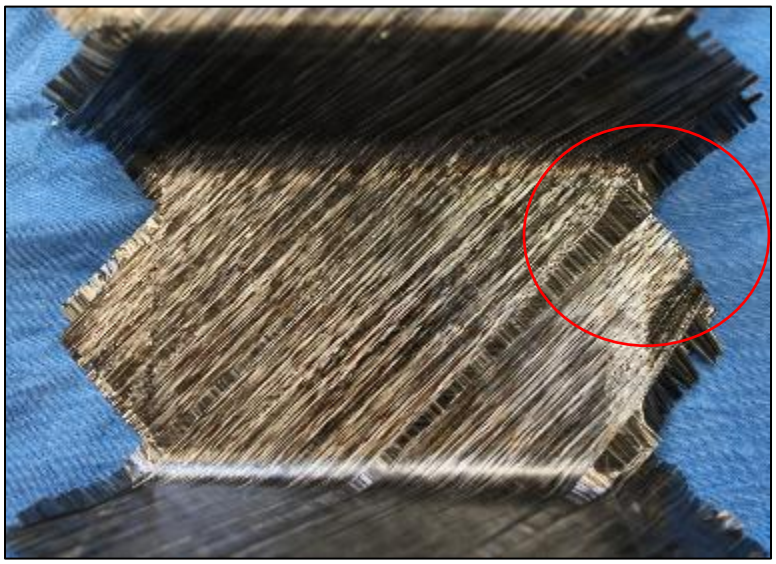

Figure B-16: 45° IE 5842b showing tape shrinkage

B.2.12 0°/90° IE 5842b

These parts showed many of the same issues as the others including fiber wash, tape shrinkage and losing the desired geometry as the corners flattened out. Overall these were the most efficient to manufacture, since the layups were produced by the automated tape layup machine, and the extra manufacturing step of trimming the excess material was not required..

B.2.13 Measurements

Thicknesses were measured with a micrometer at each section of each part. Each top flange, web, and bottom flange was measured in three locations. The average of those measurements for each resin and location are shown in Table B-1. The general trend of this data is that the bottom flange is the thickest, then the web, then the top flange. This might be caused by the top flange being unrestrained so the material there could spread out and get thinner.

Table B-1: Average thicknesses (mm)

Location	45° IE 5842	0°/90° IE 5842	45° IE 5842b	0°/90° IE 5842b
Top Flange	2.28	2.26	1.98	2.15
Bottom Flange	2.43	2.45	2.13	2.23
Web	2.36	2.37	2.13	2.20

B.2.14 Second Trial Results

For the second set of trials, the tailored blank was put into the oven and transported to the mold with thin sheets of silicone on either sides of it. The main function of the silicone was to restrain the outer layers of the tailored blanks to prevent tape shrinkage. The silicone also helped to insulate the part during transport into the mold to reduce the springback observed in previous trials. For this set of trials, two parts were made with each fiber layup. The manufactured proof-of-concept parts are shown in Figure B-17 through Figure B-20.

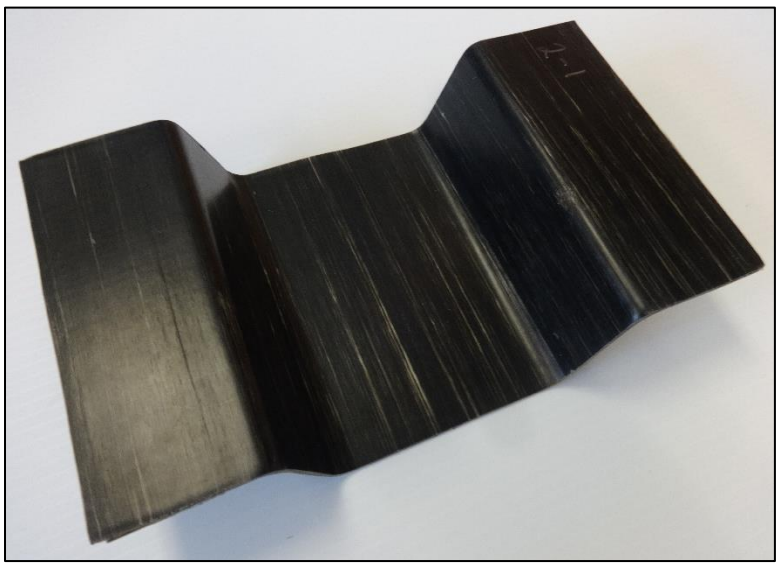

Figure B-17: 0°/90° IE 5842b Specimen 1

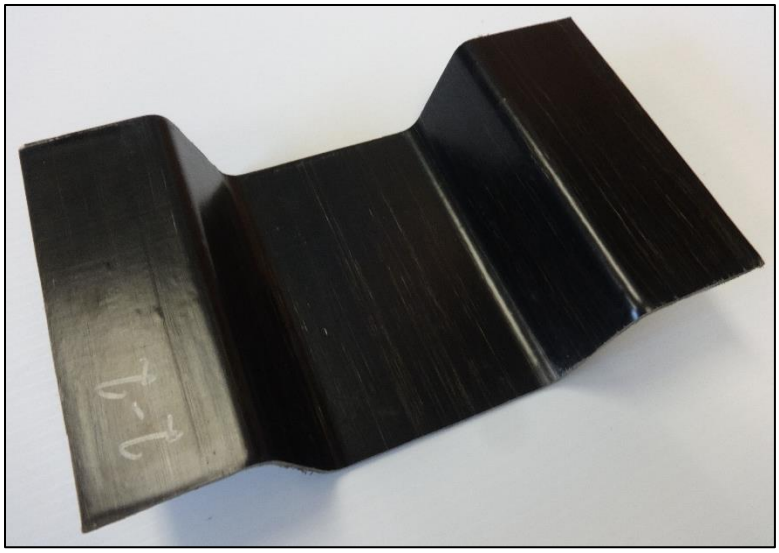

Figure B-18: 0°/90° IE 5842b Specimen 2

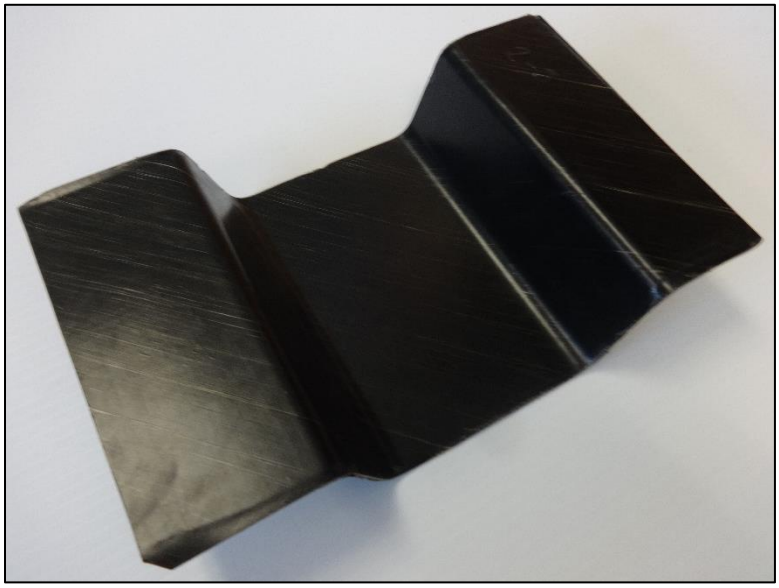

Figure B-19: ±45° IE 5842b Specimen 3

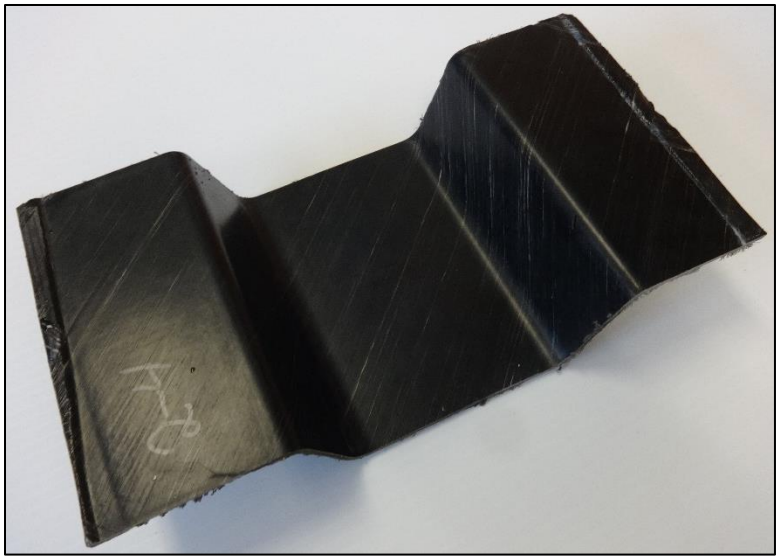

Figure B-20: ±45° IE 5842b Specimen 4

B.3 Corrugated Panel Configuration Trial Parts

Two corrugated parts were manufactured in the Alfond Advanced Manufacturing Laboratory for Structural Thermoplastics at the ASCC to validate the planned manufacturing methods for the full-scale beams.

B.3.1 Manufacturing Process

The two short corrugated CFRTP panels were manufactured using the process given in Appendix A. A slightly different design from the final design for the composite laminate given in Section 4.2.1 was used for these specimens. The same number of unidirectional and biaxial fibers were used, but they were arranged differently. The lamina were arranged in this manner to create a balanced and symmetric laminate in which the biaxial lamina are distributed evenly throughout the laminate.

$$Bottom\ Flange = [0_5/\pm 45/0_5/\pm 45/0_5/\pm 45/0_5/\mp 45/0_5/\mp 45/0_5/\mp 45/0_5]$$

$$Web = [0_5/\pm 45/0_2/\pm 45_2/0_2/\pm 45/0_2/\pm 45/\mp 45/0_2/\mp 45/0_2/\mp 45_2/0_2/\mp 45/0_5]$$

The dimensions of the tailored blank for the trial parts are shown in Figure B-21. The portion that would end up in the bottom flange was 47 layers thick and $102\ mm$ wide. The portions on either side of that which would end up in the webs and top flanges were 42 layers thick and $165\ mm$ wide. The total width of the tailored blank was 432 mm wide, which was larger than the 429 mm needed to form the designed part. This oversizing allowed the part to be trimmed to size after forming.

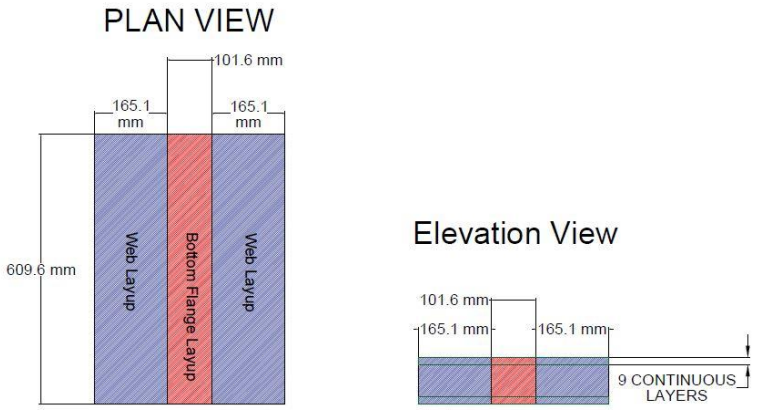

Figure B-21: Dimensions of the tailored blank for the trial corrugated CFRTP panels

The tailored blank was created in four sections on the tape layup machine. The layers that were in each section are shown in Table B-2. Each section was created by laying down each layer successively. For some layers, the tape was put down in same direction across the entire part. This mainly occurred in sections one and four. The other layers had varying fiber directions between the different layups. The continuity of the fibers between the different layups is only important for the biaxial fibers, which have individual fibers crossing the boundary between layups. The longitudinal fibers would not cross the boundary with only the PETg matrix being continuous between the layups. The continuous fibers between the layups were needed to transfer shear between the web and bottom flange effectively. Without a method to transfer shear between the web and bottom flange beyond the resin strength, the bottom flange could potentially shear off the structure.

Table B-2: Trial corrugated CFRTP panel layups

Layer	Bottom Flange Layup	Web Layup	Section
1	0	0	
2	0	0	
3	0	0	
4	0	0	
5	0	0	1
6	45	45	
7	-45	-45	
8	0	0	
9	0	0	
10	0	-	
11	0	-	
12	0	45	
13	45	-45	
14	-45	45	
15	0	-45	
16	0	0	
17	0	0	2
18	0	45	
19	0	-45	
20	45	0	
21	-45	0	
22	0	45	
23	0	-45	
24	0	-	
25	0	-45	
26	0	45	
27	-45	0	
28	45	0	
29	0	-45	
30	0	45	
31	0	0	
32	0	0	3
33	0	-45	
34	-45	45	
35	45	-45	
36	0	45	
37	0	-	
38	0	-	
39	0	0	
40	0	0	
41	-45	-45	
42	45	45	
43	0	0	4
44	0	0	
45	0	0	
46	0	0	
47	0	0	

Two flat trial panels were consolidated using the process described in Appendix A. Figure B-22shows the consolidated flat CFRTP panels made from tailored blanks by pressing them in the hydraulic press between heated consolidation platens.

Figure B-22: Consolidated trial flat CFRTP panels

These flat plates were consolidated fully, however, the multi-thickness nature of the composite plates created some dry spots in the outer region where the initial thickness of the plate was less than in the center where a nice finish was achieved.

The consolidation platens were then removed from hydraulic press and replaced with a mold that would form the consolidated panels into a corrugated shape. For the trials, an oriented strand board (OSB) mold with silicone-covered surfaces was constructed to explore the manufacturing feasibility of the designed corrugated cross-section. An OSB mold was chosen because it was a quick, inexpensive solution. The OSB mold was constructed by layering sheets of OSB and securing them together with construction adhesive and screws. The surface was machined with a computer numerical control (CNC) router to achieve the designed cross-section. A cross-sectional view of a 3-D model of the mold is shown in Figure B-23.

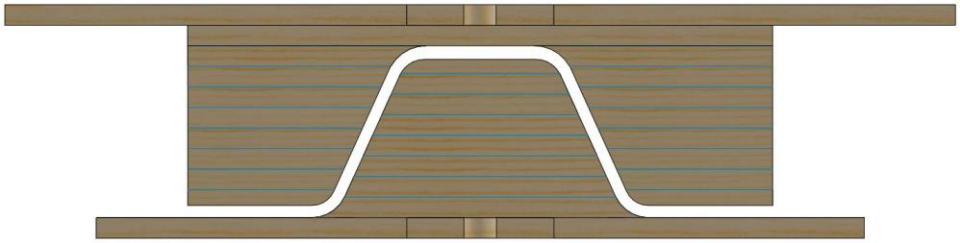

Figure B-23: 3-D model showing cross-section of OSB mold

Figure B-24 shows the final OSB mold constructed at the ASCC. The surface was covered with a $1/16\ inch$ silicone sheet adhered to the mold in order to provide temperature resistance and a smooth surface for the part.

Figure B-24: OSB Corrugated mold mounted in the hydraulic press

The two consolidated blanks were then formed into corrugations using the parameters given in Table B-3. Each panel was heated in the IR oven for 120 seconds at a temperature of $218°C$. The 120-second dwell time was separated into four increments with 30 seconds between each heating pulse. This was done to allow for adequate resin heating for flow during forming. The heated panels were then moved into the mold and stamp formed with a pressure of $517\ kPa$ across the entire area of the panel.

Table B-3: Summary of automated stamp forming processing parameters

Processing Trial Number	Material System	Part Length (mm)	IR-Oven Temperature (°C)	IR-Oven Dwell Time (seconds)	Stamping Pressure (kPa)
Trial 1	IE 5842b	432	218	120	517
Trial 2	IE 5842b	584	218	120	517

B.3.2 Results

Both trial specimens were successfully formed. Figure B-25, Figure B-26, and Figure B-27 show the $432\ mm$-long corrugated CFRTP panel. The $584\ mm$-long panel is shown in Figure B-28, Figure B-29, and Figure B-30.

Figure B-25: Trial 1 corrugated CFRTP top view

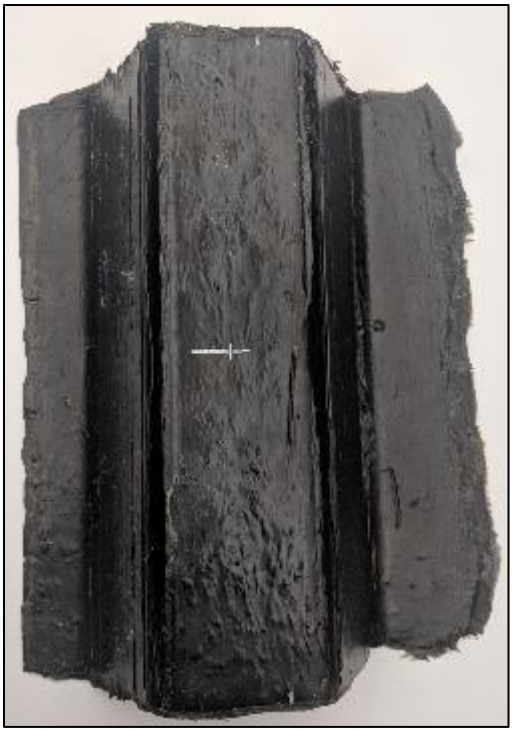

Figure B-26: Trial 1 corrugated CFRTP bottom view

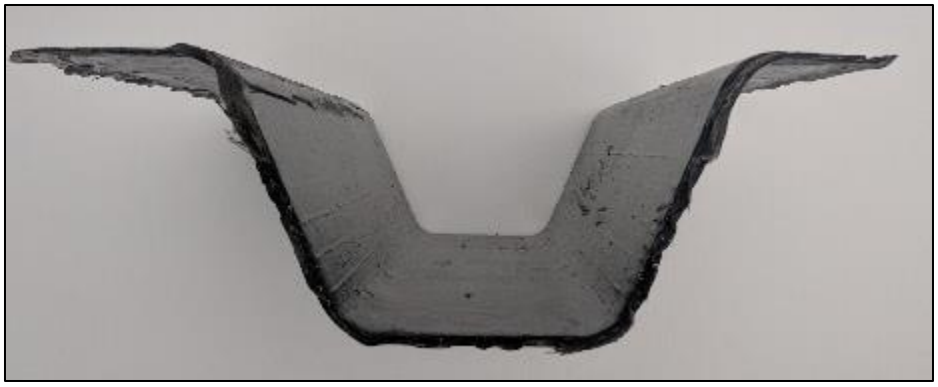

Figure B-27: Trial 1 corrugated CFRTP cross-sectional view

Figure B-28: Trial 2 corrugated CFRTP top view

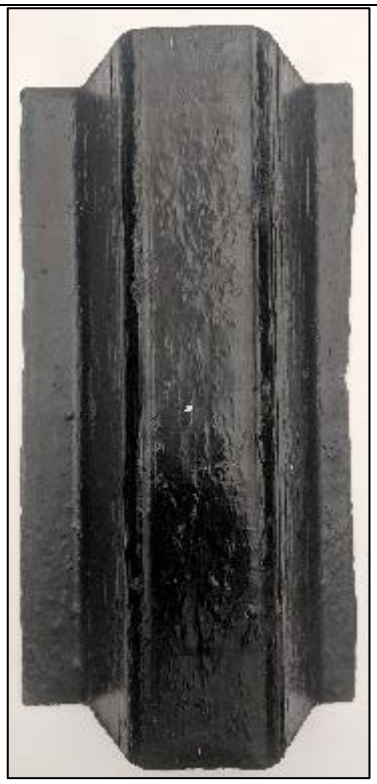

Figure B-29: Trial 2 corrugated CFRTP bottom view

Figure B-30: Trial 2 corrugated CFRTP cross-sectional view

Once the flat plates were stamp formed into corrugated sections in the mold the dry regions were mostly mitigated by movement of the resin during the reheating process. Both trial show minimal evidence of dry spots. Some surface imperfections are visible in the corrugations, such as resin

wrinkles and indents in the part. These were caused by wrinkling of the silicone on the mold surface and imperfections in the wood composite mold surface from the connection mechanism used on the press. Alignment issues were also observed which were caused by the panel being placed on the mold unsymmetrically. This caused one of the top flanges to be noticeably wider than the other. This misalignment also caused the bottom flange laminate to not line up directly with the physical bottom flange of the corrugation.

It was decided that the stamp forming process showed the potential to be suitable for future manufacturing. However, the OSB mold was unsuitable for repeated manufacturing so a new mold needed to be created. Most of the male OSB mold tore away from the base plate after the second trial. The damage to the mold is shown in Figure B-31.

Figure B-31: Broken OSB Corrugated mold after forming trials

APPENDIX C

CALCULATIONS

This appendix contains the programming and calculation sheets created during this research.

C.1 MATLAB Codes

- 200) Analysis Tool Box for Corrugated Panel
- 220) Analysis Tool Box for Stiffened Panel
- 238) F4 Calculation: F4PETg
- 239) CLT Matrix Calculations: GetCLTStuffInput
- 242) CLT Moduli Calculations: GetModuli
- 243) CLT Strength Calculations: GetStrengthsInput
- 246) Maximum Strain Failure Criteria: SR_Max_Strain
- 247) Hashin Failure Criteria: FS_Hashin_KW
- 248) Tsai-Wu Failure Criteria: SR_TsaiWu

C.2 Mathcad Sheets

- 249) Beam Shear Stud Calculations
- 252) Design of Bearing Test
- 255) Bearing Test Results
- 256) AASHTO Live Load Calculations

Table of Contents


```
function Driver_CorrugationV3

%%%%%%%%%%%%%%%%%%%%%%%%%%%%%%%%%%%%%%%%%%%%%%%%%%%%%%%%%%%%
% Analysis Tool Box for Angle Corrugated Panel V3 %
%%%%%%%%%%%%%%%%%%%%%%%%%%%%%%%%%%%%%%%%%%%%%%%%%%%%%%%%%%%%

% Author: Benjamin Smith
% Start Date: July 20, 2018
% Advanced Structures and Composites Center, University of Maine
% Project: ERDC Task 2, 1355.11

% Changes: Incorporate Hashin Failure and Poisson's effects, clean up
% variables and stress computations

%----Units----

% All units are in pounds and inches

% z measured positive up

% compression is positive

%----Drawings----

% See cross-section sketches here:

%----References----


clc
```

Inputs

```
%--Geometry--

% Length of the beam, Assume 4" supports 60" total length
L = 56; %in
% Width of top face of bottom flange,(in)
Wb=4;
% Width of bottom face of EACH top flange,(in)
Wt=2;
```

```
% Vertical height between bottom face of top flange
% and top face of bottom flange,(in)
h=4;
% Angle of webs from vertical
theta=24.4*pi()/180; %radians, input should be typed in degrees
% Depth of concrete above top of FRP,(in)
dc=2.5;

%--FRP inputs--

% Unit weight of FRP, Aerial weight from PETg data sheet with
%   measured 0.2mm thickness
UWfrp=0.073158; %pci
% Thickness of a single lamina
tl   = 0.2/25.4; %in

%-Lamina Strengths-

%Material: E-glass/PETg

%Longitudinal Tensile Strength
F1t = 9.036*10^4; %psi
%Transverse Tensile Strength
F2t = 2.103*10^3; %psi
%Longitudinal Compressive Strength
F1c = 4.495*10^4; %psi
%Transverse Compressive Strength
F2c = 9.427*10^3; %psi
%Longitudinal Elastic Modulus
E1 = 4.096*10^6; %psi, from tension test (comp=3.408*10^6)
%Transverse Elastic Modulus
E2 = 6.425*10^5; %psi, from tension test (comp=7.223*10^5)
%In-Plane Shear Strength
F6 = 4.183*10^3; %psi
%In-Plane Shear Modulus
G12 = 2.147*10^5; %psi
%In-Plane Poisson's Ratio
nu12 = 0.353; %-, from tension test (comp=0.298)
%Out-of-Plane Shear Strength
F4 = F4PETg; %psi

%-Bottom Flange-
layupb = [ 0 0 0 0 0 45 -45 0 0 0 0 0 45 -45 0 0 0 0 0 45 -45 0 0 0 0
 0 ...
    -45 45 0 0 0 0 0 -45 45 0 0 0 0 0 -45 45 0 0 0 0
 0 ]*pi()/180; %radians, 0 is longitudinal

%-Top Flange-
layupt = [ 0 0 0 0 0 45 -45 0 0 45 -45 45 -45 0 0 45 -45 0 0 45
 -45 ...
    -45 45 0 0 -45 45 0 0 -45 45 -45 45 0 0 -45 45 0 0 0 0
 0 ]*pi()/180; %radians, 0 is longitudinal

%-Web-
```

```
layupw = [ 0 0 0 0 0 45 -45 0 0 45 -45 45 -45 0 0 45 -45 0 0 45
 -45 ...
    -45 45 0 0 -45 45 0 0 -45 45 -45 45 0 0 -45 45 0 0 0 0
 0 ]*pi()/180; %radians, 0 is longitudinal

%--Shear Rod--

%Assumed material: Steel

%Diameter of rod
D = 0.75; %in
%Shear Strength of Rod
Tur = 0.6*60*10^3; %psi
%Center to center spacing between rods
pitch = 6; %in
% Depth to the center of the top rod from the top of the FRP
dr(1) = 1; %in
% Depth to the center of the bottom rod from the top of the FRP
dr(2) = 2.5; %in

%--Concrete--

% Unit weight of reinforced concrete
UWc = 150/12^3; %pci
% 28-day Concrete Compressive strength f'c (psi)
fc = 4200;
% Modulus of Rupture (psi)
MoR = 7.5*sqrt(fc);
```

Initial Calculations

```
% Elastic modulus of concrete,(psi)
Ec=57000*sqrt(fc); %(Wight Equation 3-18)

%[thickness of composite (in),thickness of each layer in composite
 (in)]
[tb,tlb]=thickness(layupb,tl);
[tt,tlt]=thickness(layupt,tl);
[tw,tlw]=thickness(layupw,tl);

% Full height of FRP
ht = tt+h+tb; %in
% Full height of composite section
htc = ht+dc;
% local width of the web,(in) (aka diagonal length)
Ww=h/cos(theta);
% Global width of of the web
ww=tw/cos(theta);
%Height of web above the first hole, top web
hwt = dr(1)-tt-D/2; %in
%Local width of top web
Wwt = hwt/cos(theta); %in
```

```
%Height of web between holes, middle web
hwm = dr(2)-dr(1)-D; %in
%Local width of middle web
Wwm = hwm/cos(theta); %in
%Height of web below the second hole, bottom web
hwb = h-(dr(2)+D/2-tt);
%Local width of bottom web
Wwb = hwb/cos(theta); %in
% Full width of section
b=2*Wt+Wb+2*h*tan(theta)+2*ww; %in
% Width of concrete at top of web
bt=Wb+2*(h+tt)*tan(theta); %in

% Area of concrete below bottom bottom hole
Acb = (hwb*(Wb+hwb*tan(theta))); %in^2
% Area of concrete between the holes
Acm = (hwm*(Wb+2*(hwb+D+hwm/2)*tan(theta))); %in^2
% Area of concrete above the top hole and below the top of the FRP
Act = (hwt*(bt-hwt*tan(theta))); %in^2
% Area of the concrete deck
Acd = b*dc; %in^2
% Total concrete area
Ac = Acb+Acm+Act+Acd; %in^2

%Cross-sectional area of the bottom flange
Ab = Wb*tb; %in^2
%Cross-sectional area of top of EACH web
Awt = Wwt*tw; %in^2
%Cross-sectional area of middle of EACH web
Awm = Wwm*tw; %in^2
%Cross-sectional area of bottom of EACH web
Awb = Wwb*tw; %in^2
%Cross-sectional area of EACH top flange
At = Wt*tt; %in^2
%Cross-sectional area of FRP
Ax = Ab + 2*(Awt+Awm+Awb) + 2* At; %in^2
```

Classical Lamination Theory

```
[ Sb,Qb,Tb,Sbarb,Qbarb,zbarb,ABDb,abdb ] = ...
    GetCLTStuffInput( layupb,E1,E2,G12,nu12,tlb );
[ St,Qt,Tt,Sbart,Qbart,zbart,ABDt,abdt ] = ...
    GetCLTStuffInput( layupt,E1,E2,G12,nu12,tlt );
[ Sw,Qw,Tw,Sbarw,Qbarw,zbarw,ABDw,abdw ] = ...
    GetCLTStuffInput( layupw,E1,E2,G12,nu12,tlw );
[Exb,Eyb,Gxyb,nuxyb,Exbb,Eybb,Gxybb,nuxybb]=GetModuli(ABDb,abdb,tb);
[Ext,Eyt,Gxyt,nuxyt,Exbt,Eybt,Gxybt,nuxybt]=GetModuli(ABDt,abdt,tt);
[Exw,Eyw,Gxyw,nuxyw,Exbw,Eybw,Gxybw,nuxybw]=GetModuli(ABDw,abdw,tw);
[ Fxtb,Fxcb,Txyb ] = GetStrengthsInput...
    ( tlb,tb,abdb,zbarb,Qbarb,Tb,Sb,E1,E2,G12,F1t,F2t,F1c,F2c,F6 );
[ Fxtt,Fxct,Txyt ] = GetStrengthsInput...
    ( tlt,tt,abdt,zbart,Qbart,Tt,St,E1,E2,G12,F1t,F2t,F1c,F2c,F6 );
[ Fxtw,Fxcw,Txyw ] = GetStrengthsInput...
```

```
    ( tlw,tw,abdw,zbarw,Qbarw,Tw,Sw,E1,E2,G12,F1t,F2t,F1c,F2c,F6 );
```

Wet Concrete Loads

```
disp('Wet Concrete Loads')

%-Loads-

% Constant distributed load on beam (AASHTO (2012) 9.7.4.1)
w=(UWc*dc+(0.05*1000/12^2))*b+UWc*(h+tt)*(Wb+bt)/2+UWfrp*Ax; %pli
%Maximum moment in beam, assuming simply supported (AISC Table 3-23)
M=w*L^2/8; %in*lb
%Maximum shear force in simply supported beam
V=w*L/2; %lb

%Moment from 4-point bend
M = V*L/3; %in*lb

%-Geometry-

%Location of the neutral axis, from bottom
NA = (Exb*Ab*(tb/2) + 2*Exw*(Awb*(tb+hwb/2) + Awm*(tb+hwb+D+hwm/2)
 + ...
    Awt*(tb+hwb+D+hwm+D+hwt/2)) + Ext*(2*At)*(tb+h+tt/2)) / ...
    (Exb*Ab+2*Exw*(Awt+Awm+Awb)+2*Ext*At); %in

%Bending Stiffness
EI = Exb*(Wb*tb^3/12 + Ab*(NA-tb/2)^2) + ...
    2*Exw*(ww*(hwt^3+hwm^3+hwb^3)/12 + ...
    Awb*(NA-(tb+hwb/2))^2 + Awm*(NA-(tb+hwb+D+hwm/2))^2 + ...
    Awt*(NA-(tb+hwb+D+hwm+D+hwt/2))^2) + 2*Ext*(Wt*tt^3/12 + ...
    At*(NA-(tb+h+tt/2))^2); %lb*in^2
%Curvature
K = M/EI; %in^-1

%--Checks--

%-Strength-

%Top Flange

%Distance from NA to centroid of the top flange, positive up
zo = tb+h+tt/2-NA; %in
%Distance from NA to center of each lamina in top flange
z1 = zo+zbart; %in
%Longitudinal strain at each lamina
ex = K*z1;
%Transverse strain at each lamina
ey = -nuxyt*ex;
%In-plane shear strain
gammaxy = zeros(1,length(z1));
for k = 1:length(z1)
    [~,gammaxy(k)] = shear_strain(z1(k));
```

```
end
%Strain at each lamina, - because failure criteria assumes tension is
%positive
strains = [-ex;-ey;gammaxy];
[SRHa1,MODE1,SRMS1,SRTW1] = strH(layupt,Qbart,Tt);

gamma = gammaxy;

%Web

%Location of each point along web to check, starting at top of web
x = 0:0.05:h; %in
%Distance from NA to each point along web to check, starting at top of
 web
z2 = ht-NA-tt-x; %in
%Longitudinal strain at each point to check
ex = K*z2;
%Transverse strain at each point to check
ey = -nuxyw*ex;
%In-plane shear strain at each point to check
gammaxy = zeros(1,length(z2));
Tauxy = gammaxy;
for k = 1:length(z2)
    [Tauxy(k),gammaxy(k)] = shear_strain(z2(k));
end
%Strain at each lamina, - because failure criteria assumes tension is
%positive
strains = [-ex;-ey;gammaxy];
[SRHa2,MODE2,SRMS2,SRTW2] = strV(layupw,Qbarw,Tw,z2);

gamma = [gamma gammaxy];

%Bottom Flange

%Distance from NA to centroid of the bottom flange, positive up
zo = tb/2-NA; %in
%Distance from NA to center of each lamina in bottom flange
z3 = zo+zbarb; %in
%Longitudinal strain at each lamina
ex = K*z3;
%Transverse strain at each lamina
ey = -nuxyb*ex;
%In-plane shear strain
gammaxy = zeros(1,length(z3));
for k = 1:length(z3)
    [~,gammaxy(k)] = shear_strain(z3(k));
end
%Strain at each lamina, - because failure criteria assumes tension is
%positive
strains = [-ex;-ey;gammaxy];
[SRHa3,MODE3,SRMS3,SRTW3] = strH(layupb,Qbarb,Tb);

gamma = [gamma gammaxy];
```

```
%Summary
SRHa = [SRHa1,SRHa2,SRHa3];
MODE = [MODE1,MODE2,MODE3];
z = [z1,z2,z3];
SRMS = [SRMS1,SRMS2,SRMS3];
SRTW = [SRTW1,SRTW2,SRTW3];

addpath('\\storage-01.umcomposites.umaine.edu\ERDC Projects\1355 &
 1554\T2\Project Work\Design\MATLAB Code\Analysis Toolbox')
figure(1)
clf
hold on
box on
plot(SRHa,z*25.4,'*')
plot(SRMS,z*25.4,'*')
plot(SRTW,z*25.4,'*')
plot(linspace(0,100,1000),(-NA+tb)*ones(1,1000)*25.4)
plot([linspace(0,100,1000) linspace(0,100,1000)],[(-NA+tb
+hwb)*ones(1,1000)*25.4 (-NA+tb+hwb+D)*ones(1,1000)*25.4])
plot([linspace(0,100,1000) linspace(0,100,1000)],[(-NA+tb+hwb+D
+hwm)*ones(1,1000)*25.4 (-NA+tb+hwb+D+hwm+D)*ones(1,1000)*25.4])
plot(linspace(0,100,1000),(-NA+tb+hwb+D+hwm+D+hwt)*ones(1,1000)*25.4)
axis([0 100 -NA*25.4 (ht-NA)*25.4])
xlabel('Strength Ratio (Capacity/Load)')
ylabel('Vertical Distance From the Neutral Axis (mm)')
% title('Corrugation - Strength Ratios Over the Section Under Wet
 Concrete Loads')
legend('Hashin','Max Strain','Tsai-Wu','Top of bottom flange','Bottom
 Hole','Top Hole','Bottom of top flange','location','east')

thesisfig
saveas(gcf,'\\aewc-dc05\Grads\benjamin.t.smith\Thesis\THESIS\FIGURES
\corrconstructionfailure','emf')

[SR_Hash,index] = min(SRHa);
MODE = MODE(index);
fail_mode = {'fiber tension','fiber compression','matrix
 tension','matrix compression'};
locs = {'top flange','web','bottom flange'};
MODE = fail_mode{MODE};
d_Hash = ht-(z(index)+NA);
if d_Hash < tt
    loc_Hash = locs{1};
elseif d_Hash < tt+h
    loc_Hash = locs{2};
else
    loc_Hash = locs{3};
end

[SR_MS,index] = min(SRMS);
d_MS = ht-(z(index)+NA);
if d_MS < tt
    loc_MS = locs{1};
elseif d_MS < tt+h
```

```
    loc_MS = locs{2};
else
    loc_MS = locs{3};
end

[SR_TW,index] = min(SRTW);
d_TW = ht-(z(index)+NA);
if d_TW < tt
    loc_TW = locs{1};
elseif d_TW < tt+h
    loc_TW = locs{2};
else
    loc_TW = locs{3};
end

fprintf('The minimum SR of the FRP is in %s in the %s under wet
 concrete loads: %1.1f (Hashin)\n',MODE,loc_Hash,SR_Hash)
fprintf('The minimum SR of the FRP is in the %s under wet concrete
 loads: %1.1f (Max Strain)\n',loc_MS,SR_MS)
fprintf('The minimum SR of the FRP is in the %s under wet concrete
 loads: %1.1f (Tsai Wu)\n',loc_TW,SR_TW)

%-Stability-

%AASHTO Deflection

%Deflection in simply supported beam (AISC Table 3-23)
defl=5*w*L^4/384/EI; %in
%Max allowable deflection for spans up to 10 feet from (AASHTO (2012)
 9.7.4.1)
deflmax=min(L/180,0.5); %in

if defl<deflmax
    disp('The AASHTO requirement for deflection in the beam of SIP
 formwork is met')
else
    disp('The AASHTO requirement for deflection in the beam of SIP
 formwork is not met')
end

%ASCE Web Shear Buckling (Roberto)

%Factor (Eqn. 7.7.3-3)
etaLT = (2*Gxyw+Eyw*nuxyw)/sqrt(Exw*Eyw);
if etaLT > 1
    Fcr = (3.9+0.47/(etaLT^2))*(tw/L)^2*sqrt(Eyw*(Eyw*nuxyw+2*Gxyw));
elseif etaLT > 0
    Fcr = (2.7+1.7*etaLT)*(tw/L)^2*(Exw*Eyw^3)^(1/4);
else
    error('web shear buckling equation problem')
end
Nu = max(Tauxy);
phi_WSB = 0.7;
FS = phi_WSB*Fcr/Nu;
```

```
fprintf('The FS against the web failing in web shear buckling under
 wet concrete loads: %1.1f\n',FS)

INT = 0.05*trapz(abs(Tauxy));
Dev_Len = INT/F6;

fprintf('Development length needed in flanges: %1.1f inches
 \n',Dev_Len)

fprintf('\nAASHTO Load: %1.2f kips\n',V*2/1000)
fprintf('Shear Buckling Load: %1.2f kips\n',V*2/1000*FS)

NAw = NA;
```

AASHTO Loads for Bridge Decking

```
disp(' ')
disp('AASHTO Loads')

%-Loads-

% Maximum live load moment from AASHTO Live Load Calculation Mathcad
 Sheet (lb-in)
M_LL = 6.294 * 1000 * b;
% Self-Weight of concrete and FRP (lb/in)
% w_DC = UWc*b*db + UWfrp*Ax;
w_DC = 0;
% Maximum DC moment assuming simply supported (lb-in)
M_DC = w_DC*L^2/8;
% Weight of assumed 2" wearing surface (lb/in)
w_DW = 140/12^3*2*b;
% Maximum DW moment assuming simply supported (lb-in)
M_DW = w_DW*L^2/8;
% Maximum factored moment (lb-in)
Mu = 1.75*M_LL + 1.25*M_DC + 1.5*M_DW;

%-Geometry-

%First crack

%Elastic NA (distance from bottom of FRP)
eNA = (Exb*Ab*(tb/2) + 2*Exw*(Awb*(tb+hwb/2) + Awm*(tb+hwb+D+hwm/2)
 + ...
    Awt*(tb+hwb+D+hwm+D+hwt/2)) + Ext*(2*At)*(tb+h+tt/2) + ...
    Ec*((Acb*(tb+hwb/2) + Acm*(tb+hwb+D+hwm/2) + Act*(tb+h-hwt/2)
 + ...
    Acd*(tb+h+tt+dc/2)))) / (Exb*Ab+2*Exw*(Awt+Awm+Awb)+2*Ext*At
+Ec*Ac); %in

%Bottom concrete
A = Wb;
B = Wb+2*hwb*tan(theta);
```

```
cybarb = hwb - (hwb*(2*A+B))/(3*(A+B));
Icb = hwb^3*(A^2+4*A*B+B^2)/(36*(A+B));
%Middle Concrete
A = Wb+2*(hwb+D)*tan(theta);
B = Wb+2*(hwb+D+hwm)*tan(theta);
cybarm = hwm - (hwm*(2*A+B))/(3*(A+B));
Icm = hwm^3*(A^2+4*A*B+B^2)/(36*(A+B));
%Top Concrete
A = bt-2*(hwt+tt)*tan(theta);
B = bt;
cybart = hwt - (hwt*(2*A+B))/(3*(A+B));
Ict = hwt^3*(A^2+4*A*B+B^2)/(36*(A+B));
%Deck Concrete
cybard = dc/2;
Icd = b*dc^3/12;

%Elastic bending stiffness
eEI = Exb*(Wb*tb^3/12 + Ab*(eNA-tb/2)^2) + ...
    2*Exw*(ww*(hwt^3+hwm^3+hwb^3)/12 + ...
    Awb*(eNA-(tb+hwb/2))^2 + Awm*(eNA-(tb+hwb+D+hwm/2))^2 + ...
    Awt*(eNA-(tb+hwb+D+hwm+D+hwt/2))^2) + 2*Ext*(Wt*tt^3/12 + ...
    At*(eNA-(tb+h+tt/2))^2) + Ec*(Icb+Acb*(eNA-(cybarb+tb))^2+...
    Icm+Acm*(eNA-(cybarm+D+hwb+tb))^2+Ict+...
    Act*(eNA-(cybart+2*D+hwm+hwb+tb))^2+Icd+...
    Acd*(eNA-(tb+h+tt+cybard))^2); %lb*in^2

crackload = 6*eEI*(MoR/Ec)/(L*(eNA-tb));

%Cracked NA (distance from bottom of FRP)
cNA = (Exb*Ab*(tb/2) + 2*Exw*(Awb*(tb+hwb/2) + Awm*(tb+hwb+D+hwm/2)
 + ...
    Awt*(tb+hwb+D+hwm+D+hwt/2)) + Ext*(2*At)*(tb+h+tt/2) + ...
    Ec*(Acd*(tb+h+tt+dc/2))) / (Exb*Ab+2*Exw*(Awt+Awm+Awb)+2*Ext*At
+Ec*Acd); %in

%Cracked bending stiffness
cEI = Exb*(Wb*tb^3/12 + Ab*(cNA-tb/2)^2) + ...
    2*Exw*(ww*(hwt^3+hwm^3+hwb^3)/12 + ...
    Awb*(cNA-(tb+hwb/2))^2 + Awm*(cNA-(tb+hwb+D+hwm/2))^2 + ...
    Awt*(cNA-(tb+hwb+D+hwm+D+hwt/2))^2) + 2*Ext*(Wt*tt^3/12 + ...
    At*(cNA-(tb+h+tt/2))^2) + Ec*(Icd+...
    Acd*(cNA-(tb+h+tt+cybard))^2); %lb*in^2

% non composite EI

frpEI = EI;

concNA = (Ec*((Acb*(tb+hwb/2) + Acm*(tb+hwb+D+hwm/2) + ...
    Act*(tb+h-hwt/2) + Acd*(tb+h+tt+dc/2)))) / (Ec*Ac); %in


concEI = Ec*(Icb+Acb*(concNA-(cybarb+tb))^2+...
    Icm+Acm*(concNA-(cybarm+D+hwb+tb))^2+Ict+...
    Act*(concNA-(cybart+2*D+hwm+hwb+tb))^2+Icd+...
```

```
    Acd*(concNA-(tb+h+tt+cybard))^2); %lb*in^2

compEI = concEI+frpEI;

% Strain in extreme concrete fiber that causes crushing
strainc=0.003;

%Save linear K and NA
K1 = K;
NA1 = NA;

%Distance to the neutral axis from the top of the concrete
c = fzero(@sum_corr,1); %in
%Distance to the neutral axis from the bottom of the FRP
NA = htc-c; %in

dNA = NA-NA1;

%Curvature
K = strainc/c; %in^-1

[~,comp,~] = intSFM(c,0,K);
[~,tens,~] = intSFM(c-dc,-NA,K);

check = comp+tens;

fprintf('The sum of forces in the beam under ultimate loads is %1.1f
 pounds\n',check)

%Nominal moment capacity, summed loads around neutral axis
[~,~,Mn] = intSFM(htc-NA,-NA,K);

phib = 1;

FS = phib*Mn/Mu;

fprintf('The FS against the beam failing in flexure under factored
 AASHTO loads is %1.1f\n',FS)

%--Checks--

%-Strength-

[~,~,M1] = intSFM(htc-NA,-NA,K);
Vu = 3*M1/L;
dx = 0.001;
K2=fzero(@MoEquil,K);

fprintf('Applied load: %1.1f kips\n',2*Vu/1000)

%Top Flange

%Distance from NA to centroid of the top flange, positive up
zo = ht-tt/2-NA; %in
```

```
%Distance from NA to center of each lamina in top flange
z1 = zo+zbart; %in
%Longitudinal strain at each lamina
ex = K*z1;
%Transverse strain at each lamina
ey = -nuxyt*ex;
%In-plane shear strain
gammaxy = zeros(1,length(z1));
for k = 1:length(z1)
    [~,gammaxy(k)] = shear_strainU(z1(k));
end
%Strain at each lamina, - because failure criteria assumes tension is
%positive
strains = [-ex;-ey;gammaxy];
[SRHa1,MODE1,SRMS1,SRTW1] = strH(layupt,Qbart,Tt);

%Web

%Location of each point along web to check, starting at top of web
x = 0:0.05:h; %in
%Distance from NA to each point along web to check, starting at top of
 web
z2 = ht-NA-tt-x; %in
%Longitudinal strain at each point to check
ex = K*z2;
%Transverse strain at each point to check
ey = -nuxyw*ex;
%In-plane shear strain at each point to check
gammaxy = zeros(1,length(z2));
for k = 1:length(z2)
    [Tau(k),gammaxy(k)] = shear_strainU(z2(k));
end
%Strain at each lamina, - because failure criteria assumes tension is
%positive
strains = [-ex;-ey;gammaxy];
[SRHa2,MODE2,SRMS2,SRTW2] = strV(layupw,Qbarw,Tw,z2);

%Bottom Flange

%Distance from NA to centroid of the bottom flange, positive up
zo = tb/2-NA; %in
%Distance from NA to center of each lamina in bottom flange
z3 = zo+zbarb; %in
%Longitudinal strain at each lamina
ex = K*z3;
%Transverse strain at each lamina
ey = -nuxyb*ex;
%In-plane shear strain
gammaxy = zeros(1,length(z3));
for k = 1:length(z3)
    [~,gammaxy(k)] = shear_strainU(z3(k));
end
%Strain at each lamina, - because failure criteria assumes tension is
%positive
```

```
strains = [-ex;-ey;gammaxy];
[SRHa3,MODE3,SRMS3,SRTW3] = strH(layupb,Qbarb,Tb);

%Summary
SRHa = [SRHa1,SRHa2,SRHa3]*Mn/Mu;
MODE = [MODE1,MODE2,MODE3];
z = [z1,z2,z3];
SRMS = [SRMS1,SRMS2,SRMS3]*Mn/Mu;
SRTW = [SRTW1,SRTW2,SRTW3]*Mn/Mu;
figure(2)
clf
hold on
box on
plot(SRHa,z*25.4,'*')
plot(SRMS,z*25.4,'*')
plot(SRTW,z*25.4,'*')
plot(linspace(0,10,1000),(-NA+tb)*ones(1,1000)*25.4)
plot([linspace(0,10,1000) linspace(0,10,1000)],[(-NA+tb
+hwb)*ones(1,1000)*25.4 (-NA+tb+hwb+D)*ones(1,1000)*25.4])
plot([linspace(0,10,1000) linspace(0,10,1000)],[(-NA+tb+hwb+D
+hwm)*ones(1,1000)*25.4 (-NA+tb+hwb+D+hwm+D)*ones(1,1000)*25.4])
plot(linspace(0,10,1000),(-NA+tb+h)*ones(1,1000)*25.4)
plot(linspace(0,10,1000),(-NA+ht)*ones(1,1000)*25.4)
axis([0 10 -NA*25.4 (htc-NA)*25.4])
xlabel('Strength Ratio (Capacity/Load)')
ylabel('Distance From the Neutral Axis (mm)')
% title('Corrugation - Strength Ratios Over the Section Under Ultimate
 Loads')
legend('Hashin','Maximum Strain','Tsai-Wu','Top of bottom
 flange','Bottom Hole','Top Hole','Bottom of top flange','Top of
 CFRTP','location','east')
thesisfig
saveas(gcf,'\\aewc-dc05\Grads\benjamin.t.smith\Thesis\THESIS\FIGURES
\corrultimate','emf')

[SR_Hash,index] = min(SRHa);
MODE = MODE(index);
fail_mode = {'fiber tension','fiber compression','matrix
 tension','matrix compression'};
MODE = fail_mode{MODE};
d_Hash = ht-(z(index)+NA);
if d_Hash < tt
    loc_Hash = locs{1};
elseif d_Hash < tt+h
    loc_Hash = locs{2};
else
    loc_Hash = locs{3};
end

[SR_MS,index] = min(SRMS);
d_MS = ht-(z(index)+NA);
if d_MS < tt
    loc_MS = locs{1};
elseif d_MS < tt+h
```

```
    loc_MS = locs{2};
else
    loc_MS = locs{3};
end

[SR_TW,index] = min(SRTW);
d_TW = ht-(z(index)+NA);
if d_TW < tt
    loc_TW = locs{1};
elseif d_TW < tt+h
    loc_TW = locs{2};
else
    loc_TW = locs{3};
end

fprintf('The minimum SR of the FRP is in %s in the %s under ultimate
 loads: %1.1f (Hashin)\n',MODE,loc_Hash,SR_Hash)
fprintf('The minimum SR of the FRP is in the %s under ultimate loads:
 %1.1f (Max Strain)\n',loc_MS,SR_MS)
fprintf('The minimum SR of the FRP is in the %s under ultimate loads:
 %1.1f (Tsai Wu)\n',loc_TW,SR_TW)

%-Shear Connector-

[~,f1,~] = intSFM(c-dc,c-dc-tt-hwt-D-hwm/2,K);
[~,f2,~] = intSFM(c-dc,c-dc-tt-hwt-D-hwm/2,K2);
Tau = (f2-f1)/(2*ww)/dx

q_top = abs(Tau)*(2*ww);

[~,f1,~] = intSFM(c-dc-tt-hwt-D-hwm/2,-NA,K);
[~,f2,~] = intSFM(c-dc-tt-hwt-D-hwm/2,-NA,K2);
Tau = (f2-f1)/(2*ww)/dx;

q_bot = abs(Tau)*(2*ww);

Frod_top = q_top*pitch;
Frod_bot = q_bot*pitch;

Fu = 2*Tur*pi*D^2/4;

FS=Fu/Frod_top;
fprintf('FS Top Shear Connector in shear (AASHTO loads): %1.1f\n',FS)
FS=Fu/Frod_bot;
fprintf('FS Bottom Shear Connector in shear (AASHTO loads): %1.1f
\n',FS)

% Bearing area of composite (in^2)
Abear = ww * D * 2;
%Bearing strength
Fbear = Fxcw/(7.672*10^4)*50000; %psi
Fbear = 1232/(8*tl)/D;
% Capacity of composite in bearing (lb)
Fcap = Fbear*Abear;
```

```
% The factor of safety against the web failing in bearing AASHTO loads
FS = Fcap/Frod_top;
fprintf('FS Web in bearing - top hole (AASHTO loads): %1.1f\n',FS)
FS = Fcap/Frod_bot;
fprintf('FS Web in bearing - bottom hole (AASHTO loads): %1.1f\n',FS)

%-Development length in flanges-

INT = 0.05*trapz(abs(Tau));
Dev_Len = INT/F6;

fprintf('Development length needed in flanges: %1.1f inches
 \n',Dev_Len)


%Drawing of shape
figure(3)
clf
axis equal
hold on
box on
%Hybrid Ultimate NA
UNA = plot([0 b],[NA NA],'r');
%Hybrid Elastic NA
ENA = plot([0,b],[eNA eNA],'y');
%Wet Concrete NA
WNA = plot([0 b],[NAw NAw],'g');
%FRP
NODES = [0 tb+h;Wt tb+h;Wt+(h+tb)*tan(theta) 0;b-(Wt+(h
+tb)*tan(theta)) ...
    0;b-Wt tb+h;b tb+h;b tb+h+tt;b-Wt-ww+tt*tan(theta) tb+h+tt;...
    b-Wt-ww-h*tan(theta) tb;Wt+ww+h*tan(theta) tb;Wt+ww-
tt*tan(theta) ...
    tb+h+tt;0 tb+h+tt];
CONNECTIVITIES = [1 2;2 3;3 4;4 5;5 6;6 7;7 8;8 9;9 10;10 11;11 12;12
 1];
for i=1:length(CONNECTIVITIES) % Draws the line for each member
    line([NODES(CONNECTIVITIES(i,1),1)
 NODES(CONNECTIVITIES(i,2),1)],...
        [NODES(CONNECTIVITIES(i,1),2) NODES(CONNECTIVITIES(i,2),2)]);
end
%Concrete
NODES = [0 tb+h+tt;0 tb+h+tt+dc;b tb+h+tt+dc;b tb+h+tt];
CONNECTIVITIES = [1 2;2 3;3 4];
for i=1:length(CONNECTIVITIES) % Draws the line for each member
    line([NODES(CONNECTIVITIES(i,1),1)
 NODES(CONNECTIVITIES(i,2),1)],...
        [NODES(CONNECTIVITIES(i,1),2) NODES(CONNECTIVITIES(i,2),2)]);
end
%rod 1
plot([0 b b 0 0],[D/2 D/2 -D/2 -D/2 D/2]+ht-dr(1),'k')
%rod 2
```

```
plot([0 b b 0 0],[D/2 D/2 -D/2 -D/2 D/2]+ht-dr(2),'k')

legend([UNA ENA WNA],{'Hybrid Ultimate NA','Hybrid Elastic NA','FRP
 NA'})

VAASHTO = 4*Mu/L;
Papp = 2*VAASHTO;

fprintf('Required AASHTO load: %1.1f kips\n',Papp/1000)
```

Subroutines

```
    function [tp,tlp] = thickness(layup,tl)
        tlp = tl*ones(1,length(layup)); % A vector of the thickness of
 each layer (in)
        tp=sum(tlp); % Thickness composite (in)
    end

    function [Tau,Gamma] = shear_strain(z)
        if z >= tb+h-NA
            t = 2*Wt;
            G = Gxyt;
        elseif z>= tb-NA
            t = 2*tw;
            G = Gxyw;
        else
            t = Wb;
            G = Gxyb;
        end
        EQ = FMA(z);
        %Shear stress
        Tau = V*EQ/EI/t; %psi
        %Shear strain
        Gamma = Tau/G; %-
    end

    function [EQ] = FMA(z)
        if NA<tb+hwb
            if z >= ht-NA
                EQ = 0;
            elseif z >= ht-tt-NA
                temp = ht-(z+NA); %in, height of top flange above z
                EQ = Ext*temp*(2*Wt)*(z+temp/2);
            elseif z >= ht-dr(1)-NA+D/2
                temp = tb+h-(NA+z); %in, height of top web above z
                EQ = Ext*tt*(2*Wt)*(tb+h+tt/2-NA) + Exw*temp*(2*ww)*(z
+temp/2);
            elseif z >= ht-dr(1)-NA-D/2
                EQ = Ext*tt*(2*Wt)*(tb+h+tt/2-NA) + ...
                    Exw*hwt*(2*ww)*(tb+h-hwt/2-NA);
            elseif z >= ht-dr(2)-NA+D/2
                temp = tb+hwb+D+hwm-(NA+z); %in, height in middle web
 above z
```

```
                EQ = Ext*tt*(2*Wt)*(tb+h+tt/2-NA) + ...
                    Exw*hwt*(2*ww)*(tb+h-hwt/2-NA) + ...
                    Exw*temp*(2*ww)*(z+temp/2);
            elseif z >= ht-dr(2)-NA-D/2
                EQ = Ext*tt*(2*Wt)*(tb+h+tt/2-NA) + ...
                    Exw*hwt*(2*ww)*(tb+h-hwt/2-NA) + ...
                    Exw*hwm*(2*ww)*(tb+hwb+D+hwm/2-NA);
            elseif z >= 0
                temp = tb+hwb-(NA+z); %in, height in bottom web above
 z
                EQ = Ext*tt*(2*Wt)*(tb+h+tt/2-NA) + ...
                    Exw*hwt*(2*ww)*(tb+h-hwt/2-NA) + ...
                    Exw*hwm*(2*ww)*(tb+hwb+D+hwm/2-NA) + ...
                    Exb*temp*(2*ww)*(z+temp/2);
            elseif z>= tb-NA
                temp = (NA-tb)+z; %in, height of bottom web below z
                EQ = Exb*tb*Wb*(NA-tb/2) + Exw*temp*(2*ww)*(NA-tb-
temp/2);
            else
                temp = NA+z; %in, height of the bottom flange below z
                EQ = Exb*temp*Wb*(NA-temp/2);
            end
        elseif NA<tb+hwb+D
            if z >= ht-NA
                EQ = 0;
            elseif z >= ht-tt-NA
                temp = ht-(z+NA); %in, height of top flange above z
                EQ = Ext*temp*(2*Wt)*(z+temp/2);
            elseif z >= ht-dr(1)-NA+D/2
                temp = tb+h-(NA+z); %in, height of top web above z
                EQ = Ext*tt*(2*Wt)*(tb+h+tt/2-NA) + Exw*temp*(2*ww)*(z
+temp/2);
            elseif z >= ht-dr(1)-NA-D/2
                EQ = Ext*tt*(2*Wt)*(tb+h+tt/2-NA) + ...
                    Exw*hwt*(2*ww)*(tb+h-hwt/2-NA);
            elseif z >= ht-dr(2)-NA+D/2
                temp = tb+hwb+D+hwm-(NA+z); %in, height in middle web
 above z
                EQ = Ext*tt*(2*Wt)*(tb+h+tt/2-NA) + ...
                    Exw*hwt*(2*ww)*(tb+h-hwt/2-NA) + ...
                    Exw*temp*(2*ww)*(z+temp/2);
            elseif z >= ht-dr(2)-NA-D/2
                EQ = Ext*tt*(2*Wt)*(tb+h+tt/2-NA) + ...
                    Exw*hwt*(2*ww)*(tb+h-hwt/2-NA) + ...
                    Exw*hwm*(2*ww)*(tb+hwb+D+hwm/2-NA);
            elseif z>= tb-NA
                temp = (NA-tb)+z; %in, height of bottom web below z
                EQ = Exb*tb*Wb*(NA-tb/2) + Exw*temp*(2*ww)*(NA-tb-
temp/2);
            else
                temp = NA+z; %in, height of the bottom flange below z
                EQ = Exb*temp*Wb*(NA-temp/2);
            end
        else
```

```
            error('change EQ function')
        end
    end

    function [SRHa,MODE,SRMS,SRTW] = strH(layup,Qbar,T)
        MODE = zeros(1,length(layup));
        SRHa = MODE;
        SRMS = MODE;
        SRTW = MODE;
        for j = 1:length(layup)
            stressxy = Qbar(:,:,j)*strains(:,j);
            stress12 = T(:,:,j)*stressxy;
            strain12 = T(:,:,j)*strains(:,j);
            [SRHa(j),MODE(j)] =
FS_Hashin_KW(stress12(1),stress12(2),0,...
                stress12(3),0,0,F1t,F1c,F2t,F2c,F6,F4);
            SRMS(j) =
SR_Max_Strain(strain12,F1t,F1c,F2t,F2c,F6,E1,E2,G12);
            SRTW(j) = SR_TsaiWu(F1t,F1c,F2t,F2c,F6,stress12);
        end
    end

    function [SRHa,MODE,SRMS,SRTW] = strV(layup,Qbar,T,z)
        for i = 1:length(z)
            for j = 1:length(layup)
                stressxy = Qbar(:,:,j)*strains(:,i);
                stress12 = T(:,:,j)*stressxy;
                strain12 = T(:,:,j)*strains(:,i);
                [StRHa(i,j),mode(i,j)] = FS_Hashin_KW(stress12(1),...

stress12(2),0,stress12(3),0,0,F1t,F1c,F2t,F2c,F6,F4);
                StRMS(i,j) =
SR_Max_Strain(strain12,F1t,F1c,F2t,F2c,F6,...
                    E1,E2,G12);
                StRTW(i,j) = SR_TsaiWu(F1t,F1c,F2t,F2c,F6,stress12);
            end
            [SRHa(i),index] = min(StRHa(i,:));
            MODE(i) = mode(i,index);
            SRMS(i) = min(StRMS(i,:));
            SRTW(i) = min(StRTW(i,:));
        end
    end

    function [sum] = sum_corr(C)
        %Finds the location of the neutral axis in inches from the top
of
        %the concrete for the composite beam with stay-in-place forms
        %under ultimate loads
        c = C;
        NA = htc-c; %in
        dNA = NA-NA1;
        K = strainc/c; %in^-1
        [~,comp,~] = intSFM(c,0,K);
        [~,tens,~] = intSFM(c-dc,-NA,K);
```

```
        sum = comp+tens;
    end

    function [Tau,Gamma] = shear_strainU(zo)
        if zo >= 0
            [~,f1,~] = intSFM(htc-NA,zo,K);
            [~,f2,~] = intSFM(htc-NA,zo,K2);
        else
            [~,f1,~] = intSFM(zo,-NA,K);
            [~,f2,~] = intSFM(zo,-NA,K2);
        end

        if zo >= -NA+tb+h
            G = Gxyt;
            t = 2*Wt;
        elseif zo >= -NA+tb
            G = Gxyw;
            t = 2*ww;
        else
            G = Gxyb;
            t = Wb;
        end

        Tau = (f2-f1)/t/dx;

        pstrain = interp1(z,gamma,zo+dNA);

        %Shear strain
        Gamma = Tau/G + pstrain; %-
    end

    function [S,F,M] = intSFM(ztop,zbot,K)
        dz = 0.0001;
        zs = (zbot:dz:ztop);
        sp = zeros(1,length(zs));
        fp = sp;
        Mp = sp;
        for m = 1:length(zs)
            if zs(m) >= 0
                sp(m) = Hognestad(fc,K*zs(m));
                fp(m) = sp(m)*b*dz;
                Mp(m) = fp(m)*zs(m);
            elseif zs(m) > c-dc
            elseif zs(m) < c-dc-tt-hwt && zs(m) > c-dc-tt-hwt-D
            elseif zs(m) < c-dc-tt-hwt-D-hwm && zs(m) > c-dc-tt-hwt-D-
hwm-D
            elseif zs(m) > c-dc-tt
                sp(m) = zs(m)*K*Ext + (zs(m)+dNA)*K1*Ext;
                fp(m) = sp(m)*(2*Wt)*dz;
                Mp(m) = fp(m)*zs(m);
            elseif zs(m) > c-dc-tt-h
                sp(m) = zs(m)*K*Exw + (zs(m)+dNA)*K1*Exw;
                fp(m) = sp(m)*(2*ww)*dz;
```

```
                Mp(m) = fp(m)*zs(m);
            else
                sp(m) = zs(m)*K*Exb + (zs(m)+dNA)*K1*Exb;
                fp(m) = sp(m)*Wb*dz;
                Mp(m) = fp(m)*zs(m);
            end
        end
        M = sum(Mp);
        F = sum(fp);
        S = sum(sp);
    end

    function zero = MoEquil(K2)
        [~,~,M2] = intSFM(htc-NA,-NA,K2);
        zero = (M2-M1)/dx-Vu;
    end

end
```

Published with MATLAB® R2017a

Table of Contents


```
function Driver_AngleV3

%%%%%%%%%%%%%%%%%%%%%%%%%%%%%%%%%%%%%%%%%%%%%%%%%%%%%%%%
% Analysis Tool Box for Angle Stiffened Panel V3 %
%%%%%%%%%%%%%%%%%%%%%%%%%%%%%%%%%%%%%%%%%%%%%%%%%%%%%%%%

% Author: Benjamin Smith
% Start Date: July 17, 2018
% Advanced Structures and Composites Center, University of Maine
% Project: ERDC Task 2, 1355.11

% Changes: simplify calculations

%----Units----

% All units are in pounds and inches

% z measured positive up

% compression is positive

%----Drawings----

% \\storage-01.umcomposites.umaine.edu\ERDC Projects\1355 ERDC CEED
 2015-17\Task 2 - Thermoplastics\03 - Project Work\02 - CAD Modeling
\2D Modeling\2-006-1-2 2D AutoCad Models\Stiffened Panel Concept

%----References----


clc
```

Inputs

```
metric = 1; %if you want plots in metric =1, else =0 (does not change
 axis labels)
if metric == 1
    mm = 25.4;
    kN = 0.0044482216;
else
    mm = 1;
```

```
    kN = 1;
end


%--Geometry--

L = 56; %in, Length of the beam, Assume 4" supports 60" total length


%--FRP inputs--

%Width of the flange of the angle
Wa = 4; %in
%Width of the plate
Wp = 8; %in
%Unit weight of FRP (Aerial weight from PETg data sheet with measured
 0.2mm thickness)
UWfrp = 0.073158; %pci
%Thickness of a single lamina
tl = 0.2/25.4; %in

%-Lamina Strengths-

%Material: E-glass/PETg

%Longitudinal Tensile Strength
F1t = 9.036*10^4; %psi
%Transverse Tensile Strength
F2t = 2.103*10^3; %psi
%Longitudinal Compressive Strength
F1c = 4.495*10^4; %psi
%Transverse Compressive Strength
F2c = 9.427*10^3; %psi
%Longitudinal Elastic Modulus
E1 = 4.096*10^6; %psi, from tension test (comp=3.408*10^6)
%Transverse Elastic Modulus
E2 = 6.425*10^5; %psi, from tension test (comp=7.223*10^5)
%In-Plane Shear Strength
F6 = 4.183*10^3; %psi
%In-Plane Shear Modulus
G12 = 2.147*10^5; %psi
%In-Plane Poisson's Ratio
nu12 = 0.353; %-, from tension test (comp=0.298)
%Out-of-Plane Shear Strength
F4 = F4PETg; %psi

%Plate Layup
layupp = [0 0 0 45 -45 0 0 0 45 -45 -45 45 0 0 0 -45 45 0 0
 0]*pi/180; %radians, 0 is longitudinal

%Angle Layup
layupa = [0 0 45 -45 0 0 45 -45 0 0 45 -45 0 0 45 -45 -45 45 0 0 -45
 45 0 0 -45 45 0 0 -45 45 0 0]*pi/180; %radians, 0 is longitudinal
```

```
%--Bearing Connection--

%Distance from the top of the angle to the center of the hole
dr = 2; %in
%Diameter of the hole
D = 2.5; %in
%Center to center longitudinal spacing of holes
pitch = 6; %in


%--Concrete--

%Unit weight of unreinforced concrete
UWc = 145/12^3; %pci
%28-day compressive strength (f'c)
fc = 6000; %psi
%Depth of concrete above the top of the angle
dc = 2.5; %in
```

Initial Calcs

```
%Elastic modulus of concrete ( Wight Equation 3-18)
Ec = 57000*sqrt(fc); %psi

%[thickness of plate,thickness of each lamina in the plate]
[tp,tlp] = thickness(layupp,tl); %in
%[thickness of angle,thickness of each lamina in the angle]
[ta,tla] = thickness(layupa,tl); %in

%Full width of section
b = Wp; %in
%Width of concrete around angle
bc = b-2*ta; %in
%Total height of the FRP
h = Wa+tp; %in
%Height of web area above the hole
ht = dr-D/2; %in
%Height of web area below the hole
hb = Wa-ta-ht-D; %in
if hb<0
    error('Hole in tension flange')
end
%Cross-sectional area of the plate
Ap = Wp*tp; %in^2
%Cross-sectional area of the top portion of the web above hole
At = ht*(2*ta); %in^2
%Cross-sectional area of the bottom portion of the web below hole
Ab = hb*(2*ta); %in^2
%Cross-sectional area of the horizontal portion of the angles
Aa = (Wa*2)*ta; %in^2
%Cross-sectional area of the concrete
Ac = b*dc + 2*(Wa-ta)*(b/2-ta);
```

```
%Cross-sectional area of FRP
Ax = Ap+Aa+Ab+At; %in^2
```

Laminate Moduli

```
[ Sp,Qp,Tp,Sbarp,Qbarp,zbarp,ABDp,abdp ] =
 GetCLTStuffInput( layupp,E1,E2,G12,nu12,tlp );
[ Sa,Qa,Ta,Sbara,Qbara,zbara,ABDa,abda ] =
 GetCLTStuffInput( layupa,E1,E2,G12,nu12,tla );

[Exp,Eyp,Gxyp,nuxyp,Exbp,Eybp,Gxybp,nuxybp]=GetModuli(ABDp,abdp,tp);
[Exa,Eya,Gxya,nuxya,Exba,Eyba,Gxyba,nuxyba]=GetModuli(ABDa,abda,ta);

[ Fxtp,Fxcp,Txyp ] =
 GetStrengthsInput( tlp,tp,abdp,zbarp,Qbarp,Tp,Sp,E1,E2,G12,F1t,F2t,F1c,F2c,F6 );
[ Fxta,Fxca,Txya ] =
 GetStrengthsInput( tla,ta,abda,zbara,Qbara,Ta,Sa,E1,E2,G12,F1t,F2t,F1c,F2c,F6 );
```

Wet Concrete Loads

```
disp('--Wet Concrete Loads--')

%-Loads-

%Constant distributed load on beam (AASHTO (2012) 9.7.4.1)
w = (0.05*1000/12^2*b) + UWc*(b*dc+bc*(Wa-ta)) + UWfrp*Ax; %pli
%Maximum moment in beam, assuming simply supported (AISC Table 3-23)
M=w*L^2/8; %in*lb

%Maximum shear force in simply supported beam
V=w*L/2; %lb

% fprintf('The load required for construction loading is %1.0f pounds
\n',2*V)


%-Geometry-

%Location of neutral axis, from bottom
NA = ( Exp*Ap*tp/2 + Exa*Aa*(tp+ta/2) + Exa*Ab*(tp+ta+hb/2) + ...
    Exa*At*(h-ht/2) ) / ( Exa*(Ax-Ap + Exp/Exa*Ap)); %in
%Bending stiffness
EI = Exp*(Wp*tp^3/12 + Ap*(NA-tp/2)^2) + Exa*(2*Wa*ta^3/12 + ...
    Aa*(NA-tp-ta/2)^2 + 2*ta*hb^3/12 + Ab*(NA-tp-ta-hb/2)^2 +
 2*ta*ht^3/12 +...
    At*(h-NA-ht/2)^2); %lb*in^2
%Curvature
K = M/EI; %in^-4

%Expected Deflection at AASHTO Load
delta = V*L^3/28/EI;
% fprintf('Expected Deflection under AASHTO construction loads is
 %1.1f inches\n',delta)
```

```
%--Checks--

%-Strength-

%Vertical Laminates
x = 0:0.05:h-tp-ta;
z1 = h-NA-x;
ex = K*z1;
ey = -nuxya*ex;
gammaxy = zeros(1,length(x));
for i = 1:length(x)
    [~,gammaxy(i)] = shear_strain(z1(i));
end
strains = [-ex;-ey;gammaxy];

[SRHa1,MODE1,SRMS1,SRTW1] = strV(layupa,Qbara,Ta,z1);

gamma = gammaxy;

clear gammaxy
%Horizontal Angle
zo = NA-tp-ta/2;
z2 = -(zo+zbara);
ex = K*z2;
ey = -nuxya*ex;
for i = 1:length(z2)
    [~,gammaxy(i)] = shear_strain(z2(i));
end
strains = [-ex;-ey;gammaxy];

[SRHa2,MODE2,SRMS2,SRTW2] = strH(layupa,Qbara,Ta);

gamma = [gamma gammaxy];

clear gammaxy
%Horizontal Plate
zo = NA-tp/2;
z3 = -(zo+zbarp);
ex = K*z3;
ey = -nuxyp*ex;
for i = 1:length(z3)
    [~,gammaxy(i)] = shear_strain(z3(i));
end
strains = [-ex;-ey;gammaxy];

[SRHa3,MODE3,SRMS3,SRTW3] = strH(layupp,Qbarp,Tp);

gamma = [gamma gammaxy];

%Summary
SRHa = [SRHa1,SRHa2,SRHa3];
MODE = [MODE1,MODE2,MODE3];
z = [z1,z2,z3];
```

```
SRMS = [SRMS1,SRMS2,SRMS3];
SRTW = [SRTW1,SRTW2,SRTW3];
addpath('\\storage-01.umcomposites.umaine.edu\ERDC Projects\1355 &
 1554\T2\Project Work\Design\MATLAB Code\Analysis Toolbox')
figure(1)
clf
hold on
plot(SRHa,z*mm,'*')
plot(SRMS,z*mm,'*')
plot(SRTW,z*mm,'*')
plot(linspace(0,200,10),(-NA+tp)*ones(1,10)*mm)
plot(linspace(0,200,10),(-NA+tp+ta)*ones(1,10)*mm)
plot([linspace(0,200,10) linspace(0,200,10)],[(h-NA-ht)*ones(1,10)*mm
 (-NA+tp+ta+hb)*ones(1,10)*mm])
axis([0 200 -NA*mm (h-NA)*mm])
xlabel('Strength Ratio (Capacity/Load)')
ylabel('Distance From the Neutral Axis (in)')
% title('Angle - Strength Ratios Over the Section Under Wet Concrete
 Loads')
legend('Hashin','Max Strain','Tsai-Wu','Top of Backer Plate',...
    'Bottom of Vertical Flange','Hole')
thesisfig
saveas(gcf,'\\aewc-dc05\Grads\benjamin.t.smith\Thesis\THESIS\FIGURES
\stiffconstructionfailure','emf')

[SR_Hash,index] = min(SRHa);
MODE = MODE(index);
fail_mode = {'fiber tension','fiber compression','matrix
 tension','matrix compression'};
locs = {'angle','plate'};
MODE = fail_mode{MODE};
d_Hash = h-(z(index)+NA);
if d_Hash < Wa
    loc_Hash = locs{1};
else
    loc_Hash = locs{2};
end

[SR_MS,index] = min(SRMS);
d_MS = h-(z(index)+NA);
if d_MS < Wa
    loc_MS = locs{1};
else
    loc_MS = locs{2};
end

[SR_TW,index] = min(SRTW);
d_TW = h-(z(index)+NA);
if d_TW < Wa
    loc_TW = locs{1};
else
    loc_TW = locs{2};
end
```

```
fprintf('The minimum SR of the FRP is in %s in the %s under wet
 concrete loads: %1.1f (Hashin)\n',MODE,loc_Hash,SR_Hash)
fprintf('The minimum SR of the FRP is in the %s under wet concrete
 loads: %1.1f (Max Strain)\n',loc_MS,SR_MS)
fprintf('The minimum SR of the FRP is in the %s under wet concrete
 loads: %1.1f (Tsai Wu)\n',loc_TW,SR_TW)

%-Stability-

%AASHTO Deflection

defl=5*w*L^4/384/EI; % Deflection in simply supported beam (in) (AISC
 Table 3-23)
deflmax=min(L/180,0.5); % max allowable deflection for spans up to 10
 feet from (AASHTO (2012) 9.7.4.1)
rat = defl/deflmax;

if defl<deflmax
    fprintf('The AASHTO requirement for deflection in the beam of SIP
 formwork is met (%1.1f%% of limit) \n',rat*100)
else
    fprintf('The AASHTO requirement for deflection in the beam of SIP
 formwork is not met (%1.1f%% of limit) \n',rat*100)
end

% Local Buckling (Angle)
%AISC pg 16.1-62

Sx = (EI/Exa)/(h-NA);
Sc = 0.8*Sx;
Fcr = 0.71*Exba/(Wa/(ta))^2;
MnLBA = Fcr*Sc;
% phib = 0.9;
phib=1;
SR = phib*MnLBA/(M/2);

fprintf('The SR against the FRP failing in local buckling of an Angle
 under wet concrete loads is %1.1f\n',SR)
Buck_Load=SR*V*2;
fprintf('--AISC Buckling Load: %1.0f pounds\n',Buck_Load)

% Roberto's Check

    function [Fcr] = RLABuck(t,a,b)
        Fcr=(t/b)^2*(pi^2/6)*(1/2*(b/a)^2*Exba+6/pi^2*Gxyba);
    end

Fcr = RLABuck(ta,L/3,Wa);

P = (M/2)*(h-NA-ht/2)/(EI/Exa)*ta*ht;

FS = Fcr/(P/ta/ht);
fprintf('--ASCE Buckling Load: %1.0f pounds\n',FS*V*2)
```

```
fprintf('The FS against Robertos check under wet concrete loads is
 %1.1f\n',FS)

NAw = NA;

% Load needed for test:

etop = Fxca/Exa;
Ktest = etop/(h-NA);

zztop = h-NA-ht/2; %A haw haw haw
eetop = Ktest*zztop;
sstop = eetop*Exa;
FFtop = sstop*At;

zzbot = h-NA-ht-D-hb/2;
eebot = Ktest*zzbot;
ssbot = eebot*Exa;
FFbot = ssbot*Ab;

zzang = -NA+tp+ta/2;
eeang = Ktest*zzang;
ssang = eeang*Exa;
FFang = ssang*Aa;

zzpla = -NA+tp/2;
eepla = Ktest*zzpla;
sspla = eepla*Exp;
FFpla = sspla*Ap;

Mn_wc = FFtop*zztop + FFbot*abs(zzbot) + FFang*abs(zzang) -
 FFpla*zzpla;

FS_flex = Mn_wc/M;

fprintf('The FS against the beam failing in flexure under wet concrete
 loads is %1.1f\n\n',FS_flex)

a = L/3; % Distance between load and support

Vn_wc = Mn_wc/a;

deltan_wc = Vn_wc*L^3/28/EI;

fprintf('--AASHTO Load: %1.0f pounds\n',V*2)
fprintf('--Failure Load: %1.0f pounds\n',V*2*SR_MS)
fprintf('--AASHTO Deflection: %1.2f inches\n',delta)
fprintf('--Failure Deflection: %1.2f inches\n',deltan_wc)

[~,comp,~] = intSFMcon(h-NA,0,K);
[~,tens,~] = intSFMcon(0,-NA,K);

check = comp+tens;
```

```
fprintf('\nThe sum of forces in the beam under construction loads is
 %1.1f pounds (numerical)\n',check)

check = FFtop+FFbot+FFang+FFpla;

fprintf('\nThe sum of forces in the beam under construction loads is
 %1.1f pounds (analytical)\n\n',check)
```

AASHTO Loads for Bridge Decking

```
disp('--AASHTO Loads--')

%-Loads-
M_LL = 6.294 * 1000 * b; % Maximum live load moment from AASHTO Live
 Loads Mathcad calc sheet (lb-in)

%w_DC = UWc*(b*dc+(b-2*ta)*(Wa-ta)) + UWfrp*Ax; % self weight of
 concrete and FRP (lb/in)
w_DC = 0;
M_DC = w_DC*L^2/8; % Maximum DC moment assuming simply supported (lb-
in)

w_DW = 140/12^3*2*b; % weight of assumed 2" wearing surface (lb/in)
M_DW = w_DW*L^2/8; % Maximum DW moment assuming simply supported (lb-
in)

gamma_LL = 1.75;
gamma_DC = 1.25;
gamma_DW = 1.5;

Mu = gamma_LL*M_LL + gamma_DC*M_DC + gamma_DW*M_DW; % Maximum factored
 moment (lb-in)

%Save linear K and NA
K1 = K;
NA1 = NA;

%-Geometry-

h = h+dc;

strainc=0.003; % strain in extreme concrete fiber that causes crushing

c = fzero(@sum_ang,1); % Finds location of neutral axis from the top
 of the section
NA = h-c; % Location of the neutral axis from the bottom of the
 section

dNA = NA-NA1;

%Curvature
K = strainc/c; %in^-1
```

```
[~,comp,~] = intSFM(c,0,K);
[~,tens,~] = intSFM(c-dc,-NA,K);

check = comp+tens;

fprintf('\nThe sum of forces in the beam under ultimate loads is %1.1f
 pounds\n',check)

%Nominal moment capacity, summed loads around neutral axis
[~,~,Mn] = intSFM(h-NA,-NA,K);

phib = 1;%0.65; % AASHTO CFFT 2.7.3.2 for compression controlled
 failure

FS_flex = phib*Mn/Mu;

fprintf('The LRFD ratio against the beam failing in flexure under
 factored AASHTO loads is %1.1f (concrete crushing)\n',FS_flex)

%--Checks--

%-Strength-

[~,~,M1] = intSFM(h-NA,-NA,K);
Vu = 3*M1/L;
dx = 0.01;
K2=fzero(@MoEquil,K);

%Vertical Laminates
clear gammaxy
z1 = c-dc-x;
ex = K*z1;
ey = -nuxya*ex;
gammaxy = zeros(1,length(x));
SR = zeros(length(x),length(layupa));
mode = zeros(length(x),length(layupa));
for i = 1:length(x)
    [~,gammaxy(i)] = shear_strainU(z1(i));
end
strains = [-ex;-ey;gammaxy];

[SRHa1,MODE1,SRMS1,SRTW1,loc] = strV(layupa,Qbara,Ta,z1);

clear gammaxy
%Horizontal Angle
zo = NA-tp-ta/2;
z2 = -(zo+zbara);
ex = K*z2;
ey = -nuxya*ex;
for i = 1:length(z2)
    [~,gammaxy(i)] = shear_strainU(z2(i));
end
strains = [-ex;-ey;gammaxy];
```

```
[SRHa2,MODE2,SRMS2,SRTW2] = strH(layupa,Qbara,Ta);

clear gammaxy
%Horizontal Plate
zo = NA-tp/2;
z3 = -(zo+zbarp);
ex = K*z3;
ey = -nuxyp*ex;
for i = 1:length(z3)
    [~,gammaxy(i)] = shear_strainU(z3(i));
end
strains = [-ex;-ey;gammaxy];

[SRHa3,MODE3,SRMS3,SRTW3] = strH(layupp,Qbarp,Tp);

%Summary
SRHa = [SRHa1,SRHa2,SRHa3]*Mn/Mu;
MODE = [MODE1,MODE2,MODE3];
z = [z1,z2,z3];
SRMS = [SRMS1,SRMS2,SRMS3]*Mn/Mu;
SRTW = [SRTW1,SRTW2,SRTW3]*Mn/Mu;
figure(2)
clf
plot(SRHa,z*mm,'*')
hold on
plot(SRMS,z*mm,'*')
plot(SRTW,z*mm,'*')
plot(linspace(0,400,1000),(-NA+tp)*ones(1,1000)*mm)
plot(linspace(0,400,1000),(-NA+tp+ta)*ones(1,1000)*mm)
plot([linspace(0,10,1000) linspace(0,200,1000)],[(-NA+tp+ta+hb
+D)*ones(1,1000)*mm (-NA+tp+ta+hb)*ones(1,1000)*mm])
plot(linspace(0,400,1000),(h-dc-NA)*ones(1,1000)*mm)

axis([0 10 -NA*mm (h-NA)*mm])
xlabel('Strength Ratio (Capacity/Load)')
ylabel('Distance From the Neutral Axis (mm)')
% title('Angle - Strength Ratios Over the Section Under Ultimate
 Loads')
legend('Hashin','Max Strain','Tsai-Wu','Top of plate',...
    'Bottom of Flange','Hole','Top of CFRTP')
thesisfig
saveas(gcf,'\\aewc-dc05\Grads\benjamin.t.smith\Thesis\THESIS\FIGURES
\stiffultimate','emf')

[SR_Hash,index] = min(SRHa);
MODE = MODE(index);
fail_mode = {'fiber tension','fiber compression','matrix
 tension','matrix compression'};
MODE = fail_mode{MODE};
d_Hash = h-(z(index)+NA);
if d_Hash < Wa+dc
    loc_Hash = locs{1};
else
    loc_Hash = locs{2};
```

```
end

[SR_MS,index] = min(SRMS);
d_MS = h-(z(index)+NA);
if d_MS < Wa+dc
    loc_MS = locs{1};
else
    loc_MS = locs{2};
end

[SR_TW,index] = min(SRTW);
d_TW = h-(z(index)+NA);
if d_TW < Wa+dc
    loc_TW = locs{1};
else
    loc_TW = locs{2};
end

fprintf('The minimum SR of the FRP is in %s in the %s under ultimate
 loads: %1.1f (Hashin)\n',MODE,loc_Hash,SR_Hash)
fprintf('The minimum SR of the FRP is in the %s under ultimate loads:
 %1.1f (Max Strain)\n',loc_MS,SR_MS)
fprintf('The minimum SR of the FRP is in the %s under ultimate loads:
 %1.1f (Tsai Wu)\n',loc_TW,SR_TW)

V=3*Mu/L; % Maximum shear force in section from 4 point bend test (lb)

[~,f1,~] = intSFM(c-dc,-NA,K);
[~,f2,~] = intSFM(c-dc,-NA,K2);
Tau = (f2-f1)/b/dx;

q = abs(Tau)*(2*ta);

Fb = q*pitch; % Force carried by one bearing connection (lb)

Sb = 25996; % Bearing capacity of angle (psi) from material testing

Fnb = Sb*2*ta*D; % Bearing capacity of angle (lbf)

phi_bear = 1;%0.7; % AASHTO 5.5.4.2.1

FS_bear = phi_bear*Fnb/Fb;
fprintf('The LRFD ratio against the angle failing in bearing under
 ultimate loads is %1.1f\n',FS_bear)

Vnc = 2*sqrt(fc)*Ac; % Shear capacity of concrete (lb)

phi_shear = 1;%0.75; % AASHTO CFFT 2.7.3.2

FS_shear = phi_shear*Vnc/V;
fprintf('The LRFD ratio against the concrete failing in shear under
 ultimate loads is %1.1f\n',FS_shear)

%Drawing of shape
```

```
figure(3)
clf
axis equal
hold on
%Ultimate NA
UNA = plot([0 Wp],[NA NA],'r');
%Wet concrete NA
WNA = plot([0 Wp],[NAw NAw],'g');
legend([UNA WNA],{'Ultimate NA','Wet Concrete NA'})

%plate
NODES = [0 0;Wp 0;Wp tp;0 tp];
CONNECTIVITIES = [1 2;2 3;3 4;4 1];
for i=1:length(CONNECTIVITIES) % Draws the line for each member
    line([NODES(CONNECTIVITIES(i,1),1)
 NODES(CONNECTIVITIES(i,2),1)],...
        [NODES(CONNECTIVITIES(i,1),2) NODES(CONNECTIVITIES(i,2),2)]);
end
%angles
NODES = [0 tp;Wa tp;2*Wa tp;2*Wa tp+ta;Wa+ta tp+ta;Wa+ta tp+Wa;Wa tp
+Wa;...
    Wa-ta tp+Wa;Wa-ta tp+ta;0 tp+ta];
CONNECTIVITIES = [1 3;3 4;4 5;5 6;6 8;8 9;9 10;10 1;2 7];
for i=1:length(CONNECTIVITIES) % Draws the line for each member
    line([NODES(CONNECTIVITIES(i,1),1)
 NODES(CONNECTIVITIES(i,2),1)],...
        [NODES(CONNECTIVITIES(i,1),2) NODES(CONNECTIVITIES(i,2),2)]);
end
%concrete
NODES = [0 ta+tp;0 tp+Wa+dc;Wp tp+Wa+dc;Wp ta+tp];
CONNECTIVITIES = [1 2;2 3;3 4];
for i=1:length(CONNECTIVITIES) % Draws the line for each member
    line([NODES(CONNECTIVITIES(i,1),1)
 NODES(CONNECTIVITIES(i,2),1)],...
        [NODES(CONNECTIVITIES(i,1),2) NODES(CONNECTIVITIES(i,2),2)]);
end
%hole
plot([Wa-ta Wa-ta Wa+ta Wa+ta Wa-ta],[tp+Wa-dr-D/2 tp+Wa-dr+D/2 ...
    tp+Wa-dr+D/2 tp+Wa-dr-D/2 tp+Wa-dr-D/2],'b')


legend([UNA WNA],{'Ultimate NA','Wet Concrete NA'})

if min([SR_Hash,SR_MS,SR_TW])>1
    [min_FS,index] = min([FS_flex,FS_bear,FS_shear]);
    FSs = {'flexure','bearing','shear'};
    fprintf('\nThe load needed for the ultimate test is %1.1f kips
\n',min_FS*(V*2)/1000)
    fprintf('Expected failure mode: %s\n',FSs{index})
    fprintf('AASHTO force: %1.1f kips\n',(V*2)/1000)
    fprintf('Minimum factor of safety: %1.1f\n',min_FS)
else
    disp('FRP fails before concrete')
end
```

```
Ahole = pi*D^2/4;

Vc = 2*sqrt(fc); %Shear strength of concrete

As = 0.11; %in^2 #3 bar

Acv = Ahole-As; %in^2

Fy = 60000; %Rebar strength

Fv = 0.6*Fy; % Shear strength of rebar

Vns = 2 * Fv*As;

Vnc = 2* Vc*Acv;

Vn = Vns + Vnc;

FS_cbs = Vn/Fb;

P = 8*Mu/L;
Pc = P*FS_flex;%/phib;
Pu = 2*Vu; %Load for concrete crack
fprintf('\n--AASHTO Load: %1.0f pounds\n',P)
fprintf('--Concrete Crush Load: %1.0f pounds\n',Pc)
fprintf('--FRP Fail Load: %1.0f pounds\n',Pc*SR_MS)
fprintf('--FRP Bearing Load: %1.0f pounds\n',Pc*FS_bear)
fprintf('--Concrete bearing shear fail load: %1.0f pounds
\n',Pc*FS_cbs)
fprintf('--Concrete Shear Load: %1.0f pounds\n',P*FS_shear)
fprintf('--FRP bot uni Fail Load: %1.0f pound\n',Pc*2.9393)
```

Subroutines

```
    function [vector] = vec(L,x)
        vector=x*ones(1,L);
    end

    function [tp,tlp] = thickness(layup,tl)
        tlp=vec(length(layup),tl); % A vector of the thickness of each
 layer (in)
        tp=sum(tlp); % Thickness composite (in)
    end

    function [EQ] = FMA(z)
        %Finds the First Moment of Area of the area on the far side of
 the
        %point of interest about the neutral axis multiplied by the
 elastic
        %modulus
        if z >= h-NA
            EQ = 0;
```

```
        elseif z >= h-NA-ht
            temp = h-(z+NA); % height of top above z
            EQ = Exa*temp*(2*ta)*(z+temp/2);
        elseif z >= h-NA-ht-D
            EQ = Exa*ht*(2*ta)*(h-NA-ht/2);
        elseif z >= 0
            temp = tp+ta+hb-NA-z; % height of bottom above z
            EQ = Exa*ht*(2*ta)*(h-NA-ht/2) + Exa*temp*(2*ta)*(z
+temp/2);
        elseif z >= tp+ta-NA
            temp = NA+z-tp-ta; % height of bottom below z
            EQ = Exp*Wp*tp*(NA-tp/2) + Exa*(2*Wa)*ta*(NA-tp-ta/2)
 + ...
                Exa*temp*(2*ta)*(temp/2-z);
        elseif z >= tp-NA
            temp = NA+z-tp; % height of angle below z
            EQ = Exp*Wp*tp*(NA-tp/2) + Exa*(2*Wa)*temp*(temp/2-z);
        else
            temp = NA+z; % height of panel below z
            EQ = Exp*Wp*temp*(temp/2-z);
        end
    end

    function [Tau,Gamma] = shear_strain(z)
        if z >= -(NA-tp-ta)
            t = 2*ta;
        else
            t = Wp;
        end
        if z >= -(NA-tp)
            G = Gxya;
        else
            G = Gxyp;
        end
        EQ = FMA(z);
        %Shear stress
        Tau = V*EQ/EI/t; %psi
        %Shear strain
        Gamma = Tau/G; %-
    end

    function [Tau,Gamma] = shear_strainU(zo)



        if zo >= 0
            [~,f1,~] = intSFM(h-NA,zo,K);
            [~,f2,~] = intSFM(h-NA,zo,K2);
        else
            [~,f1,~] = intSFM(zo,-NA,K);
            [~,f2,~] = intSFM(zo,-NA,K2);
        end

        if zo >= -NA+tp+ta
```

```
            be = 2*ta;
        else
            be = b;
        end

        Tau = (f2-f1)/be/dx;

        if zo >= -(NA-tp)
            G = Gxya;
        else
            G = Gxyp;
        end

        %Shear strain
        Gamma = Tau/G; %-
    end

    function [sum] = sum_ang(C)
        %Finds the location of the neutral axis in inches from the top
of
        %the concrete for the composite beam with stay-in-place forms
        %under ultimate loads
        c = C;
        NA = h-c; %in
        dNA = NA-NA1;
        K = strainc/c; %in^-1
        [~,comp,~] = intSFM(c,0,K);
        [~,tens,~] = intSFM(c-dc,-NA,K);

        sum = comp+tens;
    end

    function zero = MoEquil(K2)

        [~,~,M2] = intSFM(h-NA,-NA,K2);
        zero = (M2-M1)/dx-Vu;
    end

    function [S,F,M] = intSFM(ztop,zbot,K)
        dz = 0.0001;
        zs = (zbot:dz:ztop);
        sp = zeros(1,length(zs));
        fp = sp;
        Mp = sp;
        for m = 1:length(zs)
            if zs(m)>0
                sp(m) = Hognestad(fc,K*zs(m));
                fp(m) = sp(m)*b*dz;
                Mp(m) = fp(m)*zs(m);
            elseif zs(m)>c-dc
            elseif zs(m)<c-dc-ht && zs(m)>c-dc-ht-D
            elseif zs(m)>(-NA+tp+ta)
                sp(m)=zs(m)*K*Exa + (zs(m)+dNA)*K1*Exa;
                fp(m)=sp(m)*(2*ta)*dz;
```

```
                Mp(m)=fp(m)*zs(m);
            elseif zs(m)>(-NA+tp)
                sp(m)=zs(m)*K*Exa + (zs(m)+dNA)*K1*Exa;
                fp(m)=sp(m)*(2*Wa)*dz;
                Mp(m)=fp(m)*zs(m);
            else
                sp(m)=zs(m)*K*Exp + (zs(m)+dNA)*K1*Exp;
                fp(m)=sp(m)*Wp*dz;
                Mp(m)=fp(m)*zs(m);
            end
        end
        M = sum(Mp);
        F = sum(fp);
        S = sum(sp);
    end

    function [S,F,M] = intSFMcon(ztop,zbot,K)
        dz = 0.00001;
        zs = (zbot:dz:ztop);
        sp = zeros(1,length(zs));
        fp = sp;
        Mp = sp;
        for m = 1:length(zs)
            if zs(m) > -NA+tp+ta+hb && zs(m) < -NA+h-ht
            elseif zs(m) > -NA+tp+ta
                sp(m) = zs(m)*K*Exa;
                fp(m) = sp(m)*(2*ta)*dz;
                Mp(m) = fp(m)*zs(m);
            elseif zs(m) > -NA+tp
                sp(m) = zs(m)*K*Exa;
                fp(m) = sp(m)*(2*Wa)*dz;
                Mp(m) = fp(m)*zs(m);
            else
                sp(m) = zs(m)*K*Exp;
                fp(m) = sp(m)*Wp*dz;
                Mp(m) = fp(m)*zs(m);
            end
        end
        M = sum(Mp);
        F = sum(fp);
        S = sum(sp);
    end

    function [SRHa,MODE,SRMS,SRTW] = strH(layup,Qbar,T)
        MODE = zeros(size(layup));
        SRHa = MODE;
        SRMS = MODE;
        SRTW = MODE;
        for k = 1:length(layup)
            stressxy = Qbar(:,:,k)*strains(:,k);
            stress12 = T(:,:,k)*stressxy;
            strain12 = T(:,:,k)*strains(:,k);
            [SRHa(k),MODE(k)] =
FS_Hashin_KW(stress12(1),stress12(2),0,...
```

```
                stress12(3),0,0,F1t,F1c,F2t,F2c,F6,F4);
            SRMS(k) =
 SR_Max_Strain(strain12,F1t,F1c,F2t,F2c,F6,E1,E2,G12);
            SRTW(k) = SR_TsaiWu(F1t,F1c,F2t,F2c,F6,stress12);
        end
    end

    function [SRHa,MODE,SRMS,SRTW,loc] = strV(layup,Qbar,T,z)
        MODE = zeros(size(z));
        SRHa = MODE;
        SRMS = MODE;
        SRTW = MODE;
        loc = MODE;
        StRHa = zeros(length(z),length(layup));
        mode = StRHa;
        StRMS = mode;
        StRTW = mode;
        for i = 1:length(z)
            for j = 1:length(layup)
                stressxy = Qbar(:,:,j)*strains(:,i);
                stress12 = T(:,:,j)*stressxy;
                strain12 = T(:,:,j)*strains(:,i);
                [StRHa(i,j),mode(i,j)] = FS_Hashin_KW(stress12(1),...

 stress12(2),0,stress12(3),0,0,F1t,F1c,F2t,F2c,F6,F4);
                StRMS(i,j) =
 SR_Max_Strain(strain12,F1t,F1c,F2t,F2c,F6,...
                    E1,E2,G12);
                StRTW(i,j) = SR_TsaiWu(F1t,F1c,F2t,F2c,F6,stress12);
            end
            [SRHa(i),index] = min(StRHa(i,:));
            MODE(i) = mode(i,index);
            [SRMS(i),loc(i)] = min(StRMS(i,:));
            SRTW(i) = min(StRTW(i,:));
        end
    end

end
```

Published with MATLAB® R2017a

```
function F4 = F4PETg

%Calculation of the out-of-plane shear strength of a composite using a
%stress concentration factor to reduce the shear strength of the
 matrix

%Equations (21-22) taken from: L. Liu and Z.-M. Huang, “Stress
 concentration factor in matrix of a composite reinforced with
 transversely isotropic fibers,” J. Compos. Mater., vol. 48, pp. 81–
98, 2014.
```

Inputs

```
%Fiber-Volume Fraction
Vf = 0.37; %-
%Beta Factor
beta = 0.45; %-
%Longitudinal Elastic Modulus of Fibers
Ef = 1.049*10^7; %psi
%Longitudinal Elastic Modulus of Matrix
Em = 320000; %psi
%In-Plane Poisson's Ratio of Matrix
vm = 0.37; %-
%In-Plane Poisson's Ratio of Fibers
vf = 0.22; %-
%Matrix Shear Strength
Fms = 9000; %psi
```

Calculations

```
%Matrix-Volume Fraction
Vm = 1-Vf;
%A' Factor
Ap = ((1-vm-2*vm^2)*Ef-(1-vf-2*vf^2)*Em)/(Ef*(1+vm)+Em*(1-vf-2*vf^2));
%B' Factor
Bp = (Em*(1+vf)-(1+vm)*Ef)/(Ef*(vm+4*vm^2-3)-Em*(1+vf));
%Stress Concentration Factor
K = (1+sqrt(Vf)/2*Ap+sqrt(Vf)/2*(3-Vf-sqrt(Vf))*Bp)*((Vf+Vm*beta)*Ef
+Vm*(1-beta)*Em)/(beta*Ef+(1-beta)*Em);
%Out-of-Plane Shear Strength
F4 = Fms/K; %psi
```

Published with MATLAB® R2017a

```
function [ S,Q,T,Sbar,Qbar,zbar,ABD,abd ] =
 GetCLTStuffInput( layup,E1,E2,G12,nu12,tl )
%function [ S,Q,T,Sbar,Qbar,zbar,ABD,abd ] =
 GetCLTStuffInput( layup,E1,E2,G12,nu12,tl )

% Assumes all lamina are same material

% layup = vector of lamina orientations, bottom first

%Convert values to vectors for each layer
E1v=vec(length(layup),E1);
E2v=vec(length(layup),E2);
nu12v=vec(length(layup),nu12);
G12v=vec(length(layup),G12);

%Reduced compliance and stiffness matrices, Codes developed with
 Barbero
[S,Q]=GetSQ(E1v,E2v,nu12v,G12v);

%Transformation Vector, Codes developed with Barbero
T=GetT(layup);

%Transformed reduced compliance and stiffness matrices, Codes
 developed with Barbero
[Sbar,Qbar]=GetSbarQbar(Q,T);

%Distance from center of composite, Codes developed with Barbero
zbar=Getzbar(tl);

%ABD Matrix, Codes developed with Barbero
ABD=GetABD(tl,zbar,Qbar);

%abd atrix, inverse of ABD
abd=inv(ABD);

end

function [S,Q] = GetSQ(E1,E2,nu12,G12)
% Construct reduced compliance and stiffness matrices

S=zeros(3,3,length(E1));
Q=zeros(3,3,length(E1));

for i=1:length(E1)
    S(1,1,i)=1/E1(i);
    S(1,2,i)=-nu12(i)/E1(i);
    S(2,1,i)=S(1,2,i);
    S(2,2,i)=1/E2(i);
    S(3,3,i)=1/G12(i); % aka S_66

    Q(:,:,i)=inv(S(:,:,i));
end
```

```
end

function [vector] = vec(L,x)
vector=x*ones(1,L);
end

function [T] = GetT(theta)

% theta can be a vector to accomodate multiple layers
% bottom layer first

T=zeros(3,3,length(theta));

for i=1:length(theta)
    m=cos(theta(i));
    n=sin(theta(i));
    T(:,:,i)=[m^2 n^2 2*m*n;n^2 m^2 -2*m*n;-m*n m*n m^2-n^2];
end
end

function [Sbar,Qbar] = GetSbarQbar(Q,T)

% Q and T can be vectors to accomodate multiple layers
% bottom layer first

Qbar=zeros(3,3,length(T(1,1,:)));

% Compute transformed reduced stiffness and compliance matrices

for i=1:length(T(1,1,:))
    Qbar(:,:,i)=T(:,:,i)\Q(:,:,i)/T(:,:,i)';

    Sbar(:,:,1)=inv(Qbar(:,:,i));
end
end

function [zbar] = Getzbar(t)

zbar=zeros(1,length(t));
zbar(1)=t(1)/2; % sets first value

for k=2:length(t)
    zbar(k)=zbar(k-1)+t(k-1)/2+t(k)/2; % gets all distances to bottom
end

zbar=zbar-sum(t)/2;

end

function [ABD] = GetABD(t,zbar,Qbar)

% t and Qbar can be vectors to accomodate multiple layers
% bottom layer first
```

```
s=size(Qbar);

A=zeros(s(1),s(2));
B=zeros(s(1),s(2));
D=zeros(s(1),s(2));

for i=1:s(1)
    for j=1:s(2)
        for k=1:length(t)
            A(i,j)=Qbar(i,j,k)*(t(k))+A(i,j);
            B(i,j)=Qbar(i,j,k)*t(k)*zbar(k)+B(i,j);

 D(i,j)=Qbar(i,j,k)*(t(k)*(zbar(k))^2+((t(k))^3)/12)+D(i,j);
        end
    end
end

ABD=[ A B ; B D];

end
```

Published with MATLAB® R2017a

```
function [ Ex,Ey,Gxy,nuxy,Exb,Eyb,Gxyb,nuxyb ] =
 GetModuli( ABD,abd,t )
%function [ Ex,Ey,Gxy,nuxy ] = GetModuli( layup,Ef,Vf,Em,tl,t )
% Computes effective laminate moduli using classical lamination theory
% Assumes all lamina are same material

% ABD = ABD matrix
% abd = inverse of ABD matrix
% t = thickness of the laminate

Ex=1/t/abd(1,1); % Longitudinal Modulus
Ey=1/t/abd(2,2); % Transverse Modulus
Gxy=ABD(3,3)/t; % In-plane shear modulus
nuxy=ABD(1,2)/ABD(2,2); % In-plane Poisson's Ratio

d = abd(4:6,4:6);

Exb = 12/t^3/d(1,1);
Eyb = 12/t^3/d(2,2);
Gxyb = 12/t^3/d(3,3);
nuxyb = -d(1,2)/d(1,1);

end
```

Published with MATLAB® R2017a

```
function [ Fxt,Fxc,Txy ] =
 GetStrengthsInput( tl,t,abd,zbar,Qbar,T,S,E1,E2,G12,F1t,F2t,F1c,F2c,F6 )
%function [ Fxt,Fxc,Txy ] =
 GetStrengthsInput( tl,t,abd,zbar,Qbar,T,S,E1,E2,G12,F1t,F2t,F1c,F2c,F6 )
% Computes effective laminate strengths using maximum strain criteria
 and
% first ply failure
% Assumes all lamina are same material

%Laminate strengths

N=[ 1 0 0 0 0 0 ]'; % Unit load for tension

e1t=F1t/E1; % Failure strains
e2t=F2t/E2;
e1c=F1c/E1;
e2c=F2c/E2;
g6u=F6/G12;

eT=[ e1t e2t g6u ]';
ec=[ e1c e2c g6u ]';

strainxy0=abd*N; % Midsurface strains, through constitutive equations

strainxy=zeros(3,length(tl));
stressxy=zeros(3,length(tl));
stress12=zeros(3,length(tl));
strain12=zeros(3,length(tl));
FS1=zeros(1,length(tl));
FS2=zeros(1,length(tl));
FS3=zeros(1,length(tl));

for j=1:length(tl)
    strainxy(:,j)=strainxy0(1:3)+zbar(j)*strainxy0(4:6); % strain at
 each lamina in global coordinates from strain compatibility, plane
 sections remain plane
    stressxy(:,j)=Qbar(:,:,j)*strainxy(:,j); % stress at each lamina
 in global coordinates
    stress12(:,j)=T(:,:,j)*stressxy(:,j); % stress at each lamina in
 local coordinates
    strain12(:,j)=S(:,:,j)*stress12(:,j); % strain at each lamina in
 local coordinates
    if strain12(1,j)>0
        FS1(j)=eT(1)/strain12(1,j);
    end
    if strain12(2,j)>0
        FS2(j)=eT(2)/strain12(2,j);
    end
    if strain12(3,j)==0
    else
        FS3(j)=eT(3)/abs(strain12(3,j));
    end
```

```
end
Fxt=min([min(FS1(FS1>0)),min(FS2(FS2>0)),min(FS3(FS3>0))])/t;

N=[ -1 0 0 0 0 0 ]'; % Unit load for compression

strainxy0=abd*N; % Midsurface strains, through constitutive equations

for j=1:length(tl)
    strainxy(:,j)=strainxy0(1:3)+zbar(j)*strainxy0(4:6); % strain at
 each lamina in global coordinates from strain compatibility, plane
 sections remain plane
    stressxy(:,j)=Qbar(:,:,j)*strainxy(:,j); % stress at each lamina
 in global coordinates
    stress12(:,j)=T(:,:,j)*stressxy(:,j); % stress at each lamina in
 local coordinates
    strain12(:,j)=S(:,:,j)*stress12(:,j); % strain at each lamina in
 local coordinates
    if strain12(1,j)<0
        FS1(j)=ec(1)/-strain12(1,j);
    end
    if strain12(2,j)<0
        FS2(j)=ec(2)/-strain12(2,j);
    end
    if strain12(3,j)==0
    else
        FS3(j)=ec(3)/abs(strain12(3,j));
    end
end
Fxc=min([min(FS1(FS1>0)),min(FS2(FS2>0)),min(FS3(FS3>0))])/t;

N=[ 0 0 1 0 0 0 ]'; % Unit load for in-plane shear

strainxy0=abd*N; % Midsurface strains, through constitutive equations

for j=1:length(tl)
    strainxy(:,j)=strainxy0(1:3)+zbar(j)*strainxy0(4:6); % strain at
 each lamina in global coordinates from strain compatibility, plane
 sections remain plane
    stressxy(:,j)=Qbar(:,:,j)*strainxy(:,j); % stress at each lamina
 in global coordinates
    stress12(:,j)=T(:,:,j)*stressxy(:,j); % stress at each lamina in
 local coordinates
    strain12(:,j)=S(:,:,j)*stress12(:,j); % strain at each lamina in
 local coordinates
    if strain12(1,j)<0
        FS1(j)=ec(1)/-strain12(1,j);
    elseif strain12(1,j)>0
        FS1(j)=eT(1)/strain12(1,j);
    end
    if strain12(2,j)<0
        FS2(j)=ec(2)/-strain12(2,j);
    elseif strain12(2,j)>0
        FS2(j)=eT(2)/strain12(2,j);
    end
```

```
    if strain12(3,j)==0
    else
        FS3(j)=ec(3)/abs(strain12(3,j));
    end
end
Txy=min([min(FS1(FS1>0)),min(FS2(FS2>0)),min(FS3(FS3>0))])/t;

end
```

Published with MATLAB® R2017a

```
function SR = SR_Max_Strain(strain12,F1t,F1c,F2t,F2c,F6,E1,E2,G12)

%Calculates a strength ratio for a single lamina using maximum strain
%failure theory.

% E. J. Barbero, Introduction to Composite Materials Design, 2nd ed.
 New York: CRC Press, 2011.

e1t=F1t/E1;
e2t=F2t/E2;
e1c=F1c/E1;
e2c=F2c/E2;
g6u=F6/G12;

eT=[ e1t e2t g6u ]';
eC=[ e1c e2c g6u ]';

SR = 1/max((0.5*(strain12+abs(strain12)))./eT+...
    (0.5*(-strain12+abs(-strain12)))./eC);
end
```

Published with MATLAB® R2017a

```
function [FS,MODE] =
 FS_Hashin_KW(P11,P22,P33,P12,P13,P23,S1T,S1C,S2T,S2C,S12,S23)

% Calculates the factor of safety for a single lamina using Hashin
% Failure Theory. Equations gathered from Warren et al.

% K. C. Warren, R. A. Lopez-Anido, S. S. Vel, and H. H. Bayraktar,
 “Progressive failure analysis of three-dimensional woven carbon
 composites in single-bolt, double-shear bearing,” Compos. Part B
 Eng., vol. 84, pp. 266–276, 2016.

% Inputs: P's are forces, S's are strengths

% [SR(i,j),mode(i,j)] = FS_Hashin_KW(stress12(1),stress12(2),0,...
%             stress12(3),0,0,F1t,F1c,F2t,F2c,F6,F4);

FoSs = 10000*ones(4,1); %Defines FoSs as something very large so the
 not applicable cases won't be the minimum

if P11>0 % Mode 1: Fiber Tension
    F = (P11/S1T)^2+1/S12^2*(P12^2+P13^2);
    FoSs(1) = 1/F;
elseif P11<0 % Mode 2: Fiber Compression
    F = -P11/S1C;
    FoSs(2) = 1/F;
end
if (P22+P33)>0 % Mode 3: Matrix Tension
    F = 1/S2T^2*(P22+P33)^2+1/S23^2*(P23^2-P22*P33)+1/
S12^2*(P12^2+P13^2);
    FoSs(3) = 1/F;
elseif (P22+P33)<0 % Mode 4: Matrix Compression
    F = 1/S2C*((S2C/(2*S23))^2-1)*(P22+P33) + 1/(4*S23^2)*(P22+P33)^2
 + ...
        1/S23^2*(P23^2-P22*P33) + 1/S12^2*(P12^2+P13^2);
    FoSs(4) = 1/F;
end

[FS,MODE] = min(abs(FoSs));
```

Published with MATLAB® R2017a

```
%*****************************************************%
%***            Tsai-Wu failure criteria             ***%
%***    Determine factors of safety Sfa and Sfr      ***%
%*****************************************************%
function [Sfa, Sfr]=SR_TsaiWu(F1t,F1c,F2t,F2c,F6,Stresses12)
%Inputs:
%  F1t,.., F6 are the lamina strengths
%  Stresses12 is a 3x1 array of stresses in the 1-2 coordinate system
%Outputs:
%  Sfa and Sfr are the factos of safety (actual and reversed-in-sign)
%Calculate Tsai-Wu Parameters
f1 = (1 / F1t) - (1  / F1c);
f11 = 1 / (F1c * F1t);
f2 = (1 / F2t) - (1 / F2c);
f22 = 1 / (F2c * F2t);
f66 = 1 / (F6 * F6);
%Determine the Coefficients a & b
a =
 (f11*Stresses12(1)*Stresses12(1))+(f22*Stresses12(2)*Stresses12(2))...
    +(f66 * Stresses12(3)*Stresses12(3))-
(sqrt(f11*f22)*Stresses12(1)...
    *Stresses12(2));
b = (f1*Stresses12(1))+(f2 * Stresses12(2));
%Determine the Factor of Safety
%*****************************************************%
%***              Factor of Safety, Sfa              ***%
%*****************************************************%
Sfa = (-b + sqrt((b * b) + (4 * a))) / (2 * a);
%*****************************************************%
%***         Reversed Factor of Safety, Sfr          ***%
%*****************************************************%
Sfr = (-b - sqrt((b * b) + (4 * a))) / (2 * a);
end
```

Published with MATLAB® R2017a

ADVANCED STRUCTURES & composites center

35 Flagstaff Road
Orono, Maine 04669
Telephone: (207) 581-2123
Fax: (207) 581-2074
composites.umaine.edu

Project: Beam Shear Stud Calculations

By: Ben Smith
Date: 06/01/17
Checked By: --
Date: --
Job Number: 1355.5

Inputs and Initial Calculations

Thickness of FRP: $t_{frp} := 0.0630\ in = 1.6\ mm$

Concrete Compressive Strength: $f'_c := 5000\ psi$

Concrete Modulus: $E_c := 57000\ psi \cdot \sqrt{\frac{f'_c}{psi}} = \left(4.031 \cdot 10^3\right)\ ksi$

FRP Modulus: $E_{frp} := 2.9218 \cdot 10^3\ ksi$

Maximum Linear Concrete Stress: $\sigma_c := 0.45 \cdot f'_c = \left(2.25 \cdot 10^3\right)\ psi$

Concrete Strain: $\varepsilon_c := \frac{\sigma_c}{E_c} = 5.582 \cdot 10^{-4}$

Beam Dimensions: Height: $h := 5\ in + t_{frp} = 5.063\ in$

Width: $b := 5\ in$

Length: $L := 5\ ft$

Depth to Center of FRP: $d := h - \frac{t_{frp}}{2} = 5.032\ in$

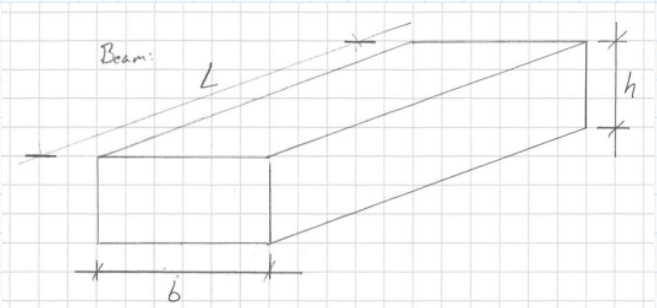

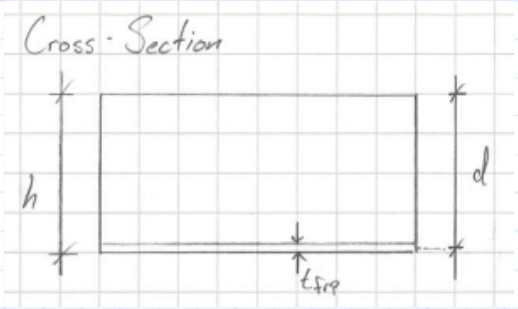

Depth to Neutral Axis:

Guess Values

$c := 1\ in$

Constraints

$$\frac{(d-c)\cdot\varepsilon_c}{c}\cdot E_{frp}\cdot t_{frp}\cdot b = \frac{\sigma_c\cdot b\cdot c}{2}$$

Sum of forces
(i.e. tension = compression)

Solver

$\mathbf{c} := \mathbf{Find}(\mathbf{c}) = 0.634\ in$

Strain in FRP: $\varepsilon_{frp} := \frac{(d-\mathbf{c})\cdot\varepsilon_c}{\mathbf{c}} = 0.004$

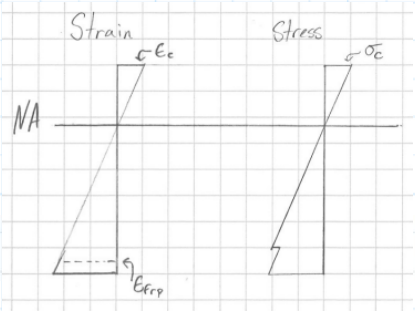

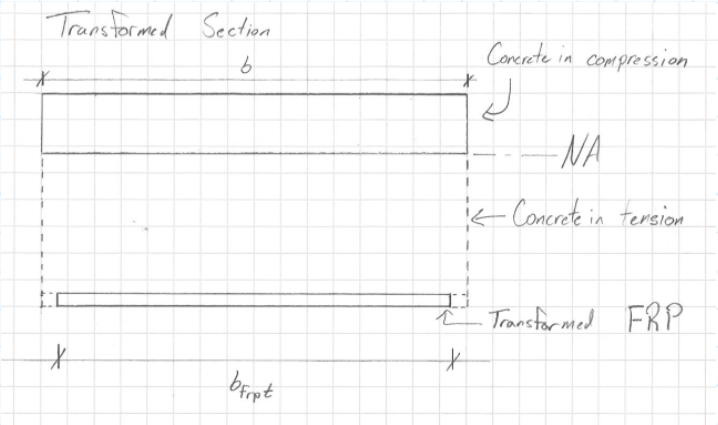

Transformed Section Analysis:

Transform FRP to Concrete: $b_{frpt} := b\cdot\frac{E_{frp}}{E_c} = 3.625\ in$

Tension Force in FRP: $F_{frp} := \varepsilon_{frp}\cdot E_{frp}\cdot t_{frp}\cdot b = \left(3.565\cdot 10^3\right)\ lbf$

Compressive Force in Concrete $F_c := \frac{\sigma_c}{2}\cdot b\cdot\mathbf{c} = \left(3.565\cdot 10^3\right)\ lbf$

Check Sum of Forces ~ 0: $sum\_forces := F_{frp} - F_c = 0\ lbf$

Moment in Section: $M := F_c\cdot\frac{2}{3}\cdot\mathbf{c} + F_{frp}\cdot(d-\mathbf{c}) = \left(1.432\cdot 10^3\right)\ lbf\cdot ft$

First Moment of Area: $Q := b_{frpt}\cdot t_{frp}\cdot(d-\mathbf{c}) = 1.004\ in^3$

Moment of Inertia: $I := \frac{b \cdot c^3}{12} + c \cdot b \cdot \left(\frac{c}{2}\right)^2 + \frac{b_{frpt} \cdot t_{frp}^3}{12} + b_{frpt} \cdot t_{frp} \cdot (d - c)^2$

I = (I_0 + Ad^2) + (I_0 + Ad^2)
Concrete FRP

$I = 4.841\ in^4$

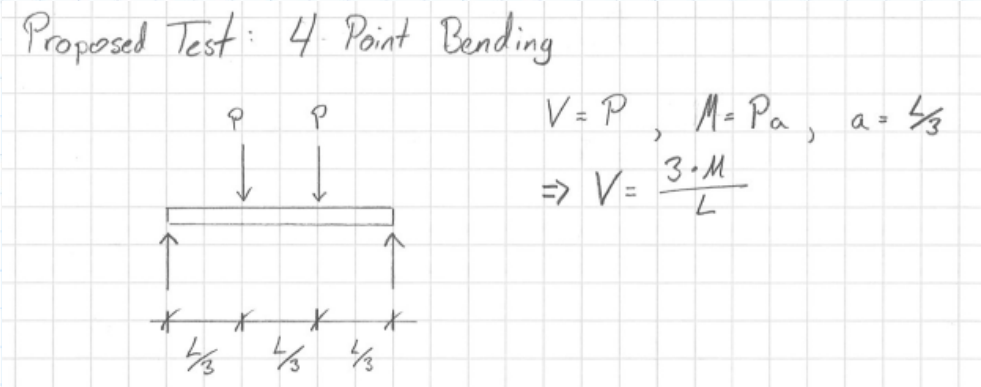

Shear Force: $V := \frac{3 \cdot M}{L} = 859.221\ lbf$

Shear Flow: $q := \frac{V \cdot Q}{I} = 178.25\ \frac{lbf}{in}$

Shear Stud Calculations

Pitch: $pitch := 3\ in$

Force carried by one row: $Force := q \cdot pitch = 534.75\ lbf$

Number of studs per row: $n := 2$

Stud diameter: $\phi := \frac{4}{8}\ in$ $b_{req} := (n) \cdot 2\ in + \frac{1}{2}\ in = 4.5\ in$
FRP , Concrete

Shear Strength: $\tau := min\left(3400\ psi, 0.5 \cdot \sqrt{f'_c \cdot E_c}\right) = \left(3.4 \cdot 10^3\right)\ psi$
FRP value includes B-Basis knockdown, should include other factors
Concrete formula from AASHTO 6.10.10.4.3-1

Allowable Force: $F_{ultimate\_capacity} := \tau \cdot \frac{\pi \cdot \phi^2}{4} \cdot n = \left(1.335 \cdot 10^3\right)\ lbf$

Percent Utilized: $percent\_capacity := \frac{Force}{F_{ultimate\_capacity}} = 40.1\%$

Factor of Safety: $FS := \frac{1}{percent\_capacity} = 2.497$

ADVANCED STRUCTURES & composites center
35 Flagstaff Road
Orono, Maine 04669
Telephone: (207) 581-2123
Fax: (207) 581-2074
composites.umaine.edu

Project: Design of Bearing Test

By: Ben Smith
Date: 06/19/2018
Checked By: Cam & Josh
Date: 6/20/2018
Job Number: 1355.11

Input

Diameter of Rod: $D := 0.5\ in$

Plate Length: $L := 6.5\ in$

Plate Width: $W := 3.75\ in$

Hole Location: $h := \frac{L}{2} = 3.25\ in$

Calculation of Approximate Bearing Strength

Compressive Strength of PETg Composite: $F_{c\_PETg} := 310\ MPa = 44.962\ ksi$

Compressive Strength of Derakane Composite: $F_{c\_Derakane} := 529\ MPa$

Bearing Strength of Derakane Composite: $F_{b\_Derakane} := 50\ ksi$

Bearing Strength of PETg Composite: $F_b := F_{b\_Derakane} \cdot \frac{F_{c\_PETg}}{F_{c\_Derakane}} = 29.301\ ksi$

Layup

Chosen Layup: $Layup := [0\ \ 0\ \ 0\ \ 0\ \ 0\ \ 45\ \ -45\ \ 45\ \ -45\ \ 45\ \ -45\ \ 45\ \ -45]\ s$

Thickness of a Lamina: $t_l := 0.2\ mm$

Thickness of Laminate $t := t_l \cdot (2 \cdot \mathrm{cols}(Layup)) = 0.205\ in$

Calculation of Load Needed

Bearing Area: $A_b := D \cdot t = 0.102\ in^2$

Load needed: $P := F_b \cdot A_b = 2.999\ kip$

Check for Tension Failure at Hole

Tension Area:	$A_t := (W - D) \cdot t = 0.665\ in^2$
Tensile Strength of Layup:	$F_{xt} := 24384.7\ psi$
Max Load	$P_{max} := F_{xt} \cdot A_t = 16.224\ kip$
FS	$FS := \frac{P_{max}}{P} = 5.409$
Total Area:	$A_{tot} := W \cdot t = 0.768\ in^2$
Max Load	$P_{max} := \frac{F_{xt} \cdot A_{tot}}{3} = 6.24\ kip$
FS	$FS := \frac{P_{max}}{P} = 2.081$

Check for Shear Failure at Hole

Shear Area:	$A_s := 2 \cdot h \cdot t = 1.331\ in^2$
Shear Strength	$T_{xy} := 4942\ psi$
Max Load	$P_{max} := T_{xy} \cdot A_s = 6.576\ kip$
FS	$FS := \frac{P_{max}}{P} = 2.193$

Check for Steel Failure

Bearing Area:	$A_{b\_s} := 2 \cdot 0.4\ in \cdot 0.2\ in = 0.16\ in^2$
Steel Tensile Strength (conservative)	$F_u := 58\ ksi$
Max Load	$P_{max} := 2.4 \cdot A_{b\_s} \cdot F_u = 22.272\ kip$
FS	$FS := \frac{P_{max}}{P} = 7.426$
Clear Distance Hole to Edge	$l_c := 0.4\ in$
Max Load	$P_{max} := 2 \cdot 1.2 \cdot l_c \cdot 0.2\ in \cdot F_u = 11.136\ kip$
FS	$FS := \frac{P_{max}}{P} = 3.713$

Tension Area: $A_{t\_s} := (0.8\ in + 0.8\ in + 1.1\ in) \cdot 0.2\ in = 0.54\ in^2$

Max Load $P_{max} := A_{t\_s} \cdot F_u = 31.32\ kip$

FS $FS := \frac{P_{max}}{P} = 10.443$

Check for Aluminum Failure

Aluminum Tensile Strength (6061) $F_u := 30\ ksi$

Tension Area: $A_{t\_a} := min(1.1\ in \cdot 4, (0.4\ in + 0.9\ in + 0.5\ in) \cdot 2) \cdot 1\ in = 3.6\ in^2$

Max Load $P_{max} := A_{t\_a} \cdot F_u = 108\ kip$

FS $FS := \frac{P_{max}}{P} = 36.009$

Bearing Area $A_{b\_a} := D \cdot 1\ in \cdot 2 = 1\ in^2$

Max Load $P_{max} := 2.4 \cdot A_{b\_a} \cdot F_u = 72\ kip$

FS $FS := \frac{P_{max}}{P} = 24.006$

Clear Distance Hole to Edge $l_c := 1\ in$

Max Load $P_{max} := 2 \cdot 1.2 \cdot l_c \cdot 1\ in \cdot F_u = 72\ kip$

FS $FS := \frac{P_{max}}{P} = 24.006$

Check for Bolt Failure

Bolt Minor Diameter: $D_s := 0.2970\ in$

Ultimate Strength: $F_{nv} := 27\ ksi$

Bolt Area: $A_{bolt} := 4 \cdot \frac{D_s^2}{4} \cdot \pi = 0.277\ in^2$

Max Load $P_{max} := F_{nv} \cdot A_{bolt} = 7.482\ kip$

FS $FS := \frac{P_{max}}{P} = 2.495$

ADVANCED STRUCTURES & composites center

35 Flagstaff Road
Orono, Maine 04669
Telephone: (207) 581-2123
Fax: (207) 581-2074
composites.umaine.edu

Project: Bearing Test Results

By: Ben Smith
Date: --
Checked By: --
Date: --
Job Number: 1355.11

Maximum Load $P := [1293.7 \ \ 1364.3 \ \ 1139.6 \ \ 1187.6 \ \ 1210.7 \ \ 1314.4 \ \ 1144.0 \ \ 1170.9]$ *lbf*

$P = [5.755 \ \ 6.069 \ \ 5.069 \ \ 5.283 \ \ 5.385 \ \ 5.847 \ \ 5.089 \ \ 5.208]$ *kN*

From Material Testing

Thickness of a lamina	$t_l := 0.2$ *mm*	$t_l = 0.008$ *in*
Number of layers in the test specimen	$n := 8$	
Thickness of the test specimen	$t := n \cdot t_l = 0.063$ *in*	$t = 1.6$ *mm*
Diameter of the hole	$D := 0.75$ *in*	$D = 19.05$ *mm*
Bearing area	$A := t \cdot D = 0.047$ *in*^{2}	$A = 30.48$ *mm*^{2}
Average maximum load	$P_{ave} := \text{mean}(P) = (1.228 \cdot 10^3)$ *lbf*	$P_{ave} = 5.463$ *kN*
Bearing Capacity	$\sigma_{max} := \frac{P_{ave}}{A} = 179.235$ *MPa*	$\sigma_{max} = 25.996$ *ksi*

ADVANCED STRUCTURES & composites center
35 Flagstaff Road
Orono, Maine 04669
Telephone: (207) 581-2123
Fax: (207) 581-2074
composites.umaine.edu

Project: AASHTO Live Load Calculations

By: Ben Smith
Date: --
Checked By: --
Date: --
Job Number: 1355.11

Spacing of girders $S := 56\ in$

Equivalent strip width for cast in place decks in positive bending $SW := 26\ in + 6.6 \cdot \frac{S}{12} = 56.8\ in$

AASHTO, Table 4.6.2.1.3-1

Wheel Load $P := 16\ kip$

Wheel Load Spacing $Sp := 6\ ft$

Spacing is larger than span, assuming single span and simply supported, highest moment is when the load is located at midspan

Maximum Moment $M := \frac{P \cdot S}{4} = 224\ in \cdot kip$

AISC, Table 3-23

Multiple Presence Factor, one lane loaded $m := 1.2$

AASHTO, Table 3.6.1.1.2-1

Impact factor, not a deck joint, not fatigue or fracture $IM := 1.33$

AASHTO, Table 3.6.2.1-1

Maximum live load moment per unit width $M_{LL} := m \cdot \frac{M}{SW} \cdot IM = 6.294\ \frac{in \cdot kip}{in}$

From Table A4-1 for comparison $M_{LL} := 4.65\ \frac{in \cdot kip}{in}$

References

AASHTO, "AASHTO LRFD Bridge Design Specifications," American Association of State Highway and Transportation Officials, Washington, D.C., 2012.

AISC, Steel Construction Manual, 14th ed. United States of America: American Institute of Steel Construction, 2011.

APPENDIX D

TECHNICAL DATA SHEETS

This appendix contains the technical data sheets for the materials used during this research.

- 258) PolyOne: Polystrand™ IE 5842 Technical Data Sheet
- 260) Vivak: PETG Product Data Sheet

Polystrand™ IE 5842

Continuous glass-reinforced thermoplastic PETG composite

Key Characteristics

Product description

Polystrand™ IE 5842 is a PETG-based thermoplastic unidirectional tape, which balances strength and toughness with excellent adhesive properties. Applications include structural components and reinforcement for wood, metal, and polymer molded or thermoformed components. The use of PETG resin imparts excellent mechanical properties, and good chemical and solvent resistance. Unidirectional tapes are available in rolls 25” wide. Custom slit widths and finished stampings are also available. Multi-ply laminates are available with plies arranged in 0 or 90 degree orientations, with maximum roll width of 125”.

Technical Properties of Unidirectional Tape

Typical Properties

PROPERTY	TEST METHOD	UNITS	DATA
Glass Content	ASTM D3647	wt%	58
Areal weight	--	oz/yd2 (g/m2)	12.0 (405)
Thickness	--	In (mm)	0.012 (0.3)
Flexural modulus	ASTM D790	MPsi (GPa)	4.18 (29)
Flexural Strength	ASTM D790	Ksi (MPa)	87 (602)
Longitudinal Tensile Modulus	ASTM D3039	MPsi (GPa)	4.14 (28.5)
Longitudinal Tensile Strength	ASTM D3039	Ksi (MPa)	82.8 (571)
In-Plane Poisson’s Ratio	ASTM D3039	--	0.27
Transverse Tensile Modulus	ASTM D3039	MPsi (GPa)	0.52 (3.6)
Transverse Tensile Strength	ASTM D3039	Ksi (MPa)	1.5 (10.0)
Longitudinal Compressive Modulus	ASTM D6641	MPsi (GPa)	0.71 (4.9)
Longitudinal Compressive Strength	ASTM D6641	Ksi (MPa)	29.5 (197)
Transverse Compressive Modulus	ASTM D6641	MPsi (GPa)	0.26 (1.8)
Transverse Compressive Strength	ASTM D6641	Ksi (MPa)	5.5 (38)
In-Plane Shear Modulus	ASTM D7078	MPsi (GPa)	0.21 (1.5)
In-Plane Shear Strength	ASTM D7078	ksi (MPa)	3.0 (21)
Transverse Shear Modulus	ASTM D7078	MPsi (GPa)	0.17 (1.2)
Transverse Shear Strength	ASTM D7078	ksi (MPa)	6.7 (46)

Notes

warranty. Buyers and users assume all responsibility and liability for loss or damage arising from the handling and use of our products, whether used alone or in combination with other products.

Processing

Polystrand™ IE 5842 process temperature is 420-470F (215-243C). Contact PolyOne for detailed set-up and processing guidelines.

Please contact PolyOne for data relating to a specific application or equipment.

Availability

Polystrand™ IE 5842 roll or laminated sheet is available in the US, EU and Asia Pacific regions.

CONTACT INFORMATION

For additional information, please contact PolyOne Advanced Composites at +1.866.POLYONE (+1.866.765.9663) or visit our web site at www.polyone.com.

PETG Sheet
Product Data

VIVAK® Sheet

VIVAK® Sheet is a transparent thermoplastic sheet. In the point of purchase industry, VIVAK Sheet is the brand and market leader for all clear plastics. Among its advantages, VIVAK Sheet offers superior impact strength over acrylic and cost effectiveness compared to polycarbonate. VIVAK Sheet offers deep draws, complex die-cuts and precise molded-in details without sacrificing structural integrity. It die-cuts and punches easily and can be bonded or fastened with adhesives, ultrasonic welding or rivets. In addition, VIVAK Sheet is easily decorated by painting, silk screening, or hot stamping. Easy to fabricate, form, bond and decorate, VIVAK Sheet is well suited for a variety of point of purchase and sign applications.

APPLICATIONS

Typical applications include video tape shelves, greeting card displays, revolving merchandise racks, indoor signs, point of purchase displays, menu displays, photo frames, and slat wall inventory displays.

Typical Physical Properties

Property	VIVAK® Sheet	Units	Test Method
GENERAL			
Specific Gravity	1.27	-	ASTM D-792
Water Absorption after 24 hrs.	0.2	%	ASTM D-570
MECHANICAL			
Tensile Strength, Ultimate .125″	7,700	psi	ASTM D-638
Tensile Modulus .125″	320,000	psi	ASTM D-638
Flexural Strength .125″	11,200	psi	ASTM D-790
Flexural Modulus .125″	310,000	psi	ASTM D-790
Izod Impact Notched .125″ at 73″	1.7	Ft-lb/in	ASTM D-256
Izod Impact Notched .125″ at 32″	1.2	Ft-lb/in	ASTM D-256
Drop Dart Impact .250″ at 73″	83	Ft-lbs	ASTM D-3763
Rockwell Hardness	115	R Scale	ASTM D-785
Shear Strength	9,000	psi	ASTM D-732
Compressive Strength	8,000	psi	ASTM D-895
THERMAL			
Heat Deflection Temperature @ 264 psi	157	°F	ASTM D-648
Heat Deflection Temperature @ 66 psi	164	°F	ASTM D-648
Coefficient of Thermal Expansion	3.8	In/in/°Fx10^{-5}	ASTM D-696
Flammability ≥ .080″	HB	-	UL 94
Glass Transition Temperature	178	°F	-
Forming Temperature	280-320	°F	-
OPTICAL			
Light Transmission	86	%	ASTM D-1003
Refractive Index	1.57	-	ASTM D-542
Haze	1.0	%	ASTM D-1003
ELECTRICAL			
Dielectric Constant, 1 kHz	2.6	-	ASTM D-150
Dielectric, 1 mHz	2.4	-	ASTM D-150
Dielectric Strength	410	v/mil	ASTM D-149

Recycle Code 2 Polyethylene Terephthalate Glycol Modified

PETG Sheet

VIVAK® Sheet

Compare VIVAK Sheet's performance for interior fabricated and formed applications. It delivers an optimum balance of performance and economy.

Performance Comparison

Impact Strength Falling Dart @ 73˝ ASTM D-5420 @ .125˝	**Acrylic**	**Polycarbonate**	**VIVAK Sheet**
10 in/lbs.	Failed	No break	No break
100 in/lbs.	Failed	No break	No break
300 in/lbs.	Failed	No break	No break
Heat Resistance @ 264 psi	190°F	270°F	157°F
@ 66 psi		280°F	164°F
Gamma Stability	Poor	Fair	Excellent
Chemical Resistance	Poor	Fair	Good

For additional or technical information please contact the Sheffield Customer Service Department:
Phone: 800/254-1707
Fax: 800/457-3553
Web Site: www.sheffieldplastics.com

Sheffield Plastics Inc.
A Bayer MaterialScience Company

119 Salisbury Road
Sheffield, MA 01257
800-628-5084
www.sheffieldplastics.com
Email: info@sheffieldplastics.com

BIOGRAPHY OF THE AUTHOR

Benjamin Smith was born in Bangor, Maine on December 6, 1994. He was raised in Old Town, Maine and graduated as valedictorian from Old Town High School in 2013. He attended the University of Maine and graduated in 2017 with a Bachelor's degree in Civil and Environmental Engineering. Upon graduation, he entered the Civil Engineering graduate program at The University of Maine and worked as a graduate research assistant at the Advanced Structures and Composites Center. He is a candidate for the Master of Science degree in Civil Engineering from the University of Maine in August 2019.